

UNRAVELING NON-CANONICAL FACETS OF TELOMERE BIOLOGY IN

*Arabidopsis thaliana*

A Dissertation

by

SREYASHREE BOSE

Submitted to the Office of Graduate and Professional Studies of  
Texas A&M University  
in partial fulfillment of the requirements for the degree of

DOCTOR OF PHILOSOPHY

Chair of Committee,	Dorothy Shippen
Committee Members,	Ping He
	Hays Rye
	Scott Dindot
Head of Department,	A. Joshua Wand

December 2020

Major Subject: Biochemistry

Copyright 2020 Sreyashree Bose

## ABSTRACT

Telomeres protect the chromosome ends from nucleolytic attack and facilitate complete replication of DNA. Telomerase is an essential enzyme composed of catalytic subunit Telomerase Reverse Transcriptase (TERT) and a long non-coding RNA (lncRNA), Telomerase RNA (TR). Telomerase, plays an indispensable role in telomere length homeostasis and a multitude of pathways have been implicated in regulating telomeres and telomerase. For example, in *Arabidopsis thaliana* a novel lncRNA named TER2 was previously identified as a negative regulator of telomerase in response to DNA damage.

In this dissertation, the role of TER2 in plant telomere biology was reevaluated. *TER2* was originally shown to partially overlap with the 5' UTR of tRNA Adenosine Deaminase (*TAD3*) gene on the complementary strand. However, updated genome annotation revealed that *TER2* was wholly embedded within the *TAD3* 5' UTR, raising the possibility that phenotypes ascribed to *TER2* could be instead derived from the *TER2/TAD3* locus. Based on the results from strand-specific qRT-PCR and RNA-Seq experiments, *TER2* is not a stable lncRNA, and instead appears to be a PCR artifact emanating from the *TAD3* 5' UTR. Further, telomerase activity assays with hypomorphic *tad3* mutant revealed that the *TER2/TAD3* locus is non-responsive to DNA damage. However, the *tad3* mutants failed to maintain proper telomere length, despite the presence of a wild type level of telomerase activity and a wild type terminal chromosome architecture. Additional genetic analysis confirmed *TAD3* contributed to telomere

maintenance via a telomerase-independent mechanism. Loss of TAD3 impacts several pathways that impinge on cell cycle, metabolism, and hormone signaling, implying that TAD3 affects telomere length maintenance indirectly by influencing cell cycle and/or metabolism-related pathways in *A. thaliana*.

I uncovered a second non-canonical mechanism in telomere biology by demonstrating that Protection Of Telomeres 1b, one of two POT1 paralogs in *A. thaliana*, is required for chromatin compaction and chromosome segregation. This function appears to be related to a role for POT1b in regulating reactive oxygen species. Overall the work presented in this dissertation provides new insights into the various non-canonical pathways involved in telomere maintenance and non-canonical functions of telomere associated protein. It also expands on understanding of the interplay between telomeres and cellular metabolism.

## DEDICATION

I want to dedicate my work and my thesis to my beautiful family: Ma, Baba, and my little brother, for their unconditional love and support and also to the love of my life, Chinmay and his family for believing in me and motivating me to keep going forward.

## ACKNOWLEDGEMENTS

The last six years have been quite a journey with countless moments, which made my time at Texas A&M University memorable. They say it takes a village to finish a Ph.D., and I couldn't agree more with that statement. Hence, I would like to use this opportunity to thank everyone from that village who has played a pivotal role in this journey called Ph.D.

Firstly, I am immensely grateful to my thesis advisor, Dr. Dorothy E. Shippen, for her continuous support, mentorship, and encouragement during the past years. My bachelor's degree is in engineering, and I did not have a formal research background before starting my lab rotations. But Dr. Shippen was extraordinarily kind and patient to believe in me and gave me the golden opportunity of becoming a part of her beautiful lab - The Shippen Lab. I remember I did a horrible job during my first lab meeting. But when the meeting was over, Dr. Shippen, instead of being disappointed with me, advised me on improving my scientific intellect and developing my overall thought process. I am thankful to her for making me push my limits and think creatively. I am fortunate to have such an amazing and strong woman of science as my boss. Although our professional journey might be date-stamped, she is my mentor for life.

Next, I would like to express my heartfelt gratitude to my committee members - Dr. Ping He, Dr. Scott Dindot, and Dr. Hays Rye - for giving me brilliant ideas for my project. Their difficult questions trained me to think on my feet, read the literature thoroughly, and develop a flexible mindset to look at scientific problems from different

perspectives. I would also like to thank all the labs where I did my 1st-year rotations in - Kunkel Lab, Rye Lab, and Kaplan Lab. A special shout out to Dr. Craig Kaplan for being the first one to teach me how to work in a research lab and how to set up a basic PCR reaction. Although after that, I have set up hundreds of PCR reactions, seeing that first band on the gel while in the Kaplan will hold a special place in my heart, forever. I am also grateful to both Dr. Kaplan and Dr. Hu for their first-year seminar class as they taught me the secret of making a great presentation and delivering an engaging talk.

For the past years, The Shippen Lab has been more than my family. I am grateful to have crossed paths with some of the most amazing scientists and learning so much from them. I am thankful to past lab members - Xiayuan for introducing me to the Shippen Lab; also, Peter and Callie, for their mentorship. I am grateful to Jiarui, Borja, and Ji-hee for their love and friendship. I am especially thankful to Pierce for giving me comments on my document and motivating me to write concisely. As a mentor, I have been blessed to have Erica and Ryan as my undergrad mentees. I am thankful to them for being patient with me and helping me with my research. A special shoutout to Helena and Laura for their love and friendship all through grad school. I am grateful to Tillie for letting me have candies from her office, helping me with all the school and lab-related paperwork, and just checking on me from time to time. I am thankful to Divina and Sherry from the stockroom and Terry and Austin from downstairs for making sure that I had the chemicals and instruments available for my research. Also, a special shout out to my graduate advisors Rafael and Justine, for their constant help with grad school-specific and life-related issues.

I am eternally grateful to my family for their unconditional love, trust, and support. I come from a country where receiving primary schooling is still an unachievable dream for many little girls. But my parents never stopped me chasing my dreams. They have taught me to work hard and remain grateful for everything we can achieve in life. The joy on their faces when they see me or hear me doing well in life is my biggest reward.

Grad school can be an emotionally draining process, and you need people around you to pull you up and walk with you. I am grateful for the 3 individuals who have been a pillar of support and strength during my Ph.D; I consider them my life coaches. First up are my lab mentors, Claudia and Vicky, whom I revere as my big sisters. They have taught me how-to do-good science and keep working hard even in the face of adversity. Beyond science, they have always been kind to hear about my life problems and advised me to do the needful. I am most eternally indebted to the love of my life, Chinmay, for being there by my side through thick and thin and for being my third pillar. I am grateful for his humor, love, and wisdom, which kept me going even on the worst days of life. I am blessed to have a partner who respects my work and pushes me to thrive beyond my comfort zone. In conclusion, thank you - Vicky, Claudia, and Chinmay- for teaching me the concept of "Philosophy" in this journey of becoming a Doctor of Philosophy.

## CONTRIBUTORS AND FUNDING SOURCES

### **Contributors**

This work was supervised by a dissertation committee consisting of Dr. Dorothy Shippen, Dr. Ping He, and Dr. Hays Rye of the Department of Biochemistry and Biophysics and Dr. Scott V Dindot from College of Medicine.

The data for Chapter II was in part provided by collaborators Dr. Ana-Victoria Súcun, Jiarui Song, Dr. Claudia Castillo-González and Dr. Behailu Birhanu Aklilu.

Data in Appendix A was produced in collaboration with Dr. Claudia Castillo-González.

Appendix B is a reprint of the publication –  
Song, J., Logeswaran, D., Castillo-Gonzalez, C., Li, Y., Bose, S., Aklilu, B.B., Ma, Z., Polkhovskiy, A., Chen, J.J.L., and Shippen, D.E. (2019). The conserved structure of plant telomerase RNA provides the missing link for an evolutionary pathway from ciliates to humans. PNAS. 116, 24542-24550.

All other work for the dissertation was completed independently by the student.

All the illustration in this document has been created using BioRender.com.

### **Funding Sources**

This work was supported by grants from NIH R01 GM065383 (to D.E.S.) and NSF MCB151787 (to D.E.S.).



## NOMENCLATURE

TERT	Telomerase Reverse Transcriptase
TER/TR	Telomerase RNA
POT	Protection of Telomeres
TAD	tRNA Adenosine Deaminase
TRF	Terminal Restriction Fragment
qTRAP	Quantitative Telomerase Repeat Addition Protocol

## TABLE OF CONTENTS

	Page
ABSTRACT .....	ii
DEDICATION.....	iv
ACKNOWLEDGEMENTS .....	v
CONTRIBUTORS AND FUNDING SOURCES .....	viii
NOMENCLATURE .....	ix
TABLE OF CONTENTS .....	x
LIST OF FIGURES .....	xiii
LIST OF TABLES .....	xvi
CHAPTER I INTRODUCTION .....	1
Tying the loose ends: genome evolution and the need for telomeres .....	1
Discovery of Telomeres and Telomerase .....	5
Telomeres and human health .....	6
Telomere length and sequence .....	8
Telomere structure: G-overhangs, Blunt ends, T-loops and G-quadruplexes .....	9
Telomerase .....	12
Telomerase RNA.....	15
Addition of telomeric repeats.....	19
Shelterin Complex.....	21
The CST Complex.....	24
POT1 proteins .....	26
Ku complex.....	29
Telomere Length Regulation .....	31
Telomere related activities across the cell cycle .....	35
<i>de novo</i> telomere formation (DNTF) at DNA Double Breaks (DSBs) .....	41
Telomerase-independent regulation of telomere length .....	43
tRNA Adenosine Deaminases.....	46
Telomere and Metabolism .....	48
ROS-induced changes to telomeric DNA.....	50
Regulation of ROS in plants .....	53

ROS, epigenome and reproductive health .....	56
<i>Arabidopsis thaliana</i> as a model organism .....	58
Dissertation Overview .....	62
CHAPTER II TRNA ADENOSINE DEAMINASE 3 IS REQUIRED FOR TELOMERE MAINTENANCE IN <i>ARABIDOPSIS THALIANA</i> .....	66
Abstract.....	66
Introduction.....	67
Results .....	71
Discussion.....	97
Material and Methods.....	101
CHAPTER III PROTECTION OF TELOMERES 1B IS NECESSARY FOR CHROMATIN COMPACTION DURING CELL DIVISION IN <i>ARABIDOPSIS THALIANA</i> .....	107
Abstract.....	107
Introduction.....	108
Results .....	112
Discussion.....	128
Materials and Methods .....	132
CHAPTER IV CONCLUSIONS AND FUTURE DIRECTIONS.....	135
The TER2 lncRNA is a PCR artifact derived from the 5'UTR of <i>TAD3</i> gene..	137
The <i>TAD3</i> locus does not respond to treatment with the DNA damage inducing agent zeocin .....	138
<i>TAD3</i> regulates telomere length via a telomerase-independent pathway in <i>A. thaliana</i> .....	140
Transcriptome analysis of <i>tad3-2</i> mutants reveal changes in metabolism and cell cycle related pathways .....	141
Future directions.....	144
Loss of POT1b induces oxidative stress in <i>A. thaliana</i> .....	148
Telomere end architecture is unperturbed in <i>pot1b</i> mutants .....	150
Aberrant chromatin and chromosome segregation in plants with elevated ROS .....	150
Future Directions.....	153
Conclusion .....	156
REFERENCES .....	159
APPENDIX A HIGH YIELD COMET ASSAY TO ASSESS DNA REPAIR COMPETENCE IN <i>ARABIDOPSIS THALIANA</i> .....	198

Abstract.....	198
Introduction.....	199
Comet Assay for plant tissue .....	202
Standard Comet Assay Protocol .....	203
Comet Assay Modification to determine DNA repair competence .....	209
Results .....	212
Discussion.....	215
APPENDIX B THE CONSERVED STRUCTURE OF PLANT TELOMERASE RNA PROVIDES THE MISSING LINK FOR AN EVOLUTIONARY PATHWAY FROM CILIATES TO HUMANS .....	219
Abstract.....	219
Introduction.....	220
Results .....	223
Discussion.....	252
Material and Methods.....	255
APPENDIX C MISCELLANEOUS INFORMATION .....	263

## LIST OF FIGURES

	Page
Figure I-1 Telomeres solve the end replication and end protection problems. ....	4
Figure I-2 Major discoveries in telomere biology over the past nine decades.....	6
Figure I-3 Telomeres form different structures. ....	11
Figure I-4 Structural elements of TERT and TER.....	14
Figure I-5 Sequential method of telomere repeat addition process. ....	20
Figure I-6 Telomere associated protein complexes. ....	22
Figure I-7 POT1 paralogs in different model organisms. ....	27
Figure I-8 The protein counting mechanism for telomere length regulation. ....	33
Figure I-9 Telomere maintenance is a cell cycle regulated process. ....	39
Figure I-10 ROS induced damage to cellular compartments. ....	52
Figure I-11 <i>Arabidopsis thaliana</i> as a model organism. ....	60
Figure II-1 Reannotation of the TER2 locus based on TAIR10_v90. ....	72
Figure II-2 TAD3 mRNA expression is regulated during plant development. ....	73
Figure II-3 Identification of a cryptic transcript produced from the TAD3 locus in <i>tad3-1</i> mutants.....	75
Figure II-4 The TAD3 locus does not modulate DNA damage related pathways. ....	77
Figure II-5 Results of zeocin treatment of WT and <i>tad3-2</i> seedlings.....	79
Figure II-6 TAD3 maintains telomeres via a telomerase-independent pathway. ....	82
Figure II-7 Exacerbated reproductive and developmental defects and genome instability in <i>pot1a tad3-2</i> mutants.....	86
Figure II-8 Combined loss of TAD3 and POT1a accelerates the onset of telomere dysfunction. ....	87

Figure II-9. Loss of TAD3 does not affect the G-overhang or blunt-end architecture of telomeres.....	91
Figure II-10 Transcriptomic analysis reveals changes in auxin signaling, plant secondary metabolism and cell cycle-related genes due to loss of TAD3..	94
Figure II-11 Cell cycle regulated expression of telomerase components and gene ontology analysis of WT and <i>tad3-2</i> transcriptomics data. ....	96
Figure III-1 Experimental model linking oxidative stress to chromosomal aberration.	112
Figure III-2 Assessment of the G-overhang structure in <i>pot1b</i> mutants.....	114
Figure III-3 Loss of POT1b generates aberrant chromatin structure in dividing cells from flowers. ....	118
Figure III-4 Chromatin bridges observed in <i>pot1b</i> are non-telomeric in origin.....	119
Figure III-5 Aberrant chromatin phenotypes of <i>cat2</i> and <i>pot1b cat2</i> mutants.....	122
Figure III-6 Chromatin structures observed during cell division in G2 and G4 <i>pot1a</i> mutants.....	125
Figure III-7 Segregating chromatin structures observed in G2 <i>tert</i> and G1 <i>tert pot1b</i> .	127
Figure III-8 A possible role for POT1b in regulating floral ROS .....	131
Figure IV-1 Potential mechanistic employed by TAD3 for maintaining telomere length in <i>A. thaliana</i> . ....	144
Figure IV-2 A potential role of POT1b in maintaining chromatin structure. ....	155
Figure A-1 Comet assay image processing. ....	211
Figure A-2 Comet assay with plant protoplasts. ....	214
Figure A-3 Ex vivo DNA Repair potential of WT extract.....	215
Figure A-4 Assessing DNA damage accumulation based on parameters beyond PDT.	218
Figure B-1 A single RNA species is enriched in active telomerase complexes.....	225
Figure B-2 AtTER1 is not recovered in an AtTERT IP.....	226
Figure B-3 AtTR is the RNA template for Arabidopsis telomerase.....	228

Figure B-4 Characterization of AtTR. ....	229
Figure B-5 AtTR is the bona fide template of <i>A. thaliana</i> telomerase. ....	230
Figure B-6 Plant TRs share a conserved secondary structure. ....	237
Figure B-7 Functional characterization of critical structural elements in AtTR. ....	241
Figure B-8 Evolution of TR pseudoknot structures. ....	242
Figure B-9 Two independent CRISPR alleles of AtTR abolish telomere maintenance. ....	243
Figure B-10 Multiple sequence alignment of plant TRs. ....	244
Figure B-11 Sequence alignments of TR structural elements from respective clades to identify group-specific co-variations. ....	245
Figure B-12 SHAPE data support the structural model of AtTR. ....	247
Figure B-13 <i>In vivo</i> DMS footprinting uncovers accessible nucleotides in AtTR. ....	248
Figure B-14 DMS MaPseq provides detailed information on accessible nucleotides in AtTR. ....	249

## LIST OF TABLES

	Page
Table III-1 Quantification of the chromosomal abnormalities from all the genotypes assessed. ....	120
Table B-1 Predictive analysis of telomerase RNA across plants. ....	250
Table C-1 Primer Sequences. ....	263



# CHAPTER I

## INTRODUCTION

### **Tying the loose ends: genome evolution and the need for telomeres**

The primitive form of the modern-day telomere emerged almost 1 billion years ago, a period in evolution marked by the transition from the circular to the linear genome (de Lange, 2015). Linear genome arose at the time when organisms decided to transfer their genetic material into their offspring through meiotic cell division (Ishikawa and Naito, 1999). Redistribution of the genetic material during meiosis involves the successful exchange of genetic information between two sister chromatids, specifically through the crossing over event. Orchestrating crossing over events using circular chromosomes generated dicentric circles (circles containing two centromeres), which were difficult to resolve. However, linear genomes circumvented this limitation. The ease of separating or segregating genomic material in a linear DNA molecule likely promoted the evolution of linear genomes (de Lange, 2015).

Although linear genomes are evolutionarily favorable to support sexual reproduction, chromosome linearization caused two distinct problems: the end replication problem and the end protection problem (Figure I-1A) (Monaghan et al., 2018). The end replication problem emerged due to the semi-conservative nature of linear DNA replication. The mechanism of replicating double-stranded DNA varies between the two antiparallel DNA strands. While a single RNA primer is sufficient to replicate the leading strand of DNA, multiple RNA primers are required to replicate the lagging strand.

Moreover, the last step of lagging strand replication involves removal of the terminal RNA primer, leaving a portion of the DNA unreplicated and resulting in loss of a DNA segment (Muller et al., 1983). The end replication problem can lead to the loss of critical genetic information every time a cell undergoes DNA replication (Garavís et al., 2013).

The second problem of the linear genome is the end protection problem (Figure I-1B). This occurs due to the structural similarity of chromosome ends to DNA double-stranded breaks (DSBs)(de Lange, 2009). DSBs can have catastrophic effect on the overall health of an organism. If not repaired efficiently, DSB can lead to translocation, deletion and fusion of the DNA that can eventually result in either cell death or increase the risk of developing chronic diseases like cancer (Scott and Pandita, 2006). As a result, robust surveillance and repair mechanisms have evolved to recognize DSBs and repair them immediately. In contrast, induction of DNA Damage Response (DDR) at the telomeres leads to multiple deleterious effects – including but not limited to – cell cycle arrest, apoptosis and telomere fusion via the non-homologous end joining pathways (Maciejowski and De Lange, 2017; Stracker and Petrini, 2011). As a result, multiple pathways have evolved to protect telomeres from the wrath of DDR pathways.

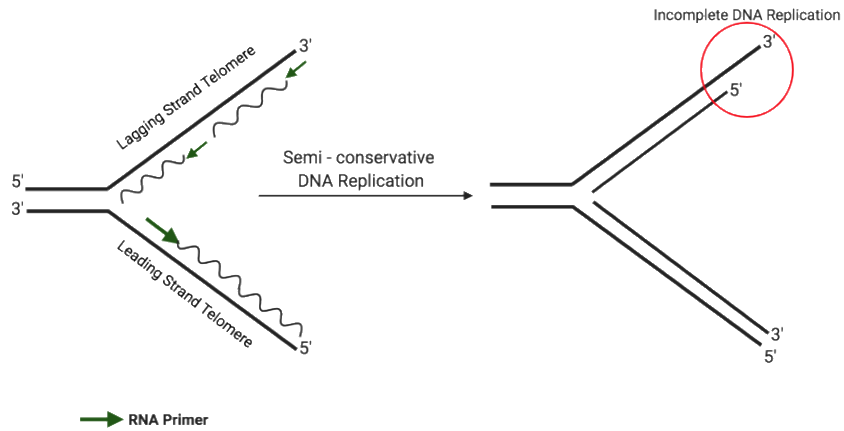
Telomeres are the repetitive DNA sequences present at the end of chromosomes and they play a critical role in solving the end replication and end protection problems (Monaghan et al., 2018). Instead of losing essential genetic information, the end replication problem allows loss of non-coding telomeric DNA. However, telomere shortening due to the end replication problem can be catastrophic. Once the telomeres reach a certain length threshold, cells undergo replicative senescence and this forms the

basis of cellular aging (Koliada et al., 2015). However, stem cells and germ cells require unlimited proliferation capacity and thus cannot afford to lose their telomeres. Therefore a specialized enzyme complex called telomerase replenishes telomeric tracts after DNA replication, thereby resolving the end replication problem (Mergny et al., 2007).

The solution to the end protection problem is offered by a myriad of protein factors recruited to telomeres (de Lange, 2018; Price et al., 2014). While some of these factors promote assembly of telomeres into specialized protective structures, others inhibit access of DNA damage repair machinery at the telomeres to prevent chromosome ends from fusing with each other, and to restrict unwanted DNA damage signaling at the chromosome ends (de Lange, 2018).

## End Replication Problem

A.



## End Protection Problem

B.

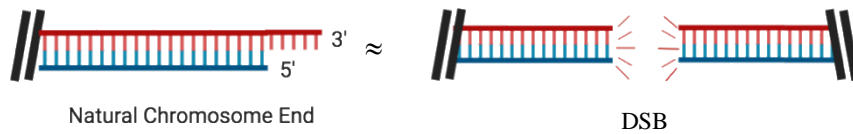


### **Figure I-1 Telomeres solve the end replication and end protection problems.**

A. The end replication problem occurs when the lagging strand cannot be fully replicated after the last RNA primer bound to the extreme 5' end of the daughter strand is removed. As a result, every time the cell divides, the chromosome ends shorten which impacts genomic integrity.

B. The end protection problem emerges due to the structural similarity between natural chromosomal ends (telomeres) and DSBs. Without telomeres, chromosome ends are predisposed to unwanted DNA damage repair pathways like recombination or fusion.

## **Discovery of Telomeres and Telomerase**

Identification of telomeres dates back to the early 1940s, when Hermann Muller (Muller, 1938), working on *Drosophila*, and Barbara McClintock, working on *Zea mays* (McClintock, 1941) reported the presence of a unique structure at chromosome ends (Figure I-2). Muller coined the "telomere" (telos – end and meros - part) for these specialized structures. Both Muller and McClintock reported that the natural ends of the chromosome behaved differently from the broken ends. The natural ends underwent a process termed chromosome healing (Sprung et al., 1999; Varela et al., 2016). However, the broken ends fused with other ends forming a dicentric chromosome. During mitotic cell division the dicentric chromosomes gave rise to anaphase bridges when the two centromeres were not segregated to opposite poles of the cell, thus initiating the break-fusion-bridge cycle (McClintock, 1939). Thus, the remarkable observation about the presence of such unique structure at chromosome termini inaugurated the branch of science known as telomere biology (Figure I-2).

In 1961, Leonard Hayflick observed that human cells could divide for only a finite number of generations *in vitro*. The term Hayflick limit or replicative senescence was introduced to explain this natural barrier (Hayflick, 1965). Ten years later, in 1972, James Watson identified the end replication problem arising from the semi-conservative nature of DNA replication (Huang and Keller, 1972). Around this same time, Alex Olovnikov proposed a link between DNA replication and the Hayflick limit, predicting that telomeres would shorten after each round of cell division (Olovnikov, 1973). Once the telomere reached a critical length, the cells would undergo cellular senescence as they would have

reached the Hayflick limit of cell division. The first telomeres were characterized in 1978 from the ciliate *Tetrahymena thermophila* (Blackburn and Gall, 1978) and the identification of telomeric sequences in other organisms followed. Both Muller and McClintock also hinted at the presence of a specific enzyme that can heal the broken ends arising from a DSB. The Nobel prize winning work of Elizabeth Blackburn and Carol Greider defined a new enzyme dubbed telomere terminal transferase, which had the ability of actively synthesizing and elongating telomeres (Greider and Blackburn, 1985; Varela and Blasco, 2010). This discovery and the close association of telomere maintenance with a cell's proliferative capacity catapulted telomere biology into one of the most highly studied areas in the scientific community (Shay and Wright, 2019).

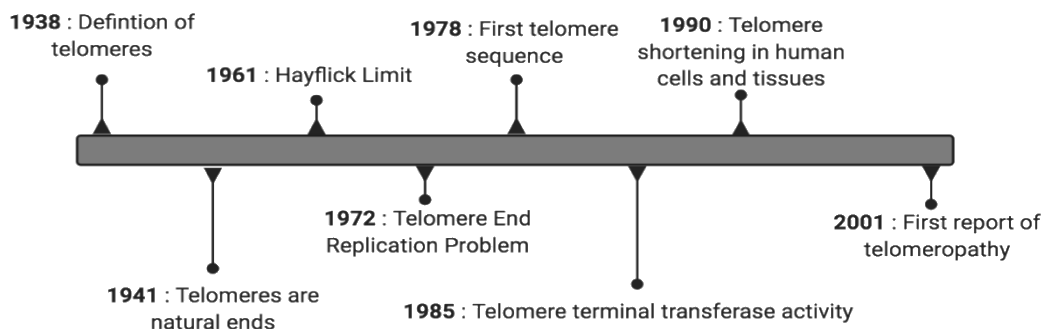


**Figure I-2 Major discoveries in telomere biology over the past nine decades.**

A timeline of the major discoveries in the field of telomere biology.

### **Telomeres and human health**

The identification of a potential link between cellular aging and telomere length in human cells dates back to 1990s. Experimental data from Calvin Harley indicated that

telomeric DNA in human cells shorten as the cell divides (Harley, 1990). Once the telomeres become critically short, the cell undergoes replicative senescence, thus supporting Olovnikov's "marginotomy theory"(Harley, 1991). The following years revealed the presence of multiple factors involved in telomere maintenance and length regulation. Interestingly, mutations in genes essential for telomere maintenance and protection are often associated with accelerated loss of telomeres and development of telomere associated diseases, also known as telomeropathies (Holohan et al., 2014). Moreover, chromosomal instability induced upon telomere shortening, in the absence of functional tumor suppressor genes, often marks the onset of tumorigenesis (Maciejowski and de Lange, 2017). Overall, unwanted loss of telomeric DNA and telomere-associated factors has a negative impact on human health.

Human telomere-related diseases include Dyskeratosis congenita, Idiopathic Pulmonary Fibrosis, Hoyeraal – Hreidarsson syndrome, aplastic anemia and cancer. The presence of critically short telomeres is a common theme for the above-mentioned diseases (Stanley and Armanios, 2015). Dyskeratosis congenita can occur due to mutations in the DKC1 gene which encodes Dyskerin, a telomerase biogenesis factor. It can also occur from mutations in the telomerase RNA subunit TERC/TR/TER (Vulliamy et al., 2001). DC patients develop defects in highly proliferative tissues like the skin and the bone marrow due to telomere shortening (Mitchell et al., 1999a). Similarly, the onset of Idiopathic Pulmonary Fibrosis (IPF) is associated with mutation in TERT and TERC genes. Such mutations also lead to aplastic anemia and acquired hematopoietic failure (Yamaguchi et al., 2005), which impairs hematopoietic stem cell production and worsens

the IPF associated symptoms including chronic scarring of the lung tissues and development of interstitial pneumonia (Barratt et al., 2018).

The failure to maintain telomeres in a defective tumor suppressor background is a hallmark for different forms of cancer. For instance, combined loss of TERC and p53 leads to the development of epithelial cancers in older adults such as breast cancer, skin cancer and cancer of the GI tract (Chin et al., 1999; Roake and Artandi, 2017). Similarly, loss of the shelterin component TRF1 in the absence of p53 causes several invasive forms of squamous cell carcinoma (Martínez et al., 2009). Several forms of lymphomas and adenocarcinomas occur due to the simultaneous loss of p53 and the shelterin protein POT1 (Akabay et al., 2013; Pinzaru et al., 2016), thus expanding the list of diseases associated with defects in proper maintenance and protection of telomeres.

### **Telomere length and sequence**

At the molecular level, telomeres consist of simple repeats of G-rich DNA. Telomeres vary in length across different organisms. The presence of highly conserved telomere-associated proteins across different kingdoms ensures little to no difference between the telomeric sequence amongst the most highly studied model organisms (Watson and Riha, 2010). *T. thermophila* has the telomere sequence TTGGGG repeated for 120-420 bp (Blackburn and Gall, 1978). While in budding yeast, *Saccharomyces cerevisiae*, telomeres span 200-300 bp and consist of  $TG_{2-3}(TG)_{1-6}$  (Shampay et al., 1984). Humans and mice occupy the other extreme of the telomere length spectrum. The vertebrate telomere sequence (TTAGGG) extends from 5 Kb – 15 Kb in humans (Moyzis



et al., 1988), while mouse telomeres are up to 150 Kb (Hemann, 2000). Hence, the disparity of telomere length between humans and mice indicates that telomere length and organismal complexity cannot be linked simplistically (Corbett and Alda, 2015). In the flowering plant, *Arabidopsis thaliana* (Col-0 ecotype) telomeres range from 2 kb – 5 kb and consist of TTTAGGG arrays (Richards and Ausubel, 1988). *A. thaliana* ecotypes (accessions) are analogous to yeast “strains”. There are >1000 ecotypes of *A. thaliana* which grow at diverse geographical locations worldwide. Notably, telomere length varies for different *A. thaliana* ecotypes (Shakirov and Shippen, 2004). In addition, There are some plants within the Asparagales clade, like *Allium cepa*, which lack a canonical telomere repeat (Sykorova et al., 2003). The plants may have telomeres similar to *Drosophila* which are composed of randomly inserted non-Long Terminal Repeat (non-LTR) retrotransposons (Healing Transposon – A or HetA, Telomere Associated Retrotransposon (TART), and Telomere Associated and HetA Related (TAHRE)) (Mason et al., 2008).

### **Telomere structure: G-overhangs, Blunt ends, T-loops and G-quadruplexes**

Due to the semiconservative nature of DNA replication, the leading strand telomeres terminate in blunt-ended telomeres whereas the lagging strand telomeres resolve into a 3' single strand extension termed as the G-overhang structure based on its G-rich sequence composition (Figure I-3A) (Sandhu and Li, 2017). The G-overhang acts as a primer for the telomerase ribonucleoprotein (RNP) complex. Thus, the length and the accessibility of the G-overhang needs to be regulated to allow the required level of

telomere addition (Rhodes and Giraldo, 1995). Along with being a major player in solving the end replication problem, G-overhang structures are equally crucial for addressing the end protection problem (Luke-Glaser et al., 2012). To prevent the chromosome ends from nucleolytic attack and recombinogenic events, G-overhangs form a lariat-like structure called the t-loop (Figure I-3B) (Griffith et al., 1999; Tomaska et al., 2019). RAP1-TRF2 proteins from the telomere-associated shelterin complex, bind to t-loops and inhibit the initiation of homologous recombination mediated DNA repair events at the telomere (Doksani et al., 2013). Besides protecting telomeres from the unwanted action of DNA damage repair machinery, the t-loops are involved in regulating access of telomerase, thereby playing a vital role in telomere length regulation (Uringa et al., 2012). According to some research models, t-loops were the ancient form of protecting the telomeres, even before the availability of the telomerase complex (de Lange, 2004). Due to their highly conserved structure, t-loops have been identified in humans, mice, plants, worms and yeast (Doksani et al., 2013; Griffith, 2013).

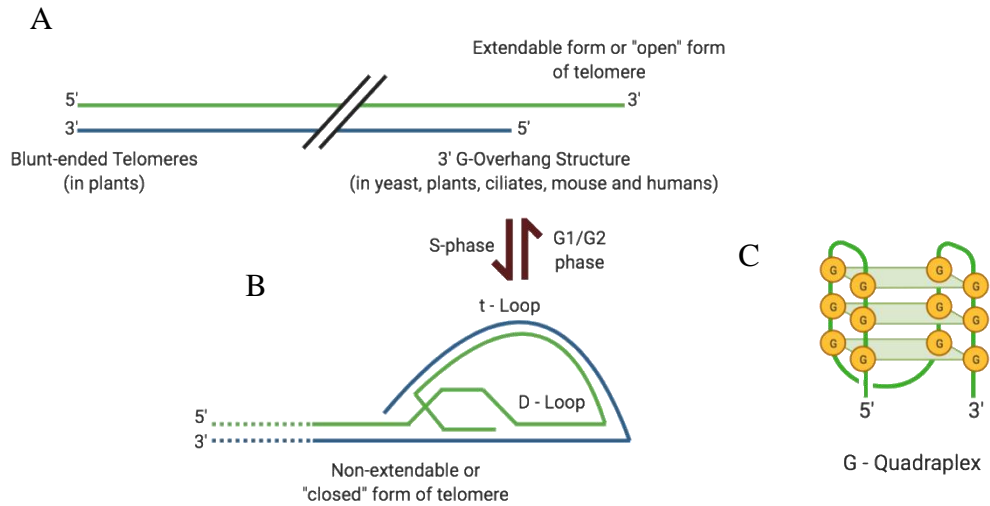


**Figure I-3 Telomeres form different structures.**

**A.** Following DNA replication, the lagging strands resolve into 3' G-overhang structures, while the leading strand gives rise to blunt-ended telomere. In most organisms, the blunt-end is converted into a G-overhang making the telomere ends symmetrical. This is not the case in plants. The accessible G-overhang allows the end of the chromosome to be extended by telomerase.

**B.** Telomeres in its non-extendible state tucks in the G-overhang giving rise to a D-loop. Similarly, the complementary C-rich strand also wraps around to form the t-loop.

**C.** The G rich sequences in the telomeres can stack upon each other to form the G-quadruplex or G-quartet structures. Specialized proteins like helicases help in resolving the G-quadruplexes.

The G-rich telomeric overhang has the ability to fold itself into a higher order structure known as the G-quadruplex or G-quartet (Figure I-3C). The G-quartet is a four-stranded structure formed by the vertical stacking of guanine-rich tetrad planes held together by a network of Hoogsten hydrogen bonding (Demkovičová et al., 2017). The presence of G-quartets limits accessibility of the telomerase enzyme and replication fork progression. As a result, G quadruplexes negatively regulate telomerase activity

(Oganesian and Karlseder, 2009). In every other organism except plants, G-overhang structures have been identified at both ends of the chromosomes (Nelson and Shippen, 2012). Enzymatic processing converts the leading strand blunt-end into G overhang structures (Bonetti et al., 2014). However, only 50% of plant chromosome ends contain a G overhang (Figure 3A). The remaining 50% are maintained as blunt ends bound by the Ku heterodimer (Valuchova et al., 2017a). Ku70-Ku80, is well known for its role in the non-homologous end joining pathway (NHEJ). The Ku complex regulates the accessibility of telomerase at blunt-ended plant telomeres (Kazda et al., 2012a; Valuchova et al., 2017b). It is hypothesized that blunt-ended telomeres reduce the rate of telomere shortening and provide additional stability to the plant genome helping to mitigate constant damage by various biotic and abiotic factors from the environment (Nelson and Shippen, 2012) (Figure I-3A).

## **Telomerase**

The discovery of telomerase dates back to 1985, when Carol Greider and Elizabeth Blackburn reported a telomere terminal transferase capability in *T. thermophila* protein extract. This activity was termed telomerase (Greider and Blackburn, 1985). Ten years later identification of telomerase activity in immortalized HeLa cells as well as the prevalence of its expression in cancer cells, accelerated telomere research (Nakamura et al., 1997). The enzyme Telomerase Reverse Transcriptase (TERT) is the catalytic component of the telomerase RNP complex (Leão et al., 2018), which acts in concert with

an integral long noncoding RNA, TERC/TR/TER (discussed later in the chapter) (Musgrove et al., 2018).

TERT is composed of four different regions – the Telomerase Essential N-terminal (TEN) domain, Telomerase RNA Binding Domain (TRBD), Reverse Transcriptase (RT) domain and C-terminal Extension (CTE) Domain (Figure I-4A) (Wyatt et al., 2010). The TEN domain traps telomeric DNA strands and associates with TR. The TRB domain binds both single-stranded and double-stranded domains in RNA. The RT domain is the catalytic core of the enzyme, which adds nucleotides in a metal ion-dependent manner to elongate the telomeres. Finally, the CTE domain stabilizes the RNA-DNA duplex at the telomeres. Mutation in any of these four regions can lead to telomeropathies (Autexier and Lue, 2006).

Telomerase activity needs to be tightly regulated for the normal growth and proliferation of human cells; its unwanted activation or repression leads to severe health complications. Insufficient telomerase activity causes bone marrow failure and pulmonary fibrosis while abnormally high levels of telomerase activity in somatic cells mark the onset of tumorigenesis and several types of cancer (Gomez et al., 2012). Similarly, plants homozygous for a null mutation in *TERT* gene show progressive telomere shortening, ultimately developing morphological defects combined with genome instability after several generations of self-propagation (Riha et al., 2001). Therefore, it is critical to regulate telomerase activity for optimal growth and development.

A Telomerase Reverse Transcriptase (TERT)



B Telomerase RNA (TR)

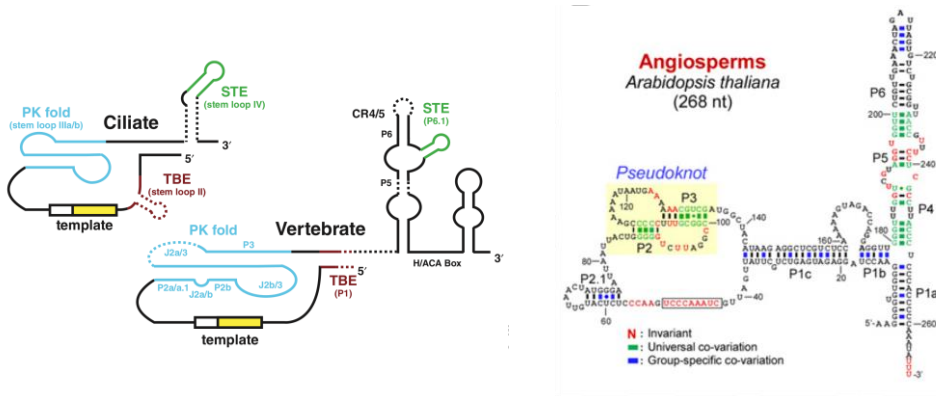


**Figure I-4 Structural elements of TERT and TER.**

**A.** The four subunits in TERT are – Telomerase Essential N-terminal (TEN) domain, Telomerase RNA-Binding Domain (TRBD), Reverse Transcriptase (RT) and C-Terminal Extension (CTE).

**B.** A schematic representation of the telomerase RNA secondary structure from ciliates, vertebrates and angiosperms. The most structural element of telomerase RNA are-the PseudoKnot (PK), Template Boundary Element (TBE), Template and a Stem Terminus Element (STE). These figures were taken from – Reprinted from Musgrove et al., 2018 and reprinted from Song et al., 2019.

## **Telomerase RNA**

TERT has the unique ability of extending telomeric DNA by reverse transcribing its internal lncRNA subunit, the telomerase RNA. TR conserved from yeast to human, but this molecule dramatically differs in size and sequence (Musgrove et al., 2018). All identified TRs possess certain basic secondary structural elements essential for proper functioning: the template, the 5' template boundary element (TBE), the pseudoknot (PK) region and the stem terminus element (STE) (Figure I-4B) (Chen et al., 2000; Lin et al., 2004; Romero and Blackburn, 1991; Theimer and Feigon, 2006). The template region, as the name suggests, acts as a template for the TERT enzyme to add telomeric repeats at chromosome ends through reverse transcription. The template region is typically comprised of 1.5 copies of the telomeric sequence (Musgrove et al., 2018). The TBE region prevents TERT from copying TR beyond the relevant template region (Chen and Greider, 2003a; Jansson et al., 2015). Although the precise role of the PK region is still under investigation, mutations in the PK region affect TR folding, which negatively impacts repeat addition processivity (RAP) of telomerase (Chen and Greider, 2005; Gilley and Blackburn, 1999; Theimer et al., 2005). The exact role of the STE region is unclear, but perturbation of the STE region diminishes telomerase activity (Zhang et al., 2011). Conservation of the secondary structural elements observed in TRs from ciliates, yeast, plants and humans underpins the importance of maintaining proper structure of this molecule *in vivo*. The structure of the PK domain and STE region have been studied extensively in vertebrate TR (Cash et al., 2013; Chen and Greider, 2005; Qiao and Cech,

2008). The STE region is resolved into a two-pronged forked structure composed of three helical segments. This region has a high affinity for TERT and undergoes several conformation changes that contribute to the regulation and activity of the telomerase complex *in vivo* (Bley et al., 2011; Mitchell and Collins, 2000). A unique triple helix RNA structure is tucked within the core of the PK region (Kim et al., 2008) and this is a target for mutations that are associated with human disease. Such mutations affect the overall stability and activity of TR (Theimer et al., 2003). In addition, structural experiments have revealed the presence of a bulged region proximal to PK which is important for facilitating dynamic movement of TR during telomere repeat addition (Jiang et al., 2015).

Despite conservation of specific structural elements, the size of TR molecules varies greatly. TRs range from ~150 nts in ciliates, ~260 nts in plants, ~450 nts in vertebrates and to over 1000 nts in budding yeast (Musgrove et al., 2018; Song et al., 2019). Ciliate TRs, which are the smallest known TRs (*T. thermophila* – 159 nts), are produced as RNA Pol III transcripts (Collins, 1999). A 9Å Cryo-EM structure of the endogenously assembled *Tetrahymena* telomerase provided the first opportunity to study full-length TR relative to its location within the RNP (Jiang et al., 2015). Extensive structural analysis of the *Tetrahymena* TR has also led to the identification of specific regions within the STE element, which mediate binding with the C-terminal domain of the p65 protein, a crucial member of the telomerase RNP in *Tetrahymena* (Jansson et al., 2015). Similar to ciliates, the 1.2 Kb yeast telomerase RNA (TLC1) has many structural similarities with TRs from ciliates and vertebrates. Most of the TLC1 is dispensable for enzyme activity and appears to function primarily as a scaffold for providing optimal



flexibility to the active TLC1 structure (Zappulla and Cech, 2004). The *Schizosaccharomyces pombe* TER is similar in length to *S. cerevisiae* TLC1 and undergoes processing via the spliceosomal complex, to generate the enzymatically active TER isoform (Box et al., 2008). Immediately following transcription, the *S. pombe* TER is bound by Sm proteins, which mediate the spliceosome-based processing. However, structural constraints within the RNA prevent a full canonical splicing reaction, thereby enabling the production of the active *S. pombe* TER (Box et al., 2008; Kannan et al., 2015). Similarly, the human TER (hTR) (451 nts long) and the mouse TER (mTR) (397 nts), possess RNA structural elements that promote RNA stability, as well as intracellular movement and biogenesis of the telomerase RNP complex (Garforth et al., 2006; Schmidt and Cech, 2015).

Previously TER1 had been reported as the plant telomerase RNA and TER2 as a novel telomerase associated regulatory RNA. However, the inability to immunoprecipitate both TER1 and TER2 from active telomerase enzyme cast doubt on the authenticity of the TER1 molecule. Independent data from three different labs, including the Shippen lab identified another lcnRNA termed AtTR as the *bona fide* plant telomerase for *A. thaliana* (Dew-Budd et al., 2020; Fajkus et al., 2019; Song, 2019), and refuted the role of TER1 as the plant telomerase RNA (Cifuentes-Rojas et al., 2011).

AtTR is a 268 nt long Pol III transcript, similar to that of TRs found in ciliates. The 9 nt template sequence within the AtTR – 5' CCAAACCCU 3' – serves as the template for telomere repeat addition *in vivo* (Song et al., 2019). Loss of AtTR leads to telomere shortening similar to the loss of TERT, indicating that AtTR is required for

telomerase activity. Plants lacking AtTR shows a discreet telomere banding pattern which is commonly seen while analyzing mutants defective in telomerase activity or processivity. This confirmed the role of AtTR as the plant telomerase RNA (Dew-Budd et al., 2020; Song et al., 2019). Bioinformatics analysis led to the identification of 85 AtTR orthologs from 70 angiosperms, 11 gymnosperms, and four lycophytes. An independent bio-informatic based experiment fueled the identification of several TRs from the Asparagales (For eg. *Rhodophiala pratensis*, *Agave tequilana*, *Nolina bigelovii*, *Allium cepa*) clades as well 75 other transcripts from eudicots, monocots and gymnosperms including the model plants *Nicotiana* and *Arabidopsis* (Fajkus et al., 2019). Cumulative structural analysis of AtTR along with most of the other plant TR revealed that the telomerase RNA in land plants possesses the conserved secondary structural elements – the template region, the pseudo knot or PK, and a long stem region expected for a true telomerase RNA. A plant-specific stem called P1.1 has been identified in the PK domain of AtTR, which is similar to the stem region found in invertebrate echinoderms and fungal TRs (Song et al., 2019). Based on its secondary structure, AtTR acts as a kind of evolutionary bridge to unify the structural components observed in TR from primitive ciliates to the more complicated vertebrate TRs. Interestingly, AtTR was originally identified as an RNA responsive to hypoxic stress that accumulates primarily in the cytoplasm under normal conditions (Wu et al., 2012).

### **Addition of telomeric repeats**

The mechanism of addition of telomere repeats by telomerase can be divided into two steps (Podlevsky and Chen, 2012a) - extension and translocation. The first step involves base-pairing the 3' end of telomeric DNA to the 5' end of the template sequence of TR, which occupies the active site of TERT (Qi et al., 2012). A single round of reverse transcription typically includes addition of 6-7 nucleotides to the telomeric DNA primer. After completing one round of repeat addition, the telomerase RNP can either recopy its template for another round of repeat addition or completely dissociate from the DNA thus marking the end of telomere repeat addition (Figure I-5). Hence, the second step of telomere repeat addition comprises of translocating the RNP such that the TR anchors to the newly synthesized telomeric repeat and continues extending the telomeres (Berman et al., 2011). The translocation process usually occurs outside of the telomerase active site (Figure I-5). Also, given that the process of repeat addition is relatively quick, the translocation step is typically the rate-limiting step for the process of telomere repeat addition (Qi et al., 2012).

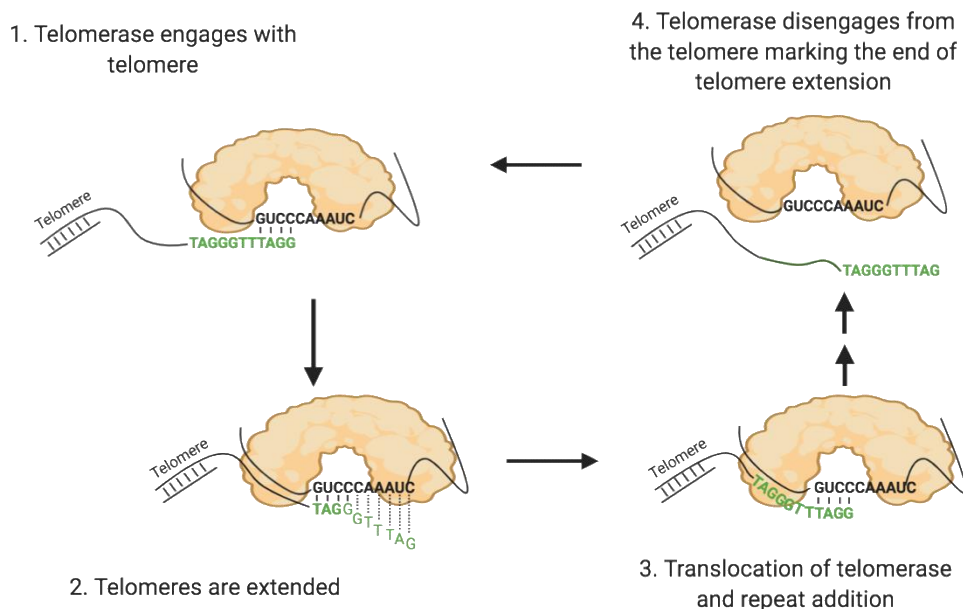


**Figure I-5 Sequential method of telomere repeat addition process.**

1. The template sequence of the TR aligns with the telomeric repeat (the first 4 bases)
2. TERT reverse transcribes TR template sequence to mediate nucleotide addition.
3. Telomerase translocates across the telomere to continue adding nucleotides. This mode represents repeat addition processivity.
4. Telomerase disengages from the telomeric repeats to terminate the repeat addition process by releasing the DNA.

Structures flanking the TR template region, i.e the Template Boundary Elements (TBE) play a crucial role in the error-free addition of telomeric repeats. For example, in ciliates the Template Recognition Element present on the 3' end of the template region of TER mediates the preferential placement of the DNA primer at the 3' end of template and not the 5' end. The 5' end of the template is thought to loop out during the initial annealing process. As the process of telomere repeat addition continues, the 5' end is gradually roped

into the active site for reverse transcription. As a result, the 5' Template Boundary Element (TBE) is crucial for preventing TERT from reverse transcribing regions, beyond the TER template sequence (Wu et al., 2017). Interestingly, the length of the template sequence is found to affect template realignment efficiency, which eventually regulates telomere repeat addition processivity (Chen and Greider, 2003b). Several conserved motifs within TERT molecule and various telomere bound protein complexes also regulate the telomerase processivity in different organisms, usually by regulating telomerase accessibility (Finger and Bryan, 2008; Xie et al., 2009) (Figure I-5) .

### **Shelterin Complex**

Shelterin is one of the most well-studied telomere protection complexes. It plays myriad of roles at telomeres including protecting telomeres from DDR, specifically aversion from activation of ATM, ATR, PARP1-related DNA damage pathways, and inhibiting non-homologous end joining (conventional and alternative) and homology-directed pathways (de Lange, 2018). Vertebrate shelterin contains six proteins – TRF1, TRF2, RAP1, TIN2, TPP1, and POT1 (de Lange, 2005) (Figure I-6). The proteins TRF1, TRF2, and POT1 are the only factors that attach directly to the telomeres (Chen et al., 2007). TRF1 and TRF2 are predicted to bind telomeric DNA individually through their Myb-SANT domains (Galati et al., 2015). POT1, on the other hand, POT1 binds to the single-stranded G-overhang region of the telomere via its two N-terminal Oligonucleotide-Oligosaccharide (OB) folds (Michael and Söll, 1999). OB folds are comprised of five beta strands in a closed beta-barrel motif and mediate the successful binding to

oligonucleotides and other protein components (Cohn, 2013). Although TPP1 possesses an OB fold, TPP1 cannot directly interact with DNA (Wang et al., 2007).

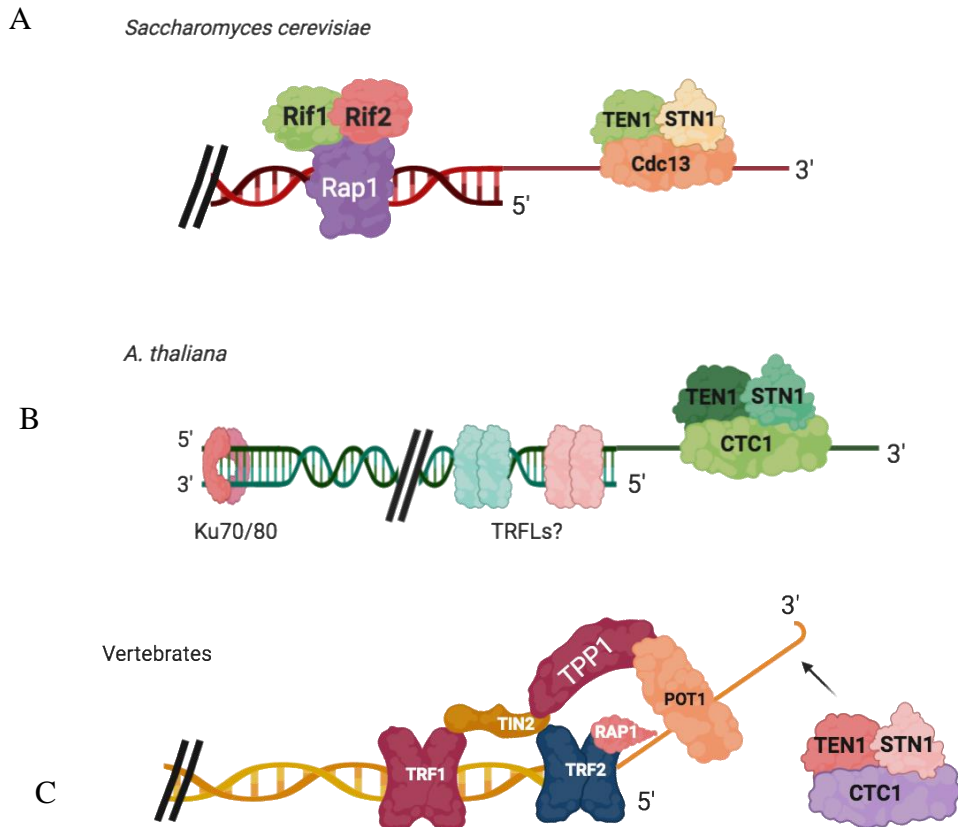


**Figure I-6 Telomere associated protein complexes.**

A. In *S. cerevisiae*, the double stranded telomeres are occupied by the RAP1-Rif1-Rif2 protein complexes while the single stranded region is occupied by the Cdc13-STN1-TEN1 complex.

B. CST (CTC1-STN1-TEN1) protein complex associates with the 3' G-overhang structure of *A. thaliana* telomeres and the blunt-ended telomeres are maintained by the Ku70/80 complex.

C. Vertebrate telomers are bound by the six membered shelterin complex and possibly by the trimeric CST complex at the single stranded region.

TIN2 is bound to TRF1 and TRF2 via different interaction surfaces. TIN2 also binds to TPP1, which in turn, is attached to the POT1 protein. Additionally, RAP1 binds to TRF2, completing the organization of the six-member complex. In addition to the interactions among the members of complex, shelterin contacts several accessory factors, most of which belong to the DDR pathways. For example, Apollo/SMNB1 interacts with shelterin via the TRF2 protein and is involved in generating G-overhang structures (Lenain et al., 2006). Tankyrase is another accessory factor that regulates telomere cohesion and telomere length homeostasis by binding to TRF1 (Dregalla et al., 2010).

Shelterin functions in different ways to keep telomeres protected from the action of ATM and ATR (Denchi and de Lange, 2007). The TRF2 protein, along with RAP1, is generally found attached to the t-loop structure to protect the telomeres from unwanted damage or attack (Denchi and de Lange, 2007; Rai et al., 2016). TRF2 maintains t-loops by wrapping around the DNA strand through their TRFH domain (Benarroch-Popivker et al., 2016). Under normal conditions, t-loops inhibit the activation of the ATM kinase signaling pathway, thus protecting the telomeres from unwanted repair activity (Bandaria et al., 2016).

Similarly, POT1 protects the telomeres from falling prey to ATR-mediated DNA damage repair. ATR signaling requires the binding of RPA to the ssDNA region of the telomeres. Although the amount of RPA present in the cell is higher than POT1, cell cycle-dependent targeted localization of the POT1 at the telomeres prevents RPA binding and wards off the ATR mediated DDR (Churikov and Price, 2008).

In addition to inhibiting the ATM at telomeres, TRF2 bound t-loops repress both the classical non-homologous end-joining and alternative non-homologous end-joining pathways (Konishi and de Lange, 2008). Similarly, Homology-Directed Repair (HDR) is inhibited at telomeres primarily by the Ku protein complex (Wang et al., 2009). In the absence of TRF2, POT1 proteins and Rap1 can block HDR activities at telomeres (Palm et al., 2009). In addition to its role of safeguarding chromosome from DDR, shelterin also facilitates recruitment of telomerase to telomeres (TIN2 & TPP1) (Xin et al., 2007) and enhances telomerase processivity (TPP1 and POT1) (Latrack and Cech, 2010). TRF1 has also been implicated in promoting replication fork progression through telomere tracts by resolving the G quadruplexes (Sfeir et al., 2009). TRF1 employs the BLM and RTEL1 helicases to remove such obstacles, thereby promoting telomere replication (Vannier et al., 2012; Zimmermann et al., 2014). Thus, shelterin is involved in a multitude of activities that addresses the “end replication problem” and the directly addresses the “end protection problem” of the linear genome.

### **The CST Complex**

CST is a trimeric protein complex comprised of Cdc13/CTC1, STN1, and TEN1 (Figure I-6). In *S. cerevisiae*, Cdc13 replaces CTC1 (Wellinger and Zakian, 2012). CST is a single-strand DNA binding complex with structural similarity to RPA (Miyake et al., 2009) that specifically binds to the G-overhang. It is involved in both telomere end protection and telomere length regulation by modulating the activity of telomerase enzyme



in some organisms (Feng et al., 2018). Like RPA, components of CST are characterized by OB-fold domains of varying numbers.

In addition to OB-folds, STN1 and TEN1 typically have a Winged-Helix-Turn-Helix (WHTH) domain, which mediates interactions with other protein components (Gao et al., 2007). Notably, the plant STN1 does not possess a WHTH domain (Song et al., 2008). In yeast, telomerase activity is modulated through various post-translation modifications of Cdc13 across the cell cycle (Churikov et al., 2013). During mid S phase, Cdc13 undergoes SUMOylation, which enhances the interaction of Cdc13 with STN1. This interaction promotes a closed telomere state and telomere extension is prohibited before completion of telomere DNA replication. On the contrary, phosphorylation of Cdc13 protein during late S to G2 phase disrupts the interaction of Cdc13 with STN1 and enhances the binding of Est1 (Ever Shorter Telomeres 1) to Cdc13. Est1 directly contacts the yeast telomerase RNA promoting telomerase engagement with single-stranded region of the telomere. Thus, interaction of Cdc13 with Est1 facilitates telomerase recruitment to telomeres (Chandra et al., 2001; Churikov et al., 2013; Zhou et al., 2000).

STN1 interacts with CTC1/Cdc13 and TEN1 for different purposes (Price et al., 2014). STN1 binds tightly to TEN1 via its C-terminal OB-fold, which creates a DNA binding pocket on the surface of STN1 and TEN1. Cdc13/CTC1 interacts with STN1 to mediate regulation of telomerase binding and recruitment of Pol alpha primase for the addition of the C-strand (Feng et al., 2018). TEN1 is the smallest subunit of the CST complex with potential telomere capping activities with Cdc13/CTC1 protein (Feng et al., 2018; Rice and Skordalakes, 2016). In addition, recent studies in *A. thaliana* show that

TEN1 has an intrinsic protein chaperone activity that may facilitate conformational changes in the CST complex to regulate telomerase accessibility (Lee et al., 2016).

As mentioned above, Cdc13/CTC1-STN1-TEN1 is structurally similar to the components of the Replication Protein A (RPA) complex (Miyake et al., 2009). RPA binds ssDNA and thus can help to mitigate G-quadruplex formation to allow replication fork progression (Ray et al., 2013). The G-rich overhang poses a similar structural challenge, and the CST complex is thought to work as a telomere-specific RPA complex that can mitigate formation of higher order DNA complexes as well as prevent induction of DDR (Feng et al., 2018; Gao et al., 2007; Rice and Skordalakes, 2016). Along with its role in promoting telomere protection, CST is also involved in recruiting and stabilizing the pol alpha enzyme, thereby regulating C-strand synthesis (Stewart et al., 2018).

### **POT1 proteins**

Protection of Telomeres 1 (POT1) is a core component of shelterin in mammals and fission yeast (Baumann and Price, 2010). POT1-like proteins were first identified in the ciliate *Oxytricha nova*, where they were known as the Telomere End Binding Protein or TEBP (Gottschling and Zakian, 1986; Price and Cech, 1987). TEBP is comprised of 2 $\alpha$  and 2 $\beta$  subunits which forms a tight ternary complex (Fang and Cech, 1993). The  $\alpha$  subunit has three OB-folds, while  $\beta$  subunit has only a single OB fold (Horvath et al., 1998). The TEBP protein protects the telomeres from any damage or degradation. Although POT1 orthologs have not been identified in budding yeast, POT1 from *S. pombe*

is involved in regulating telomere length as well as chromosome end protection (Baumann and Cech, 2001; Bunch et al., 2005; Miyoshi et al., 2008) (Figure I-7)

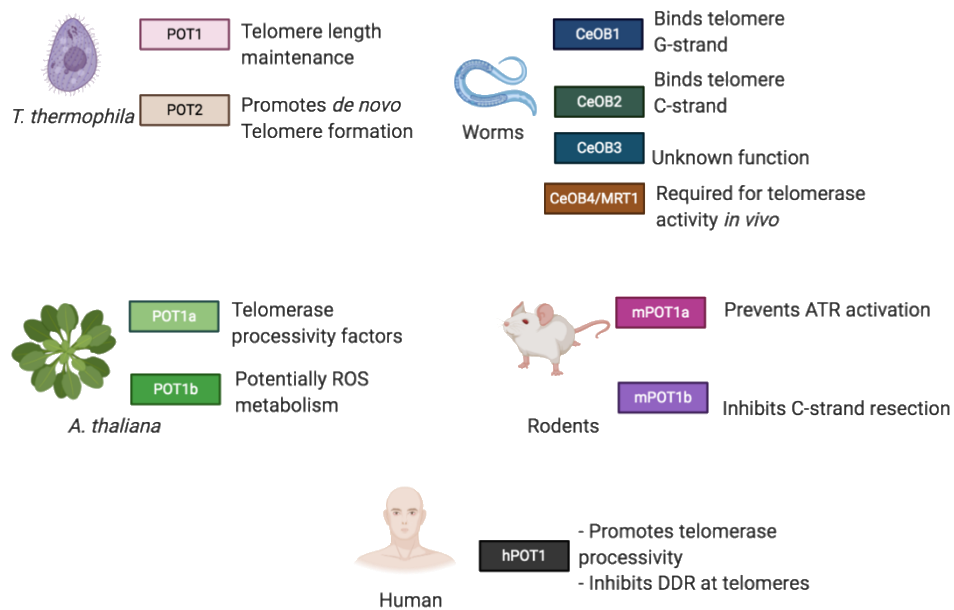


**Figure I-7 POT1 paralogs in different model organisms.**

Varying numbers of POT1 paralogs are found across different studied model organism. Each of these paralogs either have a direct involvement in telomere maintenance or they can also undergo neo-functionalization and participate in other biological pathways.

Although most organisms possess a single POT1 gene, several organisms harbor multiple POT1 paralogs and in each case have acquired distinct roles in the cell (Barcenilla and Shippen, 2019; Baumann and Price, 2010). There are two *POT1* paralogs in *T. thermophila*, POT1 and POT2. Primarily localized at the macronuclear telomeres of the vegetative cells, TtPOT1 is involved in telomere length maintenance and preventing checkpoint activation, similar to POT1 in *S. pombe*. In contrast, TtPOT2 is found in the

developing macronucleus of mated cells, where it is involved in *de novo* Telomere Formation (DNTEF) at the newly forming chromosome ends (Jacob et al., 2007). Similarly, the four paralogs of *POT1* in *Caenorhabditis elegans* (CeOB1, CeOB2, CeOB3 and CeOB4/MRT1) play various roles related to telomere protection and maintenance. Notably, *C. elegans* possesses both 3' and 5' telomere overhangs. CeOB1 binds to the 3' overhang region whereas CeOB2 binds to the 5' overhang. Telomere elongation and increased recombination at telomeres are the dominant phenotypes exhibited upon loss of CeOB1 or CeOB2 (Raices et al., 2008). While the function of CeOB3 remains elusive, the fourth POT1-like protein in *C. elegans*, CeOB4/MRT1 binds to both 3' and 5' telomere overhangs and plays a critical role in telomere maintenance (Meier et al., 2009).

Mice also possess two *POT1* paralogs, mPOT1a and mPOT1b, which have 72% sequence similarity. mPOT1b regulates resection of the 5' telomere overhang. In contrast, mPOT1a works in concert with mTOR to diminish ATR signaling at the telomeres (Hockemeyer et al., 2006). Humans have only a single copy of the *POT1* gene (Veldman et al., 2004). hPOT1 inhibits the activity of the various DNA damage pathways at the telomeres, and it plays an essential role in regulating access of telomerase at the telomeres (Churikov et al., 2006; Hockemeyer et al., 2006; Wu et al., 2006). In addition, hPOT1 acts in concert with TPP1 to promote processivity of the telomerase RNP (Wang et al., 2007).

Although plants exhibit frequent gene duplication, most plants harbor a single *POT1* gene, which appears to house the ancestral function of telomere end protection and telomerase regulation (Shakirov et al., 2010). *A. thaliana*, however, is an exception as it contains three *POT1* paralogs; *POT1a*, *POT1b*, and *POT1c*. Recent bioinformatic analysis

has revealed that *POT1c* is a pseudogene silenced by the insertion of a transposon in its promoter immediately after its genesis 5 million years ago (Kobayashi et al., 2019). POT1a and POT1b, which show only 52% similarity, are the most divergent POT1 paralogs described to date (Shakirov et al., 2005). POT1a stimulates telomerase processivity (Renfrew et al., 2014; Surovtseva et al., 2007). However, unlike other organisms, AtPOT1a accumulates at telomeres only during S phase (Surovtseva et al., 2007). Genetic analysis indicates that POT1b does not have a significant impact on telomere length (Shakirov et al., 2005). However, ongoing research in the Shippen lab indicates that POT1b plays a role ROS metabolism (Castillo-González et al., unpublished).

### **Ku complex**

Beyond its vital role in the NHEJ DNA repair pathway, the Ku70/80 complex is involved in a variety of other biological processes including antigen-receptor gene rearrangement, mobile genetic elements, transcription, apoptosis, and telomere maintenance (Downs and Jackson, 2004). Interestingly, Ku's role in telomere biology has been observed in multiple organisms from *S. cerevisiae* to humans. Ku in *S. cerevisiae* facilitates recruitment of telomerase to telomeres by binding to a specific 48 bp hairpin loop region in TLC1 (Fisher et al., 2004; Lemon et al., 2019; Pfingsten et al., 2012). yKu also protects telomeres from degradation by exonucleases and recombination processes (Polotnianka et al., 1998). Cell-cycle dependent localization of yeast telomeres to the nuclear periphery is also dependent on Ku protein (Laroche et al., 1998). Similarly, Ku70/80 proteins in both fission yeast and *Trypanosoma brucei* act as positive regulators

of telomere length and promote telomere end protection (Baumann and Cech, 2000; Conway et al., 2002).

Unlike other model organisms, plant telomeres are asymmetrical; one terminus is blunt-ended and the other contains a G-overhang. It is hypothesized that blunt-end can be detected in plants because of the lack of processing machinery (eg. the Apollo nucleases) which convert blunt-ended telomeres produced by leading strand replication into the G-overhang structure (Lenain et al., 2006). The presence of blunt-ended telomeres ensures that only one-half of the telomeres are acted upon by telomerase each cell cycle, which may provide additional genome stability (Nelson and Shippen, 2012). The Ku complex binds to blunt-ended telomeres and is critical for their maintenance (Kazda et al., 2012a). In plants null for Ku, telomeres extend up to 22 Kb in a telomerase-dependent manner (Riha and Shippen, 2003a). In addition, blunt-ended telomeres are converted to G-overhangs (Kazda et al., 2012a). Recent biochemical evidence has revealed that *Arabidopsis* Ku complex shows separation of function based on its interaction with the DNA substrate. While Ku70/80 bound at the edge of blunt-ended telomeres is sufficient to protect the terminus, Ku complex needs to translocate along the DNA tracts for fulfilling its role in the DNA damage repair pathway (Valuchova et al., 2017b). Thus, it is unclear how Ku is prevented from sliding off the telomeric DNA.

In mice, the absence of Ku leads to stunted growth and premature aging, correlating with increased telomerase recombination and telomere fusion (Hsu et al., 2000; Samper et al., 2000). Ku is essential in humans because decreased abundance of human

Ku complex leads to shortening of bulk telomeres and G-overhangs as well as increased telomere fusion (Jaco et al., 2004). Thus, Ku is an essential protein in telomere biology.

### **Telomere Length Regulation**

Telomere length homeostasis is established for each species and is dependent on a crucial balance between pathways involved in elongating telomeres or shortening them (Tomita, 2018). An optimal telomere length or set-point that is maintained indicates the existence of a feedback mechanism. Several studies indicate that telomerase preferentially extends only the shortest telomeres each cell cycle (Harrington, 2012). Regulation of telomerase-dependent telomere repeat addition has been extensively studied in yeast, where the concept of a “protein counting” mechanism was developed (Marcand et al., 1997). In this model, moderately longer telomeres are bound by specific protein complexes, which in turn inhibit the accessibility of telomerase to the telomeres. As the length of telomeres reduces due to the end replication problem, the occupancy of these telomerase regulating proteins likewise reduces, eventually allowing telomerase to bind to and elongate the short telomeres Figure (I-8) (Marcand et al., 1997).

In yeast this simple “protein counting” model has become more complex. The dynamic interplay of the proteins Rif1-Rif2-Rap1 and Tel1-MRX (Mre11-Rad50-Xrs2) is now thought to be responsible for maintaining telomere length (Vasianovich et al., 2020). Rif1 and Rif2 are telomere-associated proteins analogous to components of shelterin (Hirano et al., 2009). Short telomeres reduce the concentration of Rif2 at telomeres, which eventually relieves the inhibition of the Tel1-MRX protein complex (Martina et al., 2012).

Increased activity of the Tel1-MRX complex generates single-stranded G-rich strands, which are the optimal binding sites for Cdc13. Binding of Cdc13 at the single-stranded region is followed by the recruitment of Est1 leading to telomerase activation at telomeric DNA (Sabourin et al., 2007). The elongated telomeres eventually allow successful binding of the RAP1 protein, followed by Rif2 and Rif1 (Wotton and Shore, 1997). These Rif proteins ultimately outcompete the amount of Tel1-MRX protein bound to the telomeres, reducing the functionality of Cdc13 and shift telomeres to a non-extendible state. Overall the “protein counting” mechanism allows preferential addition of telomeric repeats to shorter telomeres, thereby keeping telomere length above a minimal threshold.



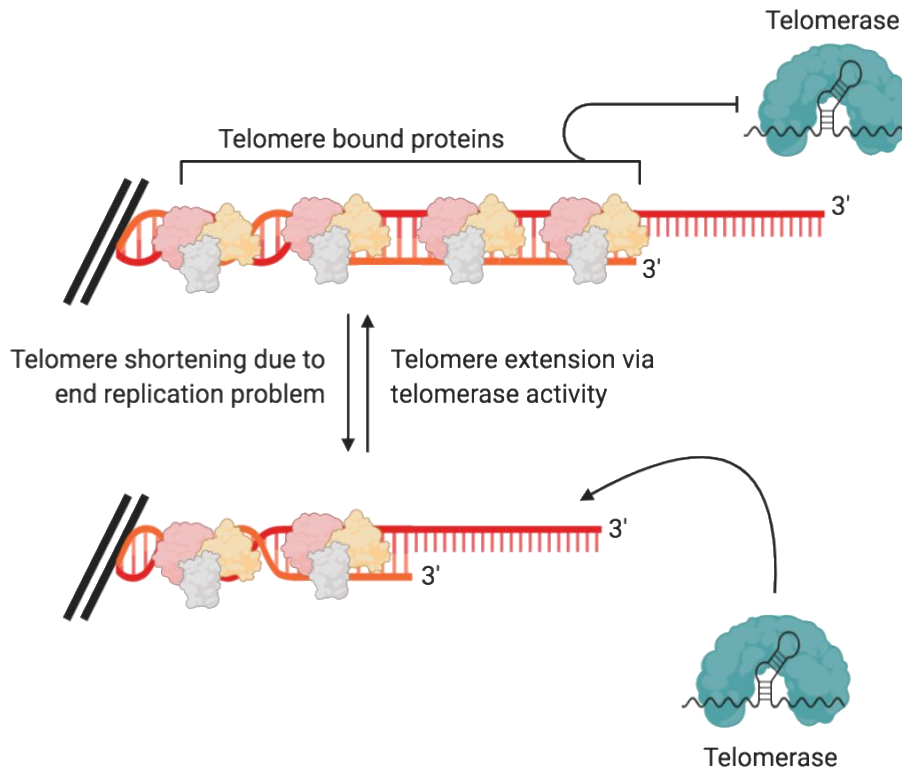


**Figure I-8 The protein counting mechanism for telomere length regulation.**

Longer telomeres are replete with telomere bound proteins (TBPs) which can inhibit telomerase from acting at chromosome ends. As telomeres shorten due to end replication problem, local concentration of the TBPs reduces. At a particular concentration, TBPs lose the ability to inhibit telomerase, which ultimately promotes telomere repeat addition.

A similar telomere length maintenance mechanism occurs in *S. pombe*, mammals, and humans, with orthologous protein components. For example, in fission yeast, transfer of the telomere-associated protein complex Poz1–Tpz1–Pot1–Ccq1 from Rap1 to the 3' overhang converts telomeres into a non-extendable state (Miyoshi et al., 2008). Similarly,

TRF1 is responsible for helping to keep human telomeres at an optimal length suitable for telomerase activity but not too short for the cells to undergo replicative senescence (Smogorzewska et al., 2000). Several reports have revealed that TRF1 controls the ability of POT1 to interact with telomeres, ultimately impacting telomerase accessibility. Therefore, both TRF1 and POT1 orchestrate a feedback loop to regulate telomere length in humans (Loayza and de Lange, 2003). In the case of *A. thaliana*, the Ku70/80 heterodimer plays a vital role in telomere length homeostasis (Riha and Shippen, 2003b). Loss of Ku70 promotes a telomerase-dependent elongation of plant telomeres perhaps because conversion of blunt end telomeres into G-overhang allows all telomeres to be accessible for telomerase extension (Kazda et al., 2012a). Thus, Ku acts as a negative regulator of telomerase (Riha and Shippen, 2003b).

Beyond the protein counting mechanism, other factors regulate telomere length, especially in higher eukaryotes (Harrington, 2012). One such factor is the RNA Pol II dependent long non-coding RNA; TELomeric Repeat-containing RNA (TERRA). TERRA is transcribed from the subtelomeric and telomeric regions and is composed of sequences and repeats complementary to the telomere G-rich strand (Azzalin and Lingner, 2015). In human cells, TERRA expression is tightly regulated by the chromatin organizing factors CTCF (CCCTC-binding factor) and cohesin RAD21 (Radiation-sensitive 21), both of which bind to the CpG TERRA promoters embedded within the CpG islands of telomeric and subtelomeric regions (Deng et al., 2012). Reduced levels of TERRA are associated with telomere shortening, telomere fusions and finally DDR activation at telomeres. TERRA may also promote replication fork progression at telomeres (Montero

et al., 2016). Interestingly, several experiments have defined TERRA as a double-edged sword in terms of telomere biology, as excess levels of TERRA can facilitate a DDR contrary to inhibiting the telomeric DDR. As a result, TERRA levels are under tight regulation (Bettin et al., 2019). Disruption of this equilibrium is associated with several telomeropathies like ICF (immunodeficiency, centromeric region instability, facial anomalies) syndrome and cancer (Maicher et al., 2012).

### **Telomere related activities across the cell cycle**

Although telomere extension occurs strictly during the late S phase all the other telomere-related activities, including telomerase biogenesis and localization of the active enzyme at telomere transpires over different stages of the cell cycle (Figure 10) (Londoño-Vallejo and Wellinger, 2012). Elegant experiments in yeast, have revealed the dance of telomerase and telomere to the symphony of the cell cycle. TLC1 assembles with other telomerase components, EST1, EST2, EST3 as well as Ku in a cell cycle-dependent manner. The regulated assembly of the telomerase complex restricts telomere repeat addition to the late S phase (Fisher et al., 2004; Gallardo et al., 2011). The minimal telomerase complex contains only Est2 (TERT) and TLC1 and these two subunits are associated with telomeres throughout the cell cycle. However, telomerase cannot actively extend telomeres until a specific time point, guided by the presence of other factors (Gallardo et al., 2008; Taggart et al., 2002). While Est2 and TLC1 levels remain constant throughout the cell cycle, Est1 and Est3 levels fluctuate. Est1 is lowly expressed during the G1 phase and then peaks during the beginning of S phase and remains high for the rest

of the cell cycle (Osterhage et al., 2006). Est3, like Est1 peaks at late S phase. Est1 is essential for the assembly of Est3 with Est2, and TLC1 into a functional complex (Tucey and Lundblad, 2014).

Similar to the Est proteins, Ku is a critical element of the yeast telomerase RNP. Broadly, yKu helps in translocating the mature TLC1 from the cytoplasm to the nucleus and handing off the active telomerase at the telomeres. The association of yKu with TLC1 is observed as early as G1 (Fisher et al., 2004). However, yKu cannot bind telomeric DNA and RNA at the same time. Thus, once yKu delivers TLC1 to the telomeres from the cytoplasm, it slides on to the telomere (Pfungsten et al., 2012). Other experiments suggest that yKu's interaction with the telomeres might help to restrict DNTFs at stalled or broken replication forks (Ribes-Zamora et al., 2007). Yeast telomerase composition changes dynamically throughout the cell cycle, and this facilitates different pathways crucial for telomere maintenance at that particular time point. A surge in the Est1 level characterizes the onset of S phase, which continues until Est1 peaks in the late S phase, for telomere elongation (Tucey and Lundblad, 2013).

As discussed above, interaction of Est1 with telomere bound Cdc13 protein facilitates the recruitment of an active telomerase complex at the yeast telomeres (Bonetti et al., 2010). A salt bridge formed between Cdc13 Glu 252 and Est1 Lys444 is critical for the interaction of Cdc13 and Est1 and subsequent activities of telomere biology during late S phase (Pennock et al., 2001). The current model (Vasianovich et al., 2020) predicts that Est1 promotes recruitment and stabilization of the active telomerase complex at telomeres during S phase by chemically interacting with the Cdc13. Given the cell cycle-

dependent increase in the level of Est1 protein, it is conceivable that yeast restricts telomerase activity to late S phase by strategically controlling the *in vivo* level of EST1, a critical telomerase recruitment factor (Vasianovich et al., 2020). Finally, TLC1 live-cell imaging has revealed that although TLC1 seems to be bound to the telomeres at even G1 and G2 phase, most of those interactions are transient, and they do not result in telomere extension (Gallardo et al., 2011). More research is needed to determine biological relevance of such futile attempts to bind the telomeres by TLC1.

In human cells, cell cycle-dependent intranuclear localization of the various telomerase components is essential for restricting the process of telomere extension to late S phase (Schmidt and Cech, 2015). At G1, hTERT accumulates as distinct foci within the nucleoplasm, whereas telomerase RNA TERC resides in the Cajal Body (CB). This strategic compartmentalization of hTERT away from hTERC inhibits telomerase activity before the initiation of S phase. TCAB1 protein present in the CB binds explicitly to the H/ACA box of TERC and stabilizes the TERC molecule for its subsequent interaction with hTERT. The subsequent onset of the S phase marks the redistribution of hTERT and TERC, ultimately leading to their localization at the nucleolus. While hTERT occupies the interior of the nucleolus, TERC within the CB exists at the periphery. During the mid-S phase, hTERT localizes with hTERC at the CB to complete the final steps of telomerase assembly, before associating with the individual telomeres throughout the cell (Hukezalie and Wong, 2013). The same TCAB1 molecule bound to the TERC-hTERT complex is hypothesized to license an active TERC-hTERT complex for telomere repeat addition. The interaction of TCAB1 with TERC reduces during the M phase of cell cycle, indicating

a cell cycle-related role of this interaction in human telomere biology (Vogan and Collins, 2015).

In addition to telomerase biogenesis and assembly of the telomerase RNP, telomere synthesis is also a cell cycle-regulated process (Vodenicharov and Wellinger, 2007). Most of the knowledge about the relationship between cell cycle and telomere dynamics is based on the extensive studies performed in yeast and humans. In *S. cerevisiae*, Cdc28p plays a major role in regulating cell cycle progression (Mendenhall and Hodge, 1998). By associating with specific cyclin D kinases (CDKs), Cdc28p controls the different activities across the cell cycle. Yeast telomere maintenance is also mostly dependent on the series of events orchestrated by the Cdc28p-C1b complex (Vodenicharov and Wellinger, 2006).

Based on experimental evidence, the process of telomere extension initiates with the replication of telomeric DNA. Passage of the replication fork through the telomeric DNA is crucial for generating the 3' G-overhang structure, the natural substrate for telomerase (Dionne and Wellinger, 1998). Following the replication of telomeric DNA, it is hypothesized that the telomeres are perceived as a DSB site for a brief period. Eliciting a DDR at the telomeres facilitates the removal of the telomere cap proteins and processing of the telomere end to elongate the 3' G-overhang structure. Cdc28p-C1b complex have been implicated in mediating the nucleolytic processing of telomeres at late S phase (Vodenicharov and Wellinger, 2007). Support for this hypothesis comes from experiments where yeast cells were found to acquire longer 3' G-overhangs transiently during the late S phase. The successive actions of some well-known nucleases, the MRX complex and

the Exo1p, are speculated to facilitate the formation of the long G overhangs, also known as G-tails (Lydall, 2003). According to the current model, exonucleolytic processing of the C-strand helps in generating the G-tails. The newly formed G-tails act as an optimal substrate for telomerase to initiate the process of telomere repeat addition. Also, as the telomere elongates, the concentration of telomere-bound protein increases. Hence based on the protein counting mechanism, the telomere bound proteins eventually terminates the repeat addition process (Vodenicharov and Wellinger, 2007).

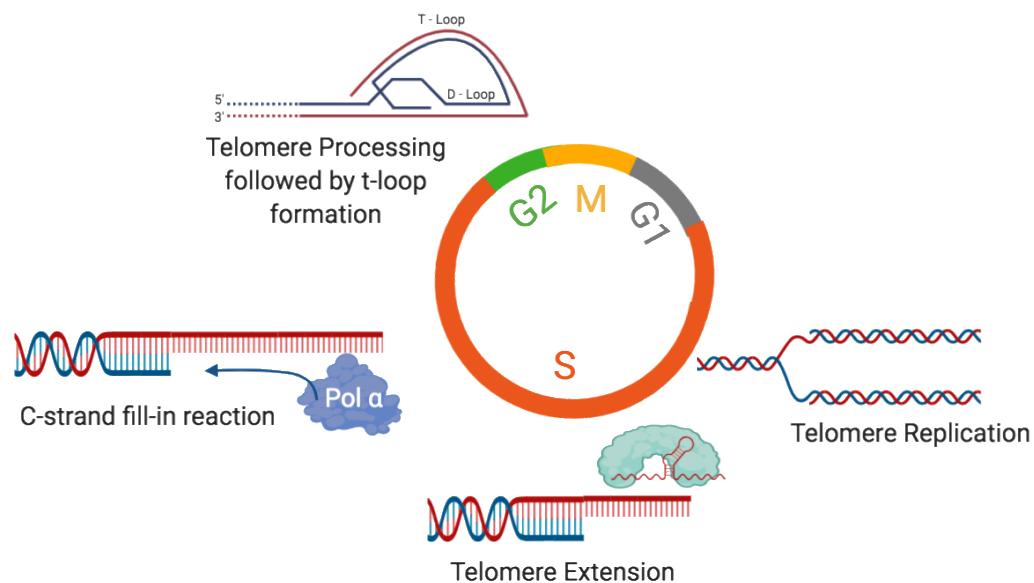


**Figure I-9 Telomere maintenance is a cell cycle regulated process.**

DNA replication commences in early S phase, towards the middle of which telomeric DNA is also replicated. Once the end replication problem occurs, telomerase complex comes to the rescue and starts adding telomeric repeats, thereby extending telomeric DNA. Note: This process occurs only with cells with active telomerase like stem cells, cancer cells and germline cells. Upon completion of telomere extension, DNA Pol  $\alpha$ -primase complex is recruited to facilitate C-strand fill in. At G2, molecular players involved in HR pathway are summoned to facilitate formation of the t-loop and D-loop and the telomeres transition to a non-extendible state.

The completion of telomere extension is followed by the C-strand fill-in reaction. During this fill-in reaction, a DNA polymerase (Pol  $\alpha$  primase) synthesizes the C-strand complementary to the newly extended telomeric G-strand to generate the species-specific length of double-stranded DNA and the 3' G-overhang (Chen and Lingner, 2013). Data from multiple model organisms have indicated the importance of the CST complex for mediating the C-strand fill-in reaction. Although the actual mechanism is still elusive, based on the current data, the CST complex bound to the newly synthesized telomeric G-overhang recruits the DNA Pol Alpha - Primase complex to initiate the C-strand fill-in reaction.

Based on human cell-cycle data, it is speculated that another DDR is induced at the telomeres while the cells are at G2. This DDR might facilitate the formation of protective t-loop structures. G2 phase of the cell cycle is notoriously famous for HR-based pathways. So maybe, the partial DDR induced by the cells at G2 provides enough time and resources to form the t-loop via HR (Verdun et al., 2005). TRF2 of the shelterin complex acts as the gatekeeper of the t-loop structures (Sarek et al., 2019). Therefore, once TRF2 binds the newly formed t-loops, it might restrict any further damage caused by the G2 specific induction of DDR.

In conclusion, DDR pathways have a unique role in telomere biology. However, strict spatio-temporal regulation of the players involved in DDR pathways is critical to favor pathways involved in telomere maintenance, rather than the ones that can damage the telomeres. Also, any perturbation to the cell cycle can directly impact the various



telomere processing pathways, which can eventually hamper the overall structure and function of telomeres.

### ***de novo* telomere formation (DNTF) at DNA Double Breaks (DSBs)**

Telomeres are structurally similar to DNA double-stranded breaks (DSBs) (Chow et al., 2013). A large number of factors ensure telomere integrity by inhibiting the DDR (DDR) machinery from wrongfully recognizing telomeres and executing DNA repair activities (Oganesian and Karlseder, 2009). On the other hand, care also needs to be taken to inhibit the action of telomerase at DSB sites within the genome to ensure telomeres are not formed instead of proper DNA repair (Ribeyre and Shore, 2013). *de novo* telomere formation (DNTF) can lead to loss of heterozygosity and genomic instability. The cell has devised regulatory pathways to restrict telomerase at DSBs. Most of the mechanistic details about these pathways come from yeast. The two major pathways that repair DSBs are homologous recombination and NHEJ. DNTF is a third and less desirable way for repairing DNA damage (Melek and Shippen, 1996). In *S. cerevisiae*, if a DSB happens near a TG-rich sequence, 99% of the time, the RAD52 HR is activated; DNTF occurs only 1% of the time (Mangahas et al., 2001). Therefore, DNTF is not a favored pathway for repair of DSBs.

Nevertheless, the presence of telomere-like sequences in the interstitial regions of the genome seed the formation of a new telomere by attracting telomere proteins or components of the telomerase. To overcome this problem in yeast, sequences homologous to TLC1 have been counter-selected from being present in the interstitial region of the

genome in *S. cerevisiae* (Mangahas et al., 2001). Although the rate of telomere addition at DSBs is normally quite low, loss of the Pif1 helicase dramatically increases the frequency of DNTF (Mangahas et al., 2001). This phenomenon can be countered only by deleting telomerase components (Myung et al., 2004). Pif1 is thought to destabilize DNA–RNA hybrid formed between the telomere and TLC1. Unwinding of the telomeric DNA–TLC1 hybrid by a Mec1-Dun1-Rad53-mediated phosphorylated form of Pif1 inhibits the addition of telomeric repeats at the DSBs (Li et al., 2009). Binding of Cdc13 to the DSB also help seed a new telomere. Cdc13 is phosphorylated by Mec1 in response to DSB. Phosphorylation of Cdc13 at S306 weakens the interaction of Cdc13 to the DSBs. Thus, Mec1 plays a critical role in inhibiting DNTF at the DSBs by phosphorylation of both Cdc13 and Pif1 (Li et al., 2009).

Resectioning of the DNA strand is the first step for the majority of DDR pathways. An incomplete resection can form a DNA substrate favorable for telomere repeat addition by telomerase, but not long enough for HR-based repair. Thus, a robust DNA resectioning mechanism helps to ensure successful DNA repair activity by HR, rather than indulging the telomerase complex for DNTF (Ribeyre and Shore, 2013; Zhu et al., 2008).

The G2 phase-specific activity of the HR pathway is the most common method of repairing DSBs in budding yeasts. Along with these elegant mechanisms of restricting DNTF DSBs, an added layer of regulation involving the TLC1 has been recently proposed for *S. cerevisiae*. Interestingly, TLC1 traffics into the nucleolus during G2, keeping the telomere addition pathway physically distant from DSBs occurring in the nucleoplasm.

Thus, spatial reorganization of the various components involved in DNTF helps block this process (Ouenzar et al., 2017).

In humans and mouse, a robust DNA damage repair mechanism competes effectively with the DNTF pathway to inhibit telomerase action at DSBs. Most of the breaks that occur at interstitial sites in the chromosome are resolved by the canonical DNA damage repair pathways. Nevertheless, further mechanistic studies are required to fully understand how DNTF is mitigated in multicellular eukaryotes (Ribeyre and Shore, 2013).

### **Telomerase-independent regulation of telomere length**

Telomere length maintenance is a multidimensional biological process, and the final telomere length set point is dependent on the optimal performance of several biological pathways besides telomerase. Three genetic screens performed in *S. cerevisiae* identified 270 non-essential and 90 essential genes important for telomere length regulation (Askree et al., 2004; Gatbonton et al., 2006; Ungar et al., 2009). Loss of majority of these genes led to telomere shortening, but in some cases, telomere lengthening occurred. Interestingly none of the genes previously known to be required for telomere maintenance (eg. the Est proteins) emerged in the screen. This may be because most of these genes are essential and even hypomorphic mutations make yeast non-viable. Nevertheless, a large number of the genes belonging to different kinds of pathways were identified (Askree et al., 2004; Gatbonton et al., 2006; Ungar et al., 2009).

The process of telomere maintenance is dependent on successful orchestration of multiple cell cycle dependent processes (Londoño-Vallejo and Wellinger, 2012;

Vodenicharov and Wellinger, 2007). Therefore, it is not surprising that defects in cell cycle-related pathways and DNA replication impact telomere length. For instance, mutation in the DNA replication genes *PRI1* (a subunit of the DNA pol  $\alpha$  primase), *MCM3/MCM6* and *CDC9* was responsible for a longer telomere phenotype, supporting hypothesis about the role of cell cycle and DNA replication in telomere maintenance (Ungar et al., 2009).

Another set of genes involved in telomere length regulation were post transcriptional processing and translation related pathways. According to the screen, mutation in six genes belonging to the pre-mRNA splicing pathway (*PRP4*, *PRP22*, *PRP31*, *PRP38*, *PRP43* and *NTR2*) generated a short telomere phenotype in yeast (Ungar et al., 2009). The gene *YLR317W* from *S. cerevisiae* was identified as one of the essential genes involved in telomere maintenance (Ungar et al., 2009). Interestingly, the transcript from this gene overlaps with the yeast tRNA Adenosine Deaminase or *TAD3* gene, which is well known for its role in tRNA editing (Torres et al., 2014a). Furthermore, mutations in genes involved in the maturation and export of 40S ribosomal units (*NET1*), as well as the production of 18S rRNA and assembly of small ribosomal units (*UTP5*) also gave rise to the short telomere phenotype. Similarly, mutation in genes involved in tRNA processing ribosome translation, RNA metabolism, were associated with both short and long telomeres in *S. cerevisiae* (Gatbonton et al., 2006; Ungar et al., 2009). The connection between translation and tRNA related pathways in telomere biology escalated when Seryl tRNA Synthetase (*SerRS*) was identified as binding partner of human *POT1* in a screen for identifying the interaction partners of the shelterin complex (Lee et al., 2011). Further

experiments revealed that SerRS association with POT1 regulates telomere length by limiting telomerase accessibility (Li et al., 2019). An additional connection between translation and telomere length regulation was recently uncovered in *A. thaliana*. QTL mapping data from *Arabidopsis* revealed a role for NOP2A, a conserved rRNA methyltransferase, in controlling telomere length (Abdulkina et al., 2019).

A third layer of telomere length regulation is offered by the pathways involved in cellular metabolism, particularly factors involved in maintaining cellular homeostasis and metabolic status of the cell. For instance, telomere extension requires a constant supply of dNTPs and as a result, perturbation to the dNTP pathway negatively impacts telomere length (Gatbonton et al., 2006). Similarly, mutations in genes involved in proteasome assembly, actin nucleation and vesicular trafficking give rise to short telomeres.

A similar screen for genes that influence telomere length performed in *S. pombe* identified a myriad of genes involved in DNA replication/repair/recombination, chromatin modification/remodeling, RNA metabolism and transcription, cell cycle regulation, vesicular trafficking, organelle organization and biogenesis (Liu et al., 2010). Interestingly, mice with short telomeres are seen to activate the mTOR pathway, which promotes cell survival and delays accelerated aging. mTOR is one of the most critical metabolism related pathways that controls growth and development through nutrient sensing (Ferrara-Romeo et al., 2020). Overall, results from multiple genetic screens and directed studies reveals surprising complexity in mechanism controlling telomere length and demonstrate that an army of interdisciplinary pathways work in harmony to guarantee telomere homeostasis.

## **tRNA Adenosine Deaminases**

RNA molecules undergo several post-transcriptional modifications depending on their biological function. One common modification in tRNAs is conversion of adenosine to inosine by tRNA editing (Schaub and Keller, 2002). Inosine is a nucleoside analog of guanosine and is rarely found in DNA, but is commonly found in both mRNA and tRNA (Lim, 1995). Two kinds of adenosine deaminase enzymes catalyze the conversion of adenosine to inosine: Adenosine Deaminase Acting on mRNA (ADAR) and Adenosine Deaminase Acting on tRNA (ADAT/TAD) (Zinshteyn and Nishikura, 2009). ADARs are exclusively present in metazoans, with three different ADAR paralogs present in vertebrates, *ADAR1*, *ADAR2*, and *ADAR3*. *ADAR1* and *ADAR2* have been well studied, but little is known about *ADAR3* as it does not participate in any known deamination reaction (Keegan et al., 2004). The A to I editing of mRNA can lead to amino acid substitutions in the proteins translated from the edited mRNA as well as modification of sites for splicing. In addition to editing mRNA, ADARs are also involved in editing lncRNAs and regulating their functions, especially in siRNA and miRNA (Zinshteyn and Nishikura, 2009).

All domains of life from Archaea to humans contain tRNA with inosine residues. However, the number of tRNA with inosine residues increases with increasing organismal complexity (Torres et al., 2014a). Inosine can occur in three different positions in a tRNA, position 34: the first nucleotide position of the anticodon also known as the wobble position; position 37: adjacent to the anticodon region; and position 57: TΨ loop of the tRNA (Jühling et al., 2009). There are specific ADATs dedicated to catalyzing each of

these modifications within the tRNA molecule. I<sub>37</sub> and I<sub>57</sub> are further modified by the addition of a methyl group through a tandem modification process (Jühling et al., 2009). I<sub>57</sub> is found only in Archaea and is generated by a currently uncharacterized enzyme (Grosjean et al., 1995). I<sub>34</sub> is found in both bacteria and eukaryotes. In bacteria only tRNA<sup>Arg</sup> undergoes the A to I modification, in a reaction catalyzed by tRNA Adenosine Deaminase A or TadA. Seven to eight cytosolic tRNAs in eukaryotes possess I<sub>34</sub>, which is generated by the action of the various tRNA Adenosine Deaminases (Torres et al., 2014a). I<sub>34</sub>, also known as the wobble position, can bind to A, U, C bases in the codon. On the contrary, adenosine at the same position can bind to only U. Thus, editing tRNA at position 34 expands the codon binding capacity of a specific tRNA. Moreover, presence of I<sub>34</sub> in the anticodon loop facilitates successful decoding of codons ending in C - the most preferred codons in the eukaryotic genome (Grosjean et al., 2010; Lyu et al., 2020).

tRNA structure plays an essential role in recognition by a specific ADAT. For example, in bacteria, the structure of the anticodon loop including size, and sequence are essential for the proper activity of the TadA enzyme (Wolf et al., 2002). In contrast, tertiary structure of the tRNA, is essential for carrying out a successful deamination reaction (Haumont et al., 1984). The conversion of A to I in tRNA is independent of the successful 5' or 3' processing of tRNA, indicating that the deamination reaction can take place immediately after the biogenesis of the tRNA molecules (French and Trewyn, 1990).

ADATs are essential enzymes. Null mutations in *TAD2* or *TAD3* in *S. cerevisiae* are lethal, and may reflect a need for these enzymes in the stress response (Maas et al., 1999). Fission yeast *TAD3* mutants display growth defects, mainly due to problems in G1-

S and G2-M cell cycle transitions (Tsutsumi et al., 2007). *A. thaliana* harbors 5 different ADATs. Only four of these, TADA, TAD1, TAD2, and TAD3, have biological functions. TADA is involved in generating I<sub>34</sub> for the tRNA<sup>Arg</sup> in the chloroplast. Plants lacking the TADA enzyme exhibit defective chloroplast translation and impaired photosynthesis (Delannoy et al., 2009). TAD1 is needed for editing A<sub>37</sub> of tRNA<sup>Ala</sup> into I<sub>37</sub>. Plants devoid of this enzyme accumulate low biomass under stressful environmental conditions (Zhou et al., 2013). Difficulty in respiration might be attributed to the role of TAD1 in controlling mitochondrial translation. TAD2 and TAD3 form a heterodimer and are involved in editing several tRNA : alanine, serine, leucine, isoleucine, arginine, and threonine at A<sub>34</sub>. Plants lacking either TAD2 or TAD3 are inviable, signifying the importance of these genes in plant growth and survival. TAD2 and TAD3 colocalize in the nucleus and interact with DEAD box helicase proteins to unwind tRNAs for editing (Zhou et al., 2014).

Interestingly, the ADAT1 transcript from *Drosophila* shows a concentrated localization in the central nervous system, where its tRNA editing role might be critical for brain development (Keegan et al., 2000). In humans, mutation in *TAD3* is associated with chronic diseases like myositis – an inflammatory muscle disorder. Moreover, defects in tRNA editing in humans are associated with intellectual disability, underscoring the importance of tRNA editing in maintaining proper health (Alazami et al., 2013).

### **Telomere and Metabolism**

Among the many factors involved in maintaining telomere length, metabolism and stress play critical but poorly understood roles. In mammals, telomere length is influenced



by lifestyle and dietary habits (Shammas, 2011). Consumption of fruits, nuts, seaweeds, vegetables, and fruits correlates with longer and healthy telomeres. However, unhealthy food habits, lack of physical exercise, and smoking negatively affect telomere length (Balan et al., 2018). Binge drinking and consumption of excessive amount of red or processed meat also correlate with telomere shortening under certain situations (Balan et al., 2018; Dixit et al., 2019). In addition, smoking and obesity have adverse effects on the overall quality of the cellular environment, and this effect correlates with overall telomere length of the organism. Finally, elevated stress is associated with the release of glucocorticoids which correlates with telomere attrition.

An influx of recent data reporting the connection between metabolism and telomere maintenance has prompted a re-examination of the metabolic attrition hypothesis for telomere length regulation (Casagrande and Hau, 2019). According to this hypothesis, organisms in response to stress redirect their cellular energy to maintain critical metabolic pathways, rather than maintaining telomeres. As a consequence, telomeres shorten. Also, since shorter telomeres are the preferred substrate for telomerase (Sabourin et al., 2007), longer telomeres may be dispensable for an organism's survival during stress. In support of this idea, arctic salmon show a higher survival rate during migration if they have short telomeres (McLennan et al., 2018). Telomere attrition in response to stress also has the advantage of producing nucleotides that can be recycled in the nucleotide salvage pathway (Aird et al., 2013). Thus, along with maintaining telomeres, various metabolic pathways may actively promote telomere shortening to better respond to stress.

Although more research is necessary to unravel the precise mechanism of telomere maintenance via metabolic pathways, many of the metabolic factors implicated in telomere length regulation ultimately converge at the phenomena of cellular oxidative stress (Shammas, 2011). Consumption of unhealthy food leads to an increase in the production of reactive oxygen species (ROS) due to the reduction of antioxidants and anti-inflammatory components in the body. Biochemical studies of obese individuals and smokers show an increased ROS level due to the deregulated production of adipocytokines. ROS converts guanine and thymine to 8-Oxo-G and Thymine Glycol (Tg), respectively. As result, telomeres with their GT rich sequences are hot-spots for ROS-induced base modification. Presence of such oxidized bases inhibits telomerase activity, which results in telomere attrition (Lee et al., 2017). Similarly, lack of antioxidant defenses and higher activity of the NADPH oxidase pathway leads to an unwanted assault of the telomeres by ROS. Likewise, elevated levels of stress-induced glucocorticoids reduce the activity of several antioxidant proteins. This, in turn, increases the accumulation of ROS, reduces telomerase enzyme activity and ultimately contributes to a reduction in telomere length (Kreuz and Fischle, 2016). Therefore, telomere homeostasis can be indirectly controlled via changes in the metabolic status of the cell.

### **ROS-induced changes to telomeric DNA**

ROS is a major byproduct of cellular metabolism (Solymosi and Schoefs, 2019) that is produced due to an imbalance between ROS generating and ROS scavenging processes. ROS impacts multiple biomolecules, including but not limited to, lipids,

proteins, DNA, and chromatin (Lonkar and Dedon, 2011). Telomeres are especially vulnerable to oxidative damage. Overaccumulation of ROS oxidizes the guanine residues to 8-Oxo-Guanine (8-Oxo-G) and thymine residue to Thymine glycol (Tg) (Lee et al., 2017). These oxidized bases are sensed and repaired primarily by the Base Excision Repair (BER) pathway enzymes, 8-Oxoguanine glycosylase (OGG1), Endonuclease III homolog 1 (NTH1) and Nei like DNA Glycosylase 1 (NEIL1) (Dizdaroglu et al., 1999; Nishioka et al., 1999; Zhou et al., 2017). Failure to remove 8-Oxo-G and Tg can result in DNA strand breaks and stalling of replication forks, leading to cancer and neurodegenerative diseases (Cooke et al., 2003).

There are two known ways in which 8-Oxo-G can impact telomere length. First, telomerase-mediated incorporation of 8-Oxo-G from 8-Oxo-dGTP during telomere repeat addition terminates the telomere elongation process. As a result, telomeres shorten. Second, failure to remove 8-Oxo-G within telomeric DNA promotes unfolding of G-quartet structures. Telomeres with disrupted G-quartets have increased accessibility to the telomerase enzyme, which leads to inappropriate telomere elongation (Fouquerel et al., 2016). Similarly, the presence of Tg in telomeres also alters the G-quartet conformation, resulting in increased accessibility to telomerase and telomere elongation (Lee et al., 2017). Accumulation of oxidized bases in telomeric DNA also hampers the interaction of the shelterin proteins TRF1 and TRF2 which in turn prevents proper t-loop formation and eventually leads to telomere shortening (Opresko et al., 2005). Thus, ROS disrupts the telomere homeostasis in several ways, by altering length regulation and by promoting other structural changes to the nuclear DNA in mammalian cells (Coluzzi et al., 2014).

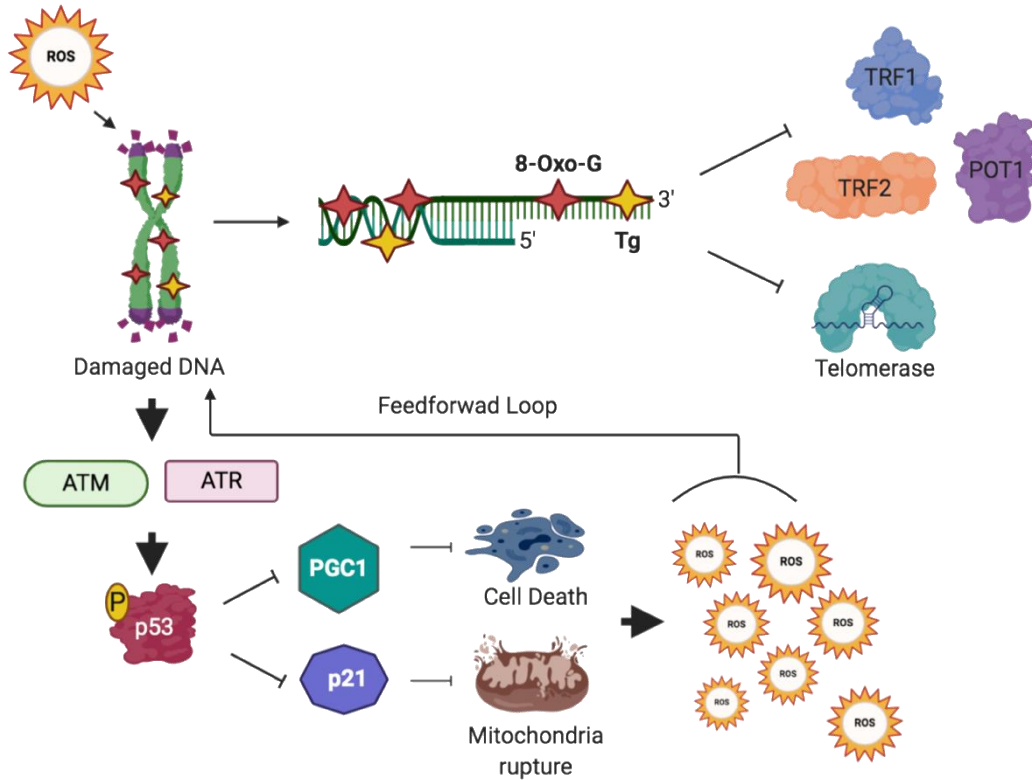


**Figure I-10 ROS induced damage to cellular compartments.**

Overaccumulation of ROS oxidizes DNA bases. The GT-rich telomeres are a hotspot of ROS-induced DNA damage. Conversion of guanine and thymine to 8-OxoG and Thymine glycol, respectively inhibits the TRF1, TRF2, POT1 from binding telomeres and telomerase from adding telomeric repeats.

DNA damage activates ATM and ATR followed by activation p53 via phosphorylated p53. Activated p53 inhibits p21 and PGC1 which leads to cell death and rupture of mitochondria. The freshly generated ROS leaking from degrading mitochondria damages the DNA further, thus creating a feedforward loop.

ROS-induced damage at the telomeres is associated with several diseases. For example, ROS exposure reduces telomere length in muscle cells, which promotes the progression of Duchenne muscular dystrophy (Ahmed and Lingner, 2018; Sacco et al., 2010). Telomeres damaged by ROS activate ATM and ATR, which then phosphorylate p53, making it biologically active. Active p53 eventually inhibits p21 and PGC1. Inhibition of p21 leads to permanent cellular growth arrest followed by cellular senescence, and repression of PGC1 affects the mitochondrial structure, which leads to leakage of oxygen radicals. This creates a feed-forward loop of inducing more stress at the telomeres and compromising the overall health of the genome (Figure I-10) (Sahin and DePinho, 2012).

In conclusion, modification of telomeric nucleotides due to oxidative stress is a common phenomenon; specialized pathways have evolved to keep telomeres and the rest of the genome healthy under oxidative stress (Lord and Aitken, 2015).

### **Regulation of ROS in plants**

Chemically reactive oxygen radicals, as well as the nonradical forms, are termed as Reactive Oxygen Species (ROS). The reactivity profile of ROS is highly variable, and impacts biological processes in different capacities (Sharma et al., 2012). The most well-known ROS are free radicals like superoxide anion ( $O_2^{\cdot-}$ ), hydroxyl radical ( $\cdot OH$ ) and the nonradical molecules such as hydrogen peroxide ( $H_2O_2$ ) and singlet oxygen ( $^1O_2$ ). In plants, ROS is generated either by the leakage of electrons from the electron transport chain or as a byproduct of various metabolic processes. The main sites of ROS production

include the chloroplast, cell wall, endoplasmic reticulum, mitochondria, plasma membrane and peroxisomes (Møller et al., 2007). Environmental stressors such as drought, salinity, chilling, metal toxicity, UV-B radiation, and biotic agents (pathogens) lead to significant accumulation of ROS. For example, under drought stress, closure of the stomata inhibits CO<sub>2</sub> fixation causing a reduction in NADP<sup>+</sup> production via the Calvin Cycle (Biehler and Fock, 1996). The problem with CO<sub>2</sub> fixation coupled with changes in the photosystem activities and photosynthetic transport capacity in response to drought leads to accelerated production of ROS in plant cells.

Unchecked levels of ROS impact different biomolecules. Higher levels of ROS increases lipid peroxidation. Peroxidation of unsaturated fatty acids leads to the generation of malondialdehyde (MDA), ultimately causing extensive damage to the cellular membrane (Su et al., 2019). Elevated cellular ROS can also take a heavy toll on the activity and stability of different protein molecules. ROS can modify proteins directly via nitrosylation, carbonylation, disulfide bond formation and glutathionylation, which ultimately hampers protein activity. Oxidation of amino acid side chains and the protein backbone leads to protein degradation and formation of protein-protein linkages (Zhang et al., 2013). Nucleic acids, particularly DNA, are affected extensively by ROS. Elevated ROS result in the removal of nucleotides, strand breakage, modification in the organic bases of the nucleotide, deoxyribose oxidation and generation of DNA-protein crosslinks (Liu et al., 2000). These DNA-protein crosslinks can impede replication and transcription, further impairing damage to the cellular processes. Subsequent mutations occur when nucleotide changes of one strand cause mismatches in the other strand. Lack of protective

proteins, along with proximity to the source of ROS production, increases the chance of mitochondrial and chloroplast DNA to undergo ROS mediated damage (Richter, 1992).

Although overwhelming levels of ROS are clearly toxic for cells (bad ROS), moderate levels of ROS can function as important signaling molecules in plants (good ROS) (Mittler, 2017). As a result, plants have employed rigorous pathways to maintain a balance between good ROS and bad ROS. Spatially controlling ROS levels is the key to successfully managing ROS's impact on plant growth and development (Huang et al., 2019). Regulated levels of ROS are critical for development of the root apical meristem (RAM) and the shoot apical meristem (SAM). For example,  $O_2^-$  and  $H_2O_2$  accumulate in the meristematic and the elongation zones of the root, respectively, under normal conditions. The ratio of  $O_2^-$  to  $H_2O_2$  determines the proliferative activity of the root cells, thereby controlling root growth and development (Dunand et al., 2007; Tsukagoshi et al., 2010). Similarly, a delicate balance of  $O_2^-$  and  $H_2O_2$  is essential for maintaining stem cell activities at the SAM as well as the cell differential processes in the peripheral zone (Zeng et al., 2017). In addition to its role in vegetative organs, optimal ROS levels are required for the plant reproduction. As flower development progresses, ROS levels increase gradually (Zimmermann et al., 2006). At the same time, an optimal level of ROS is essential for initiating pollen development in the anthers (Hu et al., 2011). Finally, ROS works in concert with various plant hormones, like auxin to regulate root hair development, thereby positively impacts plant growth and development (Mangano et al., 2017).

## **ROS, epigenome and reproductive health**

Changes to the epigenetic landscape are a major fallout from the overaccumulation of systemic ROS and Reactive Nitrogen Species (RNS) in plants. These reactive species can impact the epigenome by regulating the activity of different enzymes involved in adding specific epigenetic marks to the genome (Kumar R. M. et al., 2020). In plants increased ROS causes hypomethylation of the epigenome. For example, overaccumulation of free radicals in a *Pisum sativum* suspension culture leads to a global reduction of DNA methylation (Berglund et al., 2017). Similar effects are observed in the case of oxidative stress induced by Nitric Oxide (NO), which leads to DNA hypomethylation at CHG sites in rice seedlings (Ou et al., 2015). The most common mechanisms employed by ROS to modify the epigenome involve changing the steady-state level of the methyl donor: S-Adenosyl Methionine (Šalplachta et al., 2005) or affecting the enzymatic activities of the DNA methyltransferases and DNA demethylases (Xu et al., 2015b). ROS can also impact the production of siRNAs critical for maintaining the methylome (Charbonnel et al., 2017; Seta et al., 2017) and modulate the activity of various histone methyl transferases and histone de-methylases (Hussain et al., 2016). Histone hyperacetylation is also one of the consequences of ROS accumulation. Based on observations from different plant species, a surge in ROS impairs the histone deacetylases (Hu et al., 2019) and imbalances Acetyl Co-A levels (Ojima et al., 2012), the donor substrate for histone acetylases. In addition to a role for ROS in regulating deposition of epigenetic marks, higher ROS levels can influence the epigenome by modulating the activities of various chromatin remodelers. For instance, rice seedlings exposed to sodium nitroprusside show downregulated



expression of two genes involved in chromatin remodeling, *deficient in DNA methylation 1a* and *1b* (*DDM1a* and *DDM1b*), which eventually lead to DNA hypomethylation of the rice genome (Ou et al., 2015).

Similar to plants, genome instability due to ROS-induced epigenetic changes is a phenomenon widely observed in cancer cells (Bhat et al., 2018). For example, increased DNA hypomethylation is often associated with early oncogenesis, whereas site-specific hypermethylation mediates cancer metastasis (Fang et al., 2013). ROS-induced hyperacetylation also forms the molecular basis for progression of several aggressive cancers like breast cancer (Kamiya et al., 2016). Thus, robust ROS scavenging machinery appears to be critical to sustain a healthy epigenome in both plants and mammalian cells.

Stressed-induced accumulation of cellular ROS is one of the leading causes for defects in male and female gametes. The presence of a lipid heavy cell wall along with reduced levels of ROS scavenging enzymes makes sperm cells highly susceptible to ROS-induced damage. Overaccumulation of ROS in sperm cell is associated with reduced motility and inability to fertilize the oocytes (Agarwal and Saleh, 2002; John Aitken et al., 1989). In the zygote, any damaged sperm DNA is repaired by the BER pathway derived from the oocyte (Lord and Aitken, 2015). Such repair pathways fragment DNA which primarily affects the paternal genetic contribution to the developing embryo (Tremellen, 2012). Moreover, energy invested in BER, compromises the essential epigenetic reprogramming of the sperm DNA, thereby impacting embryo quality (Wyck et al., 2018). Interestingly, in humans anti-oxidants are the major line of defense against male infertility (Martin-Hidalgo et al., 2019). Female reproductive health (eg. the oocyte) can also be

negatively impacted by ROS (Sasaki et al., 2019). Oocyte quality decreases with increasing reproductive age (May-Panloup et al., 2016) and mitochondrial ROS appears to be the culprit (Wiener-Megnazi et al., 2004). Therefore, keeping ROS levels in check is crucial for maintaining a healthy germline genome in mammals.

Notably, a moderate level of ROS is essential to drive several developmental processes in flowers. An intricate balance of ROS is needed to produce healthy pollen grains in rice (Hu et al., 2011), and disruption of this balance leads to over-accumulation of ROS in anthers that make pollen grains inviable (Zheng et al., 2019c). An optimal amount of ROS at the flower stigma is also required for a successful pollination event (Zhang et al., 2020). Efficient ROS mediated signaling facilitates pollen tube growth within the style and its eventual penetration into the ovary followed by pollen tube rupture to release the male germ cell (Duan et al., 2014). However, overaccumulation of ROS in the female gametophyte impairs embryo sac development and results in unsuccessful fertilization events (Martin et al., 2014). Thus, ROS levels must be strictly maintained to favor the pathways essential for growth and development in both plants and animals (Mittler, 2017).

### **Arabidopsis thaliana as a model organism**

*A. thaliana* is a small dicotyledonous flowering plant belonging to the family of *Brassicaceae*. This simple weed has garnered the status as model organism of choice for plant biology for several reasons ([https://www.nsf.gov/pubs/2002/Arabidopsis thaliana/model.htm](https://www.nsf.gov/pubs/2002/Arabidopsis_thaliana/model.htm)). The minimal requirements for its growth - light, air, water, and

limited soil minerals - along with *A. thaliana*'s short stature, make it easy to grow and propagate in a small laboratory space. *A. thaliana* takes only 6 weeks to complete its life cycle, and each healthy plant can produce more than 10,000 seeds because of its ability to self-pollinate. After proper dehydration, seeds can be stored at room temperature for several years or in colder temperatures for over more extended periods. A complete collection of *A. thaliana* knockout mutants can be stored in a room no larger than a closet, something not feasible for other larger model organisms like mouse, flies, or fish. *Arabidopsis* exhibits the typical and specialized features of seed plants including perfect flowers, stems, apical meristem, trichomes, stomatal structure, pollen grains and female gametophytes. Being a winter annual, *A. thaliana* has biphasic development with vegetative growth of a compact set of rosette leaves. Later on, depending on the availability of favorable environmental conditions, the plant grows a single primary stem that harbors all the flowers and the siliques (Woodward and Bartel, 2018).

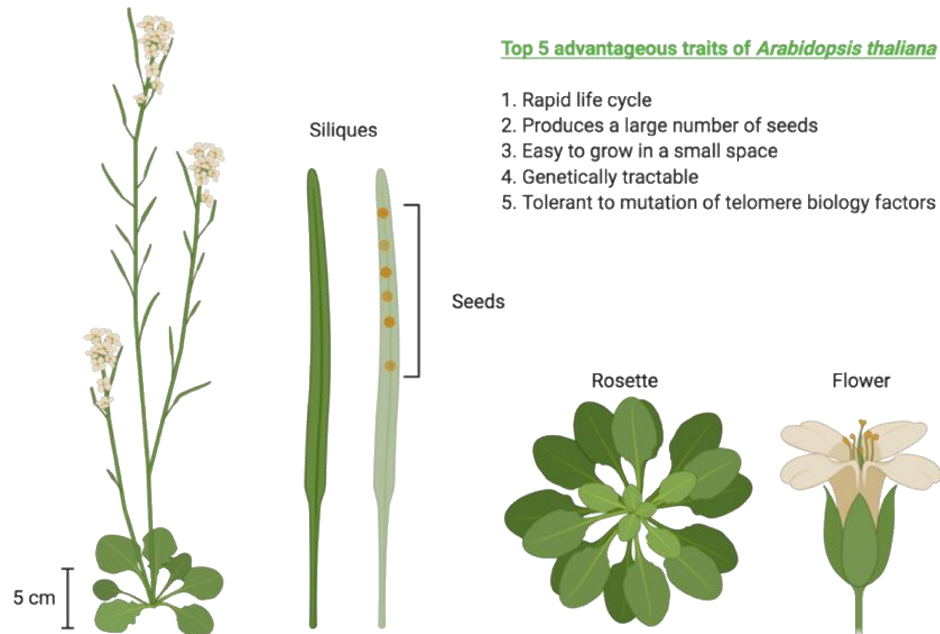


**Figure I-11 *Arabidopsis thaliana* as a model organism.**

Another advantage of using *A. thaliana* as a model organism is its genome size and genetic tractability. *A. thaliana* has a comparably small genome of ~132 Mbp has 38000 loci, which include more than 20,000 genes distributed on five different chromosomes (Cheng et al., 2017). It can tolerate a high degree of homozygosity and is self-fertile. The genes present in *A. thaliana* account for most of the genes present in higher plants (Provar et al., 2016). Hence, many observations made in *Arabidopsis* are applicable in other higher plants. *A. thaliana* also has an advanced toolkit available for genetic manipulation (Bortesi and Fischer, 2015; Koornneef and van der Veen, 1980; Zhang et al., 2006). Forward and reverse genetic screens are routinely performed in addition to more advanced gene-editing strategies like CRISPR-Cas9. The plants can be easily transformed

through *Agrobacterium*-mediated transformation and floral dipping. Moreover, the large number of ecotypes or (accessions) available for *Arabidopsis thaliana* act as complementary resources to analyze the genome functionally, especially identification of novel genes contributing to unique phenotypes and for population-wide mapping studies such as quantitative trait loci (QTL) mapping and genome-wide association studies (GWAS) (Fulcher et al., 2014).

For more than two decades, *A. thaliana* has served as an excellent model to study telomeres in the Shippen Lab. This telomere system was pioneered by the Shippen Lab. Several novel discoveries, like the identification of the CST complex in *A. thaliana*, was the starting point for identifying and characterizing such similar complexes in humans. There are several reasons for the success of *A. thaliana* as a model organism to study telomere biology. First, plants show exceptional tolerance to the loss of critical components of the telomere maintenance pathways (McKnight and Shippen, 2004). Plants lacking telomerase can survive for up to six generations without showing any phenotypic defect or growth abnormality (Riha et al., 2001). Second telomeres are short (2 kb to 5 kb) in *A. thaliana*. The presence of restriction enzyme sites within the subtelomeric regions helps resolve the telomeres using standard Southern blotting techniques. In addition, eight out of ten chromosome arms have a unique subtelomeric sequence, enabling design of assays to monitor the telomere length of individual chromosome arms and also to gauge the occurrence of chromosome fusion events at the telomeres (Watson and Shippen, 2007). Overall, the biological and genomic features along with its genetic tractability and

tolerance to genomic stress makes *A. thaliana* an excellent organism for telomere biology (Figure I-11).

## **Dissertation Overview**

The underlying theme of this dissertation is exploring non-canonical aspects of telomere biology in *Arabidopsis thaliana*. The three major discoveries reported in this thesis are: 1) The previously described telomerase-associated lncRNA TER2 is a PCR artifact; 2) tRNA Adenosine Deaminase 3 (TAD3), an enzyme in the tRNA editing pathway regulates *A thaliana* telomere length via a telomerase-independent mechanism; and 3) Loss of AtPOT1b, a paralog of the Protection of Telomeres 1 (POT1) gene, manifests a novel chromatin decondensation phenotype that appears to reflect mis-regulation of ROS, rather than a canonical telomerase-protection pathway.

The first half of Chapter II contains data obtained from the re-evaluation of the *TER2/TAD3* locus. A combination of robust stranded RNA-Seq experiments followed by cross-validation using published RNA-Seq data revealed that a PCR artifact from the *TAD3* locus was misidentified as the TER2 lncRNA (Bose et al., submitted). Previously studies implicated a role for the *TAD3/TER2* locus in response to DNA damage (Cifuentes-Rojas et al., 2012). However, I did not observe any surge in transcripts from the *TAD3/TER2* locus following DNA damage induction with the radiomimetic drug, zeocin. Moreover, I found that the *TER2/TAD3* locus is not involved in regulating telomerase activity during DNA damage. Although *tad3* seedlings are sensitive to DNA damage treatment, defect in the DNA damage response pathway is not an underlying

mechanism for the observed sensitivity. Furthermore, the same hypomorphic *tad3* mutant shows a subtle but progressive telomere shortening phenotype in successive generations. Therefore, while TER2 is a PCR artifact, the *TER2/TAD3* locus seems to have a potential role in telomere biology of *A. thaliana*.

The second half of Chapter II takes a deep dive to investigate the potential mechanism of TAD3-mediated telomere length maintenance. *TAD3* is an essential gene involved in tRNA editing (Zhou et al., 2014). Unexpectedly, I found that telomeres shorten progressively in *tad3* mutants. I report that loss of TAD3 does not affect telomerase activity and plants lacking both TAD3 and POT1a display accelerated telomere shortening, indicating that TAD3 contributes to telomere length maintenance independent of telomerase. Finally, data obtained from transcriptomics analysis of *tad3* mutants shows extensive downregulation of genes involved in auxin-related pathways and upregulation of genes involved in secondary metabolite pathways. In addition, Fluorescence-Activated Cell Sorting (FACS) analysis revealed a cell cycle-dependent expression pattern of the *TAD3* mRNA, which was distinct from *TERT* and *POT1a* mRNA, suggesting that TAD3 contributes to telomere length regulation via a cell cycle-dependent mechanism. Taken together, my data identify TAD3 as a new player involved in telomere length regulation. This regulation occurs via a telomerase-independent non-canonical mechanism that may reflect altered plant metabolism.

Chapter III aims to examine the role of POT1b on chromosome structure and integrity. Using cytology-based assays, I discovered a unique chromatin decondensation phenotype and other aberrant chromatin structures in mitotically dividing cells from

flower pistils in the *pot1b* mutant. The unusual chromatin structures were partially rescued by complementing *pot1b* by overexpressing wild type POT1b. Interestingly, I observed similar chromatin structures in mitotically dividing cells from *catalase 2* mutants, which over accumulate ROS. In addition, *pot1a* and *tert* mutants also display similar aberrant chromatin phenotypes including chromatin decondensation. I hypothesize that overaccumulation of ROS alters chromatin structure across the genome and not just at telomeres. Furthermore, POT1b plays an important but unanticipated role in modulating genome architecture.

Appendix I provides a detailed protocol for a modified plant-based comet assay. There are two improvements in this assay compared to the previously published protocols. First, this new version uses >200 data points for generating a statistically robust result, that provides a more rigorous measure of the amount DNA damage present in a particular sample. Second, the new protocol includes development of a modified *ex vivo* version of the comet assay. In the *ex vivo* version, comets from mutants with damaged DNA are incubated with wild type protein followed by assessing the amount of DNA repaired after the incubation step. The results from this new method can provide new insight into DNA damage repair competency of the constituent molecules in the extract or a specific genotype.

Appendix II presents a published manuscript from 2019 which details the identification and characterization of the bona fide telomerase RNA (TR) from plants.

Altogether this dissertation clarifies the nature of a previously reported telomerase regulatory molecule. It reveals a novel connection between metabolism-related activities,



particularly a tRNA deaminase, and plant telomere maintenance. In addition, observations presented in this dissertation elucidates a novel non-telomeric role for POT1 proteins concerning the maintenance of global chromatin structure. Overall the results reported in this document provide novel insight and open new avenues for future investigation into non-canonical facets of telomere biology in *A. thaliana*.

## CHAPTER II

### tRNA ADENOSINE DEAMINASE 3 IS REQUIRED FOR TELOMERE

#### MAINTENANCE IN *Arabidopsis thaliana*

#### **Abstract**

Telomere length maintenance is influenced by a complex web of chromatin and metabolism-related factors. We previously reported that a lncRNA termed AtTER2 regulates telomerase activity in *Arabidopsis thaliana* in response to DNA damage. AtTER2 was initially shown to partially overlap with the 5' UTR of the *tRNA ADENOSINE DEAMINASE 3 (TAD3)* gene. However, updated genome annotation showed that AtTER2 was completely embedded in TAD3, raising the possibility that phenotypes ascribed to AtTER2 could be derived from TAD3. Here we show through strand-specific RNA-Seq, strand-specific qRT-PCR and bioinformatic analyses that AtTER2 does not encode a stable lncRNA. Further examination of the original *tad3 (ter2-1/tad3-1)* mutant revealed expression of an antisense transcript driven by a cryptic promoter in the T-DNA. Hence, a new hypomorphic allele of TAD3 (*tad3-2*) was examined. *tad3-2* mutants showed hypersensitivity to DNA damage, but no deregulation of telomerase, suggesting that the telomerase phenotype of *tad3-1* mutants reflects an off-target effect. Unexpectedly, however, *tad3-2* plants displayed progressive loss of telomeric DNA over successive generations that was not accompanied by alteration of terminal architecture or end protection. The phenotype was exacerbated in plants lacking the telomerase processivity factor POT1a, indicating that TAD3 promotes telomere maintenance in a noncanonical, telomerase-independent pathway. The transcriptome

of *tad3* mutants revealed significant dysregulation of genes involved in auxin signaling and glucosinolate biosynthesis, pathways that intersect the stress response, cell cycle regulation and DNA metabolism. These findings indicate that the *TAD3* locus indirectly contributes to telomere length homeostasis by altering the metabolic profile in *Arabidopsis*.

## **Introduction**

Telomeres safeguard the genome by preventing chromosome ends from eliciting a DNA damage response and ensuring that terminal DNA sequences can be faithfully maintained (Shay and Wright, 2019). Due to the nature of eukaryotic DNA replication, telomeres culminate in a single-stranded extension termed the G-overhang (Sandhu and Li, 2017), which acts as a substrate for the addition of telomeric repeats by telomerase. Plant telomeres are unusual in that one-half of their chromosome ends terminate in a G-overhang, and the other half in a blunt end bound by the Ku complex (Kazda et al., 2012b). Loss of Ku triggers extensive telomerase-dependent telomere elongation, presumably because blunt ends are converted to telomerase-accessible G-overhangs (Kazda et al., 2012b; Valuchova et al., 2017b). This unusual telomere architecture may further enhance genome stability, which seems advantageous given the sessile lifestyle of plants (Nelson and Shippen, 2012).

Telomere length homeostasis is modulated by a wide range of factors. At the telomere, components of the shelterin complex, particularly the TTP1/POT1 heterodimer, enhance telomerase activity and processivity on human telomeric DNA (Wang et al.,

2007). In *Arabidopsis* POT1a associates with the telomerase ribonucleoprotein complex (RNP) and stimulates its repeat addition processivity (Arora et al., 2016; Renfrew et al., 2014; Surovtseva et al., 2007). Plants deficient in POT1a undergo telomeric DNA attrition at a rate similar to the amorphic telomerase (*AtTERT*) mutant (Surovtseva et al., 2007). The progressive loss of telomeric DNA in telomerase mutants ultimately causes a critical length threshold to be breached, activating a DNA damage response that leads to telomere fusion and genome-wide instability. *Arabidopsis* telomeres normally span 2–5 kb in length; telomere tracts shorter than 1kb have an increased probability of being recruited into end-to-end chromosome fusions (Heacock et al., 2004). Thus, an optimal telomere length setpoint must be established to maintain genome integrity (Jeffrey Chiang et al., 2010; Watson and Shippen, 2007).

In addition to canonical telomere-associated factors, genetic screens performed in *Saccharomyces cerevisiae* and *Schizosaccharomyces pombe* demonstrate that telomere length is also influenced by a wide variety of “non-telomeric” genes that function in various aspects of DNA metabolism, chromatin modification, vesicular trafficking, RNA metabolism, ribosome metabolism and translation (Askree et al., 2004; Ungar et al., 2009). Perturbation of cell cycle progression can also alter telomere length. For example, mutation of *RAD1*, a component of the intra-S DNA damage checkpoint, leads to telomere shortening in *S. pombe* (Nakamura et al., 2002). Similarly, Rad1 functions as a positive regulator of telomere length in mammals, working in concert with Hus1 and Rad9 in the 911 complex (Rad9-Hus1-Rad1) (Francia et al., 2007).

Telomere dysfunction induces Programmed Cell Death (PCD) in plant meristems to eliminate genetically unstable cells (Amiard et al., 2014; Boltz et al., 2012). PCD activation is essential for cell differentiation and proper development and is also involved in pathogen and environmental stress responses (Locato and De Gara, 2018). PCD activation involves various kinds of molecular signals including plant hormones, calcium and reactive oxygen species (ROS) (Huysmans et al., 2017). Different hormonal pathways are interconnected to fine-tune PCD via transcriptional regulation. The auxin hormone regulates plant growth, and under normal conditions concentrates at the quiescent center of the root stem cell niche. Under abiotic stresses, many of which induce the accumulation of ROS, auxin levels decline causing PCD in root tissues (Hong et al., 2017; Krishnamurthy and Rathinasabapathi, 2013). Auxin signaling also controls cell cycle progression by mediating activation of Cdc2 (Yang et al., 2002). Cdc2/Cdk2 kinase activity is necessary for expression of telomerase activity at early S phase (Ren et al., 2004; Tamura et al., 1999; Yang et al., 2002). Thus, telomerase is a downstream target of auxin signaling pathway.

Telomerase is comprised of two core components, the catalytic subunit TERT and a long non-coding RNA (lncRNA) TER/TR (Musgrove et al., 2018) that serves as a template for telomere repeat addition (Egan and Collins, 2012). In *A. thaliana*, two lncRNAs were initially identified as telomerase subunits (Cifuentes-Rojas et al., 2011). AtTER1 was uncovered through partial purification of telomerase, and proposed to be the canonical telomerase RNA subunit. AtTER2, expressed from a locus partially overlapping the tRNA Adenosine Deaminase 3 (*TAD3*) gene, was uncovered by BLAST based on its

high sequence similarity to AtTER1 (Cifuentes-Rojas et al., 2011, 2012). Subsequent studies indicated that AtTER2 was stabilized and function to down-regulate telomerase activity in response to DNA double-strand breaks (Cifuentes-Rojas et al., 2012; Xu et al., 2015a). We recently employed an unbiased RIP-seq approach to identify lncRNAs associated with active telomerase under native conditions and failed to recover AtTER1 (Song et al., 2019). Instead, a single lncRNA, AtTR, was significantly enriched. Further analyses by our lab and others revealed that AtTR was the *bona fide* telomerase RNA subunit in *A. thaliana* (Fajkus et al., 2019; Song et al., 2019).

A new annotation of the *A. thaliana* genome, Araport11, extended the 5' UTR of TAD3 to now fully embed AtTER2. This updated annotation prompted us to re-examine the TER2/TAD3 locus to assess whether the phenotypes originally ascribed to TER2 might instead result from mutation of TAD3. tRNA Adenosine Deaminase 3 (TAD3) catalyzes the deamination of adenosine at position 34 of the tRNA anticodon loop into inosine to facilitate wobble base pairing (Torres et al., 2014a). Yeast and plant TAD3 amorphic mutants are inviable (Gerber and Keller, 2017; Zhou et al., 2013). Similarly, loss of TAD3 in fission yeast compromises cell survival by affecting cell cycle progression (Tsutsumi et al., 2007). Decreased expression of human TAD3 impacts RNA editing for several tRNA species and is associated with intellectual disability (Torres et al., 2014b). Notably, *TAD3* was uncovered in a genetic screen in *S. cerevisiae* as one of the essential genes that impacts telomere length maintenance (Ungar et al., 2009).

Here we show through strand-specific RNA-Seq, strand-specific qRT-PCR, and bioinformatic analyses that AtTER2 does not encode a stable lncRNA, and the telomere-

related functions from this locus derive from the TAD3 gene. Through analysis of additional TAD3 mutant alleles, we report that hypomorphic *tad3* mutants are hypersensitive to DNA damage, but TAD3 is not required to regulate telomerase activity in response to DNA damage. However, TAD3 is required for telomere length maintenance. This unanticipated function is independent of telomerase, and appears to reflect a broader role for TAD3 in modulating cellular metabolism.

## Results

### Reexamination of *AtTER2* locus

The initial characterization of *AtTER2* was based on annotation of the *Arabidopsis* genome published by The Arabidopsis Information Resource, TAIR10 (Release date, November 2010) (Berardini et al., 2015). *AtTER2* is located in the Crick strand on Chromosome 5, partially overlapping the 5' UTR of *TAD3*, encoded in the Watson strand (Figure II-1A) (Cifuentes-Rojas et al., 2012). The non-overlapping region of *AtTER2* was used to design *AtTER2*-specific primers to trace the molecule by RT-PCR. Given that the current genome annotation for *A. thaliana*, Araport11 (Release date, June 2016), extended the 5' UTR of *TAD3* to fully embed *AtTER2* (Figure II-1A), we designed a strand-specific RT-PCR approach to exclusively detect the *AtTER2* transcript. We were unable to detect *AtTER2* in flowers, leaves, and seedlings from wild type plants grown under normal conditions (Figure II-2A). Cq values > 31 were obtained for *AtTER2* amplification compared to Cq  $\cong$  19 for the internal control ACT2 (AT3G18780) (Figure II-2A).

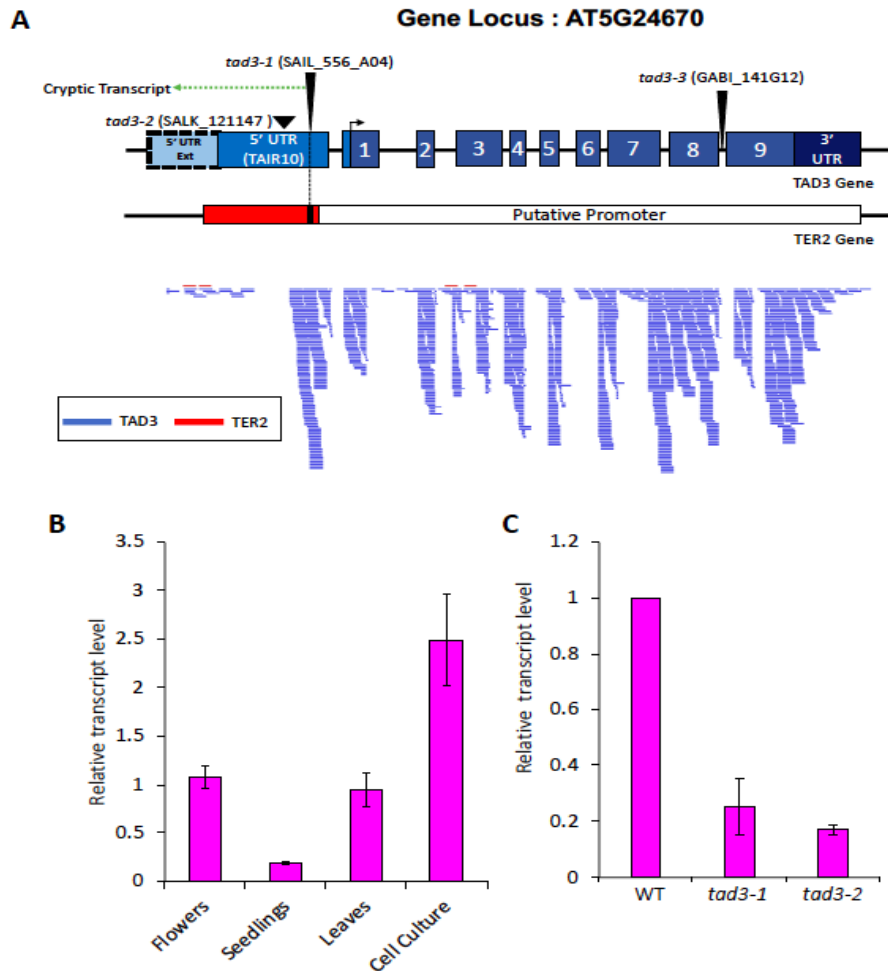


**Figure II-1 Reannotation of the TER2 locus based on TAIR10\_v90.**

(A) Schematic representation of the *TER2* and *TAD3* loci in *Arabidopsis thaliana* based on the Araport11 version of genome annotation. The *TAD3* gene (AT5G24670) is represented in blue and *TER2* in red. The previous genome annotation (TAIR10 + Araport11 5' Ext) placed *TER2* within the 5' UTR of *TAD3*. The putative promoter would span the *TAD3* gene. The positions of the *tad3-1*, *tad3-2* and *tad3-3* T-DNA insertions are indicated by the black triangles. The short horizontal blue (*TAD3*) and red (*TER2*) lines below top panel denote stranded RNA-Seq reads from six-day-old wild type (WT) Col-0 seedlings. A cryptic transcript emanating from the *tad3-1* insertion is indicated by the dotted green line. (B) qRT-PCR data for *TAD3* mRNA in flowers, seedlings, leaves and cell culture. Data from two biological replicates are shown as fold change with respect to WT flowers. (C) qRT-PCR data for *TAD3* mRNA in flowers from WT, *tad3-1* and *tad3-2* plants. Data from two biological replicates are shown as fold change with respect to WT samples.



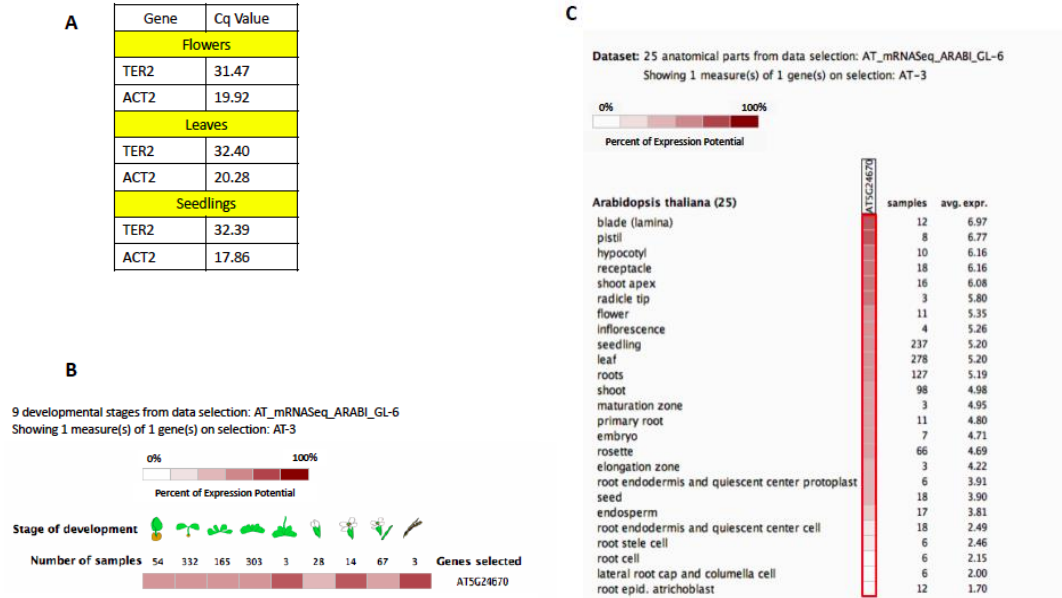


**Figure II-2 TAD3 mRNA expression is regulated during plant development.**

(A) Results from strand-specific qPCR. Cq values for TER2 and the ACT2 gene amplified using WT flowers, leaves and seedlings are shown. (B) Genevestigator-based analysis of TAD3 mRNA expression during different stages of plant growth and development. (C) Genevestigator analysis of organ-specific expression of TAD3 mRNA.

Previous studies indicated that AtTER2 was stabilized and accumulated in response to DNA damage (Cifuentes-Rojas et al., 2012). To thoroughly explore AtTER2 expression, we performed total RNA sequencing on *tad3-2* mutants (see below) and wild type seedlings with and without zeocin treatment. Stranded RNAseq libraries were prepared from total RNA after depletion of ribosomal RNAs. Sequencing of untreated *tad3-2* and wild type seedlings produced a total of 51,194.244 (91.17%) and 59,996.775

(91.47%) reads, respectively, uniquely mapped to the reference genome. While sequencing of zeocin treated produced 46,127.084 (91.59%) and 53,093.124 (89.75%) uniquely mapped to the reference genome in the *tad3-2* and wild type, respectively. *TAD3* expression in *tad3-2* mutants was ~33% of wild type (see below). However, we found no change in *TAD3* expression in wild type plants upon zeocin treatment. Moreover, negligible number of reads aligned to *AtTER2* in either the *tad3-2* or wild type datasets from mock (Figure II-1A) or zeocin treated seedlings. Together, these data indicate that *AtTER2* is not a stable lncRNA, and the previously detected PCR products likely reflect artifactual amplification of the Crick strand of the *TAD3* 5' UTR. Therefore, any functions previously ascribed to this locus derive from *TAD3*.

#### **Identification of *TAD3* mutant alleles**

*TAD3* is widely expressed, with peaks during bolting, formation of mature flowers and silique development (Figure II-2B). *In silico* analysis of publicly available transcriptomic data using Genevestigator (Hruz et al., 2008) indicated *TAD3* is most highly expressed in leaves, flowers and root apical meristem (Figure II-2C). We verified this finding experimentally using qRT-PCR, and also found high *TAD3* expression in cell culture (Figure II-1B).

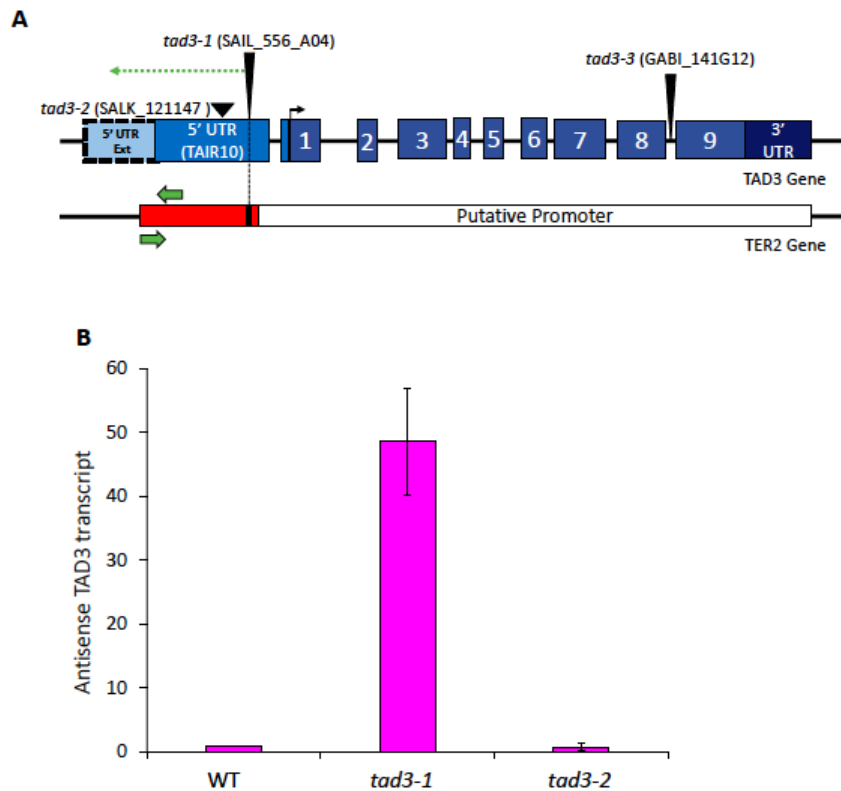


**Figure II-3 Identification of a cryptic transcript produced from the TAD3 locus in *tad3-1* mutants.**

(A) Schematic representation of the TAD3 locus (see legend for Figure 1). Green arrows denote forward and reverse primers used to detect expression. (B) qRT-PCR results obtained with these primers with WT, *tad3-1* and *tad3-2* samples. PCR product size = 108 nts. Data from two biological replicates are shown as fold change with respect to WT samples.

Our previous analyses of the *TAD3* locus utilized the T-DNA insertion line SAIL\_556\_A04 (*ter2-1*) (Cifuentes-Rojas et al., 2012), now designated *tad3-1*, which resides in the 5' UTR of *TAD3* (Figure II-1A). Although no transcript spanning the T-DNA insertion in *tad3-1* could be detected (Cifuentes-Rojas et al., 2012) (Figure II-1A), qRT-PCR with strand-specific primers targeting a region 770 nt downstream of the T-DNA revealed the presence of an RNA transcript (Figure II-3A and II-3B), suggesting the activation of a cryptic promoter within the T-DNA (Mengiste and Paszkowski, 1999). As

this transcript could have indirect effects, we considered the *tad3-1* allele suboptimal for further studies, and characterized two additional T-DNA lines. One allele termed *tad3-3* carries a T-DNA in the intron between exons 8 and 9, but embryonic lethality was previously reported in homozygous mutants (Zhou et al., 2014). The third T-DNA line (SALK\_121147) termed *tad3-2* contains a T-DNA 902 nt downstream from the start of the *TAD3* 5' UTR (Figure II-1A). In contrast to *tad3-1*, *tad3-2* does not produce an antisense transcript (Figure II-3B). qRT-PCR analysis of floral RNA indicated that *TAD3* mRNA is reduced by ~75% (p-value=0.06) in *tad3-1* and by 83% (p-value=0.01) in *tad3-2* mutants respectively (Figure II-1C). Because of the higher knockdown and the absence of a potentially confounding antisense transcript, downstream analyses were performed using the *tad3-2* allele.

***Plants deficient in TAD3 exhibit hypersensitivity to DNA damage and elevated programmed cell death***

It was previously reported that *tad3-1* mutants exhibit an increased incidence of programmed cell death (PCD) in the Root Apical Meristem (RAM) after zeocin treatment (Cifuentes-Rojas et al., 2012). We re-examined this response in *tad3-2* mutants by imaging the RAM of seedlings stained with Propidium Iodide (PI) four- and six-hours post-treatment with 20  $\mu$ M zeocin. At four hours, 70% of the *tad3-2* seedlings displayed PCD, compared to 0% of wild type seedlings (Figure II-4A and II-4B). Thus, *tad3-2* mutants are hypersensitive to DNA damage, consistent with the previous results obtained in *tad3-1* mutants (Cifuentes-Rojas et al., 2012). The prior study indicated that *tad3-1*

mutants have an intrinsically elevated accumulation of DDR-related transcripts, including *BRCA1* (Cifuentes-Rojas et al., 2012). However, transcriptomic analysis of *tad3-2* and wild type seedlings grown under normal conditions revealed only a slight increase in *BRCA1* expression (1.8-fold (FDR<0.05)) in *tad3-2* (Figure II-5A).

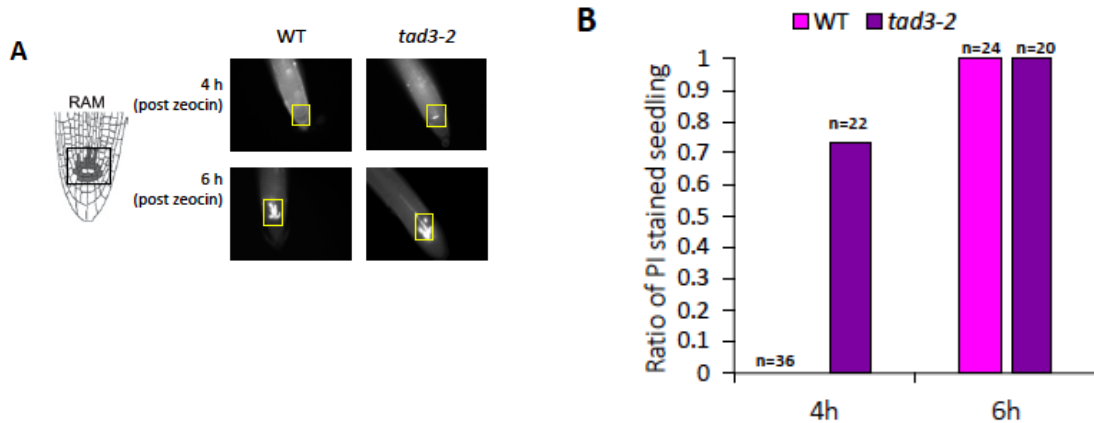


**Figure II-4 The TAD3 locus does not modulate DNA damage related pathways.**

(A) Schematic representation of an *A. thaliana* root tip with the Root Apical Meristem (RAM) highlighted in gray (left). On the right, images of roots from *A. thaliana* seedlings stained with Propidium Iodide solution (PI) following treatment with 20  $\mu$ M zeocin. Photos are shown of representative 4-days old WT and *tad3-2* seedlings treated with zeocin for 4 hours and 6 hours followed by PI staining. Yellow box highlights the RAM and Programmed Cell Death. (B) Quantification of PI staining in the RAM of WT and *tad3-2* seedlings treated with zeocin for 4 or 6 hours. Numerical values indicate total number of roots imaged for each condition. 0 out of the 36 WT seedlings showed RAM PCD at 4 hours post-zeocin treatment. (C) Representative images of data obtained from comet assays performed on protoplasts extracted from seedlings. The length and intensity of the comet tail indicates the level of DNA damage. (D) Values for percentage DNA in tail (%PDT) from the comet assay plotted using a box and whisker plot. Top and bottom edges of the box represent the first and the third quartiles, respectively. The length of the whisker spans the minimum to maximum values. The straight line inside the box represents the median and ‘X’ stands for sample mean. Normally distributed data have an overlapping mean and median. More than 1000 comets were scored for each genotype. \*\*p-value <0.001 and NS = not significant. (E) Data obtained for quantitative Telomere Repeat Amplification Processivity (qTRAP) assays performed with flower bundles from WT and *tad3-2* mutants. Data from three biological replicates are shown as fold change with respect to WT samples. NS = not significant. (F) qTRAP results for 7-day old seedlings untreated (mock) or treated with 20  $\mu$ M zeocin for 6 hours. Data are shown for three biological replicates as fold change with respect to WT samples at 0 h mock treated. NS = not significant. \*\* = p-value <0.01 based on u-test.

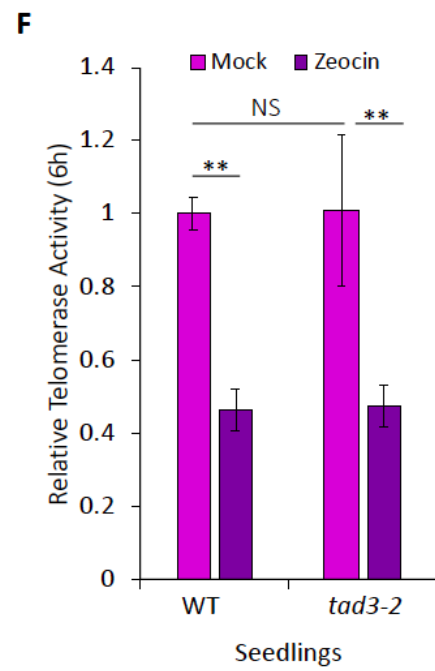
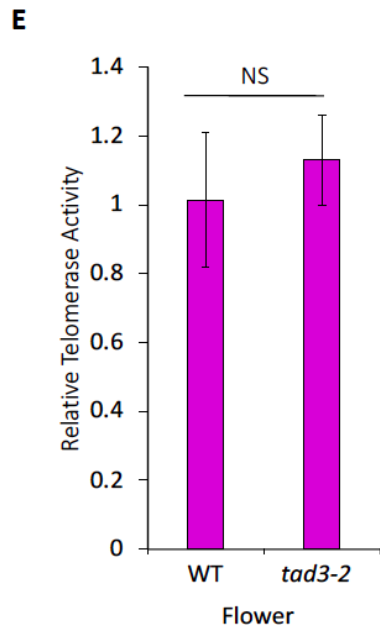
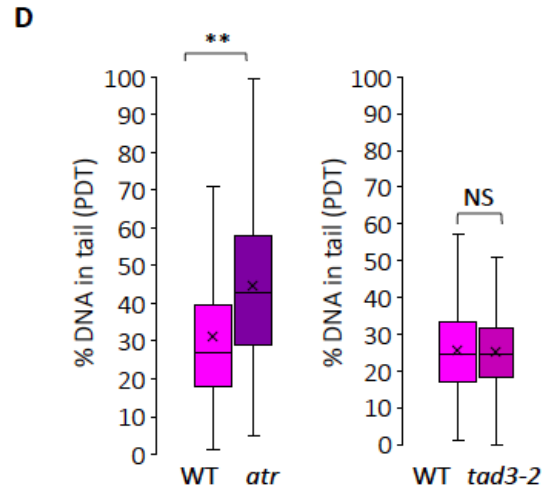
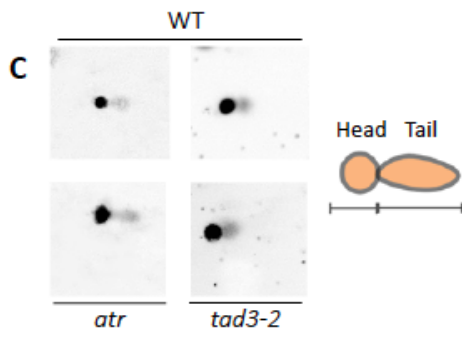


**Figure II-4 Continued**

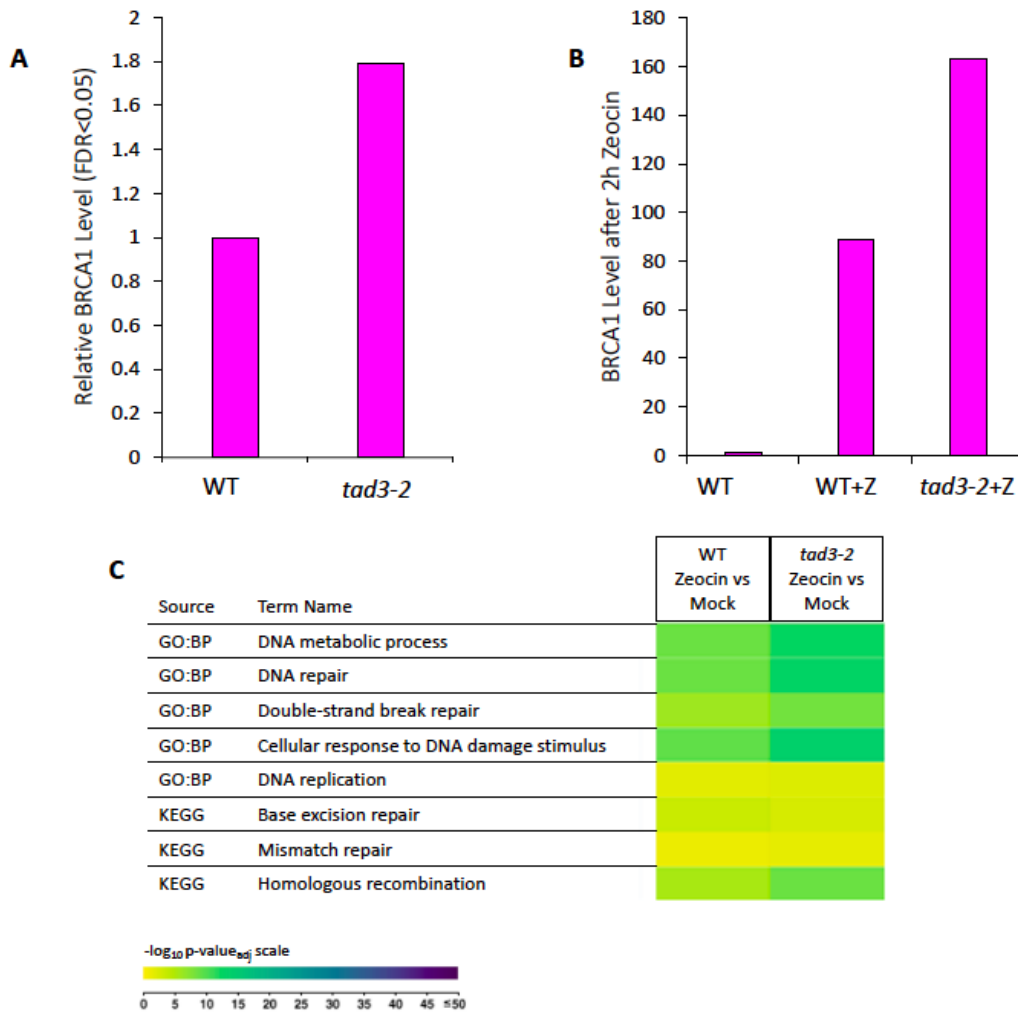


**Figure II-5 Results of zeocin treatment of WT and *tad3-2* seedlings.**

(A) Graphical representation of the RNA-Seq data obtained for BRCA1 expression in untreated WT and *tad3-2* mutant seedlings. (B) Results for qRT-PCR experiments performed to detect BRCA1 gene expression samples treated with 20  $\mu$ M zeocin for 2 hours. The mean of three biological replicates is shown as fold change with respect to untreated WT samples. (C) Gene ontology analysis performed using G profiler with the genes upregulated in 6-days old WT and *tad3-2* seedlings treated with 20  $\mu$ M zeocin for 2 hours.

To test if increased PCD in *tad3-2* seedlings correlates with accumulation of endogenous DNA damage, we performed a modified version of the single cell comet assay using protoplasts extracted from 7 days old seedlings. We measured Percentage DNA in the comet Tail (PDT) and Tail Length (TL) to calculate Tail Moment (TM) (Olive and Banáth, 2006). Statistical analysis of any of these three parameters gauges the level of DNA damage (Beedanagari et al., 2014) and can be confirmed by the other two parameters. For convenience, we represented DNA damage as a function of PDT (%PDT). As a positive control, assays were performed on cells from plants lacking ATR, a master regulator of the DNA damage response machinery (Wang et al., 2016). As expected, PDT was significantly higher in *atr* mutants compared to wild type (Figure II-4C and II-4D). However, the level of PDT observed in *tad3-2* mutant was similar to wild type. To confirm that DNA damage sensing and repair capabilities were intact in *tad3-2* mutants, we performed a gene ontology analysis of the differentially regulated genes in zeocin treated wild type and *tad3-2* seedlings (Figure II-5C). Results from G profiler (<https://biit.cs.ut.ee/gprofiler/gost>) revealed a similar induction of all the major DNA damage signaling and repair pathways in both wild type and *tad3-2* seedlings. We conclude that reduced expression of TAD3 gene does not lead to accumulation of damaged DNA, and existing DNA damage is not an underlying cause of the PCD in *tad3-2* mutants.



Finally, since AtTER2 was reported to negatively regulate telomerase activity in response to DNA double-strand breaks (Xu et al., 2015a), we re-assessed this conclusion using the *tad3-2* allele. We found no difference in telomerase activity levels of *tad3-2* flowers or seedlings relative to wild type (Figure II-4E and II-4F). Two hours of zeocin treatment induced a robust DNA damage response as evidenced by a 100-fold increase in *BRCA1* expression (Figure II-5B). Telomerase activity was decreased by ~50% in both wild type and *tad3-2* mutants, after six hours of zeocin treatment (Figure II-4F), arguing that the telomerase response to zeocin is not dependent on *TAD3*. Altogether, these findings indicate that *tad3* mutants are hypersensitive to DNA damage, but *TAD3* does not regulate the response to DNA damage.

#### **A telomere maintenance defect in *tad3-2* mutants is independent of telomerase**

As part of our characterization of the *TAD3* locus, we monitored bulk telomere length over three consecutive generations in *tad3-2* mutants. Terminal Restriction Fragment (TRF) analyses revealed a subtle but progressive loss of high molecular weight telomere tracts in the *tad3-2* mutants relative to wild type siblings (Figure II-6A). Genetic complementation was used to test if the telomere maintenance defect was due to the loss of *TAD3*. *tad3-2* mutants were transformed with a full-length *TAD3* gene under the control of its native promoter ( $P_{TAD3}::TAD3$ ) (Figure II-6B). Within a single generation, three of the nine independent transformants showed complete recovery of telomere length to wild type, and in five others some telomere tracts were longer than in *tad3-2* mutants (Figure II-6B), supporting a role for *TAD3* in telomere length maintenance.

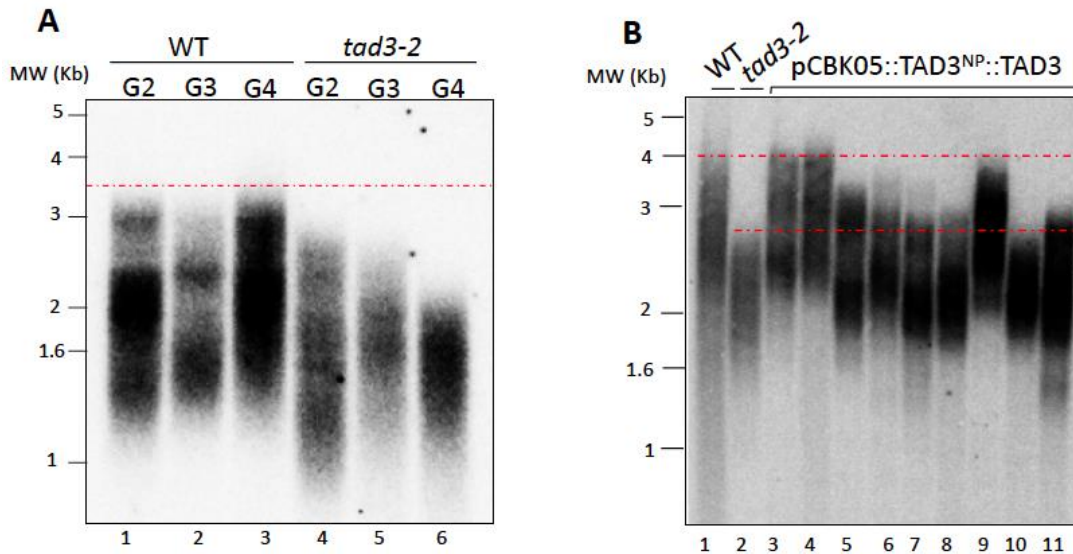


**Figure II-6 TAD3 maintains telomeres via a telomerase-independent pathway.**

(A) Results of Terminal Restriction Fragment (TRF) analysis to measure bulk telomere length in WT and *tad3-2* mutants from second (G2), third (G3) and fourth (G4) generations of homozygosity. WT samples were from segregating siblings of the *tad3-2* heterozygous parent. Red dotted line indicates the maximum telomere length for the WT samples from this cross. (B) Results of TRF analysis performed for genetic complementation of *tad3-2* mutants. 4-week-old G2 *tad3-2* mutants were transformed with pCBK05::NPTAD3::TAD3. Results are shown for WT (lane 1), G3 *tad3-2* (lane 2) and complementation lines (lanes 3-11). Red dashed line indicates maximum telomere lengths for WT and *tad3-2* samples. Lanes 1 and 2 contains DNA derived from a pool of ~100 seedlings and lane 3-11 contains DNA from individual transformants. (C) Results from TRF analysis of WT, G2 *tad3-2*, G2 *pot1a* and G2 *pot1a tad3-2* mutants. DNA samples are derived from individual plants of each genotype. Red line indicates the critical telomere length threshold of 1 Kb.

(D) Quantification of the TRF gel from panel D determined by TeloTool (Göhring et al. 2014). Data are represented as box and whisker plot. Red dot within the box represents the mean value. (E) Results from qTRAP assays performed with flowers from WT, G2 *tad3-2*, G2 *pot1a* and G2 *pot1a tad3-2* samples. Data from three biological replicates are shown as fold change with respect to WT samples

(F) Results of TRF analysis for WT, *tad3-2*, *tad3-2 ku70* and *ku70* mutants. DNA was analyzed from individual segregating siblings from a *tad3-2* X *ku70* cross. The gel has been sliced to highlight the lane for *ku70*. A vertical line separates the *ku70* lane from the rest of the gel.

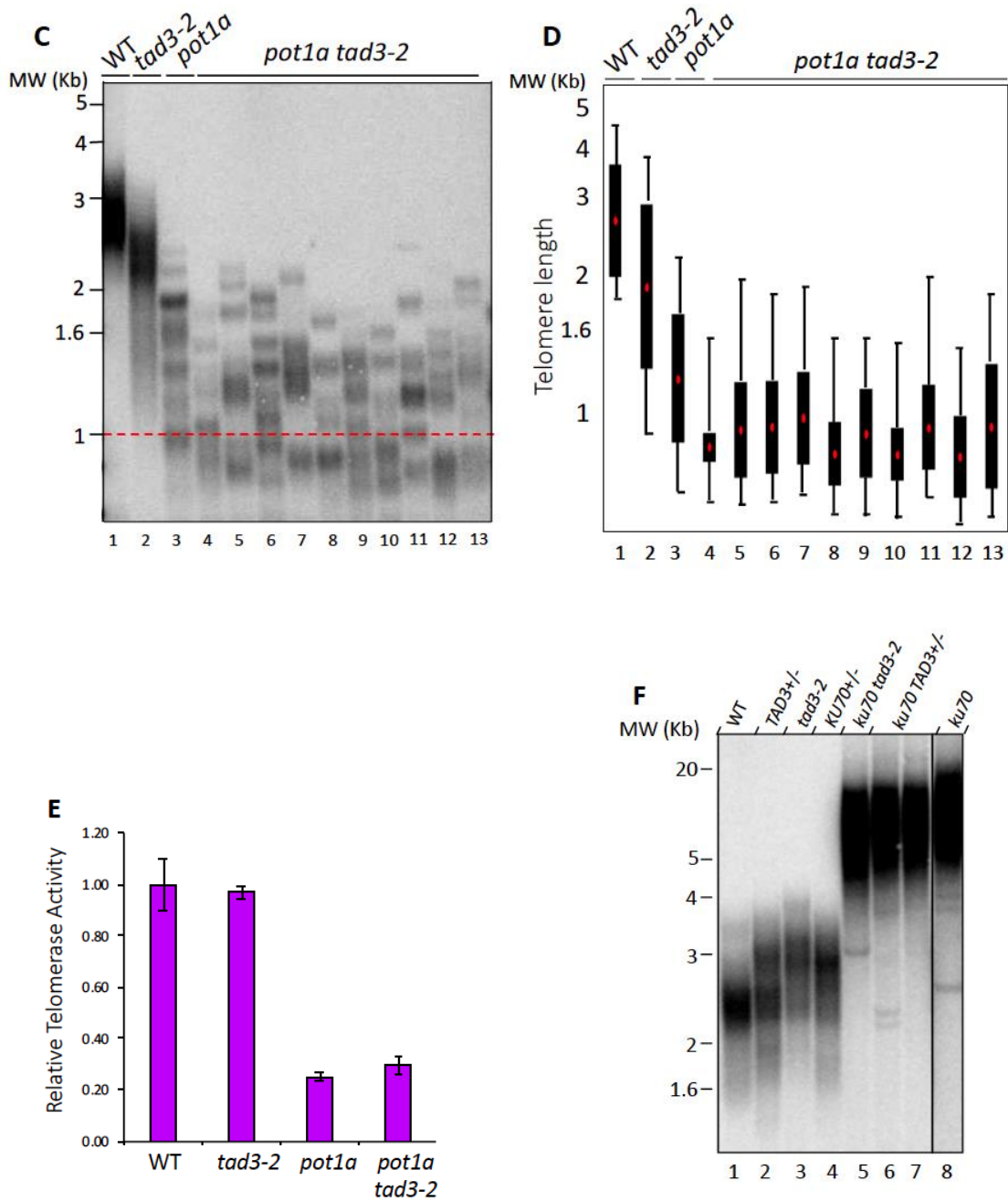


Figure II-6 Continued

When telomerase activity is limiting, shorter telomeres are preferentially elongated (Armanios et al., 2005; Goldman et al., 2005; Harrington, 2012; Marcand et al., 1997). To investigate if depletion of long telomeres in *tad3-2* mutants reflects a defect in telomerase, we generated double mutant plants. Our initial goal was to obtain plants lacking *TAD3* and *TERT*. Both genes are situated on chromosome 5, approximately 2.9 Mb apart with *TAD3* proximal to the centromere (Berardini et al., 2015). Linkage calculations indicated that Mendelian segregation of the two loci was possible, and predicted 25% of the offspring of *TAD3-2<sup>+/-</sup> TERT<sup>+/-</sup>* would be *tad3-2<sup>-/-</sup> tert<sup>-/-</sup>*. Nevertheless, we failed to recover any homozygous double mutants among ~200 offspring analyzed, suggesting that *TERT* and *TAD3* may cooperate for some essential non-telomeric function. As an alternative strategy, we made crosses to generate plants doubly deficient in *TAD3* and *POT1a*. First-generation (G1) *pot1a tad3-2* plants were readily obtained and were self-pollinated to produce second-generation (G2) *pot1a tad3-2* mutants. In parallel, we propagated wild type, *pot1a* and *tad3-2* single mutants. Each line was grown for several consecutive generations (G2-G4).

We assessed how the combined loss of POT1a and TAD3 impacted telomere length using TRF (Figure II-6C). As expected, telomeres in G2 *pot1a* mutants were shorter than wild type and displayed a discrete banding pattern indicative of a telomerase deficiency (Surovtseva et al., 2007) (Figure II-6C). Strikingly, telomeres in G2 *pot1a tad3-2* were even shorter than the *pot1a* single mutants (Figure II-6C). A banding pattern was visible for longer telomeres, but telomere tracts shorter than 1kb were more heterogeneous (Figure II-6C). Quantification of telomere length using TeloTool (Göhring

et al., 2014) showed wild type spanned 2.0-5.0 kb with a mean telomere length (MTL) of 3kb (Figure II-6D). *tad3-2* telomeres were similar though slightly shorter (range=1.2-4.0 kb; MTL= 2.1 kb). In contrast, telomeres in G2 *pot1a tad3-2* plants were significantly shorter (range=0.5-2.1 kb; MTL=1 kb) than telomeres in G2 *pot1a* mutants (range=0.8-2.8 kb; MTL=1.7 kb) (Figure II-6D). We conclude that combined loss of TAD3 and POT1a accelerates telomere shortening relative to the loss of POT1a alone.

Progressive telomere shortening ultimately causes profound developmental defects as a consequence of genome instability (Riha et al., 2001). Consistent with the hypothesis that TAD3 acts additively with telomerase, there was accelerated shortening of telomeres in *pot1a tad3-2* mutants (Figure II-6C and II-8A), which correlated with an early onset of stem cell-related defects (Figure II-7A and II-8B). *tad3-2* mutants displayed no visible developmental defects for three generations (Figure II-7A and II-8B). Importantly, *pot1a* single mutants were indistinguishable from wild type in G2 (Figure II-7A). We categorized *pot1a tad3-2* plants into three groups: class I mutants were similar to wild type; class II plants had stunted growth with leaf abnormalities, constricted rosettes, and occasional hook-shaped siliques; and class III mutants were more severely impacted than class II (Figure II-7A). The number of class II and class III mutants increased with each generation (Figure II-7B). Pollen viability of G2 *pot1a tad3-2* was decreased relative to wild type or either single mutants (Figure II-7C), and later generation *pot1a tad3* plants were sterile, failing to produce any siliques (Figure II-7A).

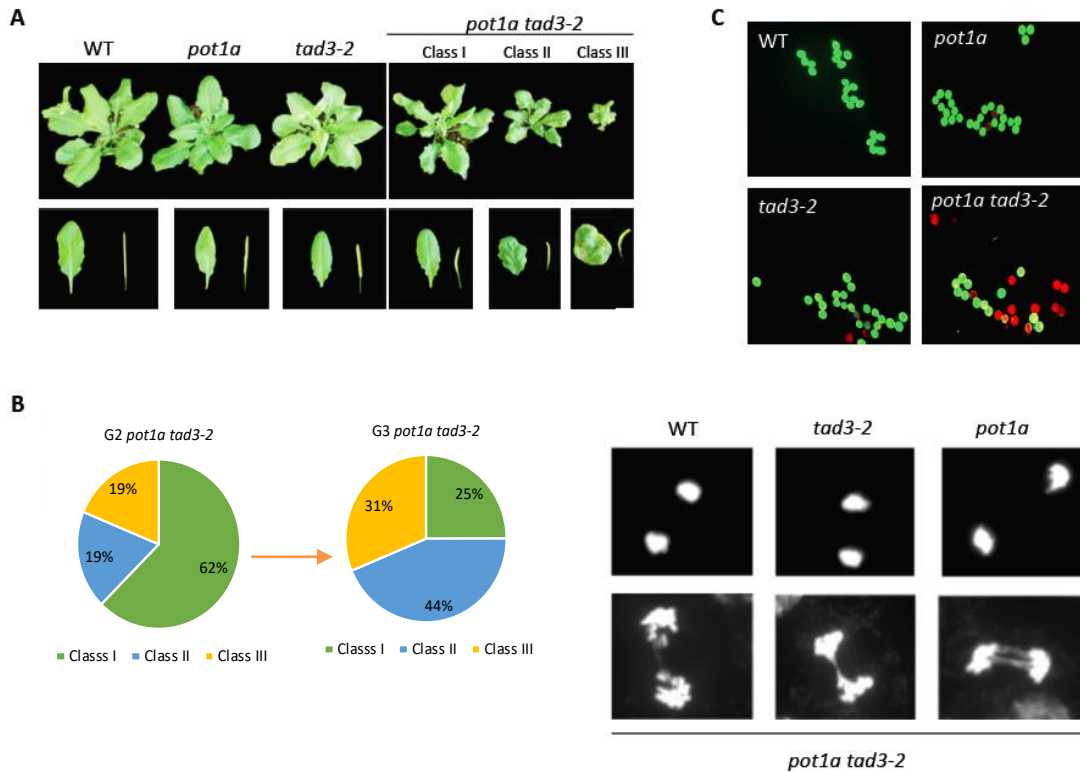


**Figure II-7 Exacerbated reproductive and developmental defects and genome instability in *pot1a tad3-2* mutants.**

(A) Photos of rosettes, individual leaves and siliques from three-week-old WT, G2 *tad3-2*, G2 *pot1a* and G2 *pot1a tad3-2* plants. Siliques and leaves were collected from the same position for all samples. For G2 *pot1a tad3-2* mutants representative images from three phenotypic classes (I, II, and III) are shown. (B) Pie chart illustrating the relative fraction of plants belonging to each phenotypic class of G2 *pot1a tad3-2* double mutants. (C) Viability of pollen grains produced by WT, G2 *tad3-2*, G2 *pot1a* and G2 *pot1a tad3-2* assessed with the FDA staining protocol (Li 2011) in combination with PI staining. Live pollen metabolizes the FDA into green colored fluorescein. PI stains dead pollen. (D) Mitotic spreads of anaphase were made from flower pistils of four-week-old WT, G2 *tad3-2*, G2 *pot1a* and G2 *pot1a tad3-2* plants using previously published protocol (Surovtseva et al. 2009). Chromatin was stained with DAPI and observed with 100X magnification on a fluorescent microscope.

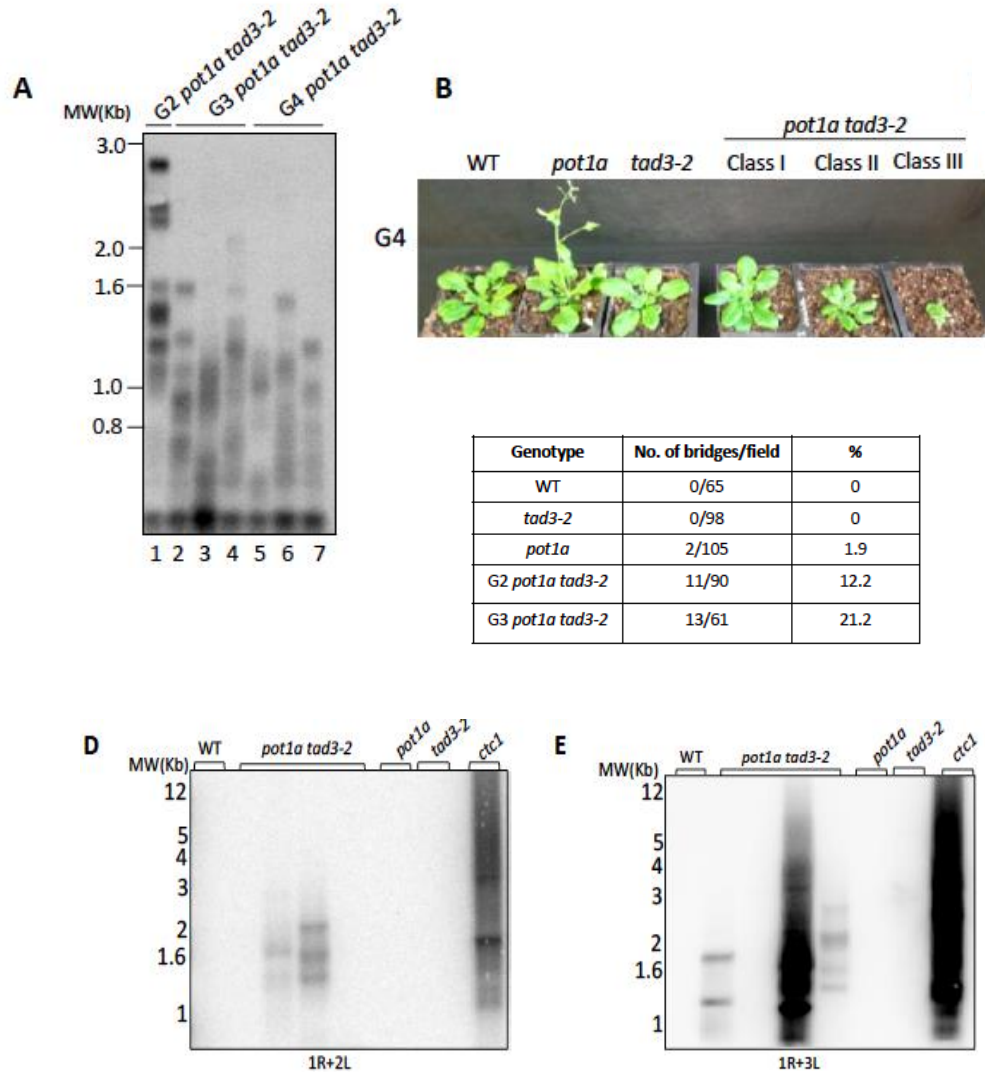


**Figure II-8 Combined loss of TAD3 and POT1a accelerates the onset of telomere dysfunction.**

(A) Results of TRF analysis for consecutive generations of individual *pot1a tad3-2* mutants from G2 (lane 1), G3 (lanes 2-4) and G4 (lanes 5-7). (B) Images of rosettes from three-week-old WT, G4 *tad3-2*, G4 *pot1a* and G4 *pot1a tad3-2* plants. Examples of plants from the different classes of G4 *pot1a tad3-2* mutants are shown. (C) Quantification of anaphase bridges obtained from analysis of mitotic figures of plants with the genotypes indicated (refer to materials and methods for the protocol used). (D) and (E) Results from Telomere Fusion PCR with WT, *tad3-2*, *pot1a* and *pot1a tad3-2* samples. DNA from a *ctc1* null mutant (Surovtseva et al., 2009) served as the positive control. The sub-telomeric primers used for PCR amplification are indicated below each blot.

The worsening of developmental phenotypes correlated with an increased incidence of telomere tracts below the critical 1kb length threshold (Heacock et al., 2004) (Figure II-8A). Analysis of mitotically dividing cells revealed 12% of the anaphases in G2 *pot1a tad3-2* harbored bridged chromosomes, consistent with telomere-to-telomere fusion, compared to 1.9% in *pot1a* and 0% in *tad3-2* and wild type siblings (Figure II-7D and II-8C). The percentage of anaphase bridges increased to 21% in G3 *pot1a tad3-2* (Figure II-8C). Telomere fusion PCR experiments confirmed that the chromatin bridges reflected end-to-end chromosome joining through telomeres (Figure II-8D and II-8E).

The data presented thus far suggest that TAD3 and telomerase act in parallel pathways to maintain telomere length. However, an alternative possibility is that TAD3 acts in a pathway overlapping with telomerase. Although repeat addition processivity of telomerase is severely compromised in *pot1a* mutants, enzyme activity is not entirely abrogated (Surovtseva et al., 2007). Thus, with both TAD3 and POT1a simultaneously inactivated, telomerase activity could be entirely abolished. To test this, qTRAP was performed with *pot1a tad3-2* mutants. There was no difference in telomerase activity in *pot1a tad3-2* mutants compared to *pot1a* (Figure II-6E), indicating that TAD3 is not required for maximal telomerase stimulation.

Finally, we asked if TAD3 was required for telomerase recruitment and enzymology at chromosome ends *in vivo* by assessing how the loss of TAD3 impacted telomere elongation in plants lacking Ku70. If telomere elongation in *ku70* mutants requires TAD3, then plants doubly deficient in both Ku70 and TAD3 should not have ultra-long telomeres. To test this hypothesis, we crossed *ku70* and *tad3-2* single mutants



and segregated double mutants from *Ku70*<sup>+/-</sup> *TAD3-2*<sup>+/-</sup> parents. TRF analysis performed with the G2 siblings, revealed no difference in telomere length in G2 *ku70 tad3-2* plants compared to G2 *ku70* (Figure II-6F). Thus, TAD3 does not appear to play a critical role in promoting telomerase engagement and extension at chromosome ends. Altogether, our results support the conclusion that TAD3 acts independently of telomerase for telomere length maintenance.

### **Telomere terminal architecture is unperturbed in *tad3-2* mutants**

Another explanation for the telomere shortening phenotype is that telomere architecture is compromised in *tad3-2* mutants, leaving chromosome ends vulnerable to inappropriate nucleolytic processing. Telomere integrity cannot be grossly altered since *tad3-2* mutants do not suffer end-to-end fusions, but to test for subtle perturbation, we measured the status of the G-overhang using in-gel hybridization (Riha et al., 2000). The G-overhang signal was increased in *ku70* mutants by 2.5-fold (Figure II-9A), consistent with the conversion of blunt-end telomeres into G-overhangs (Kazda et al., 2012b). In contrast, we found no difference in the G-overhang signal in G2 *pot1a tad3-2*, G2 *tad3-2*, and G2 *pot1a* mutants compared to wild type (Figure II-9A). Next, we examined the integrity of blunt end telomeres using the dUTP-PENT assay (Kazda et al., 2012b). As expected, approximately 55% of the signal was retained in wild type samples after UDG treatment, confirming half the telomeres are blunt ended, while in *ku70* mutants, the signal was reduced by ~89%, consistent with conversion of most blunt ends into G overhangs (Figure II-9B). *tad3-2* mutants exhibited a wild type level signal (~50%) after UDG

treatment. We verified blunt end telomeres in *tad3-2* mutants using a hairpin ligation assay (Kazda et al., 2012a; Valuchova et al., 2017b). Blunt-ended telomeres migrate as a higher molecular weight smear and then are lost upon BamHI digestion. A high molecular weight smear sensitive to BamHI was observed in both wild type and *tad3-2* samples, but not in *ku70* (Figure II-9C). We conclude that TAD3 does not play an essential role in maintaining the proper architecture of chromosome termini.



### **Loss of TAD3 impacts many cellular pathways**

Given the essential role of tRNA deaminases in translation (Torres et al., 2014a), TAD3 is expected to impinge on many cellular pathways. To gain insight into the global impact of TAD3 mutation, we further analyzed RNA-seq data from *tad3-2* and wild type seedlings to identify differentially expressed genes (DEGs). We used Limma-Voom on the web-based program Galaxy (Afgan et al., 2018), with FDR<0.05. DEG with more than two-fold change in *tad3-2* compared with wild type was fed into G: Profiler (Reimand et al., 2007) to determine the functional enrichment of gene ontology (GO) terms. A total of 980 RNAs were differentially accumulated in *tad3-2* mutants; 598 were upregulated and 382 were downregulated. Notably, no telomere-related gene was identified as a DEG.

GO terms are categorized by Molecular Function (MF), Biological Pathway (BP) and Cellular Compartment (CC). We observed significant enrichment of GO terms in the BP category, with a large number of downregulated genes associated with auxin signaling, auxin transport, and cellular response to auxin. Other downregulated genes were associated with the cellular response to chemicals and growth, both of which are also related to auxin-related processes (Figure II-10A). In contrast, upregulated genes showed significant enrichment of GO terms related to secondary metabolic processes, secondary metabolite synthesis, and particularly with the glucosinolate biosynthetic pathway (Figure II-10A).

Since based on the RNA-Seq experiments *tad3-2* mutants respond to zeocin treatment in a manner indistinguishable from wild type, we re-examined our RNA-seq dataset in an effort to find more direct targets of TAD3 by looking at DEGs between

zeocin-treated *tad3-2* and wild type seedlings. This stringent analysis resulted in 166 differentially accumulated RNAs in *tad3-2* mutants, of which 105 were upregulated and 61 were downregulated (Figure II-11A). GO analysis of the new gene pool was consistent with the previous analysis: the downregulation of auxin homeostasis and signal transduction pathway and upregulation of glucosinolate biosynthesis as the most affected processes in the hypomorphic *tad3-2* mutant (Figure II-11A).

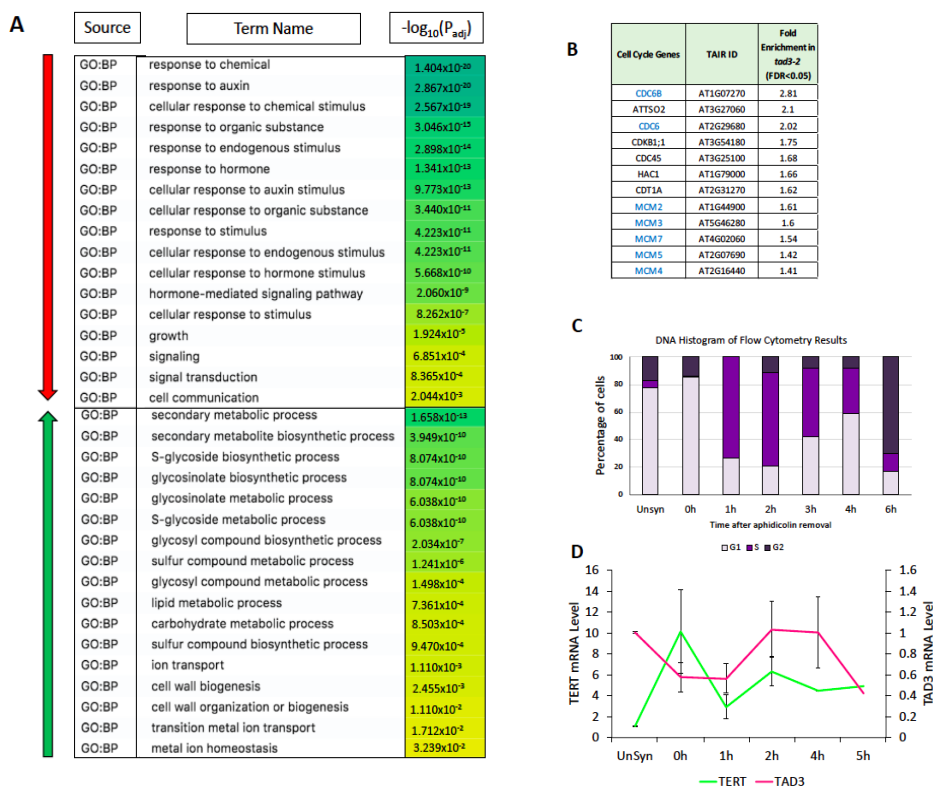


**Figure II-10 Transcriptomic analysis reveals changes in auxin signaling, plant secondary metabolism and cell cycle-related genes due to loss of TAD3.**

(A) Gene ontology analysis performed with differentially regulated genes in 6-day-old *tad3-2* seedlings compared to 6-day-old WT seedlings. Table contains GO term source, term name and with the numerical p-value expressed as a function of intensity of the green color. p-values greater than  $10^{-16}$  are highly significant (Reimand et al. 2007). Red and the green arrows represent genes downregulated or upregulated in the *tad3-2* mutants, respectively. (B) Expression data for some critical cell cycle and DNA replication related genes in *tad3-2* mutants derived from transcriptome data. (C) FACS data obtained from Aphidicolin-synchronized T87 cell culture. Graph shows a time course of the fraction of cells in each phase of the cell cycle post release from the drug. (D) qRT-PCR results for TAD3 and TERT mRNA levels in synchronized T87 cell culture. Each data point represents the mean value from two biological replicates.

Finally, given the importance of TAD3 in cell cycle progression in fission yeast (Tsutsumi et al., 2007), we specifically looked for changes in expression of 150 critical cell cycle regulators and DNA replication factors in *tad3-2* mutants. We found that the MCM gene cluster (MCM2, MCM3, MCM4, MCM5, MCM7) exhibited a 1.5 - 1.8-fold increase in *tad3-2*, while CDC6 and CDC6B expression increased by almost 2.1-fold (Figure II-10B). Both CDC6 and MCM gene clusters initiate S phase by licensing origins for DNA replication (Borlado and Méndez, 2008; Das et al., 2014). Loss of TAD3 also led to elevated expression for some cell cycle regulators including CDKB11 (1.6 fold), HAC1 (1.66), CDC45 (1.69) and CDT1 (1.62) (Figure II-10B). Thus, TAD3 modulates expression of numerous cell cycle related genes.

We investigated the expression pattern of TAD3 across the cell cycle in *Arabidopsis* using synchronized T87 *A. thaliana* cell culture (Menges and Murray, 2006). Cells were treated with Aphidicolin to arrest them in G1/early S phase. FACS analysis was done at various points after releasing the block to monitor cell cycle progression (Figure II-10C) and transcript levels were measured. TERT and POT1a mRNA peaked during the G1/S phase transition (Figure II-10D and II-11B). In contrast, TAD3 mRNA levels declined during the G1/S transition and early S phase, rising again during late S phase through the middle of G2 (Figure II-10D). The data suggest that TAD3 expression is regulated across the *Arabidopsis* cell cycle, but in a manner distinct from telomerase components.

**A**

Source	Term Name	$-\log_{10}(P_{adj})$
GO:BP	auxin homeostasis	$1.4761 \times 10^{-7}$
GO:BP	regulation of biological quality	$1.805 \times 10^{-3}$
GO:BP	regulation of hormone levels	$1.652 \times 10^{-2}$
GO:BP	response to auxin	$2.416 \times 10^{-2}$
GO:BP	thalianol metabolic process	$2.648 \times 10^{-5}$
GO:BP	tricyclic triterpenoid metabolic process	$1.057 \times 10^{-4}$
GO:BP	triterpenoid metabolic process	$3.905 \times 10^{-4}$
GO:BP	secondary metabolic process	$6.438 \times 10^{-4}$
GO:BP	indole glucosinolate metabolic process	$4.562 \times 10^{-3}$
GO:BP	sulfur compound metabolic process	$8.658 \times 10^{-3}$
GO:BP	S-glycoside metabolic process	$9.573 \times 10^{-3}$
GO:BP	glucosinolate metabolic process	$9.573 \times 10^{-3}$
GO:BP	glycosyl compound metabolic process	$1.203 \times 10^{-2}$

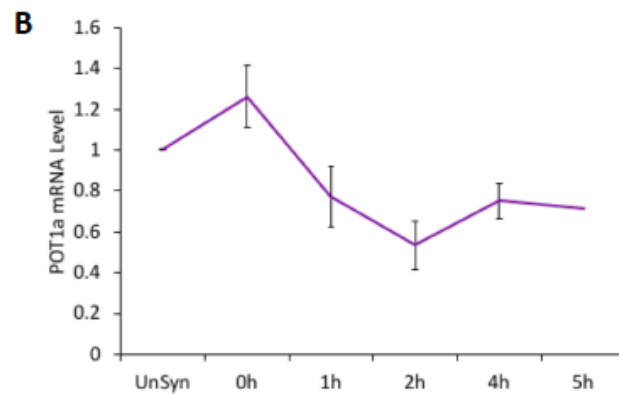


**Figure II-11 Cell cycle regulated expression of telomerase components and gene ontology analysis of WT and *tad3-2* transcriptomics data.**

(A) Gene ontology analysis performed with differentially regulated genes in zeocin treated six days old *tad3-2* seedlings compared to zeocin treated 6-day-old WT seedlings. (B) Results for qRT-PCR performed for POT1a mRNA in T87 synchronized cell culture. Each data point represents the mean value from two biological replicates.



## Discussion

Telomere length maintenance is essential for the stability of linear genomes. Over the past two decades, multiple genetic screens, interactome assays, and QTL mapping experiments illustrate the influence of "non-canonical" pathways in telomere length regulation. Remarkably, genome-wide studies in *S. cerevisiae* revealed that >5% of nonessential (Askree et al., 2004) and >11% of essential (Ungar et al., 2009) genes are necessary for telomere maintenance. Recently, translation-related factors have emerged as critical determinants of telomere length homeostasis (Abdulkina et al., 2019; Askree et al., 2004; Fu and Collins, 2007; Gatbonton et al., 2006; Gupta et al., 2013; Heiss et al., 1998; Lin and Zakian, 1996; Maas et al., 1999; Ungar et al., 2009; Walne et al., 2007). One of essential gene affecting telomere length in budding yeast is YLR317W, a transcript produced from the *TAD3* locus (Ungar et al., 2009). Here we demonstrate the importance of *TAD3* in telomere length maintenance in *A. thaliana*. We further show that this function is mediated by a noncanonical, telomerase-independent mechanism, highlighting the importance of cross-functional pathways in telomere biology.

Previously we described a telomerase regulatory function for the long non-coding RNA *AtTER2* encoded on the opposite strand and partially overlapping with the 5' UTR of *TAD3* (Cifuentes-Rojas et al., 2012). In considering updated *A. thaliana* genome annotation (Araport 11) showing that *AtTER2* is fully embedded into the 5' UTR of *TAD3* and the demonstration that TER1 was not the true telomerase RNA subunit (Dew-Budd et

al., 2020; Fajkus et al., 2019) led us to revisit the *TER2* locus using strand-specific qRT-PCR and transcriptomic analyses. We report that *TAD3* does not give rise to a stable lncRNA, and hence telomere-related functions derive from the *TAD3* gene itself.

Because a null mutation in *TAD3* leads to embryonic lethality (Agorio et al., 2017), we obtained a new hypomorphic *tad3* mutant (*tad3-2*) to further explore its function in telomere biology. We discovered that in *tad3-2* mutants, the longest telomere tracts shortened progressively over successive generations, while shorter telomeres remained unchanged. A similar profile is observed in cells haploinsufficient for key telomerase components (Armanios et al., 2005; Goldman et al., 2005; Harrington, 2012). However, *ex vivo* qTRAP assays indicated wild type levels of telomerase activity in *tad3-2* mutants. In addition, analysis of *ku70 tad3-2* mutants revealed that telomerase can fully access and extend telomeres in plants deficient in TAD3. Strikingly, defective telomere maintenance in *tad3-2* mutants is strongly exacerbated in plants also lacking the telomerase processivity factor POT1a, with double mutants exhibiting an early onset of developmental defects and genome instability arising from telomere dysfunction. Thus, TAD3 facilitates telomere length homeostasis via a telomerase-independent pathway.

How could TAD3 promote telomere maintenance? TAD3 encodes a tRNA-editing deaminase that converts adenosine to inosine at the wobble 34 position of the tRNA anticodon loop (Torres et al., 2014a). This modification expands pairing to A, U, C at the 3rd position of a codon (Crick, 1966; Grosjean et al., 2010). I34 is critical for reading and translating C-ended codons (Lim, 1995) for Ala, Ser, Pro, and Thr (Rafels-Ybern et al., 2015, 2018). Consequently, compromising TAD3 is expected to impact many cellular

pathways (Schimmel, 2018a). Analysis of human transcriptome and proteome data confirm the importance of adenosine deaminases (ADATs) in translating transcripts rich in these same four codons (Rafels-Ybern et al., 2015). Because such translation-related data are unavailable for *A. thaliana*, we performed a transcriptome analysis on *tad3-2* mutants to examine how decreased expression of *AtTAD3* impacts plant metabolism.

Over 6000 genes are differentially regulated upon loss of TAD3, but intriguingly none are associated with known telomere pathways. Instead the genes are concentrated in two major areas with significant downregulation of the auxin signal transduction pathways and significant upregulation of the glucosinolate biosynthetic pathway. Notably, both metabolic processes intersect stress response, cell cycle regulation and DNA metabolism. Reduced auxin signaling may account for the elevated PCD in the RAM of *tad3-2* mutants in response to zeocin. Our RNA-seq data and comet assays showed that *tad3-2* mutants mount a normal DDR and do not accumulate more DNA damage than wild type under normal conditions. Auxin inhibits PCD during plant development and in response to stress (Awwad et al., 2019). Under normal conditions, auxin concentrations in root stem cell niche peak in the quiescent center and follow a local gradient at the root tip. However, in response to environmental stress, auxin levels decline, leading to PCD induction in roots (Hong et al., 2017). Thus, lower levels of auxin in *tad3-2* mutants may sensitize plants to PCD in response to stress. Alternatively, down regulation of auxin signaling may render chromatin more vulnerable to zeocin treatment. Auxin has recently been shown to increase chromatin compaction, and its inhibition results in increased DNA damage upon zeocin treatment (Hasegawa et al., 2018).

Our transcriptomic data analyses also revealed that *tad3-2* mutants significantly upregulate genes in the glucosinolate biosynthetic pathway. Glucosinolates are secondary metabolites in cruciferous plants that serve as antimicrobials and defend against herbivory. Interestingly, glucosinolate accumulation regulates cell cycle progression in *Arabidopsis* and reduces the rate of DNA replication in wild type plants, causing cells to accumulate in S phase (Åsberg et al., 2015; Chezem and Clay, 2016). Despite the wide array of mutant phenotypes expected for TAD3 mutation, the predominant feature of *tad3* mutation in fission yeast is a cell cycle defect (Tsutsumi et al., 2007). While the changes were not as dramatic as in other metabolic pathways, we observed a surge in expression of genes that regulate cell cycle and promote DNA replication. In addition, we found that *TAD3* expression peaks during mid S phase, after *TERT* and *POT1a*. Telomere replication and processing require a dynamic switch from a protective state to an open conformation and back again (Gobbini et al., 2014), and thus cell cycle perturbation can alter telomere length and terminal architecture (Londoño-Vallejo and Wellinger, 2012; Sarek et al., 2019; Verdun et al., 2005; Vodenicharov and Wellinger, 2007). Although we saw no obvious change in the status of G-overhangs or blunt end telomeres in *tad3* mutants, our experiments were performed on asynchronously growing seedlings. It is possible that a subtle shift in cell cycle progression in *tad3* mutants decreases telomerase access to telomeres or increases access for nucleolytic processing enzymes, either of which would lead to telomere shortening.

We conclude that the *TAD3* locus indirectly contributes to telomere length homeostasis in *Arabidopsis* by altering the metabolic profile. Understanding precisely

how cross-functional pathways influence telomere biology may shed new light on how telomeres serve as both sentinels and elicitors of physiological stress.

## **Material and Methods**

### *Plant materials, genotyping and genetic complementation*

Seeds for *tad3-1* (SAIL\_556\_A04), *tad3-2* (SALK\_121147) and WT Col-0 accessions along with T87 cell culture for the Col-0 accession were obtained from the ABRC stock center. Seeds were sterilized using 70% ethanol, 10% bleach and 0.1% Triton X-100 followed by vernalization for 2 days at 4°C. Seeds were plated on half Murashige and Skoog (RPI M10500) and 1% agar (Caisson A038) supplemented with 1% sucrose. Plants were grown in soil in controlled growth chambers maintained at 22°C under long day light conditions. Photographs to assess plant growth and development were captured using a digital camera.

Genotyping (primer sequences in Supplemental Table I) was performed with leaf DNA and emerald enzyme master mix (Clontech RR310A). *pot1a tad3-2* double mutants and *ku70 tad3-2* double mutants were generated by crossing plants heterozygous for *pot1a* and *tad3-2* or *ku70* and *tad3-2* followed by segregating progeny for multiple generations. For genetic complementation, 3-week-old G2 *tad3-2* plants were transformed with *Agrobacterium* (GV3101) cells harboring the plasmid pCBK05::NP<sup>TAD3</sup>::TAD3 using the floral dip method (Zhang et al., 2006). Resistance to BASTA and Carbenicillin was used to select for true transformants in the next generation (G3).

### RNA-Seq, transcriptome data visualization and analysis, and qRT-PCR

RNA extracted from 6-day-old seedlings was used to make RNA libraries in triplicate using the Illumina TruSeq® Stranded Total RNA Library Prep Plant (Catalog no. 2002061). After trimming the raw sequences using the Trimomatic program (Galaxy Europe), datasets were concatenated for each biological replicate and aligned to the *A. thaliana* reference genome sequence (TAIR10\_v90) using RNA\_STAR. The Bed file generated by RNA\_STAR was visualized in SeqMonk to determine the density of raw reads aligning to various locations in the genome. To obtain the dataset for the Differentially Expressed Genes (DEG), the bed file was processed using the featurecounts program followed by the limma-voom software. For Gene Ontology analysis, the list was fed into G:Profiler(Reimand et al., 2007). For qRT-PCR, the Zymo Research kit (R2051) was used for RNA extraction. Strand-specific qRT-PCR was performed using cDNA synthesized from 1 µg total RNA using Super Scriptase IV (Thermo Fisher:18090050) and strand-specific primers (primer sequences in Supplemental Table I) followed by qPCR using PowerUp SyBr Green (Thermo Fisher: A25741). For non-stranded cDNA synthesis, a cDNA synthesis kit (Quanta:95047) was used with the same protocol for qPCR.

### Zeocin treatment, PI staining and pollen viability assays

4- or 5-day-old seedlings grown on 0.5X MS media with 1% sucrose and 1% agar were transferred to six well plates containing MS media (Mock) or MS media plus 20 µM of Zeocin (Thermo Fisher Scientific - R25001). Plates were wrapped in aluminum foil and left on a shaker (100 RPM) for 2, 4 and 6 h. After treatment, seedlings were transferred to six well plates filled with PI stain solution (10 mg/ml; Sigma P4170) dissolved in H<sub>2</sub>O.

After 30 sec, seedlings were washed in ddH<sub>2</sub>O, transferred to slides in a droplet of H<sub>2</sub>O, sealed with a cover slip and imaged at 10X using a dsRED filter and brightfield of a Zeiss fluorescence microscope. Pollen viability was assessed as described (Li, 2011). For accuracy and highest yield, the assay was performed with flowers collected between 6 AM and 8 AM. Slides containing pollen grains were imaged using a GFP filter (blue light, wavelength = 495 nm) on a Zeiss fluorescence microscope.

#### Comet Assay

The comet assay was performed with protoplasts using a comet assay kit from Trevigen (4250-050-K) following the manufacturer's directions with minor modifications. Protoplasts were extracted (He et al., 2006) from 6- or 7-day-old WT, *atr* (At5g40820) and *tad3-2* seedlings. A concentration of  $2 \times 10^5$  cells/ml was used for the assay. Slides were run in an electrophoretic set up at 18 V for 10 minutes in complete darkness. After drying the agarose, slides were stained with PI stain (100 µg/ml), sealed with a cover slip and imaged using a Zeiss fluorescence microscope at 5X magnification with a dsRED filter. The parameters (Percentage DNA in tail, Tail Length, Tail Moment) were calculated using Open Comet Software (<http://www.cometbio.org/>). Refer to Appendix A for a detailed description of the comet assay.

#### Telomere and telomerase analysis

TRF assays were performed with 3- to 4-week-old plants as described (Kobayashi et al., 2019). To obtain high quality DNA, phenol chloroform extraction was performed twice while extracting the DNA from plant tissues. Telomere length was quantified using TeloTool (Göhring et al., 2014). Telomere fusion PCR was performed using 2 µg of DNA

as described (Heacock et al., 2004). Fusions were monitored between the right arm of chromosome 1 (1R) and left arm of chromosome 2 (2L), and between 1R and the left arm of chromosome 3 (3L) using primer indicated in Supplemental Table I. G-overhangs were assessed using in-gel hybridization as described previously (Riha and Shippen, 2003a) with slight modifications. Plants no older than 3 weeks were used for the assay to obtain high-quality DNA. To assess blunt end telomeres, the hairpin-ligation assay and the UDG PENT assays were performed using 150 µg of high quality DNA quantified using a Qubit Analyzer as described (Kazda et al., 2012b). Quantitative TRAP was conducted as described (Song et al., 2019) with two minor modifications. Buffer W+ (1M Tris-Acetate pH 7.5, 1M MgCl<sub>2</sub>, 2M KGlu, 0.5M EGTa, 30% PVP, Glycerol, 1µM DTT, 0.6 nM VRC, 1µM PMSF) was used to resuspend ground tissues (flowers or seedlings). The protein pellet was resuspended in buffer W+ supplemented with RNaseOUT (Thermo – 10777019). Debris were removed before measuring the protein concentration using Bradford reagent. Primer extension was performed with primer sequences in Supplemental Table I for 45 min at 25°C followed by qPCR using Dynamo SyBr mix (Thermo: F410L).

### Anaphase bridges

Mitotic spreads from flower pistils were prepared and analyzed as described (Heslop-Harrison, 1998; Surovtseva et al., 2009). The spreads were stained with commercial DAPI solution (IHC-Tek 1W-1404), and imaged at 100X using a DAPI filter in Nikon Ti fluorescence microscope.



Cell culture synchronization and flow cytometry

T87 cell culture was maintained in NT-1 media on a rotary shaker (120 RPM) under continuous light for 24 h and every 7 days cells were subcultured into fresh NT-1 media (1:2 v/v). For cell synchronization, 5 mL of early stationary phase T87 cell suspension (7 days after previous subculture) was subcultured into 75 ml fresh NT-1 medium in a 250 mL Erlenmeyer flask. The flask was incubated at 24°C, 120 rpm under constant light for 7 days. 12 mL of the cell suspension was transferred into 60 ml fresh NT-1 medium to achieve a dilution of 1:5. 10 mL cell suspension was cleaned by filtration through sterilized miracloth. Excess liquid was removed with a paper towel, and an aliquot of unsynchronized cells was frozen in liquid nitrogen. To block cells in G1/early S phase 173 µl aphidicolin stock solution of 5mg/ml (Sigma Aldrich, Catalog no. A0781) was added to 72 mL of diluted cell suspension to obtain a final concentration of 12 µg/mL. The culture was incubated at 24°C, 120 rpm under constant light for 23 h. To release the block, cells were filtered through miracloth, washed vigorously with 500 ml NT-1 medium and resuspended in 60 ml NT-1 medium. Aliquots were taken at various times for DNA content analysis. The first aliquot was labeled “T0”. The remaining cell culture continued to incubate at 24°C, 120 RPM under constant light and samples were collected each hour. For FACS analysis, frozen cells were transferred to a clean petri dish and 1 ml of cold homogenization buffer (25 mM PIPES (pH 7), 10 mM NaCl, 5 mM EDTA (pH 8), 250 mM Sucrose, 0.15 mM Spermine, 0.5 mM Spermidine, 20 mM -mercaptoethanol, 1% NP-40, 1 mM PMSF) was added. Cells were chopped with a razor blade to release nuclei followed by addition of 1 ml homogenization buffer. Cells were resuspended using a

p1000 pipet and transferred into a new tube for 2 min. A 40  $\mu\text{m}$  cell strainer (Merck or BD Falcon) was placed into a 50 ml falcon tube and the tube placed on ice. Resuspended cells were strained and collected into the cold falcon tube. Nuclei were collected by centrifugation at 7000 RPM for 20 min at 4°C then resuspended in homogenization buffer. Samples were treated with RNaseA at a final concentration of 15  $\mu\text{g}/\text{mL}$  followed by incubation at RT for 10 min. Nuclei were stained with 60  $\mu\text{g}/\text{ml}$  of propidium iodide (PI) and samples were run on a Becton-Dickinson FACSCalibur at 488 nm at the Flow Cytometry Core Facility, VMBS, Texas A&M University. DNA content was analyzed using CellQuest (Becton-Dickinson) and ModFit LT (Verity) programs.

## CHAPTER III

### PROTECTION OF TELOMERES 1B IS NECESSARY FOR CHROMATIN

#### COMPACTION DURING CELL DIVISION IN *Arabidopsis thaliana*

##### **Abstract**

Telomeres are repetitive DNA sequences present at chromosome ends, which shield chromosomes from unwanted damage and degradation through binding of multiple protein complexes. Protection of Telomeres 1 (POT1), a member of the shelterin complex, safeguards telomeres from damage and is important for telomere length maintenance. *A. thaliana* encodes two POT1 proteins, POT1a and POT1b. While the telomeric roles of POT1a are understood, the function of POT1b remains elusive. Recent data showed that loss of POT1b increased telomerase activity, but did not impact telomere length. Transcriptomics data indicated that loss of POT1b upregulates several oxidative stress related pathways, and *pot1b* mutants overaccumulate reactive oxygen species (ROS). Moreover, POT1b is dually localized to the nucleus and to peroxisomes and it interacts with the peroxisomal enzymes CAT2 and CAT3 in yeast-two-hybrid (Y2H) experiments. In multiple organisms, ROS overaccumulation impacts chromatin architecture. Here, I investigate the effects of loss of POT1b function on genome structure, locally at telomere-ends and globally on chromatin structure during cell division. Through biochemical and cytological approaches, I found that POT1b does not affect telomere-end architecture, but *pot1b* mutants exhibit aberrant chromatin phenotypes particularly chromatin decondensation, that can be partially rescued by POT1b complementation. Aberrant

chromatin was also observed in *cat2* and *pot1a* mutants, which incidentally also over accumulate ROS. I conclude that POT1b is essential for maintaining proper chromatin compaction and integrity of dividing cells in *Arabidopsis thaliana*, beyond telomeres.

## **Introduction**

Protection of Telomeres 1 (POT1) proteins are one of the solutions to the end protection problem of linear genomes. Their primary roles include protecting telomeres from unwanted nucleolytic attack and inhibiting telomeric fusions (Calvete et al., 2017). However, the exact mechanism of POT1-mediated telomere protection varies among organisms (Baumann and Price, 2010). For instance, *S. pombe* POT1 protects telomeres from degradation, and loss of SpPOT1 leads to telomere shortening and chromosome fusions (Baumann and Cech, 2001). On the other hand, human POT1 regulates telomere length by both positively and negatively regulating the telomerase complex (Veldman et al., 2004). By associating with TPP1, hPOT1 acts as a telomerase processivity factor, thereby facilitating telomere repeat addition (Latrick and Cech, 2010; Wang et al., 2007). However, during late S phase, hPOT1 limits telomerase accessibility to elongated telomeres and negatively regulates telomere lengthening (Chen et al., 2007; Kelleher et al., 2005). hPOT1 also protects telomeres from eliciting a DNA damage response (DDR) by inhibiting Replication Protein A (RPA) binding to telomeres. Upon binding, RPA activates ATR-mediated DNA damage repair, which at the telomeres leads to genomic instability (Hockemeyer et al., 2005). Loss of hPOT1 results in chromosome fusions that impede proper chromatin segregation during cell division. Therefore, hPOT1 in addition

to being critical for genome stability and telomere maintenance, plays an important role in chromatin segregation (Gu et al., 2017).

Along with their telomere-specific roles, some telomere-associated proteins (TAPs) also function beyond telomeres. For example, hPOT1 facilitates the repair of DNA double-strand breaks (DSBs) at non-telomeric regions by promoting precise DDR via the Non-Homologous End Joining Pathway (NHEJ) (Yu et al., 2017). Similarly, hTERT translocates to mitochondria upon oxidative stress where it promotes mitochondrial functions and stability (Gordon and Santos, 2010).

Although most organisms encode a single *POT1* gene multiple *POT1* paralogs are observed in protozoa, worms, plants and rodents, each with specific functions (Barcenilla and Shippen, 2019). For example, mice harbor two *POT1* paralogs, *POT1a* and *POT1b*. Both mPOT1a and mPOT1b are essential, and largely non-redundant (Palm et al., 2009). However, mPOT1a restricts ATR-mediated DNA damage signaling at telomeres (Hockemeyer et al., 2006; Kratz and de Lange, 2018) while mPOT1b is critical for maintenance of telomeric architecture. Loss of mPOT1b results in altered G-overhang structures, compromises telomere-end architecture (Palm et al., 2009; Wu et al., 2012b). The single copy hPOT1, on the other hand, fulfills the molecular functions of both mPOT1a and mPOT1b (Palm et al., 2009).

In *A. thaliana*, three *POT1* paralogs were originally identified, *POT1a*, *POT1b*, and *POT1c*. Recent exhaustive biochemical and bioinformatics analysis revealed *POT1c* is a pseudogene (Kobayashi et al., 2019). In contrast, *POT1a* and *POT1b* were found to play important roles in telomere biology and genomic stability, respectively (Shakirov et

al., 2005; Surovtseva et al., 2007). POT1a and POT1b display only 52% similarity (Shakirov et al., 2005), making them the most divergent POT1 paralog characterized to date. Analogous to its human counterpart, AtPOT1a functions as a telomerase processivity factor (Renfrew et al., 2014; Surovtseva et al., 2007). In most organisms, POT1 constitutively binds telomeric DNA; however, AtPOT1a accumulates at telomeres only during S phase (Arora et al., 2016; Surovtseva et al., 2007). This observation fits well with FACS data showing a surge in AtPOT1a mRNA during S phase (Bose et al., submitted).

Precisely how POT1b contributes to genome stability or plant biology is still unknown. Loss of POT1b does not have any impact on telomere length in *A. thaliana*, although these mutants showed increased telomerase activity (B. Barbero, unpublished). Based on recent transcriptomics analyses, there are five-fold more upregulated genes in *pot1b* mutants than downregulated genes. Moreover, the majority of the differentially regulated genes are implicated in the oxidative stress response and glutathione metabolism. Thus, the data suggests a potential role for POT1b in transcriptional repression and reactive oxygen species (ROS) homeostasis (C. Castillo-González, unpublished).

ROS are by-products of aerobic respiration and in plants they are produced in different subcellular compartments including mitochondria, chloroplasts, and peroxisomes (Janků et al., 2019). Specialized biochemical assays (e.g. 3,3'-diaminobenzidine (DAB) staining) revealed overaccumulation of ROS in *pot1b* mutants supporting a role for POT1b in ROS regulation. Notably, POT1b is present in both the nucleus and peroxisomes, and yeast-two-hybrid (Y2H) data showed that POT1b interacts

with Catalase 2 (CAT2) and Catalase 3 (CAT3), the major anti-oxidants in peroxisomes (J. H. Min, unpublished).

The findings suggest that POT1b may play an important role in peroxisomal function. One of the fallouts of elevated ROS is alteration of the global chromatin architecture (Fransen et al., 2012). Overwhelming levels of systemic ROS can modify the epigenetic marks on histones and DNA, which can lead to development of chronic ailments like cancer, diabetes and neurodegenerative disorders (Kreuz and Fischle, 2016). ROS-induced changes to the epigenome and chromatin architecture have also been reported in several plant species, (Kumar R. M. et al., 2020). For instance, tobacco cell culture exposed to oxidative stress displays DNA hypomethylation, which eventually triggers programmed cell death (Poborilova et al., 2015)

Based on (1) the dispensability of POT1b for maintenance of bulk telomere length and telomere end architecture; (2) POT1b's localization to the peroxisomes; (3) its interaction with CAT2 and CAT3; and (4) the higher levels of cellular ROS in *pot1b* mutants, we were motivated to investigate if the loss of POT1b spurs changes in global chromatin architecture. Here, I report observations from cytology-based experiments performed with *pot1b*, *pot1a*, *tert*, *cat2*, *pot1b cat2* and *tert pot1b* to explore the contribution of these proteins in chromatin structure. Compared to wild type flowers, *pot1b* mutants display multiple aberrant chromatin structures including a chromatin decondensation phenotype. Similar phenotypes were observed in *cat2*, *pot1a* and *tert* mutants, which are also found to overaccumulate ROS. I conclude that POT1b is essential

for maintaining proper chromatin structure of dividing cells in *Arabidopsis thaliana* (Figure III-1).

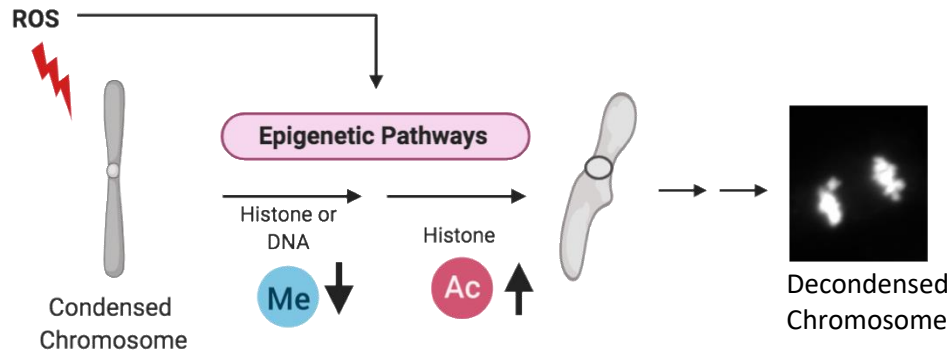


**Figure III-1 Experimental model linking oxidative stress to chromosomal aberration.**

Systemic oxidative stress in plants leads to either hypomethylation of DNA and histone or hyperacetylation of the histone, eventually modifying the level of chromatin compaction. Defects in chromosomal structure during anaphase of TAP mutants is proposed to reflect ROS induced epigenetic modifications.

## Results

### *Telomere end architecture is unperturbed in pot1b mutants*

Following the identification of *POT1b* as a paralog of *POT1a*, it was critical to decipher the role of POT1b in plant telomere biology. Two different mutant lines exist for the *POT1b* gene: *POT1b*<sub>S273F</sub> (*pot2\_110E1*) and *pot1b*Δ89. The hypomorphic *pot1b* S273F is a tilling line with a missense mutation that significantly reduces POT1b protein accumulation, while the null mutant *pot1b*Δ89 was generated by CRISPR-Cas9 and has an 89bp deletion in the first exon. Interestingly, neither *pot1b* mutant displayed a telomere



length phenotype, indicating that POT1b is not essential for telomere length maintenance in *A. thaliana* (B. Barbero, unpublished). However, the telomerase activity was slightly increased in homozygous plants of both *pot1b* mutant alleles suggesting that POT1b negatively regulates telomerase activity.

Increased telomerase activity can alter the G-overhang (Zhao et al., 2009). To ask if *pot1b* mutants display perturbation in chromosome end architecture, I monitored the intensity of the G-overhang signal by in-gel hybridization assay, and blunt-end telomeres using a hairpin-based ligation assay (Kazda et al., 2012b; Riha and Shippen, 2003b). For the G-overhang assay, *ku70* mutants were used as a positive control, respectively. For biological homogeneity, I tested the null mutant, *pot1b* $\Delta$ 89. *ku70*, as expected, showed a 2-fold enrichment of the G-overhang signal due to the previously reported phenomenon of converting the blunt-ended telomeres into G-overhangs (Kazda et al., 2012a). Interestingly, the G-overhang signal in *pot1b* $\Delta$ 89 was similar to that of wild type and *pot1a* mutants (Figure III-1). The G-overhang results were corroborated by the blunt-end assay, which also showed the same relative amount of intact blunt-ended telomeres in the *pot1b* mutants as in wild type plants (J. Song, unpublished). Therefore, the increased telomerase activity in *pot1b* mutants does not correlate with changes in bulk telomere length or perturbation of telomere-end architecture.

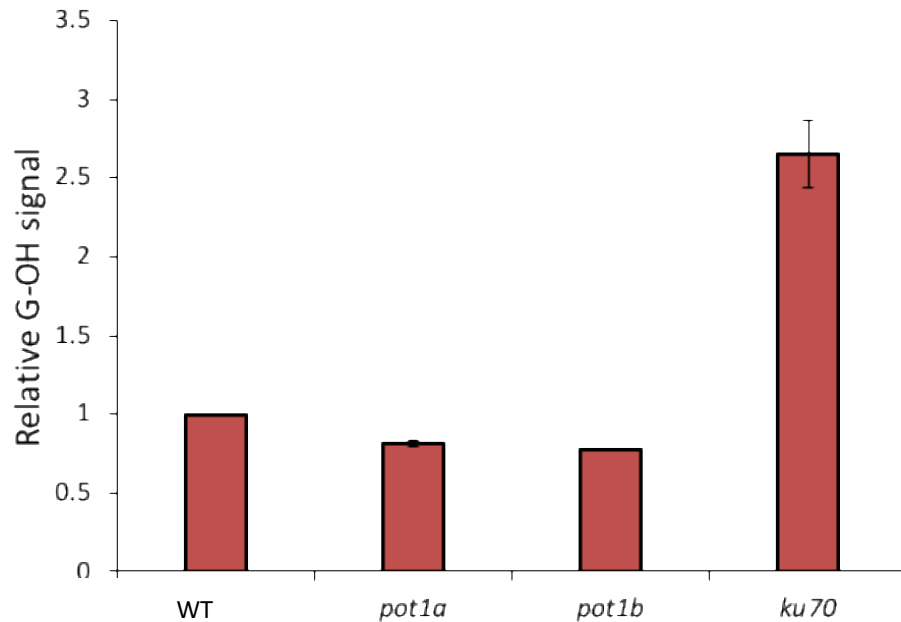


**Figure III-2 Assessment of the G-overhang structure in *pot1b* mutants**

Quantity One based quantification of the G-overhang signal plotted as a bar graph. *ku70* served as a positive control. Values greater 1 indicates more G-overhang signal relative to WT. Signal for each sample is relative to WT signal (set to 1). Results from two or more biological replicates are shown.

**Loss of *POT1b* spurs chromosomal aberrations in mitotically dividing cells**

According to the Klepikova Atlas transcriptome data, *POT1b* mRNA is expressed in young flowers, seeds (young, dry and germinating) and roots (Klepikova et al., 2016 C. Castillo-González, unpublished). Among them, the female reproductive organs carpel and stigma accumulated the highest amount of *POT1b* mRNA (Klepikova et al., 2016). Interestingly, the carpel and stigma harbors moderate levels of ROS to facilitate successful pollination and fertilization events (Duan et al., 2014). Inability to regulate floral ROS

level causes damage to the embryo sac which eventually hampers fertilization (Martin et al., 2014).

Subcellular localization experiments indicate that POT1b accumulates in the peroxisomes and nucleus (C. Castillo-González, unpublished). Peroxisomes play a critical role in redox homeostasis and peroxisomal defects are often associated with overaccumulation of cellular ROS (Fransen et al., 2012). Oxidative stress negatively impacts a large number of biomolecules and cellular components, including but not limited to, lipid peroxidation, protein degradation, mitochondrial dysfunction, DNA oxidation, and post-translation modifications of histones and other DNA binding proteins (Czarnocka and Karpiński, 2018; Kreuz and Fischle, 2016; Møller et al., 2007). Experimental data from DAB staining assays revealed accumulation of H<sub>2</sub>O<sub>2</sub> in *pot1b* mutants, which can be rescued by overexpression of wild type POT1b (J.H. Min, unpublished). Since oxidative stress is known to disrupt chromatin architecture in higher eukaryotes (Halicka et al., 2009), I asked whether *pot1b* mutants also have defects in chromatin structure and organization.

I performed cytology-based assays on pistils from second generation (G2) and fourth generation (G4) *pot1b* mutants and compared them to wild type samples. Pistils are a good source of dividing cells, and cytological analysis of pistils can offer a snapshot of on-going mitotic events (Heslop-Harrison, 1998). During anaphase, the segregating chromosomes appear as two compact balls of chromatin positioned opposite from each other. If chromosome segregation is delayed, a hook-like structure may protrude from the otherwise dense chromatin material. This structure corresponds to a "lagging

chromosome." After multiple rounds of cell division, lagging chromosome(s) may separate themselves from properly segregating chromatin to form a chromosome fragment called "micronuclei" (Thompson and Compton, 2011).

A more extreme example of chromosome segregation defects is seen with a "chromatin bridge" or "anaphase bridge," which is characterized by a thin thread-like structure stretched between segregating chromosomes (Fernández-Casañas and Chan, 2018). Defective telomeres can cause chromosomes to undergo the break-fusion-bridge cycle which entails fusion of telomeres to form dicentric chromosomes that form anaphase bridges and genome rearrangements (McClintock, 1941). Most commonly, under conditions of accelerated telomere shortening, the chromosomes eventually lose the telomeric protection which leads to chromosome fusion and formation of dicentric chromosomes (Fernández-Casañas and Chan, 2018). During anaphase, as the dicentric chromosome is pulled apart by the corresponding spindle fibers, a portion of the segregating chromatin is extended between the separating chromatin and this gives rise to the anaphase bridge structure. Internal DSBs, including those induced by ROS can also lead to chromosome fusion and corresponding formation of anaphase bridges (Wang et al., 2013).

To assess chromatin segregation in *pot1b* mutants, I analyzed 57 fields from a total of three pistils of G2 *pot1b* and 73 fields from two pistils of G4 *pot1b* and ~100 fields from three pistils of wild type. Lagging chromosomes, micronuclei, and chromatin bridges were observed in *pot1b* flowers. The number of lagging chromosomes and micronucleus in G2 *pot1b* (1.7%) increased to 5.4% in G4 *pot1b* mutants. Chromatin bridges appeared

only in G4 *pot1b* (4%). Wild type samples did not show lagging chromosomes, micronuclei or anaphase bridges (Figure III-3, Table III-1). Given that loss of POT1b did not affect the bulk telomere length, I performed telomere fusion PCR (TF-PCR) assays to determine if the chromatin bridges observed in G4 *pot1b* samples were a result of telomere dysfunction. In this assay, sub telomeric sequence specific primers are used to amplify covalently joined chromosome ends (Heacock et al., 2004). No TF-PCR product were obtained from G2 and G4 *pot1b* mutants, indicating that the anaphase bridges observed in the G4 *pot1b* mutant has a non-telomeric origin (Figure III-4).

In addition to the aberrant chromosome structures, an unusual non-uniform pattern of DAPI staining was observed in mitotically dividing cells. Specifically, segments of chromatin showed decreased DAPI signals. Occasionally, fragments of chromatin appeared to be detached from the bulk of condensed chromatin, and the overall structure looked like a fuzzy orb rather than the typical dense ball of condensed chromosomes. At times, the fainter chromatin portions looped out or formed a clawed structure. We interpret these images as decondensed chromatin. Wild type samples exhibited this phenotype in ~12% of the fields, but the frequency was much higher in G2 and G4 *pot1b* mutants, at 47% and 50, respectively (Figure III-3, Table III-1).

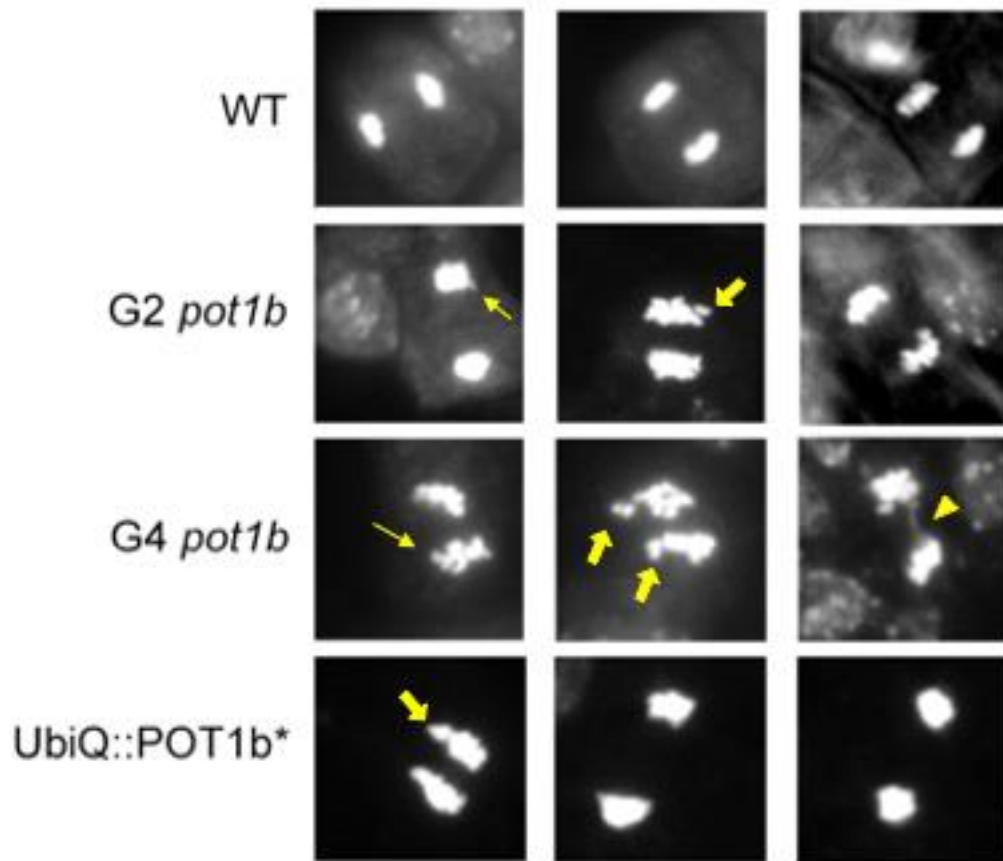


**Figure III-3 Loss of POT1b generates aberrant chromatin structure in dividing cells from flowers.**

Mitotic spreads of anaphase were made from pistils of four-week-old WT, G2 and G4 *pot1b* mutants. Chromatin was stained with DAPI and visualized at 100X magnification on a fluorescent microscope. Thin yellow arrows denote lagging chromosomes, thick yellow arrows denote micronuclei and yellow triangles denote chromatin bridges. Table III-1 has the quantification data from this experiment.


To investigate whether loss of POT1b caused these chromosomal aberrations, cytological analysis was repeated with third generation transformants (T3) of *Gn pot1b* mutants complemented with wild type POT1b expressed from a ubiquitin promoter ( $P_{UBQ}::Flag-Myc_4-gPOT1b-3'UTR_{POT1b}$ ). I analyzed 124 fields from eight pistils of the

POT1b complementation line. The percentage of fields with decondensed chromatin decreased to 17% compared to 50% in G4 *pot1b* mutants. However there remained a large number of fields with lagging chromosomes and anaphase bridges (Figure III-3, Table III-1). These results indicate that POT1b only partially rescued the chromatin defects. This may be because the *pot1b* mutant line was propagated for many generations prior to the rescue, and additional generations are needed to rescue the chromatin structure. Nevertheless, the partial rescue of the decondensed phenotype of the *pot1b* mutants suggests that the chromatin decondensation is caused by loss of POT1b function rather than a pleiotropic effect of telomere dysfunction.

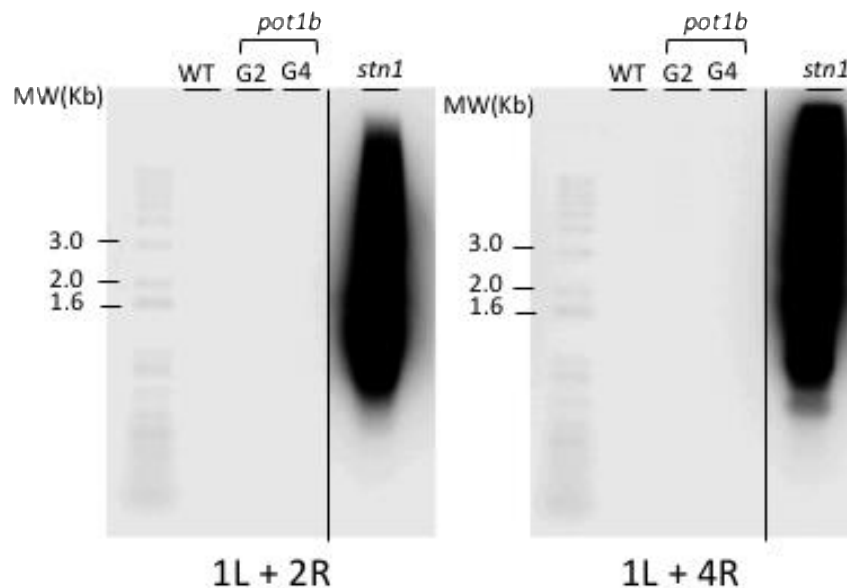


**Figure III-4 Chromatin bridges observed in *pot1b* are non-telomeric in origin.**

Results from Telomere Fusion PCR with WT, G2 and G4 *pot1b* samples. DNA from a *stn1* null mutant served as the positive control (Heacock et al., 2004). The sub-telomeric primers used for PCR amplification are indicated below each blot.



Genotype	Normal	Bridge	Lagging/Micronuclei	Decondensed Chromatin
WT (n=96)	88.54%	0%	0%	11.46%
G2 <i>pot1b</i> (n=57)	50.8%	0%	1.75%	47.36%
G4 <i>pot1b</i> (n=73)	39.7%	4.1%	5.4%	50.68%
pUbQ:: <i>POT1b</i> * (n=124)	68.54%	3.22%	11.29%	16.93%
G2 <i>pot1a</i> (n=150)	73.33%	2.67%	2%	22%
G4 <i>pot1a</i> (n=155)	39.68%	34.84%	4.51%	23.22%
G3 <i>pot1b</i> (n=77)	54.5%	0%	20.7%	24.6%
G3 <i>cat2</i> (n=162)	69.13%	0.62%	14.81%	16.04%
G3 <i>cat2 pot1b</i> (n=116)	62%	0%	12.9%	25%
G2 <i>tert</i> (n=123)	65.85%	4.06%	5.69%	24.39%
G1 <i>pot1b tert</i> (n=121)	67.76%	0%	13.23%	19%

**Table III-1 Quantification of the chromosomal abnormalities from all the genotypes assessed.**

The grey colored cartoons on the top indicate the type of chromosomal aberration.  
\* = unknown generation.

***POT1b and CAT2 act in the same pathway for maintaining chromatin structure***

Peroxisomes are a major source of endogenous cellular ROS and harbor highly effective enzymatic systems to scavenge the byproducts. Catalases, superoxide dismutases



and components of the ascorbate-glutathione cycle are three of the most critical peroxisomal antioxidants that maintain ROS homeostasis. Loss of any of these enzymes leads to overaccumulation of cellular ROS (Corpas et al., 2017).

*A. thaliana* has three different *CATALASE* genes - *CATALASE 1 (CAT1)*, *CATALASE 2 (CAT2)*, and *CATALASE 3 (CAT3)*, and all of them are important in the regulation of cellular ROS (Mhamdi et al., 2010). Loss of CAT2 leads to overaccumulation of H<sub>2</sub>O<sub>2</sub>, and *cat2* mutants were used as a positive control in the DAB staining experiments (J.H. Min, unpublished). Strikingly, Y2H experiments show CAT2 specifically interacts with POT1b (X. Xie, J.H. Min, unpublished). Therefore, given the role of CAT2 in maintaining redox homeostasis, I asked if POT1b and CAT2 act in the same pathway for maintenance of chromatin structure.

I analyzed the chromatin architecture of segregating siblings obtained after crossing *cat2* and *pot1b* single mutants (B. Barbero, unpublished). 162 fields from seven pistils of G3 *cat2* along with 77 fields from five pistils of G3 *pot1b*, and 101 fields from four pistils of G3 wild type were used for the initial analyses. ~16% of the *cat2* fields exhibited the chromatin decondensation phenotype, compared to ~25% in *pot1b* mutants and ~11% in wild type flowers. Lagging chromosome/micronuclei were present in ~15% of the *pot1b* fields, ~21% of *cat2* and ~9% of the wild type fields. The percentage of chromatin bridges was negligible for all the three genotypes examined (Figure III-5, Table III-1). Therefore, the ROS overaccumulating *cat2* mutants also display the aberrant chromosome phenotypes during cell division, including chromatin decondensation.

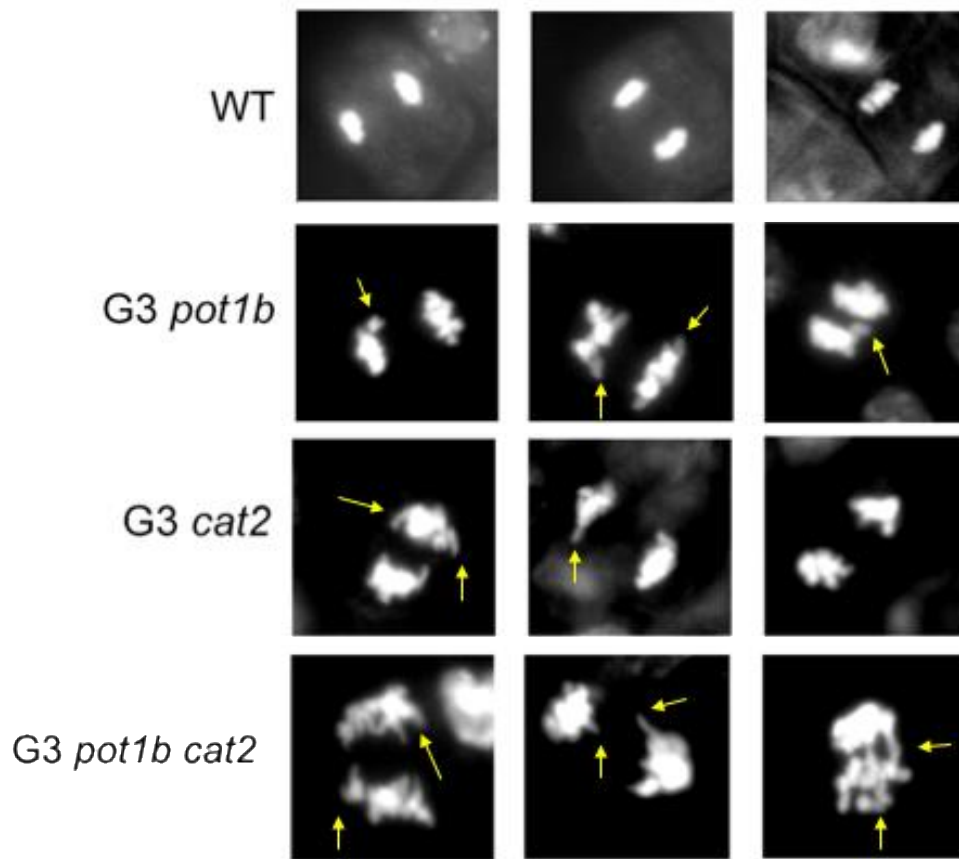


**Figure III-5 Aberrant chromatin phenotypes of *cat2* and *pot1b cat2* mutants**  
 Mitotic spreads of anaphase were made from pistils of four-week-old G3 *cat2*, G3 *pot1b* mutants, G3 *pot1b cat2* and WT samples. Chromatin was stained with DAPI and observed with 100X magnification on a fluorescent microscope. Thin yellow arrows denote lagging chromosomes, thick yellow arrows denote micronuclei and yellow triangles denote chromatin bridges. Table III-1 has the quantification data from this experiment.

To determine whether *POT1b* and *CAT2* function in the same genetic pathway, I assessed the anaphase fields in flowers from the *pot1b cat2* double mutants. Similar to the single mutants, I did not observe chromatin bridges in *pot1b cat2* flowers. However, like

G3 *pot1b* mutants, G3 *pot1b cat2* double mutants showed lagging chromosomes and decondensed chromatin in ~13% and 25% of the fields, respectively. (Figure III-5, Table I). Therefore, it is possible that *CAT2* and *POT1b* function in the same pathway, where *CAT2* is epistatic to *POT1b* for chromatin structure. Interestingly loss of POT1b results in reduced activity of the CAT2 enzyme, which might also suggest that POT1b and CAT2 work in the same pathway for ROS metabolism and chromatin structure maintenance. Even though the percentage of decondensed chromatin in both *pot1b* and *pot1b cat2* mutants were similar, the chromatin decondensation phenotype was noticeably more severe in the G3 *pot1b cat2* double mutant compared to either of the *cat2* and *pot1b* single mutants, possibly due to pleiotropic effects.

**Early generation *pot1a* mutants also have a defect in chromatin condensation**

Although POT1a functions as a part of the telomerase RNP, we asked if POT1a and POT1b exhibit functional overlap for ROS metabolism and chromatin structure. DAB staining of *pot1a* mutants showed elevated ROS accumulation (J.H. Min, unpublished). It is not clear if this increase in ROS reflects telomere dysfunction from shortened telomeres or it reflects some other perturbation in metabolism.

I examined the chromatin architecture of segregating chromosomes in *pot1a* pistils. As discussed earlier, when telomeres become critically short due to telomerase insufficiency, telomere fusion occurs leading to dicentric chromosomes and anaphase bridges. To avoid the negative impact of short telomeres, I compared results from early generation (G2) *pot1a* and later generation (G4) *pot1a* mutants for the analysis of

chromatin structure. I examined 150 fields from five pistils of G2 *pot1a* and 155 fields from eight pistils of G4 *pot1a*. G2 *pot1a* samples showed chromatin bridges and lagging chromosome in only 2.7% and 2% of the fields, respectively. Telomeres were expected to be in the wild type size range of 2-5 Kb and not below the critical length of 1 Kb (Heacock et al., 2004). The number of bridges spiked to ~34% in G4 *pot1a* correlating with more extensive telomere shortening (Figure III-6, Table III-1). Interestingly, decondensed chromatin was seen in 22% and 23.2% of the fields in G2 and G4 *pot1a*, respectively (Figure III-6, Table III-1). Given the role of POT1a in telomere maintenance, it is reasonable to hypothesize that some of the chromosome aberrations of the *pot1a* mutants are a manifestation of telomere dysfunction. However, since some of these phenotypes are evident in mutants whose telomeres are not critically short, elevated ROS may play a role in chromatin defects of *pot1a* mutants.

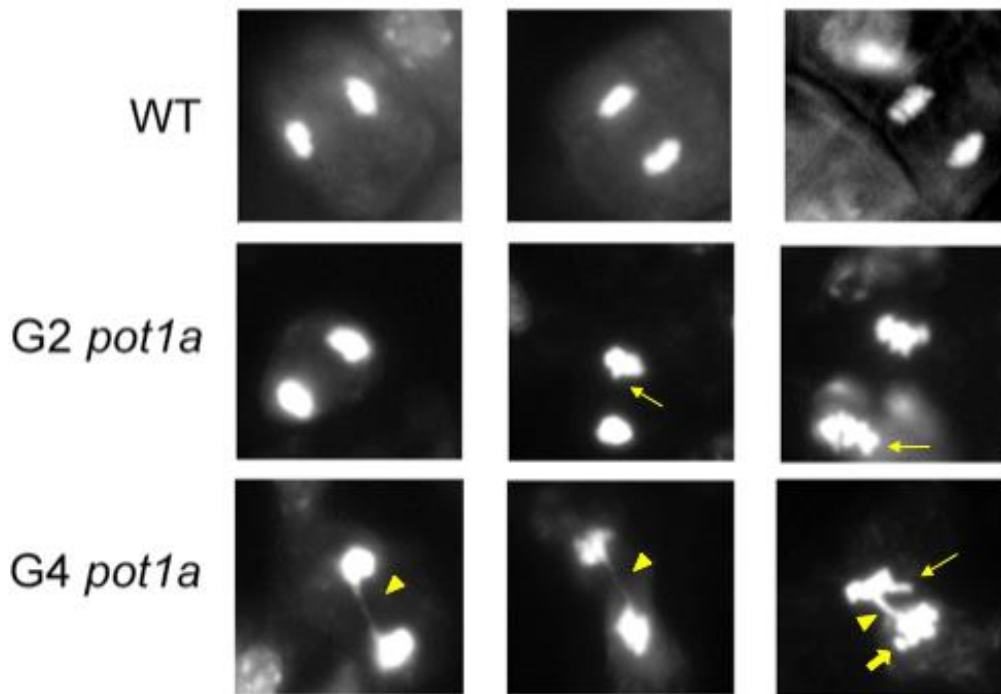


**Figure III-6 Chromatin structures observed during cell division in G2 and G4 *pot1a* mutants.**

Mitotic spreads of anaphase were made from pistils of four-week-old G2 and G4 *pot1a* mutants and WT. Chromatin was stained with DAPI and observed with 100X magnification on a fluorescent microscope. Thin yellow arrows denote lagging chromosomes, thick yellow arrows denote micronuclei and yellow triangles denote chromatin bridges. Table III-1 has the quantification data from this experiment.

**Aberrant chromatin is also observed in early generation *tert* and *tert pot1b* mutants**

Recent experimental data from mice has revealed that TERT also localizes to the mitochondria and plays an essential role in ROS homeostasis. The inability of TERT to traffic into mitochondria leads to a reduction in mitochondrial integrity and an increase in

mitochondria generated ROS (Zheng et al., 2019a). We recently found that ROS accumulates in *tert* mutants as it does in *pot1b* and *pot1a* plants (J.H. Min, unpublished). Therefore, I asked if loss of AtTERT also gives rise to the aberrant chromatin structure, as observed in *pot1a* and *pot1b* mutants. Like *pot1a* mutants, I analyzed flowers from early generation *tert* mutants with telomere in wild type range to avoid any secondary effect of short telomeres.

I examined 123 fields from seven pistils of G2 *tert*. ~4% and 5.7% of the fields displayed anaphase bridges and lagging chromosomes, respectively (Figure III-7, Table III-1). Interestingly, I observed the same number of fields with decondensed chromatin in G2 *pot1a* and G2 *tert* mutants. Therefore, it is possible that overaccumulation of ROS in G2 *tert* mutants contributes to the aberrant chromatin structures, including chromatin decondensation phenotype.

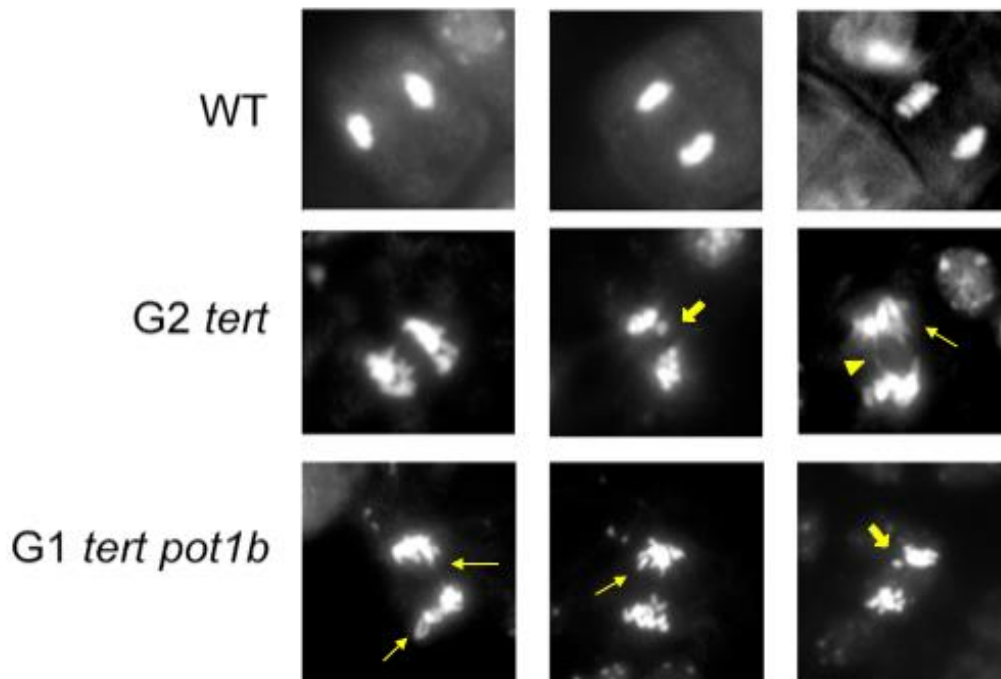


**Figure III-7 Segregating chromatin structures observed in G2 *tert* and G1 *tert pot1b***

Mitotic spreads of anaphase were made from pistils of four-week-old G2 *tert* and G1 *tert pot1b* mutants and WT. Chromatin was stained with DAPI and observed with 100X magnification on a fluorescent microscope. Thin yellow arrows denote lagging chromosomes, thick yellow arrows denote micronuclei and yellow triangles denote chromatin bridges. Table III-1 has the quantification data from this experiment.

Based on the cytology data from G2 *tert* and G2 *pot1a*, I was curious to investigate the biological relationship between TERT and POT1b for chromatin structure maintenance. To unravel a potential overlap between TERT and POT1b, I examined *tert pot1b* double mutants. Interestingly, the G1 *tert pot1b* double mutants were very sick. As a result, to avoid any additional stress impacting the chromatin structure, I analyzed the chromatin structure in dividing cells from G1 *tert pot1b* flowers. I examined a total of 121

fields from eight pistils (Figure III-7, Table III-1). ~13.2% of the fields displayed lagging chromosome compared to ~19% of the fields with decondensed chromatin. None of the fields showed any chromatin bridges indicating that the telomeres were potentially in a healthy range in the G1 *tert pot1b* mutants.

Interestingly, the chromatin defects observed in G1 *tert pot1b* mutants were much more pronounced than the abnormalities observed in G2 *tert* and G2 *pot1b* single mutants. Therefore, the current data indicates that, POT1b and TERT work synergistically for maintaining the chromatin structure. However, the conclusion must be confirmed with cytology data from G1 *pot1b* and G1 *tert* mutants.

## **Discussion**

Oxidative stress can negatively impact a multitude of cellular components and biological processes (Møller et al., 2007). Recent experimental data in *A. thaliana* shows that loss of the telomere-related protein POT1b results in oxidative stress. POT1b localizes to both the nucleus and peroxisomes, and CAT2, the major antioxidant enzyme in peroxisomes, is one of the binding partners of POT1b (C. Castillo-González et al., unpublished). Interestingly, changes to the overall chromatin structure and epigenome are widely documented downstream effects of ROS overaccumulation (Poetsch, 2020). In this chapter, I report the presence of an unexpected chromatin decondensation phenotype in *pot1b* mutants. The same chromatin decondensation phenotype was observed in *cat2* mutants and early generation *pot1a* and *tert* mutants, all of which have elevated ROS. My data also indicate that *CAT2* is epistatic to *POT1b* for chromatin structure maintenance



given the phenotype of *pot1b cat2* double mutants. Finally, based on the preliminary data from *tert pot1b* mutants, both TERT and POT1b appear to have a role in chromatin structure via two independent pathways. Altogether, these data suggest that POT1 protein play a critical role in modulating chromatin compaction by regulating ROS.

While analyzing data from the segregants of the cross made with *cat2* and *pot1b* single mutants, I found that ~25% of the G3 *pot1b* (-/-) *cat2* (+/+) fields showed chromatin decondensation compared to ~50% of the fields in G2 and G4 *pot1b* mutants. The *pot1b* mutant line used for generating the *pot1b cat2* double mutants was different from the one used for analyzing the single mutant of G2 and G4. Therefore, the two different *pot1b* mutant lines might differ in the number of fields displaying the chromatin decondensation phenotype due to genetic variability or other conditions unaccounted for in my experiments. As a result, a critical experiment will be to determine the generational chromatin decondensation phenotype in *pot1b* mutants by comparing that to wild type segregants from the same cross. Only 10.8% of the fields showed the chromatin decondensation phenotype in the G3 wild type samples compared to 24.6% in the G3 *pot1b* mutants, supporting the idea that POT1b regulates chromatin structure. Also, even though the percentage of fields displaying the chromatin decondensation phenotype was similar between *pot1b* and *pot1b cat2* double mutants, the chromatin structural defects were much more pronounced in the double mutants. Given that CAT2 is one of the primary ROS scavengers in the cell, it is expected that removal of CAT2 results in pleiotropic defects (Mhamdi et al., 2010). Alternatively, further deterioration of the chromatin

decondensation phenotype in the *pot1b cat2* double mutants could be interpreted to mean that POT1b makes contribution to chromatin compaction independent of CAT2.

Despite the deleterious impact of ROS overaccumulation on plant health, moderate ROS is required for signaling in various developmental pathways (Mittler, 2017). For example, ROS is essential for flower development and fertilization (Zhang et al., 2020). Interestingly, POT1b mRNA shows the highest accumulation in flowers, specifically at the sigma and carpel (Klepikova et al., 2016). I hypothesize that POT1b might be important for maintaining ROS homeostasis in floral tissues. If that is the case, I predict that ROS deregulation in *pot1b* mutants might be the underlying reason for the observed chromatin decondensation phenotype (Figure III-8).

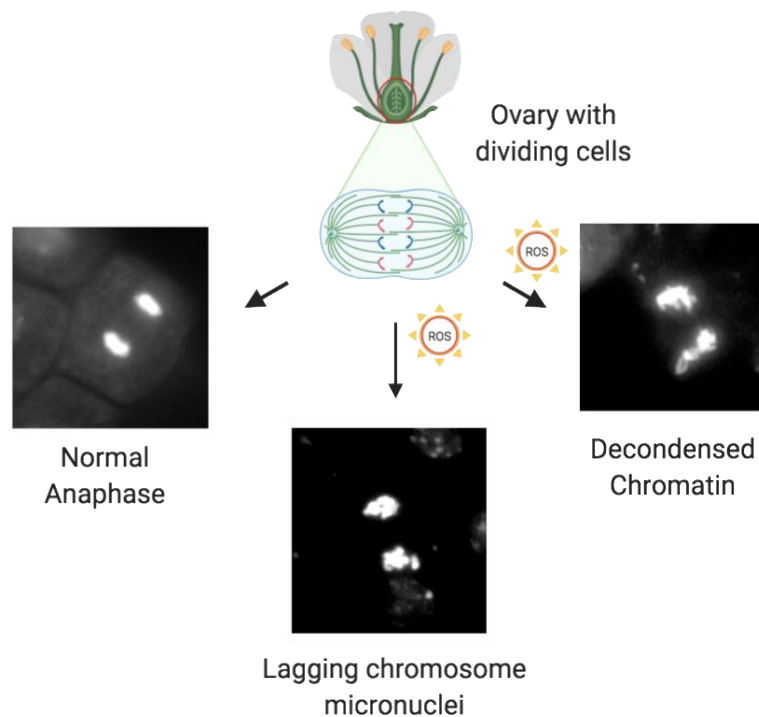


**Figure III-8 A possible role for POT1b in regulating floral ROS**

A moderate level of ROS is essential for reproductive events in the pistils. Dividing cells from *pot1b* mutants show the aberrant chromatin phenotypes. Therefore, it is possible that the presence of POT1b in flowers is necessary for regulating tissue levels of ROS. Failure to do so can lead to ROS-induced changes to the overall chromatin structure as observed in the ROS accumulating mutants: *pot1b*, *pot1a*, *cat2* and *tert*.

ROS overaccumulation leads to histone and DNA hypomethylation and histone hyperacetylation in plants (Kumar R. M. et al., 2020). Alteration of the epigenetic landscape is often associated with changes in the overall structure of chromatin and this phenotype is most evident during chromatin segregation (Sasaki et al., 2019). Thus, it is possible that the chromatin decondensation phenotype observed in the different mutants analyzed in this chapter is a downstream effect of the ROS-mediated epigenomic changes. Alternatively, nuclear POT1b, POT1a and TERT might play a role in maintaining the

epigenome and, directly affecting chromatin structure. Further investigation of the epigenetic status of *pot1a*, *pot1b*, *cat2* and *tert* mutants will be required to assess these and other possibilities.

## **Materials and Methods**

### *Plant material and growth conditions*

Seeds for *tert* +/- (CD-6, CD-7), *cat2* (SALK\_057998) were obtained from the ABRC seed center. Knockout mutants of *AtPOT1b* were created using the CRISPR/Cas9 system (*pot1b*Δ89) and EMS mutagenesis (*pot1b* S273F). Plants for *tert* +/- and *cat2* +/- were genotyped with the primers indicated in Table VII-Appendix C- Table 1. Seeds were sterilized using 70% ethanol, 10% bleach and 0.1% Triton X-100 followed by vernalization for 2 days at 4°C. The sterilized and vernalized seeds were plated on half Murashige and Skoog (0.5X MS Media: RPI M10500) and 1% agar (Caisson A038) supplemented with 1% sucrose. The seedlings and plants on soil were propagated in controlled growth chambers maintained at 22°C under long day light conditions.

### *G-overhang Assay*

The G overhang assay was performed as described previously (Riha and Shippen, 2003a). Total DNA was extracted from 3-week-old plants (WT, *pot1b*, *pot1a* and *ku70*) mutants using phenol–chloroform and chloroform-based extraction. 150 μg of the extracted DNA was digested with 40 units of MseI (NEB: R0525L) and resolved on a 1% agarose gel for 16 h. The bottom half of the gel was subjected to denatured Southern blot using 4X Telo probe (5'TTAGGGTTTAGGGTTTAGGGTTTAGGG3'). The top half

of the gel was subjected to native in-gel hybridization. A telomeric C-rich radioactive probe (5'CCCTAAACCCTAAACCCTAAACCCTAAA3') complementary to the G-overhang sequence was used to determine the G-overhang signal for each sample. Quantity One was used to calculate radioactive signal on the gels (both in-gel and Southern blot membrane). The Southern blot signal was used as the loading control. The in-gel signal was first normalized to the loading control and then everything was normalized to the wild type signal. Results were plotted on a bar graph.

#### Cytology Assay

Chromosome structure was examined based on a previously published protocol (Heslop-Harrison, 1998). Inflorescences comprising unopened buds were collected, destained and fixed in 1 ml of ethanol: acetic acid (3:1) solution overnight. The next morning the solution was replaced with a fresh solution of ethanol: acetic acid. Whole inflorescences were transferred to petri plates with the fixative and individual buds were teased apart with forceps. Each of the buds was rinsed 2X in water and 2X in 1X citrate buffer (10X citrate buffer = 4 parts of 0.1 M citric acid + 6 parts of 0.1 M tri-sodium citrate solution). Buds were transferred in a dish and submerged in the enzyme solution (1X citrate buffer + cellulase (10mg/ml) + pectolyase (10mg/ml)) at 37°C for 1.5 – h. After digestion, the enzyme solution was replaced with 1X citrate buffer and buds can be left in 1X citrate for 3 h at RT or overnight at 4°C. To make the spreads, 20 µL of 60% acetic acid was transferred to the center of a clean slide and a single bud was placed in the droplet. The pistil was dissected by removing all the other floral organs. A cover slip was applied to the pistil followed by tapping and spreading the pistil out with an eraser on the back of

a pencil. The process was continued for 3 min to allow the cells to spread evenly. The whole slide was immersed in liquid nitrogen, and taken out only after the liquid nitrogen stopped bubbling. The coverslip was removed very carefully using the sharp edge of a razor blade and the pistil spread was rinsed with 1 ml of the fixative and kept to air dry for 30 min. 20 uL of DAPI (IHC-Tek 1W-1404) was added to the spread and the slide was sealed with a cover slip. Images were captured at 100X oil immersion using a Nikon Ti microscope. ImageJ was used for processing the image and for counting the number of fields with specific chromatin abnormalities.

#### *Telomere Fusion PCR*

Telomere fusion PCR was performed using 2 µg of DNA as described (Heacock et al., 2004). Fusions were monitored between the left arm of chromosome 1 (1L) and right arm of chromosome 2 (2R), and chromosome 4 (4R) using primer indicated in Chapter VII - Appendix C-Table 1.

## CHAPTER IV

### CONCLUSIONS AND FUTURE DIRECTIONS

Telomeres are the repetitive sequences present at chromosome ends, which emerged as solutions to the end replication and end protection problems of linear DNA. The loss of telomeres is associated with chronic stem cell diseases. Thus, it is critical to maintain and replenish the telomeric DNA. The telomerase ribonucleoprotein maintains telomeric DNA via telomerase reverse transcriptase (TERT), telomerase RNA (TR), and several other accessory factors, thereby solving the end replication problem. However, given the structural similarity of telomere ends with DNA DSBs, it is essential to distinguish natural chromosome ends from DSBs, and to restrict telomerase from forming telomeres at the sites of DSBs within the chromosome body. In most organisms, telomerase action at DSBs is limited through spatio-temporal regulation of enzyme activity. In the case of plants, the previously reported lncRNA TER2 was hypothesized to act as a negative regulator of plant telomerase under DNA damage and as an inhibitor of *de novo* telomere formation at the broken double-stranded ends.

Besides controlling the time and location of telomere addition, the cell is replete with pathways involved in maintaining telomere length homeostasis. Over the past few decades, a variety of molecular players have been identified for their role in telomere length maintenance. Most of these molecular players control telomere length by impinging on the telomerase-dependent pathways. However, recent reports reveal that telomere length is influenced by various non-telomerase dependent pathways including general

DNA replication and repair factors, and proteins involved in chromatin remodeling, protein translation, and even cellular metabolism. The discovery of so-called non-canonical pathways for telomere maintenance indicates that this process is the result of complicated cross-talk between multiple pathways. Understanding how such pathways contribute to telomere length regulation will provide a more holistic view of the mechanisms that safeguard genomic integrity.

The observations reported in Chapter II of this dissertation illustrates a new pathway for telomerase-independent maintenance of telomere length. I report that tRNA Adenosine Deaminase 3 (TAD3) is required for telomere maintenance via a non-telomerase dependent pathway. Overall, the data presented in Chapter II offers novel insights into how multiple pathways can converge to maintain telomeric DNA in *A. thaliana*.

In addition to the pathways mentioned above, telomere length maintenance is also dependent on the various roles played by the telomere-associated proteins (TAPs). TAPs are involved in telomere length regulation as well as the preservation of telomere end architecture. However, recent data suggests that several of these TAPs also participate in biological processes beyond telomeres. For example, the TAP, TRF2, facilitates DNA break repair through NHEJ pathways at non-telomeric regions of the genome (Mao et al., 2007). Similarly, TERT actively translocates to mitochondria upon oxidative stress (Zheng et al., 2019b). These observations support the idea that some of the TAPs may have diversified to participate in other non-telomeric pathways.



A similar phenomenon is observed for the TAP, POT1b in *A. thaliana*. While the AtPOT1a paralog acts as the plant telomerase processivity factor (Surovtseva et al., 2007), AtPOT1b has been implicated in ROS metabolism (C. Castillo-González et al., unpublished). Furthermore, in Chapter III, I report a novel role of POT1b in maintaining chromatin structure in dividing cells. Therefore, it is possible that the TAP, POT1b, diversified to participate in non-telomeric pathways, including but not limited to ROS metabolism and maintenance of chromatin structure in dividing cells.

### **The TER2 lncRNA is a PCR artifact derived from the 5'UTR of *TAD3* gene**

Previously two telomerase RNAs were identified in *A. thaliana* - TER1 and TER2 (Cifuentes-Rojas et al., 2011). TER1 was designated as the plant telomerase RNA, and TER2, a derivative of TER1, was proposed to act as a negative regulator of telomerase, especially in response to DSBs (Cifuentes-Rojas et al., 2012; Xu et al., 2015a). However, recent RNA-Seq experiments performed with immuno-precipitated active telomerase revealed AtTR as the *bonafide* plant telomerase RNA (Song et al., 2019). Genetic studies confirmed that TER1 was not the functional TR for *A. thaliana* (Dew-Budd et al., 2020; Fajkus et al., 2019). Moreover, the gene encoding TER2 was initially identified as partially overlapping the 5' UTR but oriented in the opposite direction of the tRNA Adenosine Deaminase 3 (*TAD3*) located in the complementary strand (Bose et al., 2020 submitted). However, a more recent annotation of the *A. thaliana* genome (Araport 11) extended the 5' UTR of *TAD3* and completely embedded the *TER2* gene within the *TAD3* gene locus (Berardini et al., 2015). The new information available about TER1 and the reannotation

of the *TER2/TAD3* locus motivated us to reevaluate the contribution of the *TER2/TAD3* locus in plant telomere biology. Chapter II has a detailed description of the telomeric roles of the *TER2/TAD3* locus.

Stranded qPCR assay, for the *TER2/TAD3* locus with wild type flowers, seedlings and leaves gave a Cq value of 32 for TER2 compared to a Cq value of 19 for the internal control, *ACT2*. This result indicated that TER2 is either a very low abundance RNA or a PCR artifact. Stranded RNA-Seq experiments were performed to validate the existence of TER2 in *A. thaliana*. None of the reads generated by the RNA-Seq experiments mapped to the *TER2* locus. Therefore, based on the data from qPCR assay and RNA-Seq experiments, a PCR artifact from the 5' UTR of TAD3 was likely the source of TER2.

### **The TAD3 locus does not respond to treatment with the DNA damage inducing agent zeocin**

According to a previous publication, TER2 expression spiked in wild type seedlings treated with zeocin (Cifuentes-Rojas et al., 2012). The increase in TER2 was associated with a concomitant reduction in telomerase activity. Thus, TER2 was proposed to be a negative regulator of telomerase in response to DNA damage (Cifuentes-Rojas et al., 2012). With the new *A. thaliana* genome annotation, we reassessed the impact of zeocin treatment on transcription from *TER2/TAD3* locus. None of reads obtained from the RNA-Seq experiments performed with wild type seedlings treated with 20  $\mu$ M zeocin mapped to the predicted *TER2* locus. Moreover, the TAD3 mRNA level was unchanged

upon zeocin treatment as indicated by the number of reads mapping to the *TAD3* locus. These findings indicate that TAD3 expression is not altered in response to zeocin.

Initial analysis of TER2 employed the *ter2-1* allele, a T-DNA insertion mutant with a T-DNA embedded within the 5' UTR of *TAD3*. Because of the location of the insertion, the *TAD3* locus was impacted. As a result, *ter2-1* was renamed *tad3-1*. Further characterization of *tad3-1* revealed a transcript produced by a cryptic promoter present within the T-DNA. The potential for confounding effects due to off-target regulation caused us to look for additional *tad3* mutant alleles. We identified an additional *tad3* alleles, dubbed *tad3-2*, which resulted in a 70% knockdown of TAD3 expression. We used this allele for further analyses to determine if and how TAD3 impacts telomere biology.

TAD3 mRNA is non-responsive to zeocin treatment, and telomerase regulation during DNA damage is independent of the *TER2/TAD3* locus. The reason for the discrepancy between our current study and the previous study is unknown. One possibility is that the amount of zeocin used in the earlier experiments was much higher which disrupts cell cycle progression and caused downregulation of telomerase activity. In the case of the *tad3-1* mutant, the added complication of a cryptic transcript derived from the locus may have had off target effects that led to changes in telomerase activity. Whatever the cause, my work on TER2 was important to set the record straight. At the present time, there is no evidence that *A. thaliana* telomerase is associated with any other functional lncRNA besides AtTR.

### **TAD3 regulates telomere length via a telomerase-independent pathway in *A. thaliana***

While reevaluating the effect of *TER2/TAD3* locus, we examined the bulk telomere length in *tad3-2* mutants. Unexpectedly, we observed progressive telomere shortening in successive generations of the mutants, implying that TAD3 played an important role in telomere maintenance. Consistent with this conclusion, the telomere shortening phenotype was completely rescued by overexpressing TAD3. The telomere-shortening could not be attributed to the altered telomerase activity in *tad3-2* samples. Moreover, plants lacking TAD3 and the telomerase processivity factor, POT1a, showed accelerated telomere shortening compared to the single mutant, *tad3-2* indicated that TAD3 and telomerase act in separate pathways for telomere maintenance. Consistent with this proposal, loss of TAD3 did not compromise the recruitment and enzymatic activity of telomerase, as indicated by the presence of long telomeres in *ku70 tad3-2* double mutants. Therefore, TAD3 is involved in maintaining telomere length in *A. thaliana* through a telomerase-independent pathway.

Various protein complexes associated with telomeric DNA are also involved in maintaining the telomere end architecture. Defects in telomere end architecture can predispose telomeric ends to nucleolytic attack which can eventually impact bulk telomere length. Therefore, we asked if the telomere shortening phenotype in *tad3-2* plants was due to defects in maintaining the telomere end architecture. The presence of intact G-overhangs and blunt-ends indicated that telomere shortening in *tad3-2* mutant does not occur due to defect in telomere end architecture.

HR mediated shortening and lengthening of telomere is one of the most well studied telomerase-independent methods for telomere length maintenance. Telomere Rapid Deletion employs HR to shorten telomeric DNA (Lustig, 2003). Branch migration of the G overhang structure into the t-loop region generates a Holliday junction. Resolving the Holliday junction shortens telomeric DNA by creating extra chromosomal t-circles or ECTCs (Lustig, 2003). *A. thaliana* mutants such as *ku70*, *stn1*, and G6 *ddm1* mutants exhibits characteristics of TRD (Watson and Shippen, 2007; Xie and Shippen, 2018). Interestingly, all of these above-mentioned mutants display stronger G overhang signal due to defect in telomere end protection. It is possible that the excess G-overhang mediates TRDs by forming ECTCs. But based on the G-overhang and blunt-end analysis, loss of TAD3 does not impinge on the telomere end protection pathways. However, further investigation is needed to rule out the possibility that HR plays a role in telomere shortening in *tad3-2* mutants. Altogether, we hypothesize that multiple metabolic pathways are responsible for telomere length perturbation rather than the known telomerase-dependent and recombination-based pathways.

### **Transcriptome analysis of *tad3-2* mutants reveal changes in metabolism and cell cycle related pathways**

To elucidate the mechanism of TAD3-mediated telomere maintenance, we analyzed RNA-seq data from wild type and *tad3-2* seedlings. A total of 6102 genes were differentially regulated with an FDR<0.05 in *tad3-2* mutants, of which 598 genes showed a 2-fold or higher upregulation and 382 genes had a 0.5-fold or lower downregulation

relative to wild type. Such a high number of differentially regulated genes indicate that loss of *TAD3* has a global impact on a wide range of biological pathways. The two major biological processes that were most affected by the loss of *TAD3* were auxin-related pathways and secondary metabolism, which were downregulated and upregulated, respectively. Also, given the cell cycle regulated activities of the telomerase complex (Londoño-Vallejo and Wellinger, 2012), we checked whether *TAD3* mRNA was cell cycle-regulated. FACS analysis with T87 cell culture revealed a surge in *TAD3* mRNA during late S phase, contrary to *TERT* and *POT1a* mRNA which spiked during early S phase. Interestingly, according to the transcriptome data, loss of *TAD3* was associated with increased expression of some of the major cell cycle progression genes like the Cell Division Cycle 6 (*CDC6*) complex and the Minichromosome Maintenance (*MCM*) complex.

Glucosinolates are secondary metabolites generated by plants as a defense response against micro-organisms and herbivory. Interestingly, glucosinolate accumulation in *A. thaliana* is associated with disruption of cell cycle progression along with overaccumulation of S phase cells (Awwad et al., 2019). Increased expression of the *CDC6* and *MCM* is therefore consistent with a possible perturbation to cell cycle progression in *tad3-2* mutants. Interestingly, loss of *TAD3* in *S. pombe* is also associated with defects in cell cycle progression. Therefore, it is possible that *TAD3* plays a role in cell cycle progression which directly or indirectly regulates telomere length.

The process of telomere replication and processing is highly dependent on the successful execution of several cell-cycle dependent processes. For example, following

replication, yeast telomeres are subjected to nucleolytic processing to generate the optimal amount of G overhang DNA that acts as a substrate for telomerase (Vodenicharov and Wellinger, 2007). As a result, any perturbation to the cell cycle progression can result in an unwanted level of nucleolytic processing of the telomeres, which can eventually give rise to a short telomere phenotype. Therefore, defect in cell cycle progression in the *tad3-2* might lengthen or shorten the window available for the optimal nucleolytic processing of the telomeres. Such uncontrolled nucleolytic processing, even for a short period of time, might be responsible for the short telomere phenotype observed in *tad3-2* mutants (Figure IV-1).

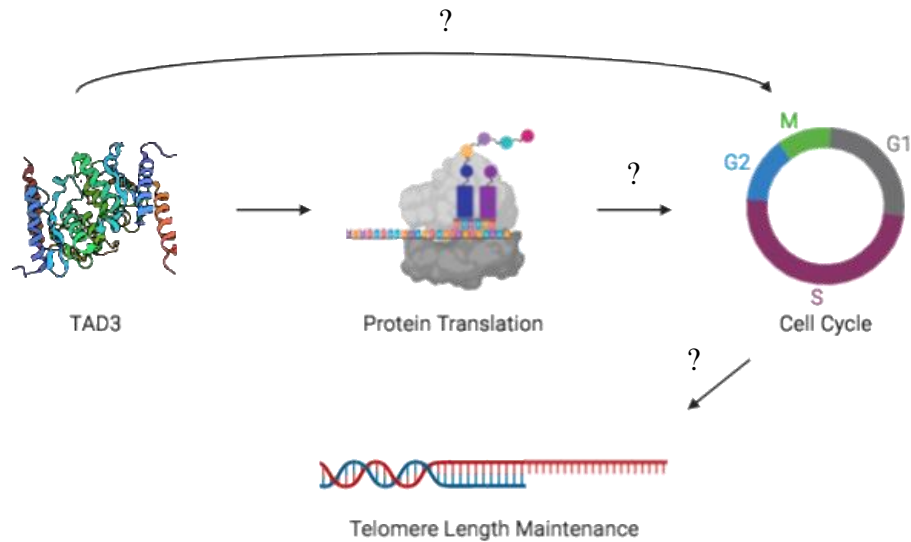


**Figure IV-1 Potential mechanistic employed by TAD3 for maintaining telomere length in *A. thaliana*.**

TAD3 controls cellular protein translation through tRNA editing activity. Some of these proteins might have direct or indirect roles in cell cycle regulation. Error-free progression of the cell cycle plays an important role in telomere length maintenance. Therefore, changes in the protein translation processes might have a role in indirectly regulating telomere length via the cell cycle.

### **Future directions**

*Determine how loss of TAD3 impacts protein regulation*

*TAD3* is an essential gene which plays a critical role in protein translation by facilitating tRNA editing (Schimmel, 2018b). Ergo, to unravel the telomere maintenance mechanism employed by TAD3, an important future direction would be to examine the biological processes impacted by TAD3's role in protein translation. The classical Bradford assay can be used as a preliminary experiment to evaluate the impact of TAD3 knockdown on global protein translation. Defects in tRNA editing enzymes or ADARs reduce available tRNAs required for translating mRNA with rare codons (Schaub and Keller, 2002). Ribosome footprinting assays performed in organisms with ADAR defects



revealed disruption of decoding activities at cognate codons, which eventually led to ribosome stalling at the ADAR specific-codons followed by reduction of protein levels *in vivo* (Kapur and Ackerman, 2018). Therefore, it is possible that knocking down the *A. thaliana* specific TAD3 enzyme impairs the protein translation fidelity of mRNAs due to ribosome stalling at the TAD3 dependent codons. Identification of the mRNAs that accumulate at stalled ribosomes might reveal the specific protein factors and functional pathways involved in maintaining plant telomeres (Brar and Weissman, 2015).

Ribosome profiling experiments or computational studies could be performed with wild type and *tad3-2* flower samples to calculate (1) the codon occupancy for individual codon families; (2) codon decoding rates; and (3) the global ribosome density (Lyu et al., 2020). Furthermore, sophisticated deep learning-based frameworks like RibosOme Stalling Estimator (ROSE) can be used to generate a targeted list of genes whose mRNAs accumulate stalled ribosomes in the *tad3-2* mutants compared to wild type (Zhang et al., 2017). Gene Ontology analysis of the ROSE generated list of genes can reveal biological pathways having the highest number of mRNAs with stalled ribosomes in *tad3-2* (Zhang et al., 2017). Estimating the protein levels for some of the most affected genes will help assess the downstream impact of translation-specific ribosome stalling in *tad3-2* mutants. In conclusion, the ribosome profiling technique may provide a more targeted list of genes to work with for elucidating the TAD3 dependent telomere maintenance pathway(s) in *A. thaliana*. A recent publication by Lyu and colleagues may be helpful in analyzing the ribosome profiling data and for other computational techniques to further characterize the plant TAD3 enzyme (Lyu et al., 2020).

*Determine if TAD3 and TAD2 cooperate to maintain plant telomeres*

In *A. thaliana* TAD3 edits tRNAs by working in a complex with tRNA Adenosine Deaminase 2 (TAD2) protein (Zhou et al., 2014). Therefore, it would be interesting to determine whether TAD3 works in concert with TAD2 for telomere maintenance in *A. thaliana* or if TAD3 has a unique role in telomere maintenance. Similar to TAD3, homozygous mutants of *tad2* are non-viable. The existing TAD2 knockdown mutant as described by Zhou et al., 2014 shows only a 50% reduction in TAD2 mRNA. The *tad3-2* mutant analyzed by our lab is an 85% knockdown mutant. So, to probe for the telomere phenotype most effectively, we should work with a *tad2* knockdown mutants with a similar level of TAD2 mRNA knockdown. CRISPR Cas9 (Bortesi and Fischer, 2015) can be used to generate an array of *tad2* knockdown mutants. The presence of a similar short telomere phenotype in the *tad2* knockdown mutants, would indicate both TAD2 and TAD3 are involved in telomere maintenance in *A. thaliana*. If *tad2 tad3* are viable, measuring the telomere length in these plants will help confirm whether TAD2 and TAD3 belong to the same pathway for telomere maintenance.

Both TAD3 and TAD2 are highly conserved tRNA editing enzymes that play similar roles in tRNA editing in humans (Torres et al., 2014a). Thus, it would be interesting to check the telomere length in TAD2 and TAD3 knockdown mutants from humans and mice, as well. If a short telomere phenotype is observed in mammalian mutants, the data would argue for a conserved role of the tRNA editing pathway in telomere maintenance.

### *Relationship between cell cycle progression of tad3-2 mutants and short telomeres*

Successful extension of telomeric DNA depends on precise orchestration of multiple cell cycle-regulated pathways. Studies performed in yeast have played a pivotal role in deciphering the crosstalk between cell cycle and telomere dynamics. The process of telomere extension starts with telomere replication in early S phase. Passage of the replication fork through the telomeres is essential to generate the 3' G-overhang structure (Dionne and Wellinger, 1998). Next the telomeric C-strand undergoes nucleolytic processing via the MRX complex (Mre11, Rad50, Xrs2) to create longer G-overhang structures, also called the G-tails. Telomerase initiates the process of telomere repeat addition using the G-tail as the substrate (Vodenicharov and Wellinger, 2007). Once the telomeres are extended to an optimal length, a DNA polymerase (mostly Pol alpha primase) is recruited to replicate the C-strand via the C-strand fill-in reaction (Zhao et al., 2009). Once the telomeres are capped, they are subjected to G2 specific HR dependent pathways to generate the t-loop structure (Verdun et al., 2005). Perturbation to cell cycle progression is often associated with an increased level of resectioning, which ultimately results in telomere failure, genome instability and, eventually, cell death (Vodenicharov and Wellinger, 2007). Interestingly, loss of TAD3 in *S. pombe* impairs cell cycle progression between G1 to S and G2 to M phases, which supports the cell cycle specific roles of tRNA editing enzymes (Tsutsumi et al., 2007).

FACS data from *A. thaliana* cell culture revealed a cell cycle-dependent expression pattern of TAD3. Moreover, transcriptome data from *tad3-2* seedlings showed overexpression of CDC6 and some of the MCM complex genes. Deregulation of either of

CDC6 and MCM gene complexes alters cell cycle timing, which can eventually destabilize DNA replication and induce cellular stress (Borlado and Méndez, 2008; Das et al., 2014). Therefore, it is possible that TAD3 mRNA mediates specific timed activities involving telomere length maintenance during cell cycle progression in *A. thaliana*. If that is the case, deregulation of the such timed activities in the *tad3-2* mutants might be an underlying reason for the telomere shortening phenotype. Unfortunately, the lack of *tad3* mutant cell culture restricts us from answering such cell cycle related questions directly. However, preliminary data about cell cycle progression of the *tad3-2* mutants could be obtained using EdU labeling experiments, which identifies S phase cells that incorporate the fluorescent EdU dye. Edu serves as a proxy for the number of dividing cells (Aklilu et al., 2014). Differences in EdU labeling patterns of *tad3-2* and wild type seedlings would imply disruption of cell cycle progression upon loss of *TAD3*. Similar experiments should be performed with *tad2* mutants to generate a comprehensive model about the cell cycle dependent roles of tRNA editing enzymes in telomere maintenance.

### **Loss of POT1b induces oxidative stress in *A. thaliana***

Besides solving the end replication problem, telomeres also participate in resolving the end protection problem through numerous protein complexes bound to the telomeres (Baumann and Price, 2010; Gottschling and Zakian, 1986; Price et al., 2010; Schmutz and de Lange, 2016). Protection of Telomeres 1 (POT1) is an indispensable component of the shelterin complex, plays critical roles in telomere protection complex and telomere length maintenance (Baumann and Price, 2010). Loss of POT1 is often associated with telomere

length deregulation and genomic instability. *A. thaliana* possesses three different paralogs of the *POT1* gene - *POT1a*, *POT1b* and *POT1c* (Kobayashi et al., 2019; Shakirov et al., 2005; Surovtseva et al., 2007). Recent experimental data has identified *POT1c* as a pseudogene (Kobayashi et al., 2019). While *POT1a* has been extensively characterized for its role in facilitating telomerase processivity (Arora et al., 2016; Renfrew et al., 2014; Surovtseva et al., 2007), *POT1b*'s role in telomere biology and plant biology remains elusive.

Meta-analyses of the *pot1b* transcriptome data revealed an upregulation of multiple stress-related pathways, including oxidative stress and glutathione metabolism (C. Castillo-González, unpublished). Biochemical experiments conducted in the Shippen lab for gauging the amount of reactive oxygen species (ROS) revealed overaccumulation of ROS in *pot1b* mutants indicating that *POT1b* has a role in ROS metabolism. In addition, subcellular localization experiments showed that *POT1b* accumulates in both the nucleus and the peroxisomes.

Peroxisomes are single membraned organelles that act as sole cellular compartment for facilitating  $\alpha$  and  $\beta$  oxidation reactions in plants (Corpas et al., 2017). ROS are typical byproducts of peroxisome-based biochemical reactions. As a result, peroxisomes also house several highly efficient ROS scavenging machineries, including the enzymes, catalases and superoxide dismutases (Schrader and Fahimi, 2006). Deregulation of these enzymatic pathways, including mutation of Catalase 2 (*CAT2*) leads to overaccumulation of cellular ROS. Yeast two-hybrid data from the Shippen lab indicate that the peroxisome enzyme, *CAT2*, is a specific binding partner of *POT1b*.

Studies in mammals demonstrate that overaccumulation of ROS alters chromatin structure. Therefore, based on the (1) overaccumulation of ROS in *pot1b* mutants; (2) POT1b's localization to the peroxisomes; and (3) interaction of POT1b with CAT2, I sought to investigate the effect of ROS overaccumulation on the chromatin structure in *pot1b* mutants. In Chapter III, I reported my observations of aberrant chromatin phenotypes in the dividing cells from *pot1b*, *cat2*, *pot1a*, and *tert* flowers.

### **Telomere end architecture is unperturbed in *pot1b* mutants**

Although POT1b is dispensable for telomere length maintenance, *pot1b* mutants show slightly elevated telomerase activity (B. Barbero, unpublished). This observation and the critical role of POT1 proteins in chromosome end protection in yeast and mammals prompted me to investigate how loss of POT1b impacts telomere end architecture. Based on results from G-overhang analysis and blunt end assays, the loss of POT1b does not affect either of the G-overhang or the blunt end structures. These findings indicate that POT1b does not make the same contribution to telomere structure as POT1 proteins from other organisms.

### **Aberrant chromatin and chromosome segregation in plants with elevated ROS**

Since POT1 is critical for end protection of chromosomes, I examined the chromatin structure of the segregating chromosomes in dividing cells from the flower pistils of *pot1b* mutants. Interestingly, the mutants displayed multiple aberrant chromatin structures, including lagging chromosomes, micronuclei, and anaphase bridges.

Chromosomes with extensively short telomeres or unrepaired DNA double-strand breaks undergo end-to-end fusion, which generates dicentric chromosomes. Segregation of these dicentric chromosomes during anaphase gives rise to a bulky chromatin material situated between the segregating chromatin. This structure is known as the "chromatin bridge" or "anaphase bridge". The cycle of break-fusion-bridge continues in the next rounds of cell division, ultimately leading to genome rearrangements and loss of chromatin material (Fernández-Casañas and Chan, 2018). Apart from the anaphase bridges, errors in microtubule formation and spindle-assembly organization gives rise to lagging chromosomes. The lagging chromosomes can eventually get wrapped within a membrane-based structure called the micronuclei. Defects in telomere end protection or general genomic instability play a significant role in generating aberrant chromatin structures. However, unperturbed telomere end architecture and lack of products in TF-PCR from *pot1b* mutants rule out the possibility that the aberrant chromatin structures are a manifestation of defects in telomeric end protection pathways. Therefore, the aberrant chromatin structure might be a result of rampant global genomic instability in *pot1b* mutants.

Additionally, I discovered a peculiar chromatin decondensation phenotype in *pot1b* mutants. Segments of the genome that were faintly stained by DAPI, at times, looped out from the dense chromatin or resolved into a clawed structure. Overexpressing POT1b partially rescued the chromatin decondensation phenotype. Why the rescue is only partial is not known, but it is possible that an optimal level of the POT1b protein is essential for genome stability. In other words, overexpression of POT1b may be

detrimental as under expression. Also given the role of POT1b in ROS metabolism, it is possible that overexpression of POT1b takes a toll on the ROS that have beneficial roles in plant growth and development. As mentioned earlier, plants use ROS in moderation as signaling molecules (Mittler, 2017). Therefore, reduction in ROS involved in signaling might also have a negative impact on the chromatin structure. Strikingly, *cat2*, *pot1a* and *tert* mutants, which also overaccumulate ROS, displayed a similar chromatin decondensation phenotype as *pot1b* mutants. They also show aberrant chromatin structures including lagging chromosome and micronuclei. Further genetic analysis suggests that *CAT2* and *POT1b* belong to the same pathway for maintaining chromatin structure, where *CAT2* is epistatic to *POT1b*. In conclusion, my work provides a novel link between telomere related genes, ROS metabolism and chromatin decondensation.

Finally, besides ROS accumulation, loss of telomeric DNA is also reported to cause changes to the epigenome and a chromatin decondensation phenotype (Galati et al., 2013). Although I analyzed early generation *pot1a* and *tert* mutants for the cytology-based assays, the telomeres are still shorter than wild type samples. As a result, it is possible that the chromatin phenotype observed in the *pot1a* and *tert* mutants is a manifestation of both ROS induced decondensation and short telomere induced chromatin modification. As a result, it is critical to assess the epigenetic landscape of these mutants with their corresponding wild types to parse the impact of ROS and telomere length on overall chromatin structure.



## **Future Directions**

### *Determine if aberrant chromatin structures are telomeric in nature*

Overwhelming levels of ROS can damage multiple cellular components, including the telomeres (Sasaki et al., 2019). The G-T rich nature of telomeres makes them highly susceptible to base oxidation to generate 8-Oxo-G at guanine or Thymine glycol at thymine residues. The presence of 8-OxoG residues in particular is associated with telomere shortening due to replication fork arrest (Coluzzi et al., 2014). Overaccumulation of cellular ROS can also modify the telomere chromatin landscape (Nishida et al., 2013). Moreover, specific enzymes like NEIL3 are employed to repair ROS induced DNA damage at the telomeres. Failure to do so, may lead to development of aberrant chromatin structure, such as those observed in the case of *pot1a*, *pot1b*, *cat2* and *tert* mutants (Zhou et al., 2017). Therefore, it would be interesting to assess the location of the telomeres relative to the aberrant chromatin structures observed in *pot1a*, *pot1b*, *cat2* and *tert* mutants from *A. thaliana* (Zhou et al., 2017). Telomeric FISH using telomeric and subtelomeric probes will help identify the associated telomeric regions within the aberrant chromatin structures (Leehy et al., 2013; Surovtseva et al., 2009). The amount of telomeric signal associated with an aberrant chromatin structure for a specific mutant might help distinguish the different regions of the genome impacted by the overaccumulation of ROS in a particular mutant.

*Determine how overaccumulation of ROS impacts the epigenome of A. thaliana*

Based on the transcriptome data, loss of POT1b leads to enhanced gene expression indicating that POT1b might have a role in suppressing gene expression in the first place. Usually removal of histone methylation marks or inability to add methyl marks are the most common reasons behind increased gene expression. Moreover, in higher eukaryotes, overaccumulation of ROS often leads to changes to the epigenetic landscape, which eventually perturbs the chromatin structure (Kreuz and Fischle, 2016). As a result, it would be interesting to determine the epigenetic status of *pot1a*, *pot1b* and *cat2* mutants. Multiple techniques can be used for analyzing the chromatin structure of these mutants. Crude assays like HPLC-UV can provide preliminary insight about any epigenetic modifications by identifying DNA methylation marks from genomic DNA (Chen et al., 2013). The high throughput technique of Whole Genome-based Bisulfite Sequencing (WGBS) can be used for assessing genome-wide DNA methylation marks in *pot1a*, *pot1b* and *cat2* samples (Grehl et al., 2018). Histone marks can be assessed by extracting total chromatin from mutant flowers, followed by western blot with antibodies for total H3, and modified histone variants like H3K9me2, H3K9ac, H3K27me3 and H3K27ac (Castillo-González et al., 2015). ChIP-Seq experiments with antibodies against acetylated or methylated histones followed by high throughput sequencing will also help examine the chromatin structure of *pot1b*, *pot1a*, *cat2* and *tert* mutants (Rymen et al., 2019), which can be further correlated with the chromatin decondensation phenotype observed in the ROS over accumulating mutants (Figure IV-2). Along with changes to the epigenome, defects in cytoskeleton development can also be a potential underlying reason for the aberrant

chromatin structures. Therefore, it would be interesting to assess if there is any change in the activity of cytoskeleton associated proteins in the *pot1b*, *cat2*, *tert* and *pot1a* samples.

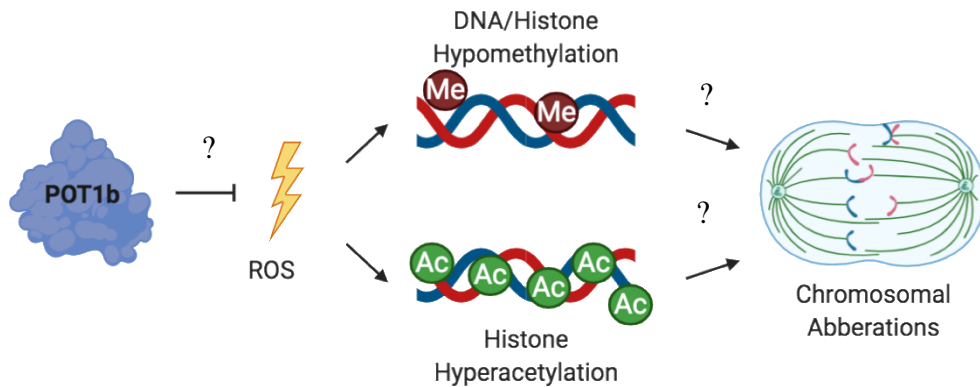


**Figure IV-2 A potential role of POT1b in maintaining chromatin structure.**

Overaccumulation of ROS in *pot1b* mutants might lead to changes to the epigenome which can eventually alter the chromatin structure. Such chromatin associated damage might be an underlying reason behind the aberrant chromatin phenotype displayed by the diving from mutants *pot1b* and other ROS over accumulating mutants.

*Determine if the chromatin decondensation phenotype is linked to a defect in POT1b organelle-specific localization*

Recent localization experiments from the Shippen lab show that POT1b is present in both peroxisomes and the nucleus, hinting at a possible dual functionality of the protein. Although chromatin organization is clearly dependent on the activity of molecular factors within the nucleus (Kaczmarczyk et al., 2020), recent studies indicate that disruption of

peroxisomal function, can also impact chromatin structure through a retrograde signaling pathway (Wang et al., 2019a). Thus, it would be interesting to delve deeper into understanding which organ-specific function of POT1b is required for maintaining chromatin structure. The Shippen lab has identified a probable peroxisomal targeting sequence 2 (PTS2) in POT1b. Therefore, *pot1b* mutants complemented with POT1b- $\Delta$ PTS2 can be assessed for the chromatin phenotype and compared to *pot1b* mutants and wild type controls. The presence of an aberrant chromatin phenotype in mutants lacking the peroxisomal localization signal would indicate a potential role of the peroxisome POT1b in maintaining chromatin structure.

Interestingly, POT1b does not have an obvious nuclear localization signal and thus it is possible that it is transported into the nucleus as a cargo. Currently, mass spectrometry-based techniques are being undertaken in the Shippen lab to identify the protein binding factors of POT1b. If we identify, a potential nuclear transporter for POT1b, then POT1b constructs unable to interact with the transporter could be used for complementing *pot1b* mutants. Inability of POT1b to localize to the nucleus due to a defect in the transporter system might give rise to the same chromatin decondensation phenotype, which would indicate that chromatin structure maintenance is dependent on the nuclear form of the POT1b protein.

## **Conclusion**

The work presented in this dissertation rectifies the identity of a previously reported negative regulator of plant telomerase, the lncRNA TER2, and reveals the

involvement of a tRNA editing enzyme called the tRNA Adenosine Deaminase 3 (TAD3), in plant telomere length maintenance. Based on rigorous experimental analyses, TER2 has been identified as an unstable lncRNA, which was generated as a PCR artifact of the TAD3 gene, located in the opposite strand. Interestingly, knocking down TAD3 expression results in telomere shortening without any measurable change in telomerase activity or any discernable perturbation to the telomere end architecture. Therefore, TAD3 maintains telomeres via a telomerase-independent pathway. Surprisingly, loss of TAD3 impacts several metabolic activities and cell cycle progression genes in *A. thaliana*. Based on several scientific reports across multiple organism, unwanted defects in the metabolic pathways induce stress, which can eventually impair high energy-requiring processes like telomere maintenance (Casagrande and Hau, 2019). Also, based on studies from yeast and humans, telomere maintenance is dependent on the successful orchestration of multiple activities across the cell cycle. As a result, any perturbation to the cell cycle can negatively impact overall telomere length and architecture. There it is possible that the newly identified player in plant telomere biology, TAD3, maintains telomeres by impinging on pathways which are at the crossroads of metabolism, cell cycle and telomeres.

In the second half of my dissertation, I describe a novel phenotype displayed by plants lacking the telomere-associated protein, POT1b. Based on experimental evidences, POT1b, unlike its paralog POT1a, is not directly involved in telomere length maintenance and telomere end architecture (C. Castillo-González, unpublished). Instead, loss of POT1b causes overaccumulation of ROS, which implies a potential role of POT1b in ROS metabolism. While investigating the downstream effects of ROS overaccumulation in

*pot1b*, I found that loss of POT1b impairs the chromatin structure compaction in dividing cells and generates chromosome with structural defects (aberrant chromosomes). I also discovered a novel chromatin decondensation phenotype exhibited by the *pot1b* mutants as well as other ROS accumulating mutants. Further genetic analyses revealed that while POT1b and the peroxisome-based antioxidant, Catalase 2, work together for chromatin structure maintenance, POT1b and TERT contribute to chromatin structure via two independent pathways. Overall, my data indicates that the telomere associated protein, POT1b is essential for regulating chromatin structure, through its possible role in ROS metabolism.

In conclusion, this dissertation offers novel insights into the non-canonical pathways involved in telomere maintenance as well as the non-canonical roles played by telomere-associated factors.

## REFERENCES

- Abdulkina, L.R., Kobayashi, C., Lovell, J.T., Chastukhina, I.B., Aklilu, B.B., Agabekian, I.A., Suescún, A. V., Valeeva, L.R., Nyamsuren, C., Aglyamova, G. V., et al. (2019). Components of the ribosome biogenesis pathway underlie establishment of telomere length set point in Arabidopsis. *Nat. Commun.* *10*, 1–21.
- Afgan, E., Baker, D., Batut, B., Van Den Beek, M., Bouvier, D., Ech, M., Chilton, J., Clements, D., Coraor, N., Grüning, B.A., et al. (2018). The Galaxy platform for accessible, reproducible and collaborative biomedical analyses: 2018 update. *Nucleic Acids Res.* *46*, W537–W544.
- Agarwal, A., and Saleh, R.A. (2002). Role of oxidants in male infertility: Rationale, significance, and treatment. *Urol. Clin. North Am.* *29*, 817–827.
- Agorio, A., Durand, S., Fiume, E., Brousse, C., Gy, I., Simon, M., Anava, S., Rechavi, O., Loudet, O., Camilleri, C., et al. (2017). An Arabidopsis Natural Epiallele Maintained by a Feed-Forward Silencing Loop between Histone and DNA. *PLoS Genet.* *13*, 1–23.
- Ahmed, W., and Lingner, J. (2018). Impact of oxidative stress on telomere biology. *Differentiation* *99*, 21–27.
- Aird, K.M., Zhang, G., Li, H., Tu, Z., Bitler, B.G., Garipov, A., Wu, H., Wei, Z., Wagner, S.N., Herlyn, M., et al. (2013). Suppression of Nucleotide Metabolism Underlies the Establishment and Maintenance of Oncogene-Induced Senescence. *Cell Rep.* *3*, 1252–1265.
- Akbay, E.A., Peña, C.G., Ruder, D., Michel, J.A., Nakada, Y., Pathak, S., Multani, A.S., Chang, S., and Castrillon, D.H. (2013). Cooperation between p53 and the telomere-protecting shelterin component Pot1a in endometrial carcinogenesis. *Oncogene* *32*, 2211–2219.
- Aklilu, B.B., Soderquist, R.S., and Culligan, K.M. (2014). Genetic analysis of the Replication Protein A large subunit family in Arabidopsis reveals unique and overlapping roles in DNA repair, meiosis and DNA replication. *Nucleic Acids Res.* *42*, 3104–3118.
- Alazami, A.M., Hijazi, H., Al-Dosari, M.S., Shaheen, R., Hashem, A., Aldahmesh, M.A., Mohamed, J.Y., Kentab, A., Salih, M.A., Awaji, A., et al. (2013). Mutation in ADAT3, encoding adenosine deaminase acting on transfer RNA, causes intellectual disability and strabismus. *J. Med. Genet.* *50*, 425–430.
- Amiard, S., Da Ines, O., Gallego, M.E., and White, C.I. (2014). Responses to telomere erosion in plants. *PLoS One* *9*.

Armanios, M., Chen, J.L., Chang, Y.P.C., Brodsky, R.A., Hawkins, A., Griffin, C.A., Eshleman, J.R., Cohen, A.R., Chakravarti, A., Hamosh, A., et al. (2005).

Haploinsufficiency of telomerase reverse transcriptase leads to anticipation in autosomal dominant dyskeratosis congenita. *Proc. Natl. Acad. Sci. U. S. A.* *102*, 15960–15964.

Arora, A., Beilstein, M.A., and Shippen, D.E. (2016). Evolution of Arabidopsis protection of telomeres 1 alters nucleic acid recognition and telomerase regulation. *Nucleic Acids Res.* *44*, gkw807.

Åsberg, S.E., Bones, A.M., and Øverby, A. (2015). Allyl isothiocyanate affects the cell cycle of Arabidopsis thaliana. *Front. Plant Sci.* *6*, 1–11.

Askree, S.H., Yehuda, T., Smolikov, S., Gurevich, R., Hawk, J., Coker, C., Krauskopf, A., Kupiec, M., and McEachern, M.J. (2004). A genome-wide screen for Saccharomyces cerevisiae deletion mutants that affect telomere length. *Proc. Natl. Acad. Sci. U. S. A.* *101*, 8658–8663.

Autexier, C., and Greider, C.W. (1995). Boundary elements of the Tetrahymena telomerase RNA template and alignment domains. *Genes Dev.* *9*, 2227–2239.

Autexier, C., and Greider, C.W. (1998). Mutational analysis of the Tetrahymena telomerase RNA: Identification of residues affecting telomerase activity in vitro. *Nucleic Acids Res.* *26*, 787–795.

Autexier, C., and Lue, N.F. (2006). The Structure and Function of Telomerase Reverse Transcriptase. *Annu. Rev. Biochem.* *75*, 493–517.

Awwad, F., Bertrand, G., Grandbois, M., and Beaudoin, N. (2019). Auxin protects Arabidopsis thaliana cell suspension cultures from programmed cell death induced by the cellulose biosynthesis inhibitors thaxtomin A and isoxaben. *BMC Plant Biol.* *19*, 512.

Azqueta, A., Slyskova, J., Langie, S.A.S., Gaivão, I.O.N., and Collins, A. (2014). Comet assay to measure DNA repair: Approach and applications. *Front. Genet.* *5*, 1–8.

Azzalin, C.M., and Lingner, J. (2015). Telomere functions grounding on TERRA firma. *Trends Cell Biol.* *25*, 29–36.

Balan, E., Decottignies, A., and Deldicque, L. (2018). Physical activity and nutrition: Two promising strategies for telomere maintenance? *Nutrients* *10*.

Bandaria, J.N., Qin, P., Berk, V., Chu, S., and Yildiz, A. (2016). Shelterin protects chromosome ends by compacting telomeric chromatin. *Cell* *164*, 735–746.



Barcenilla, B.B., and Shippen, D.E. (2019). Back to the future: The intimate and evolving connection between telomere-related factors and genotoxic stress. *J. Biol. Chem.* *294*, 14803–14813.

Barratt, S., Creamer, A., Hayton, C., and Chaudhuri, N. (2018). Idiopathic Pulmonary Fibrosis (IPF): An Overview. *J. Clin. Med.* *7*, 201.

Baumann, P., and Cech, T.R. (2000). Protection of telomeres by the Ku protein in fission yeast. *Mol. Biol. Cell* *11*, 3265–3275.

Baumann, P., and Cech, T.R. (2001). Pot1, the putative telomere end-binding protein in fission yeast and humans. *Science* (80- ). *292*, 1171–1175.

Baumann, P., and Price, C. (2010). Pot1 and telomere maintenance. *FEBS Lett.* *584*, 3779–3784.

Beedanagari, S., Vulimiri, S. V, Bhatia, S., and Mahadevan, B. (2014). Chapter 43 - Genotoxicity biomarkers: Molecular basis of genetic variability and susceptibility. R.C.B.T.-B. in T. Gupta, ed. (Boston: Academic Press), pp. 729–742.

Benarroch-Popivker, D., Pisano, S., Mendez-Bermudez, A., Lototska, L., Kaur, P., Bauwens, S., Djerbi, N., Latrick, C.M., Fraasier, V., Pei, B., et al. (2016). TRF2-Mediated Control of Telomere DNA Topology as a Mechanism for Chromosome-End Protection. *Mol. Cell* *61*, 274–286.

Berardini, T.Z., Reiser, L., Li, D., Mezheritsky, Y., Muller, R., Strait, E., and Huala, E. (2015). The arabidopsis information resource: Making and mining the “gold standard” annotated reference plant genome. *Genesis* *53*, 474–485.

Berglund, T., Wallström, A., Nguyen, T. Van, Laurell, C., and Ohlsson, A.B. (2017). Nicotinamide; antioxidative and DNA hypomethylation effects in plant cells. *Plant Physiol. Biochem.* *118*, 551–560.

Berman, A.J., Akiyama, B.M., Stone, M.D., and Cech, T.R. (2011). The RNA accordion model for template positioning by telomerase RNA during telomeric DNA synthesis. *Nat. Struct. Mol. Biol.* *18*, 1371–1375.

Bettin, N., Oss Pegorar, C., and Cusanelli, E. (2019). The Emerging Roles of TERRA in Telomere Maintenance and Genome Stability. *Cells* *8*, 246.

Bhat, A. V, Hora, S., Pal, A., Jha, S., and Taneja, R. (2018). Stressing the (Epi)Genome: Dealing with Reactive Oxygen Species in Cancer. *Antioxid. Redox Signal.* *29*, 1273–1292.

Biehler, K., and Fock, H. (1996). Evidence for the contribution of the Mehler-peroxidase reaction in dissipating excess electrons in drought-stressed wheat. *Plant Physiol.* *112*, 265–272.

Bilichak, A., Yao, Y., Titov, V., Golubov, A., and Kovalchuk, I. (2014). Genome stability in the *uvh6* mutant of *Arabidopsis thaliana*. *Plant Cell Rep.* *33*, 979–991.

Blackburn, E.H., and Collins, K. (2011). Telomerase: An RNP enzyme synthesizes DNA. *Cold Spring Harb. Perspect. Biol.* *3*, 1–9.

Blackburn, E.H., and Gall, J.G. (1978). A tandemly repeated sequence at the termini of the extrachromosomal ribosomal RNA genes in *Tetrahymena*. *J. Mol. Biol.* *120*, 33–53.

Bley, C.J., Qi, X., Rand, D.P., Borges, C.R., Nelson, R.W., and Chen, J.J.L. (2011). RNA-protein binding interface in the telomerase ribonucleoprotein. *Proc. Natl. Acad. Sci. U. S. A.* *108*, 20333–20338.

Boltz, K.A., Leehy, K., Song, X., Nelson, A.D., and Shippen, D.E. (2012). ATR cooperates with CTC1 and STN1 to maintain telomeres and genome integrity in *Arabidopsis*. *Mol. Biol. Cell* *23*, 1558–1568.

Bonetti, D., Clerici, M., Manfrini, N., Lucchini, G., and Longhese, M.P. (2010). The MRX complex plays multiple functions in resection of Yku- and Rif2-protected DNA ends. *PLoS One* *5*.

Bonetti, D., Martina, M., Falcettoni, M., and Longhese, M.P. (2014). Telomere-end processing: Mechanisms and regulation. *Chromosoma* *123*, 57–66.

Borlado, L.R., and Méndez, J. (2008). CDC6: From DNA replication to cell cycle checkpoints and oncogenesis. *Carcinogenesis* *29*, 237–243.

Bortesi, L., and Fischer, R. (2015). The CRISPR/Cas9 system for plant genome editing and beyond. *Biotechnol. Adv.* *33*, 41–52.

Box, J.A., Bunch, J.T., Tang, W., and Baumann, P. (2008). Spliceosomal cleavage generates the 3' end of telomerase RNA. *Nature* *456*, 910–914.

Brar, G.A., and Weissman, J.S. (2015). Ribosome profiling reveals the what, when, where and how of protein synthesis. *Nat. Rev. Mol. Cell Biol.* *16*, 651–664.

Bunch, J.T., Bae, N.S., Leonardi, J., and Baumann, P. (2005). Distinct Requirements for Pot1 in Limiting Telomere Length and Maintaining Chromosome

Stability. *Mol. Cell. Biol.* *25*, 5567–5578.

Calvete, O., Garcia-Pavia, P., Domínguez, F., Bougeard, G., Kunze, K., Braeuninger, A., Teule, A., Lasa, A., Ramón Y Cajal, T., Llord, G., et al. (2017). The wide spectrum of POT1 gene variants correlates with multiple cancer types. *Eur. J. Hum. Genet.* *25*, 1278–1281.

Casacuberta, E. (2017). *Drosophila*: Retrotransposons making up telomeres. *Viruses* *9*.

Casagrande, S., and Hau, M. (2019). Telomere attrition: Metabolic regulation and signalling function? *Biol. Lett.* *15*.

Cash, D.D., Cohen-Zontag, O., Kim, N.K., Shefer, K., Brown, Y., Ulyanov, N.B., Tzfati, Y., and Feigon, J. (2013). Pyrimidine motif triple helix in the *Kluyveromyces lactis* telomerase RNA pseudoknot is essential for function in vivo. *Proc. Natl. Acad. Sci. U. S. A.* *110*, 10970–10975.

Castillo-González, C., Liu, X., Huang, C., Zhao, C., Ma, Z., Hu, T., Sun, F., Zhou, Y., Zhou, X., Wang, X.J., et al. (2015). Geminivirus-encoded TrAP suppressor inhibits the histone methyltransferase SUVH4/KYP to counter host defense. *Elife* *4*, 1–31.

Chandra, A., Hughes, T.R., Nugent, C.I., and Lundblad, V. (2001). Cdc13 both positively and negatively regulates telomere replication. *Genes Dev.* *15*, 404–414.

Charbonnel, C., Niazi, A.K., Elvira-Matelot, E., Nowak, E., Zytnicki, M., De Bures, A., Jobet, E., Opsomer, A., Shamandi, N., Nowotny, M., et al. (2017). The siRNA suppressor RTL1 is redox-regulated through glutathionylation of a conserved cysteine in the double-stranded-RNA-binding domain. *Nucleic Acids Res.* *45*, 11891–11907.

Chen, J.-L. (2002). A critical stem-loop structure in the CR4-CR5 domain of mammalian telomerase RNA. *Nucleic Acids Res.* *30*, 592–597.

Chen, J.L., and Greider, C.W. (2003a). Template boundary definition in mammalian telomerase. *Genes Dev.* *17*, 2747–2752.

Chen, J.L., and Greider, C.W. (2003b). Determinants in mammalian telomerase RNA that mediate enzyme processivity and cross-species incompatibility. *EMBO J.* *22*, 304–314.

Chen, J.L., and Greider, C.W. (2005). Functional analysis of the pseudoknot structure in human telomerase RNA. *Proc. Natl. Acad. Sci. U. S. A.* *102*, 8080–8085.

Chen, L.Y., and Lingner, J. (2013). CST for the grand finale of telomere

replication. *Nucl. (United States)* 4.

Chen, J.L., Blasco, M.A., and Greider, C.W. (2000). Secondary structure of vertebrate telomerase RNA. *Cell* 100, 503–514.

Chen, L.-Y., Liu, D., and Songyang, Z. (2007). Telomere Maintenance through Spatial Control of Telomeric Proteins. *Mol. Cell. Biol.* 27, 5898–5909.

Chen, Q., Tao, S., Bi, X., Xu, X., Wang, L., and Li, X. (2013). Research of total levels on DNA methylation in plant based on HPLC analysis. *Am. J. Mol. Biol.* 03, 98–101.

Cheng, C.Y., Krishnakumar, V., Chan, A.P., Thibaud-Nissen, F., Schobel, S., and Town, C.D. (2017). Araport11: a complete reannotation of the *Arabidopsis thaliana* reference genome. *Plant J.* 89, 789–804.

Chezem, W.R., and Clay, N.K. (2016). Regulation of plant secondary metabolism and associated specialized cell development by MYBs and bHLHs. *Phytochemistry* 131, 26–43.

Chin, L., Artandi, S.E., Shen, Q., Tam, A., Lee, S.L., Gottlieb, G.J., Greider, C.W., and DePinho, R.A. (1999). P53 Deficiency Rescues the Adverse Effects of Telomere Loss and Cooperates With Telomere Dysfunction To Accelerate Carcinogenesis. *Cell* 97, 527–538.

Chow, T.T., Mak, S.S., Shay, J.W., and Wright, W.E. (2013). Telomeres. *Brenner's Encycl. Genet.* Second Ed. 38–43.

Churikov, D., and Price, C.M. (2008). Pot1 and cell cycle progression cooperate in telomere length regulation. *Nat. Struct. Mol. Biol.* 15, 79–84.

Churikov, D., Wei, C., and Price, C.M. (2006). Vertebrate POT1 Restricts G-Overhang Length and Prevents Activation of a Telomeric DNA Damage Checkpoint but Is Dispensable for Overhang Protection. *Mol. Cell. Biol.* 26, 6971–6982.

Churikov, D., Corda, Y., Luciano, P., and Géli, V. (2013). Cdc13 at a crossroads of telomerase action. *Front. Oncol.* 3, 39.

Cifuentes-Rojas, C., Kannan, K., Tseng, L., and Shippen, D.E. (2011). Two RNA subunits and POT1a are components of *Arabidopsis* telomerase. *Proc. Natl. Acad. Sci. U. S. A.* 108, 73–78.

Cifuentes-Rojas, C., Nelson, A.D.L., Boltz, K.A., Kannan, K., She, X., and Shippen, D.E. (2012). An alternative telomerase RNA in *arabidopsis* modulates enzyme

activity in response to DNA damage. *Genes Dev.* *26*, 2512–2523.

Cohn, M. (2013). OB Fold Contributes to Telomere Maintenance. *Structure* *21*, 3–4.

Collins, K. (1999). Ciliate Telomerase Biochemistry. *Annu. Rev. Biochem.* *68*, 187–218.

Collins, A.R., Dušinská, M., Gedik, C.M., and Štětina, R. (1996). Oxidative damage to DNA: Do we have a reliable biomarker? *Environ. Health Perspect.* *104*, 465–469.

Coluzzi, E., Colamartino, M., Cozzi, R., Leone, S., Meneghini, C., O’Callaghan, N., and Sgura, A. (2014). Oxidative stress induces persistent telomeric DNA damage responsible for nuclear morphology change in mammalian cells. *PLoS One* *9*, e110963.

Conway, C., McCulloch, R., Ginger, M.L., Robinson, N.P., Browitt, A., and David Barry, J. (2002). Ku is important for telomere maintenance, but not for differential expression of telomeric VSG genes, in African trypanosomes. *J. Biol. Chem.* *277*, 21269–21277.

Cooke, M.S., Evans, M.D., Dizdaroglu, M., and Lunec, J. (2003). Oxidative DNA damage: mechanisms, mutation, and disease. *FASEB J.* *17*, 1195–1214.

Corbett, N., and Alda, M. (2015). On telomeres long and short. *J. Psychiatry Neurosci.* *40*, 3–4.

Corpas, F.J., Barroso, J.B., Palma, J.M., and Rodriguez-Ruiz, M. (2017). Plant peroxisomes: A nitro-oxidative cocktail. *Redox Biol.* *11*, 535–542.

Crasta, K., Ganem, N.J., Dagher, R., Lantermann, A.B., Ivanova, E. V., Pan, Y., Nezi, L., Protopopov, A., Chowdhury, D., and Pellman, D. (2012). DNA breaks and chromosome pulverization from errors in mitosis. *Nature* *482*, 53–58.

Crick, F.H.C. (1966). Codon—anticodon pairing: The wobble hypothesis. *J. Mol. Biol.* *19*, 548–555.

Czarnocka, W., and Karpiński, S. (2018). Friend or foe? Reactive oxygen species production, scavenging and signaling in plant response to environmental stresses. *Free Radic. Biol. Med.* *122*, 4–20.

Das, M., Singh, S., Pradhan, S., and Narayan, G. (2014). MCM Paradox: Abundance of Eukaryotic Replicative Helicases and Genomic Integrity. *Mol. Biol. Int.* *2014*, 1–11.

Delannoy, E., Ret, M. Le, Faivre-Nitschke, E., Estavillo, G.M., Bergdoll, M., Taylor, N.L., Pogson, B.J., Small, I., Lmbault, P., and Gualberto, J.M. (2009). Arabidopsis tRNA adenosine deaminase arginine edits the wobble nucleotide of chloroplast tRNA<sup>Arg</sup>(ACG) and is essential for efficient chloroplast translation. *Plant Cell* *21*, 2058–2071.

Demkovičová, E., Bauer, L., Kraččíková, P., Tlučková, K., Tóthová, P., Halaganová, A., Valušová, E., and Víglaský, V. (2017). Telomeric G-Quadruplexes: From Human to Tetrahymena Repeats. *J. Nucleic Acids* *2017*.

Denchi, E.L., and De Lange, T. (2007). Protection of telomeres through independent control of ATM and ATR by TRF2 and POT1. *Nature* *448*, 1068–1071.

Deng, Z., Wang, Z., Stong, N., Plasschaert, R., Moczan, A., Chen, H.S., Hu, S., Wikramasinghe, P., Davuluri, R. V., Bartolomei, M.S., et al. (2012). A role for CTCF and cohesin in subtelomere chromatin organization, TERRA transcription, and telomere end protection. *EMBO J.* *31*, 4165–4178.

Dew-Budd, K., Cheung, J., Palos, K., Forsythe, E.S., and Beilstein, M.A. (2020). Evolutionary and biochemical analyses reveal conservation of the Brassicaceae telomerase ribonucleoprotein complex. *PLoS One* *15*, 1–18.

Ding, Y., Tang, Y., Kwok, C.K., Zhang, Y., Bevilacqua, P.C., and Assmann, S.M. (2014). In vivo genome-wide profiling of RNA secondary structure reveals novel regulatory features. *Nature* *505*, 696–700.

Dionne, I., and Wellinger, R.J. (1998). Processing of telomeric DNA ends requires the passage of a replication fork. *Nucleic Acids Res.* *26*, 5365–5371.

Dixit, S., Whooley, M.A., Vittinghoff, E., Roberts, J.D., Heckbert, S.R., Fitzpatrick, A.L., Lin, J., Leung, C., Mukamal, K.J., and Marcus, G.M. (2019). Alcohol consumption and leukocyte telomere length. *Sci. Rep.* *9*, 1–10.

Dizdaroglu, M., Karahalil, B., Sentürker, S., Buckley, T.J., and Roldán-Arjona, T. (1999). Excision of products of oxidative DNA base damage by human NTH1 protein. *Biochemistry* *38*, 243–246.

Doksani, Y., Wu, J.Y., De Lange, T., and Zhuang, X. (2013). XSuper-resolution fluorescence imaging of telomeres reveals TRF2-dependent T-loop formation. *Cell* *155*, 345.

Downs, J.A., and Jackson, S.P. (2004). A means to a DNA end: The many roles of Ku. *Nat. Rev. Mol. Cell Biol.* *5*, 367–378.

Dregalla, R.C., Zhou, J., Idate, R.R., Battaglia, C.L.R., Liber, H.L., and Bailey, S.M. (2010). Regulatory roles of tankyrase 1 at telomeres and in DNA repair: Suppression of T-SCE and stabilization of DNA-pkcs. *Aging (Albany, NY)*. 2, 691–708.

Duan, Q., Kita, D., Johnson, E.A., Aggarwal, M., Gates, L., Wu, H.M., and Cheung, A.Y. (2014). Reactive oxygen species mediate pollen tube rupture to release sperm for fertilization in *Arabidopsis*. *Nat. Commun.* 5, 3129.

Dunand, C., Crèvecoeur, M., and Penel, C. (2007). Distribution of superoxide and hydrogen peroxide in *Arabidopsis* root and their influence on root development: Possible interaction with peroxidases. *New Phytol.* 174, 332–341.

Egan, E.D., and Collins, K. (2010). Specificity and Stoichiometry of Subunit Interactions in the Human Telomerase Holoenzyme Assembled In Vivo. *Mol. Cell. Biol.* 30, 2775–2786.

Egan, E.D., and Collins, K. (2012). Biogenesis of telomerase ribonucleoproteins. *Rna* 18, 1747–1759.

Fajkus, P., Peška, V., Závodník, M., Fojtová, M., Fulnečková, J., Dobias, Š., Kilar, A., Dvořáčková, M., Zachová, D., Nečasová, I., et al. (2019). Telomerase RNAs in land plants. *Nucleic Acids Res.* 47, 9842–9856.

Fang, G., and Cech, T.R. (1993). Oxytricha telomere-binding protein: DNA-dependent dimerization of the  $\alpha$  and  $\beta$  subunits. *Proc. Natl. Acad. Sci. U. S. A.* 90, 6056–6060.

Fang, X., Corrales, J., Thornton, C., Scheffler, B.E., and Willett, K.L. (2013). Global and gene specific DNA methylation changes during zebrafish development. *Comp. Biochem. Physiol. - B Biochem. Mol. Biol.* 166, 99–108.

Feng, X., Hsu, S.J., Bhattacharjee, A., Wang, Y., Diao, J., and Price, C.M. (2018). CTC1-STN1 terminates telomerase while STN1-TEN1 enables C-strand synthesis during telomere replication in colon cancer cells. *Nat. Commun.* 9.

Fernández-Casañas, M., and Chan, K.L. (2018). The unresolved problem of DNA bridging. *Genes (Basel)*. 9.

Ferrara-Romeo, I., Martinez, P., Saraswati, S., Whittemore, K., Graña-Castro, O., Thelma Poluha, L., Serrano, R., Hernandez-Encinas, E., Blanco-Aparicio, C., Maria Flores, J., et al. (2020). The mTOR pathway is necessary for survival of mice with short telomeres. *Nat. Commun.* 11, 1–17.

Finger, S.N., and Bryan, T.M. (2008). Multiple DNA-binding sites in *Tetrahymena* telomerase. *Nucleic Acids Res.* *36*, 1260–1272.

Fisher, T.S., Taggart, A.K.P., and Zakian, V.A. (2004). Cell cycle-dependent regulation of yeast telomerase by Ku. *Nat. Struct. Mol. Biol.* *11*, 1198–1205.

Fouquerel, E., Lormand, J., Bose, A., Lee, H.T., Kim, G.S., Li, J., Sobol, R.W., Freudenthal, B.D., Myong, S., and Opresko, P.L. (2016). Oxidative guanine base damage regulates human telomerase activity. *Nat. Struct. Mol. Biol.* *23*, 1092–1100.

Francia, S., Weiss, R.S., and d'Adda di Fagagna, F. (2007). Need telomere maintenance? Call 911. *Cell Div.* *2*, 1–6.

Fransen, M., Nordgren, M., Wang, B., and Apanasets, O. (2012). Role of peroxisomes in ROS/RNS-metabolism: Implications for human disease. *Biochim. Biophys. Acta - Mol. Basis Dis.* *1822*, 1363–1373.

French, B.T., and Trewyn, R.W. (1990). Modification of the anticodon wobble position of tRNA<sup>Ala</sup> in vitro does not require 5' or 3' processing. *Gene* *96*, 301–304.

Fu, D., and Collins, K. (2007). Purification of Human Telomerase Complexes Identifies Factors Involved in Telomerase Biogenesis and Telomere Length Regulation. *Mol. Cell* *28*, 773–785.

Fulcher, N., Teubenbacher, A., Kerdaffrec, E., Farlow, A., Nordborg, M., and Riha, K. (2014). Genetic architecture of natural variation of telomere length in *Arabidopsis thaliana*. *Genetics* *199*, 625–635.

Galati, A., Micheli, E., and Cacchione, S. (2013). Chromatin structure in telomere dynamics. *Front. Oncol.* *3* MAR, 1–16.

Galati, A., Micheli, E., Alicata, C., Ingegnere, T., Cicconi, A., Pusch, M.C., Giraud-Panis, M.J., Gilson, E., and Cacchione, S. (2015). TRF1 and TRF2 binding to telomeres is modulated by nucleosomal organization. *Nucleic Acids Res.* *43*, 5824–5837.

Gallardo, F., Olivier, C., Dandjinou, A.T., Wellinger, R.J., and Chartrand, P. (2008). TLC1 RNA nucleo-cytoplasmic trafficking links telomerase biogenesis to its recruitment to telomeres. *EMBO J.* *27*, 748–757.

Gallardo, F., Laterreur, N., Cusanelli, E., Ouenzar, F., Querido, E., Wellinger, R.J., and Chartrand, P. (2011). Live cell imaging of telomerase RNA dynamics reveals cell cycle-dependent clustering of telomerase at elongating telomeres. *Mol. Cell* *44*, 819–827.

Gao, H., Cervantes, R.B., Mandell, E.K., Otero, J.H., and Lundblad, V. (2007).



RPA-like proteins mediate yeast telomere function. *Nat. Struct. Mol. Biol.* *14*, 208–214.

Garavís, M., González, C., and Villasante, A. (2013). On the origin of the eukaryotic chromosome: The role of noncanonical dna structures in telomere evolution. *Genome Biol. Evol.* *5*, 1142–1150.

Garforth, S.J., Wu, Y.Y., and Prasad, V.R. (2006). Structural features of mouse telomerase RNA are responsible for the lower activity of mouse telomerase versus human telomerase. *Biochem. J.* *397*, 399–406.

Gatbonton, T., Imbesi, M., Nelson, M., Akey, J.M., Ruderfer, D.M., Kruglyak, L., Simon, J.A., and Bedalov, A. (2006). Telomere length as a quantitative trait: Genome-wide survey and genetic mapping of telomere length-control genes in yeast. *PLoS Genet.* *2*, 0304–0315.

Gerber, A.P., and Keller, W. (2017). An Adenosine Deaminase That Generates Inosine at the Wobble Position of tRNAs Published by : American Association for the Advancement of Science Stable URL : <http://www.jstor.org/stable/2900044> REFERENCES Linked references are available on JSTOR for this . *286*, 1146–1149.

Giglia-Mari, G., Zotter, A., and Vermeulen, W. (2011). DNA damage response. *Cold Spring Harb. Perspect. Biol.* *3*, 1–19.

Gilley, D., and Blackburn, E.H. (1999). The telomerase RNA pseudoknot is critical for the stable assembly of a catalytically active ribonucleoprotein. *Proc. Natl. Acad. Sci. U. S. A.* *96*, 6621–6625.

Gobbini, E., Trovesi, C., Cassani, C., and Longhese, M.P. (2014). Telomere uncapping at the crossroad between cell cycle arrest and carcinogenesis. *Mol. Cell. Oncol.* *1*, 1–7.

Göhring, J., Fulcher, N., Jacak, J., and Riha, K. (2014). TeloTool: A new tool for telomere length measurement from terminal restriction fragment analysis with improved probe intensity correction. *Nucleic Acids Res.* *42*, 1–10.

Goldman, F., Bouarich, R., Kulkarni, S., Freeman, S., Du, H.Y., Harrington, L., Mason, P.J., Londoño-Vallejo, A., and Bessler, M. (2005). The effect of TERC haploinsufficiency on the inheritance of telomere length. *Proc. Natl. Acad. Sci. U. S. A.* *102*, 17119–17124.

Gomez, D.E., Armando, R.G., Farina, H.G., Menna, P.L., Cerrudo, C.S., Ghiringhelli, P.D., and Alonso, D.F. (2012). Telomere structure and telomerase in health and disease (Review). *Int. J. Oncol.* *41*, 1561–1569.

Gordon, D.M., and Santos, J.H. (2010). The emerging role of telomerase reverse

transcriptase in mitochondrial DNA metabolism. *J. Nucleic Acids* 2010.

Gottschling, D.E., and Zakian, V.A. (1986). Telomere proteins: Specific recognition and protection of the natural termini of *Oxytricha* macronuclear DNA. *Cell* 47, 195–205.

Grehl, C., Kuhlmann, M., Becker, C., Glaser, B., and Grosse, I. (2018). How to Design a Whole-Genome Bisulfite Sequencing Experiment. *Epigenomes* 2, 21.

Greider, C.W., and Blackburn, E.H. (1985). Identification of a specific telomere terminal transferase activity in tetrahymena extracts. *Cell* 43, 405–413.

Greider, C.W., and Blackburn, E.H. (1989). A telomeric sequence in the RNA of *Tetrahymena* telomerase required for telomere repeat synthesis. *Nature* 337, 331–337.

Griffith, J.D. (2013). Many ways to loop DNA. *J. Biol. Chem.* 288, 29724–29735.

Griffith, J.D., Comeau, L., Rosenfield, S., Stansel, R.M., Bianchi, A., Moss, H., and de Lange, T. (1999). Mammalian Telomeres End in a Large Duplex Loop. *Cell* 97, 503–514.

Grosjean, H., Constantinesco, F., Foiret, D., and Benachenhou, N. (1995). A novel enzymatic pathway leading to 1-methylinosine modification in *Haloferax volcanii* tRNA. *Nucleic Acids Res.* 23, 4312–4319.

Grosjean, H., Crécy-Lagard, V. de, and Marck, C. (2010). Deciphering synonymous codons in the three domains of life: Co-evolution with specific tRNA modification enzymes. *FEBS Lett.* 584, 252–264.

Gu, P., Wang, Y., Bisht, K.K., Wu, L., Kukova, L., Smith, E.M., Xiao, Y., Bailey, S.M., Lei, M., Nandakumar, J., et al. (2017). Pot1 OB-fold mutations unleash telomere instability to initiate tumorigenesis. *Oncogene* 36, 1939–1951.

Gupta, A., Sharma, S., Reichenbach, P., Marjavaara, L., Nilsson, A.K., Lingner, J., Chabes, A., Rothstein, R., and Chang, M. (2013). Telomere length homeostasis responds to changes in intracellular dNTP pools. *Genetics* 193, 1095–1105.

Gyori, B.M., Venkatachalam, G., Thiagarajan, P.S., Hsu, D., and Clement, M.V. (2014). OpenComet: An automated tool for comet assay image analysis. *Redox Biol.* 2, 457–465.

Halicka, H.D., Zhao, H., Podhorecka, M., Traganos, F., and Darzynkiewicz, Z. (2009). Cytometric detection of chromatin relaxation, an early reporter of DNA damage response. *Cell Cycle* 8, 2233–2237.

- Harley, C.B. (1990). [Letters to nature]. *Nature* 345, 458.
- Harley, C.B. (1991). Telomere loss: mitotic clock or genetic time bomb? *Mutat. Res. DNAGing* 256, 271–282.
- Harrington, L. (2012). Haploinsufficiency and telomere length homeostasis. *Mutat. Res. - Fundam. Mol. Mech. Mutagen.* 730, 37–42.
- Hasegawa, J., Sakamoto, T., Fujimoto, S., Yamashita, T., Suzuki, T., and Matsunaga, S. (2018). Auxin decreases chromatin accessibility through the TIR1/AFBs auxin signaling pathway in proliferative cells. *Sci. Rep.* 8, 1–12.
- Haumont, E., Fournier, M., Henau, S. De, and Grosjean, H. (1984). *Nucleic Acids Research* conversion of A , into I. 12, 2705–2715.
- Hayflick, L. (1965). The limited in vitro lifetime of human diploid cell strains. *Exp. Cell Res.* 37, 614–636.
- He, P., Shan, L., and Sheen, J. (2006). *Plant-Pathogen Interactions, Methods and Protocols.* 1–9.
- He, P., Shan, L., and Sheen, J. (2007). The use of protoplasts to study innate immune responses. *Methods Mol. Biol.* 354, 1–9.
- Heacock, M., Spangler, E., Riha, K., Puizina, J., and Shippen, D.E. (2004). Molecular analysis of telomere fusions in Arabidopsis: Multiple pathways for chromosome end-joining. *EMBO J.* 23, 2304–2313.
- Heiss, N.S., Knight, S.W., Vulliamy, T., Klauck, S.M., Wiemann, S., Mason, P., Poustka, A., and Dokal, I. (1998). With Putative Nucleolar Functions. *Nat. Genet.* 19, 32–38.
- Hemann, M.T. (2000). Wild-derived inbred mouse strains have short telomeres. *Nucleic Acids Res.* 28, 4474–4478.
- Heslop-Harrison, J.S. (1998). Cytogenetic analysis of Arabidopsis. *Methods Mol. Biol.* 82, 119–127.
- Hirano, Y., Fukunaga, K., and Sugimoto, K. (2009). Rif1 and Rif2 Inhibit Localization of Tell to DNA Ends. *Mol. Cell* 33, 312–322.
- Hockemeyer, D., Sfeir, A.J., Shay, J.W., Wright, W.E., and De Lange, T. (2005). POT1 protects telomeres from a transient DNA damage response and determines how human chromosomes end. *EMBO J.* 24, 2667–2678.

Hockemeyer, D., Daniels, J.-P., Takai, H., and de Lange, T. (2006). Recent Expansion of the Telomeric Complex in Rodents: Two Distinct POT1 Proteins Protect Mouse Telomeres. *Cell* 126, 63–77.

Holohan, B., Wright, W.E., and Shay, J.W. (2014). Telomeropathies: An emerging spectrum disorder. *J. Cell Biol.* 205, 289–299.

Hong, J.H., Savina, M., Du, J., Devendran, A., Kannivadi Ramakanth, K., Tian, X., Sim, W.S., Mironova, V. V., and Xu, J. (2017). A Sacrifice-for-Survival Mechanism Protects Root Stem Cell Niche from Chilling Stress. *Cell*.

Horvath, M.P., Schweiker, V.L., Bevilacqua, J.M., Ruggles, J.A., and Schultz, S.C. (1998). Crystal structure of the *Oxytricha nova* telomere end binding protein complexed with single strand DNA. *Cell* 95, 963–974.

Hruz, T., Laule, O., Szabo, G., Wessendorp, F., Bleuler, S., Oertle, L., Widmayer, P., Gruissem, W., and Zimmermann, P. (2008). Genevestigator V3: A Reference Expression Database for the Meta-Analysis of Transcriptomes. *Adv. Bioinformatics* 2008, 1–5.

Hsu, H.L., Gilley, D., Galande, S.A., Prakash Hande, M., Allen, B., Kim, S.H., Li, G.C., Campisi, J., Kohwi-Shigematsu, T., and Chen, D.J. (2000). Ku acts in a unique way at the mammalian telomere to prevent end joining. *Genes Dev.* 14, 2807–2812.

Hu, L., Liang, W., Yin, C., Cui, X., Zong, J., Wang, X., Hu, J., and Zhang, D. (2011). Rice MADS3 regulates ROS homeostasis during late anther development. *Plant Cell* 23, 515–533.

Hu, Y., Lu, Y., Zhao, Y., and Zhou, D.X. (2019). Histone Acetylation Dynamics Integrates Metabolic Activity to Regulate Plant Response to Stress. *Front. Plant Sci.* 10, 1–9.

Huang, W.H., and Keller, W.D. (1972). © 1972 Nature Publishing Group. *Nat. New Biol.* 239, 149–151.

Huang, H., Ullah, F., Zhou, D.-X., Yi, M., and Zhao, Y. (2019). Mechanisms of ROS Regulation of Plant Development and Stress Responses. *Front. Plant Sci.* 10, 800.

Hukezalie, K.R., and Wong, J.M.Y. (2013). Structure-function relationship and biogenesis regulation of the human telomerase holoenzyme. *FEBS J.* 280, 3194–3204.

Hussain, A., Mun, B.G., Imran, Q.M., Lee, S.U., Adamu, T.A., Shahid, M., Kim, K.M., and Yun, B.W. (2016). Nitric oxide mediated transcriptome profiling reveals

activation of multiple regulatory pathways in *Arabidopsis thaliana*. *Front. Plant Sci.* 7, 1–18.

Huysmans, M., Lema A, S., Coll, N.S., and Nowack, M.K. (2017). Dying two deaths — programmed cell death regulation in development and disease. *Curr. Opin. Plant Biol.* 35, 37–44.

Ishikawa, F., and Naito, T. (1999). Why do we have linear chromosomes? A matter of Adam and Eve. *Mutat. Res. - DNA Repair* 434, 99–107.

Jaco, I., Muñoz, P., and Blasco, M.A. (2004). Role of human Ku86 in telomere length maintenance and telomere capping. *Cancer Res.* 64, 7271–7278.

Jacob, N.K., Lescasse, R., Linger, B.R., and Price, C.M. (2007). Tetrahymena POT1a regulates telomere length and prevents activation of a cell cycle checkpoint. *Mol. Cell. Biol.* 27, 1592–1601.

Janků, M., Luhová, L., and Petřivalský, M. (2019). On the Origin and Fate of Reactive Oxygen Species in Plant Cell Compartments. *Antioxidants* 8, 105.

Jansson, L.I., Akiyama, B.M., Ooms, A., Lu, C., Rubin, S.M., and Stone, M.D. (2015). Structural basis of template-boundary definition in Tetrahymena telomerase. *Nat. Struct. Mol. Biol.* 22, 883–888.

Jeffrey Chiang, Y., Calado, R.T., Hathcock, K.S., Lansdorp, P.M., Young, N.S., and Hodes, R.J. (2010). Telomere length is inherited with resetting of the telomere set-point. *Proc. Natl. Acad. Sci. U. S. A.* 107, 10148–10153.

Jiang, J., Chan, H., Cash, D.D., Miracco, E.J., Loo, R.R.O., Upton, H.E., Cascio, D., Johnson, R.O.B., Collins, K., Loo, J.A., et al. (2015). Structure of Tetrahymena telomerase reveals previously unknown subunits, functions, and interactions. *Science* (80-). 350.

John Aitken, R., Clarkson, J.S., and Fishel, S. (1989). Generation of Reactive Oxygen Species, Lipid Peroxidation, and Human Sperm Function. *Biol. Reprod.* 41, 183–197.

Jühling, F., Mörl, M., Hartmann, R.K., Sprinzl, M., Stadler, P.F., and Pütz, J. (2009). tRNADB 2009: Compilation of tRNA sequences and tRNA genes. *Nucleic Acids Res.* 37, 159–162.

Kaczmarczyk, A., Meng, H., Ordu, O., Noort, J. van, and Dekker, N.H. (2020). Chromatin fibers stabilize nucleosomes under torsional stress. *Nat. Commun.* 11, 1–12.

Kamiya, T., Goto, A., Kurokawa, E., Hara, H., and Adachi, T. (2016). Cross Talk Mechanism among EMT, ROS, and Histone Acetylation in Phorbol Ester-Treated Human Breast Cancer MCF-7 Cells. *Oxid. Med. Cell. Longev.* 2016.

Kannan, R., Helston, R.M., Dannebaum, R.O., and Baumann, P. (2015). Diverse mechanisms for spliceosome-mediated 3' end processing of telomerase RNA. *Nat. Commun.* 6, 1–8.

Kapur, M., and Ackerman, S.L. (2018). mRNA Translation Gone Awry: Translation Fidelity and Neurological Disease. *Trends Genet.* 34, 218–231.

Kazda, A., Zellinger, B., Rössler, M., Derboven, E., Kusenda, B., and Riha, K. (2012a). Chromosome end protection by blunt-ended telomeres. *Genes Dev.* 26, 1703–1713.

Kazda, A., Zellinger, B., Rössler, M., Derboven, E., Kusenda, B., and Riha, K. (2012b). Chromosome end protection by blunt-ended telomeres. *Genes Dev.* 26, 1703–1713.

Keegan, L.P., Gerber, A.P., Brindle, J., Leemans, R., Gallo, A., Keller, W., and O'Connell, M.A. (2000). The Properties of a tRNA-Specific Adenosine Deaminase from *Drosophila melanogaster* Support an Evolutionary Link between Pre-mRNA Editing and tRNA Modification. *Mol. Cell. Biol.* 20, 825–833.

Keegan, L.P., Leroy, A., Sproul, D., and O'Connell, M.A. (2004). Adenosine deaminases acting on RNA (ADARs): RNA-editing enzymes. *Genome Biol.* 5.

Kelleher, C., Kurth, I., and Lingner, J. (2005). Human Protection of Telomeres 1 (POT1) Is a Negative Regulator of Telomerase Activity In Vitro. *Mol. Cell. Biol.* 25, 808–818.

Kim, N.K., Zhang, Q., Zhou, J., Theimer, C.A., Peterson, R.D., and Feigon, J. (2008). Solution Structure and Dynamics of the Wild-type Pseudoknot of Human Telomerase RNA. *J. Mol. Biol.* 384, 1249–1261.

Klepikova, A. V., Kasianov, A.S., Gerasimov, E.S., Logacheva, M.D., and Penin, A.A. (2016). A high resolution map of the *Arabidopsis thaliana* developmental transcriptome based on RNA-seq profiling. *Plant J.* 88, 1058–1070.

Kobayashi, C.R., Castillo-González, C., Survotseva, Y., Canal, E., Nelson, A.D.L., and Shippen, D.E. (2019). Recent emergence and extinction of the protection of telomeres 1c gene in *Arabidopsis thaliana*. *Plant Cell Rep.* 38, 1081–1097.

Koliada, A.K., Krasnenkov, D.S., and Vaiserman, A.M. (2015). Telomeric aging:

Mitotic clock or stress indicator? *Front. Genet.* 5, 2003–2006.

Konishi, A., and De Lange, T. (2008). Cell cycle control of telomere protection and NHEJ revealed by a ts mutation in the DNA-binding domain of TRF2. *Genes Dev.* 22, 1221–1230.

Koornneef, M., and van der Veen, J.H. (1980). Induction and analysis of gibberellin sensitive mutants in *Arabidopsis thaliana* (L.) heynh. *Theor. Appl. Genet.* 58, 257–263.

Kratz, K., and De Lange, T. (2018). Protection of telomeres 1 proteins POT1a and POT1b can repress ATR signaling by RPA exclusion, but binding to CST limits ATR repression by POT1b. *J. Biol. Chem.* 293, 14384–14392.

Kreuz, S., and Fischle, W. (2016). Oxidative stress signaling to chromatin in health and disease. *Epigenomics* 8, 843–862.

Krishnamurthy, A., and Rathinasabapathi, B. (2013). Oxidative stress tolerance in plants. *Plant Signal. Behav.* 8, e25761.

Lange, T. de (2018). Shelterin-Mediated Telomere Protection. *Annu. Rev. Genet.* 52, 223–247.

de Lange, T. (2018). Shelterin-Mediated Telomere Protection. *Annu. Rev. Genet.* 52, 223–247.

de Lange, T. (2004). T-loops and the origin of telomeres. *Nat. Rev. Mol. Cell Biol.* 5, 323–329.

de Lange, T. (2005). Shelterin: The protein complex that shapes and safeguards human telomeres. *Genes Dev.* 19, 2100–2110.

de Lange, T. (2009). How telomeres solve the end-protection problem. *Science* (80-. ). 326, 948–952.

de Lange, T. (2015). A loopy view of telomere evolution. *Front. Genet.* 6, 1–5.

Langie, S.A.S., Azqueta, A., and Collins, A.R. (2015). The comet assay: Past, present, and future. *Front. Genet.* 6, 1–3.

Laroche, T., Martin, S.G., Gotta, M., Gorham, H.C., Pryde, F.E., Louis, E.J., and Gasser, S.M. (1998). Mutation of yeast Ku genes disrupts the subnuclear organization of telomeres. *Curr. Biol.* 8, 653–657.

Latrack, C.M., and Cech, T.R. (2010). POT1-TPP1 enhances telomerase

processivity by slowing primer dissociation and aiding translocation. *EMBO J.* 29, 924–933.

Leão, R., Apolónio, J.D., Lee, D., Figueiredo, A., Tabori, U., and Castelo-Branco, P. (2018). Mechanisms of human telomerase reverse transcriptase (hTERT) regulation: Clinical impacts in cancer. *J. Biomed. Sci.* 25, 1–12.

Lee, H.T., Bose, A., Lee, C.Y., Opresko, P.L., and Myong, S. (2017). Molecular mechanisms by which oxidative DNA damage promotes telomerase activity. *Nucleic Acids Res.* 45, 11752–11765.

Lee, J.R., Xie, X., Yang, K., Zhang, J., Lee, S.Y., and Shippen, D.E. (2016). Dynamic interactions of Arabidopsis TEN1: Stabilizing telomeres in response to heat stress. *Plant Cell* 28, 2212–2224.

Lee, O.-H., Kim, H., He, Q., Baek, H.J., Yang, D., Chen, L.-Y., Liang, J., Chae, H.K., Safari, A., Liu, D., et al. (2011). Genome-wide YFP fluorescence complementation screen identifies new regulators for telomere signaling in human cells. *Mol. Cell. Proteomics* 10, M110.001628.

Leehy, K.A., Lee, J.R., Song, X., Renfrew, K.B., and Shippen, D.E. (2013). MERISTEM DISORGANIZATION1 encodes TEN1, an essential telomere protein that modulates telomerase processivity in arabidopsis. *Plant Cell* 25, 1343–1354.

Lemon, L.D., Morris, D.K., and Bertuch, A.A. (2019). Loss of Ku's DNA end binding activity affects telomere length via destabilizing telomere-bound Est1 rather than altering TLC1 homeostasis. *Sci. Rep.* 9, 1–13.

Lenain, C., Bauwens, S., Amiard, S., Brunori, M., Giraud-Panis, M.J., and Gilson, E. (2006). The Apollo 5' Exonuclease Functions Together with TRF2 to Protect Telomeres from DNA Repair. *Curr. Biol.* 16, 1303–1310.

Li, X. (2011). Pollen Fertility/Viability Assay Using FDA Staining. *1*, 1–2.

Li, S., Makovets, S., Matsuguchi, T., Blethrow, J.D., Shokat, K.M., and Blackburn, E.H. (2009). Cdk1-Dependent Phosphorylation of Cdc13 Coordinates Telomere Elongation during Cell-Cycle Progression. *Cell* 136, 50–61.

Li, Y., Li, X., Cao, M., Jiang, Y., Yan, J., Liu, Z., Yang, R., Chen, X., Sun, P., and Xiang, R. (2019). Seryl tRNA synthetase cooperates with POT1 to regulate telomere length and cellular senescence. *Signal Transduct. Target. Ther.* 1–11.

Lim, V.I. (1995). Analysis of action of the wobble adenine on codon reading within the ribosome. *J. Mol. Biol.* 252, 277–282.



Lin, J.J., and Zakian, V.A. (1996). The *Saccharomyces* CDC13 protein is a single-strand TG1-3 telomeric DNA-binding protein in vitro that affects telomere behavior in vivo. *Proc. Natl. Acad. Sci. U. S. A.* *93*, 13760–13765.

Lin, J., Ly, H., Hussain, A., Abraham, M., Pearl, S., Tzfati, Y., Parslow, T.G., and Blackburn, E.H. (2004). A universal telomerase RNA core structure includes structured motifs required for binding the telomerase reverse transcriptase protein. *Proc. Natl. Acad. Sci. U. S. A.* *101*, 14713–14718.

Lingner, J., Hendrick, L.L., and Cech, T.R. (1994). Telomerase RNAs of different ciliates have a common secondary structure and a permuted template. *Genes Dev.* *8*, 1984–1998.

Liu, N.N., Han, T.X., Du, L.L., and Zhou, J.Q. (2010). A genome-wide screen for *Schizosaccharomyces pombe* deletion mutants that affect telomere length. *Cell Res.* *20*, 963–965.

Liu, T., Van Staden, J., and Cress, W.A. (2000). Salinity induced nuclear and DNA degradation in meristematic cells of soybean (*Glycine max* (L.)) roots. *Plant Growth Regul.* *30*, 49–54.

Loayza, D., and De Lange, T. (2003). POT1 as a terminal transducer of TRF1 telomere length control. *Nature* *423*, 1013–1018.

Locato, V., and De Gara, L. (2018). Programmed cell death in plants: An overview. *Methods Mol. Biol.* *1743*, 1–8.

Londoño-Vallejo, J.A., and Wellinger, R.J. (2012). Telomeres and telomerase dance to the rhythm of the cell cycle. *Trends Biochem. Sci.* *37*, 391–399.

Lonkar, P., and Dedon, P.C. (2011). Reactive species and DNA damage in chronic inflammation: Reconciling chemical mechanisms and biological fates. *Int. J. Cancer* *128*, 1999–2009.

Lord, T., and Aitken, R.J. (2015). Fertilization stimulates 8-hydroxy-2'-deoxyguanosine repair and antioxidant activity to prevent mutagenesis in the embryo. *Dev. Biol.* *406*, 1–13.

Luke-Glaser, S., Poschke, H., and Luke, B. (2012). Getting in (and out of) the loop: regulating higher order telomere structures. *Front. Oncol.* *2*, 1–6.

Lustig, A.J. (2003). Clues to catastrophic telomere loss in mammals from yeast telomere rapid deletion. *Nat. Rev. Genet.* *4*, 916–923.

Lydall, D. (2003). Hiding at the ends of yeast chromosomes: Telomeres, nucleases and checkpoint pathways. *J. Cell Sci.* *116*, 4057–4065.

Lyu, X., Yang, Q., Li, L., Dang, Y., Zhou, Z., Chen, S., and Liu, Y. (2020). Adaptation of codon usage to tRNA I34 modification controls translation kinetics and proteome landscape. *PLoS Genet.* *16*, e1008836.

M., S.K.R., Wang, Y., Zhang, X., Cheng, H., Sun, L., He, S., and Hao, F. (2020). Redox Components: Key Regulators of Epigenetic Modifications in Plants. *Int. J. Mol. Sci.* *21*, 1419.

Maas, S., Gerber, A.P., and Rich, A. (1999). Identification and characterization of a human tRNA-specific adenosine deaminase related to the ADAR family of pre-mRNA editing enzymes. *Proc. Natl. Acad. Sci. U. S. A.* *96*, 8895–8900.

Maciejowski, J., and De Lange, T. (2017). Telomeres in cancer: Tumour suppression and genome instability. *Nat. Rev. Mol. Cell Biol.* *18*, 175–186.

Maicher, A., Kastner, L., and Luke, B. (2012). Telomeres and disease: Enter TERRA. *RNA Biol.* *9*, 843–849.

Mangahas, J.L., Alexander, M.K., Sandell, L.L., and Zakian, V.A. (2001). Repair of chromosome ends after telomere loss in *Saccharomyces*. *Mol. Biol. Cell* *12*, 4078–4089.

Mangano, S., Denita-Juarez, S.P., Choi, H.S., Marzol, E., Hwang, Y., Ranocha, P., Velasquez, S.M., Borassi, C., Barberini, M.L., Aptekmann, A.A., et al. (2017). Molecular link between auxin and ROS-mediated polar growth. *Proc. Natl. Acad. Sci. U. S. A.* *114*, 5289–5294.

Mao, Z., Seluanov, A., Jiang, Y., and Gorbunova, V. (2007). TRF2 is required for repair of nontelomeric DNA double-strand breaks by homologous recombination. *Proc. Natl. Acad. Sci. U. S. A.* *104*, 13068–13073.

Marcand, S., Gilson, E., and Shore, D. (1997). A Protein-Counting Mechanism for Telomere Length Regulation in Yeast. *Science* (80-. ). *275*, 986–990.

Martin-Hidalgo, D., Bragado, M.J., Batista, A.R., Oliveira, P.F., and Alves, M.G. (2019). Antioxidants and male fertility: From molecular studies to clinical evidence. *Antioxidants* *8*.

Martin, M.V., Distéfano, A.M., Bellido, A., Córdoba, J.P., Soto, D., Pagnussat, G.C., and Zabaleta, E. (2014). Role of mitochondria during female gametophyte

development and fertilization in *A. thaliana*. *Mitochondrion* 19, 350–356.

Martina, M., Clerici, M., Baldo, V., Bonetti, D., Lucchini, G., and Longhese, M.P. (2012). A Balance between Tell and Rif2 Activities Regulates Nucleolytic Processing and Elongation at Telomeres. *Mol. Cell. Biol.* 32, 1604–1617.

Martínez, P., Thanasoula, M., Muñoz, P., Liao, C., Tejera, A., McNeese, C., Flores, J.M., Fernández-Capetillo, O., Tarsounas, M., and Blasco, M.A. (2009). Increased telomere fragility and fusions resulting from TRF1 deficiency lead to degenerative pathologies and increased cancer in mice. *Genes Dev.* 23, 2060–2075.

Mason, D.X., Goneska, E., and Greider, C.W. (2003). Stem-Loop IV of Tetrahymena Telomerase RNA Stimulates Processivity in trans. *Mol. Cell. Biol.* 23, 5606–5613.

Mason, J.M., Frydrychova, R.C., and Biessmann, H. (2008). *Drosophila* telomeres: An exception providing new insights. *BioEssays* 30, 25–37.

May-Panloup, P., Boucret, L., de la Barca, J.M.C., Desquirit-Dumas, V., Ferré-L'Hotellier, V., Morinière, C., Descamps, P., Procaccio, V., and Reynier, P. (2016). Ovarian ageing: The role of mitochondria in oocytes and follicles. *Hum. Reprod. Update* 22, 725–743.

McClintock, B. (1939). the Behavior in Successive Nuclear Divisions of a. 25, 405–416.

McClintock, B. (1941). The Stability of Broken Ends of Chromosomes in *Zea Mays*. *Genetics* 26, 234–282.

McKnight, T.D., and Shippen, D.E. (2004). Plant Telomere Biology. *Plant Cell* 16, 794–803.

McLennan, D., Armstrong, J.D., Stewart, D.C., McKelvey, S., Boner, W., Monaghan, P., and Metcalfe, N.B. (2018). Telomere elongation during early development is independent of environmental temperatures in Atlantic salmon. *J. Exp. Biol.* 221.

Meier, B., Barber, L.J., Liu, Y., Shtessel, L., Boulton, S.J., Gartner, A., and Ahmed, S. (2009). The MRT-1 nuclease is required for DNA crosslink repair and telomerase activity in vivo in *Caenorhabditis elegans*. *EMBO J.* 28, 3549–3563.

Melek, M., and Shippen, D.E. (1996). Meni Melek.

Mendenhall, M.D., and Hodge, A.E. (1998). Regulation of Cdc28 Cyclin-Dependent Protein Kinase Activity during the Cell Cycle of the Yeast *Saccharomyces*

*cerevisiae*. *Microbiol. Mol. Biol. Rev.* 62, 1191–1243.

Menges, M., and Murray, J.A.H. (2006). Synchronization, transformation, and cryopreservation of suspension-cultured cells. *Methods Mol. Biol.* 323, 45–61.

Mengiste, T., and Paszkowski, J. (1999). Prospects for the precise engineering of plant genomes by homologous recombination. *Biol. Chem.* 380, 749–758.

Menke, M., Chen, I.P., Angelis, K.J., and Schubert, I. (2001). DNA damage and repair in *Arabidopsis thaliana* as measured by the comet assay after treatment with different classes of genotoxins. *Mutat. Res. - Genet. Toxicol. Environ. Mutagen.* 493, 87–93.

Mergny, J.-L., Lacroix, L., and Riou, J.-F. (2007). Telomerase: A Dimeric Menage a Trois. *ChemInform* 38.

Mhamdi, A., Queval, G., Chaouch, S., Vanderauwera, S., Van Breusegem, F., and Noctor, G. (2010). Catalase function in plants: a focus on *Arabidopsis* mutants as stress-mimic models. *J. Exp. Bot.* 61, 4197–4220.

Michael, I., and Söll, D. (1999). Published by: American Association for the Advancement of Science Linked references are available on JSTOR for this article: Nanoporous Material. *Science* (80-. ). 286, 1893–1897.

Mitchell, J.R., and Collins, K. (2000). Human telomerase activation requires two independent interactions between telomerase RNA and telomerase reverse transcriptase. *Mol. Cell* 6, 361–371.

Mitchell, J.R., Wood, E., and Collins, K. (1999a). A telomerase component is defective in the human disease dyskeratosis congenita. *Nature* 402, 551–555.

Mitchell, J.R., Cheng, J., and Collins, K. (1999b). A Box H/ACA Small Nucleolar RNA-Like Domain at the Human Telomerase RNA 3' End. *Mol. Cell. Biol.* 19, 567–576.

Mittler, R. (2017). ROS Are Good. *Trends Plant Sci.* 22, 11–19.

Miyake, Y., Nakamura, M., Nabetani, A., Shimamura, S., Tamura, M., Yonehara, S., Saito, M., and Ishikawa, F. (2009). RPA-like Mammalian Ctc1-Stn1-Ten1 Complex Binds to Single-Stranded DNA and Protects Telomeres Independently of the Pot1 Pathway. *Mol. Cell* 36, 193–206.

Miyoshi, T., Kanoh, J., Saito, M., and Ishikawa, F. (2008). Fission Yeast Pot1-Tpp1 Protects Telomeres and Regulates Telomere Length. *Science* (80-. ). 320, 1341–1344.

Møller, I.M., Jensen, P.E., and Hansson, A. (2007). Oxidative Modifications to Cellular Components in Plants. *Annu. Rev. Plant Biol.* 58, 459–481.

Monaghan, P., Eisenberg, D.T.A., Harrington, L., and Nussey, D. (2018). Understanding diversity in telomere dynamics. *Philos. Trans. R. Soc. B Biol. Sci.* 373.

Montero, J.J., López De Silanes, I., Granã, O., and Blasco, M.A. (2016). Telomeric RNAs are essential to maintain telomeres. *Nat. Commun.* 7, 1–13.

Mosig, A., Sameith, K., and Stadler, P. (2006). Fragrep: An efficient search tool for fragmented patterns in genomic sequences. *Genomics, Proteomics Bioinforma.* 4, 56–60.

Moyzis, R.K., Buckingham, J.M., Crams, L.S., Dani, M., Larry, L., Jones, M.D., Meyne, J., Ratliff, R.L., Wu, J., and Rich, A. (1988). j ~ iA ( J. 85, 6622–6626.

Muller, J.H. (1938). The remaking of chromosomes. *Collect. Net* 8, 198.

Muller, H., Prize, N., McClintock, B., Prize, N., Watson, J., Crick, F., Prize, N., and Wilkins, M. (1983). *Telomere Biology : A Short History.*

Musgrove, C., Jansson, L.I., and Stone, M.D. (2018). New perspectives on telomerase RNA structure and function. *Wiley Interdiscip. Rev. RNA* 9, 1–15.

Myung, K., Ghosh, G., Fattah, F.J., Li, G., Kim, H., Dutia, A., Pak, E., Smith, S., and Hendrickson, E.A. (2004). Regulation of Telomere Length and Suppression of Genomic Instability in Human Somatic Cells by Ku86. *Mol. Cell. Biol.* 24, 5050–5059.

Nakamura, T.M., Moser, B.A., and Russell, P. (2002). Telomere binding of checkpoint sensor and DNA repair proteins contributes to maintenance of functional fission yeast telomeres. *Genetics* 161, 1437–1452.

Nakamura Nakamura, T. M., Morin, G. B., Chapman, K. B., Weinrich, S. L., Andrews, W. H., Lingner, J., ... Cecht, T. R. (2017). Telomerase Catalytic Subunit Homologs from Fission Yeast and Human American Association for the Advancement of Science Stable

Nandhakumar, S., Parasuraman, S., Shanmugam, M.M., Ramachandra Rao, K., Chand, P., and Vishnu Bhat, B. (2011). Evaluation of DNA damage using single-cell gel electrophoresis (Comet Assay). *J. Pharmacol. Pharmacother.* 2, 107–111.

Nawrocki, E.P., and Eddy, S.R. (2013). Infernal 1.1: 100-fold faster RNA homology searches. *Bioinformatics* 29, 2933–2935.

Nelson, A.D.L., and Shippen, D.E. (2012). Blunt-ended telomeres: An alternative

ending to the replication and end protection stories. *Genes Dev.* *26*, 1648–1652.

Nisa, M.-U., Huang, Y., Benhamed, M., and Raynaud, C. (2019). The Plant DNA Damage Response: Signaling Pathways Leading to Growth Inhibition and Putative Role in Response to Stress Conditions. *Front. Plant Sci.* *10*, 653.

Nishida, N., Arizumi, T., Takita, M., Kitai, S., Yada, N., Hagiwara, S., Inoue, T., Minami, Y., Ueshima, K., Sakurai, T., et al. (2013). Reactive oxygen species induce epigenetic instability through the formation of 8-hydroxydeoxyguanosine in human hepatocarcinogenesis. *Dig. Dis.* *31*, 459–466.

Nishioka, K., Ohtsubo, T., Oda, H., Fujiwara, T., Kang, D., Sugimachi, K., and Nakabeppu, Y. (1999). Expression and differential intracellular localization of two major forms of human 8-oxoguanine DNA glycosylase encoded by alternatively spliced OGG1 mRNAs. *Mol. Biol. Cell* *10*, 1637–1652.

Noël, J.F., Larose, S., Elela, S.A., and Wellinger, R.J. (2012). Budding yeast telomerase RNA transcription termination is dictated by the Nrd1/Nab3 non-coding RNA termination pathway. *Nucleic Acids Res.* *40*, 5625–5636.

Oganesian, L., and Karlseder, J. (2009). Telomeric armor: The layers of end protection. *J. Cell Sci.* *122*, 4013–4025.

Ojima, Y., Suryadarma, P., Tsuchida, K., and Taya, M. (2012). Accumulation of pyruvate by changing the redox status in *Escherichia coli*. *Biotechnol. Lett.* *34*, 889–893.

Olive, P.L., and Banáth, J.P. (2006). The comet assay: A method to measure DNA damage in individual cells. *Nat. Protoc.* *1*, 23–29.

Olovnikov, A.M. (1973). A theory of marginotomy. The incomplete copying of template margin in enzymic synthesis of polynucleotides and biological significance of the phenomenon. *J. Theor. Biol.* *41*, 181–190.

Opresko, P.L., Fan, J., Danzy, S., Wilson, D.M., and Bohr, V.A. (2005). Oxidative damage in telomeric DNA disrupts recognition by TRF1 and TRF2. *Nucleic Acids Res.* *33*, 1230–1239.

Osterhage, J.L., Talley, J.M., and Friedman, K.L. (2006). Proteasome-dependent degradation of Est1p regulates the cell cycle-restricted assembly of telomerase in *Saccharomyces cerevisiae*. *Nat. Struct. Mol. Biol.* *13*, 720–728.

Ostling and Johanson (1984). MICRDELECTKOPHORETIC STUDY OF RADIATION-INDUCED DNA DAMAGES IN INDIVIDUAL MAMMALIAN CELLS. 海洋通報marine Sci. Bull. *123*, 291–298.

Ou, X., Zhuang, T., Yin, W., Miao, Y., Wang, B., Zhang, Y., Lin, X., Xu, C., von Wettstein, D., Rustgi, S., et al. (2015). DNA Methylation Changes Induced in Rice by Exposure to High Concentrations of the Nitric Oxide Modulator, Sodium Nitroprusside. *Plant Mol. Biol. Report.* 33, 1428–1440.

Ouenzar, F., Lalonde, M., Laprade, H., Morin, G., Gallardo, F., Tremblay-Belzile, S., and Chartrand, P. (2017). Cell cycle-dependent spatial segregation of telomerase from sites of DNA damage. *J. Cell Biol.* 216, 2355–2371.

Pace, N.R., Smith, D.K., Olsen, G.J., and James, B.D. (1989). Phylogenetic comparative analysis and the secondary structure of ribonuclease P RNA - a review. *Gene* 82, 65–75.

Palm, W., Hockemeyer, D., Kibe, T., and de Lange, T. (2009). Functional Dissection of Human and Mouse POT1 Proteins. *Mol. Cell. Biol.* 29, 471–482.

Pennock, E., Buckley, K., and Lundblad, V. (2001). Cdc13 delivers separate complexes to the telomere for end protection and replication. *Cell* 104, 387–396.

Pfingsten, J.S., Goodrich, K.J., Taabazuing, C., Ouenzar, F., Chartrand, P., and Cech, T.R. (2012). Mutually exclusive binding of telomerase RNA and DNA by Ku alters telomerase recruitment model. *Cell* 148, 922–932.

Pinzaru, A.M., Hom, R.A., Beal, A., Phillips, A.F., Ni, E., Cardozo, T., Nair, N., Choi, J., Wuttke, D.S., Sfeir, A., et al. (2016). Telomere Replication Stress Induced by POT1 Inactivation Accelerates Tumorigenesis. *Cell Rep.* 15, 2170–2184.

Poborilova, Z., Ohlsson, A.B., Berglund, T., Vildova, A., Provaznik, I., and Babula, P. (2015). DNA hypomethylation concomitant with the overproduction of ROS induced by naphthoquinone juglone on tobacco BY-2 suspension cells. *Environ. Exp. Bot.* 113, 28–39.

Podlevsky, J.D., and Chen, J.J.L. (2012a). It all comes together at the ends: Telomerase structure, function, and biogenesis. *Mutat. Res. - Fundam. Mol. Mech. Mutagen.* 730, 3–11.

Podlevsky, J.D., and Chen, J.J.L. (2012b). It all comes together at the ends: Telomerase structure, function, and biogenesis. *Mutat. Res. - Fundam. Mol. Mech. Mutagen.* 730, 3–11.

Podlevsky, J.D., and Chen, J.J.L. (2016). Evolutionary perspectives of telomerase RNA structure and function. *RNA Biol.* 13, 720–732.

Podlevsky, J.D., Li, Y., and Chen, J.J.L. (2016). The functional requirement of two structural domains within telomerase RNA emerged early in eukaryotes. *Nucleic Acids Res.* *44*, 9891–9901.

Polotnianka, R.M., Li, J., and Lustig, A.J. (1998). The yeast ku heterodimer is essential for protection of the telomere against nucleolytic and recombinational activities. *Curr. Biol.* *8*, 831–835.

Pourrut, B., Pinelli, E., Mendiola, V.C., Silvestre, J., and Douay, F. (2015). Recommendations for increasing alkaline comet assay reliability in plants. *Mutagenesis* *30*, 37–43.

Price, C.M., and Cech, T.R. (1987). Telomeric DNA-protein interactions of *Oxytricha* macronuclear DNA. *Genes Dev.* *1*, 783–793.

Price, C., Boltz, K.A., Chaiken, M.F., Stewart, J.A., Beilstein, M.A., and Shippen, D.E. (2014). Evolution of CST function in telomere maintenance. *Cell Cycle* *9*, 3177–3185.

Price, C.M., Boltz, K.A., Chaiken, M.F., Stewart, J.A., Beilstein, M.A., and Shippen, D.E. (2010). Evolution of CST function in telomere maintenance. *Cell Cycle* *9*, 3177–3185.

Provart, N.J., Alonso, J., Assmann, S.M., Bergmann, D., Brady, S.M., Brkljacic, J., Browse, J., Chapple, C., Colot, V., Cutler, S., et al. (2016). 50 years of Arabidopsis research: Highlights and future directions. *New Phytol.* *209*, 921–944.

Qi, X., Xie, M., Brown, A.F., Bley, C.J., Podlevsky, J.D., and Chen, J.J.L. (2012). RNA/DNA hybrid binding affinity determines telomerase template- translocation efficiency. *EMBO J.* *31*, 150–161.

Qi, X., Li, Y., Honda, S., Hoffmann, S., Marz, M., Mosig, A., Podlevsky, J.D., Stadler, P.F., Selker, E.U., and Chen, J.J.L. (2013). The common ancestral core of vertebrate and fungal telomerase RNAs. *Nucleic Acids Res.* *41*, 450–462.

Qiao, F., and Cech, T.R. (2008). Triple-helix structure in telomerase RNA contributes to catalysis. *Nat. Struct. Mol. Biol.* *15*, 634–640.

Rafels-Ybern, À., Attolini, C.S.O., and de Pouplana, L.R. (2015). Distribution of ADAT-dependent codons in the human transcriptome. *Int. J. Mol. Sci.* *16*, 17303–17314.

Rafels-Ybern, À., Torres, A.G., Grau-Bove, X., Ruiz-Trillo, I., and Ribas de Pouplana, L. (2018). Codon adaptation to tRNAs with Inosine modification at position 34 is widespread among Eukaryotes and present in two Bacterial phyla. *RNA Biol.* *15*, 500–



507.

Rai, R., Chen, Y., Lei, M., and Chang, S. (2016). TRF2-RAP1 is required to protect telomeres from engaging in homologous recombination-mediated deletions and fusions. *Nat. Commun.* 7.

Raices, M., Verdun, R.E., Compton, S.A., Haggblom, C.I., Griffith, J.D., Dillin, A., and Karlseder, J. (2008). *C. elegans* Telomeres Contain G-Strand and C-Strand Overhangs that Are Bound by Distinct Proteins. *Cell* 132, 745–757.

Ray, S., Qureshi, M.H., Malcolm, D.W., Budhathoki, J.B., Çelik, U., and Balci, H. (2013). RPA-mediated unfolding of systematically varying G-quadruplex structures. *Biophys. J.* 104, 2235–2245.

Reimand, J., Kull, M., Peterson, H., Hansen, J., and Vilo, J. (2007). G:Profiler—a web-based toolset for functional profiling of gene lists from large-scale experiments. *Nucleic Acids Res.* 35, 193–200.

Ren, S., Johnston, J.S., Shippen, D.E., and McKnight, T.D. (2004). TELOMERASE ACTIVATOR1 induces telomerase activity and potentiates responses to auxin in *Arabidopsis*. *Plant Cell* 16, 2910–2922.

Renfrew, K.B., Song, X., Lee, J.R., Arora, A., and Shippen, D.E. (2014). POT1a and Components of CST Engage Telomerase and Regulate Its Activity in *Arabidopsis*. *PLoS Genet.* 10.

Rhodes, D., and Giraldo, R. (1995). Telomere structure and function. *Curr. Opin. Struct. Biol.* 5, 311–322.

Ribes-Zamora, A., Mihalek, I., Lichtarge, O., and Bertuch, A.A. (2007). Distinct faces of the Ku heterodimer mediate DNA repair and telomeric functions. *Nat. Struct. Mol. Biol.* 14, 301–307.

Ribeyre, C., and Shore, D. (2013). Regulation of telomere addition at DNA double-strand breaks. *Chromosoma* 122, 159–173.

Rice, C., and Skordalakes, E. (2016). Structure and function of the telomeric CST complex. *Comput. Struct. Biotechnol. J.* 14, 161–167.

Richards, E.J., and Ausubel, F.M. (1988). Isolation of a higher eukaryotic telomere from *Arabidopsis thaliana*. *Cell* 53, 127–136.

Richter, C. (1992). Reactive oxygen and DNA damage in mitochondria. *Mutat. Res. DNAGing* 275, 249–255.

Riha, K., and Shippen, D.E. (2003a). Telomere structure, function and maintenance in Arabidopsis. *Chromosom. Res.* *11*, 263–275.

Riha, K., and Shippen, D.E. (2003b). Ku is required for telomeric C-rich strand maintenance but not for end-to-end chromosome fusions in Arabidopsis. *Proc. Natl. Acad. Sci. U. S. A.* *100*, 611–615.

Riha, K., McKnight, T.D., Fajkus, J., Vyskot, B., and Shippen, D.E. (2000). Analysis of the G-overhang structures on plant telomeres: Evidence for two distinct telomere architectures. *Plant J.* *23*, 633–641.

Riha, K., McKnight, T.D., Griffing, L.R., and Shippen, D.E. (2001). Living with genome instability: Plant responses to telomere dysfunction. *Science* (80-. ). *291*, 1797–1800.

Roake, C.M., and Artandi, S.E. (2017). and Cancer by p53 Downstream of Telomeres. 1–16.

Romero, D.P., and Blackburn, E.H. (1991). A conserved secondary structure for telomerase RNA. *Cell* *67*, 343–353.

Rymen, B., Kawamura, A., Lambalez, A., Inagaki, S., Takebayashi, A., Iwase, A., Sakamoto, Y., Sako, K., Favero, D.S., Ikeuchi, M., et al. (2019). Histone acetylation orchestrates wound-induced transcriptional activation and cellular reprogramming in Arabidopsis. *Commun. Biol.* *2*, 1–15.

Sabourin, M., Tuzon, C.T., and Zakian, V.A. (2007). Telomerase and Telp Preferentially Associate with Short Telomeres in *S. cerevisiae*. *Mol. Cell* *27*, 550–561.

Sacco, A., Mourkioti, F., Tran, R., Choi, J., Llewellyn, M., Kraft, P., Shkreli, M., Delp, S., Pomerantz, J.H., Artandi, S.E., et al. (2010). Short telomeres and stem cell exhaustion model duchenne muscular dystrophy in mdx/mTR mice. *Cell* *143*, 1059–1071.

Sahin, E., and DePinho, R.A. (2012). Axis of ageing: Telomeres, p53 and mitochondria. *Nat. Rev. Mol. Cell Biol.* *13*, 397–404.

Šalplachta, J., Allmaier, G., and Chmelík, J. (2005). Proteomic identification of gluten proteins. *Chem. List.* *99*, 967–971.

Samach, A., Melamed-Bessudo, C., Avivi-Ragolski, N., Pietrokovski, S., and Levy, A.A. (2011). Identification of Plant RAD52 Homologs and Characterization of the Arabidopsis thaliana RAD52-Like Genes. *Plant Cell* *23*, 4266–4279.

- Samper, E., Goytisolo, F.A., Slijepcevic, P., Van Buul, P.P.W., and Blasco, M.A. (2000). Mammalian Ku86 protein prevents telomeric fusions independently of the length of TTAGGG repeats and the G-strand overhang. *EMBO Rep.* 1, 244–252.
- Sandhu, R., and Li, B. (2017). Telomerase activity is required for the telomere G-overhang structure in *Trypanosoma brucei*. *Sci. Rep.* 7, 1–13.
- Santos, C.L.V., Pourrut, B., and Ferreira de Oliveira, J.M.P. (2015). The use of comet assay in plant toxicology: Recent advances. *Front. Genet.* 6.
- Sarek, G., Kotsantis, P., Ruis, P., Van Ly, D., Margalef, P., Borel, V., Zheng, X.F., Flynn, H.R., Snijders, A.P., Chowdhury, D., et al. (2019). CDK phosphorylation of TRF2 controls t-loop dynamics during the cell cycle. *Nature* 575, 523–527.
- Sasaki, H., Hamatani, T., Kamijo, S., Iwai, M., Kobanawa, M., Ogawa, S., Miyado, K., and Tanaka, M. (2019). Impact of Oxidative Stress on Age-Associated Decline in Oocyte Developmental Competence. *Front. Endocrinol. (Lausanne)*. 10, 1–7.
- Schaub, M., and Keller, W. (2002). RNA editing by adenosine deaminases generates RNA and protein diversity. *Biochimie* 84, 791–803.
- Schimmel, P. (2018a). The emerging complexity of the tRNA world: mammalian tRNAs beyond protein synthesis. *Nat. Rev. Mol. Cell Biol.* 19, 45–58.
- Schimmel, P. (2018b). RNA Processing and Modifications: The emerging complexity of the tRNA world: Mammalian tRNAs beyond protein synthesis. *Nat. Rev. Mol. Cell Biol.* 19, 45–58.
- Schmidt, J.C., and Cech, T.R. (2015). Human telomerase: Biogenesis, trafficking, recruitment, and activation. *Genes Dev.* 29, 1095–1105.
- Schmutz, I., and Lange, T. de (2016). Shelterin. *Curr. Biol.* 26, R397--9.
- Schrader, M., and Fahimi, H.D. (2006). Peroxisomes and oxidative stress. *Biochim. Biophys. Acta - Mol. Cell Res.* 1763, 1755–1766.
- Scott, S.P., and Pandita, T.K. (2006). The cellular control of DNA double-strand breaks. *J. Cell. Biochem.* 99, 1463–1475.
- Seta, A., Tabara, M., Nishibori, Y., Hiraguri, A., Ohkama-Ohtsu, N., Yokoyama, T., Hara, S., Yoshida, K., Hisabori, T., Fukudome, A., et al. (2017). Post-translational regulation of the dicing activities of arabidopsis DICER-LIKE 3 and 4 by inorganic phosphate and the redox state. *Plant Cell Physiol.* 58, 485–495.

Sfeir, A., Kosiyatrakul, S.T., Hockemeyer, D., MacRae, S.L., Karlseder, J., Schildkraut, C.L., and de Lange, T. (2009). Mammalian Telomeres Resemble Fragile Sites and Require TRF1 for Efficient Replication. *Cell* *138*, 90–103.

Shakirov, E. V., and Shippen, D.E. (2004). Length regulation and dynamics of individual telomere tracts in wild-type Arabidopsis. *Plant Cell* *16*, 1959–1967.

Shakirov, E. V., Surovtseva, Y. V., Osbun, N., and Shippen, D.E. (2005). The Arabidopsis Pot1 and Pot2 Proteins Function in Telomere Length Homeostasis and Chromosome End Protection. *Mol. Cell. Biol.* *25*, 7725–7733.

Shakirov, E. V., Perroud, P.-F., Nelson, A.D., Cannell, M.E., Quatrano, R.S., and Shippen, D.E. (2010). Protection of Telomeres 1 is required for telomere integrity in the moss *Physcomitrella patens*. *Plant Cell* *22*, 1838–1848.

Shammas, M.A. (2011). Telomeres, lifestyle, cancer, and aging. *Curr. Opin. Clin. Nutr. Metab. Care* *14*, 28–34.

Shampay, J., Szostak, J.W., and Blackburn, E.H. (1984). Maintained in Yeast. *310*, 1–4.

Sharma, P., Jha, A.B., Dubey, R.S., and Pessarakli, M. (2012). Reactive Oxygen Species, Oxidative Damage, and Antioxidative Defense Mechanism in Plants under Stressful Conditions. *J. Bot.* *2012*, 1–26.

Shay, J.W., and Wright, W.E. (2019). Telomeres and telomerase: three decades of progress. *Nat. Rev. Genet.* *20*, 299–309.

Singh, M., Wang, Z., Koo, B.K., Patel, A., Cascio, D., Collins, K., and Feigon, J. (2012). Structural Basis for Telomerase RNA Recognition and RNP Assembly by the Holoenzyme La Family Protein p65. *Mol. Cell* *47*, 16–26.

Singh, N.P., McCoy, M.T., Tice, R.R., and Schneider, E.L. (1988). A simple technique for quantitation of low levels of DNA damage in individual cells. *Exp. Cell Res.* *175*, 184–191.

Smogorzewska, A., van Steensel, B., Bianchi, A., Oelmann, S., Schaefer, M.R., Schnapp, G., and de Lange, T. (2000). Control of Human Telomere Length by TRF1 and TRF2. *Mol. Cell. Biol.* *20*, 1659–1668.

Solymosi, K., and Schoefs, B. (2019). Plant cell compartments. *Bot. Lett.* *166*, 269–273.

Song, J. (2019). The conserved structure of the plant telomerase RNA provides the missing link for an evolutionary pathway from ciliates to humans. *PNAS*.

Song, J., Logeswaran, D., Castillo-González, C., Li, Y., Bose, S., Aklilu, B.B., Ma, Z., Polkhovskiy, A., Chen, J.J.L., and Shippen, D.E. (2019). The conserved structure of plant telomerase RNA provides the missing link for an evolutionary pathway from ciliates to humans. *Proc. Natl. Acad. Sci. U. S. A.* *116*, 24542–24550.

Song, X., Leehy, K., Warrington, R.T., Lamb, J.C., Surovtseva, Y. V., and Shippen, D.E. (2008). STN1 protects chromosome ends in *Arabidopsis thaliana*. *Proc. Natl. Acad. Sci. U. S. A.* *105*, 19815–19820.

Sprung, C.N., Reynolds, G.E., Jasin, M., and Murnane, J.P. (1999). Chromosome healing in mouse embryonic stem cells. *Proc. Natl. Acad. Sci. U. S. A.* *96*, 6781–6786.

Stanley, S.E., and Armanios, M. (2015). The short and long telomere syndromes: Paired paradigms for molecular medicine. *Curr. Opin. Genet. Dev.* *33*, 1–9.

Stewart, J.A., Wang, Y., Ackerson, S.M., and Schuck, P.L. (2018). Emerging roles of CST in maintaining genome stability and human disease. *Front. Biosci. (Landmark Ed.)* *23*, 1564–1586.

Stracker, T.H., and Petrini, J.H.J. (2011). The MRE11 complex: Starting from the ends. *Nat. Rev. Mol. Cell Biol.* *12*, 90–103.

Su, L.J., Zhang, J.H., Gomez, H., Murugan, R., Hong, X., Xu, D., Jiang, F., and Peng, Z.Y. (2019). Reactive Oxygen Species-Induced Lipid Peroxidation in Apoptosis, Autophagy, and Ferroptosis. *Oxid. Med. Cell. Longev.* *2019*.

Surovtseva, Y. V., Shakirov, E. V., Vespa, L., Osbun, N., Song, X., and Shippen, D.E. (2007). *Arabidopsis* POT1 associates with the telomerase RNP and is required for telomere maintenance. *EMBO J.* *26*, 3653–3661.

Surovtseva, Y. V., Churikov, D., Boltz, K.A., Song, X., Lamb, J.C., Warrington, R., Leehy, K., Heacock, M., Price, C.M., and Shippen, D.E. (2009). Conserved Telomere Maintenance Component 1 Interacts with STN1 and Maintains Chromosome Ends in Higher Eukaryotes. *Mol. Cell* *36*, 207–218.

Sykorova, E., Lim, K.Y., Chase, M.W., Knapp, S., Leitch, I.J., Leitch, A.R., and Fajkus, J. (2003). The absence of *Arabidopsis*-type telomeres in *Cestrum* and closely related genera *Vestia* and *Sessea* (Solanaceae): First evidence from eudicots. *Plant J.* *34*, 283–291.

Taggart, A.K.P., Teng, S., Zakian, V.A., Science, S., Series, N., and Aug, N. (2002). Est1p as a Cell Cycle-Regulated Activator of Telomere-Bound Telomerase  
Published by: American Association for the Advancement of Science Stable URL :

<http://www.jstor.com/stable/3832054>. 297, 1023–1026.

Tamura, K., Liu, H., and Takahashi, H. (1999). Auxin induction of cell cycle regulated activity of tobacco telomerase. *J. Biol. Chem.* 274, 20997–21002.

Theimer, C.A., and Feigon, J. (2006). Structure and function of telomerase RNA. *Curr. Opin. Struct. Biol.* 16, 307–318.

Theimer, C.A., Finger, L.D., and Feigon, J. (2003). YNMG tetraloop formation by a dyskeratosis congenita mutation in human telomerase RNA. *Rna* 9, 1446–1455.

Theimer, C.A., Blois, C.A., and Feigon, J. (2005). Structure of the human telomerase RNA pseudoknot reveals conserved tertiary interactions essential for function. *Mol. Cell* 17, 671–682.

Thompson, S.L., and Compton, D.A. (2011). Chromosome missegregation in human cells arises through specific types of kinetochore-microtubule attachment errors. *Proc. Natl. Acad. Sci. U. S. A.* 108, 17974–17978.

Tomaska, L., Nosek, J., Kar, A., Willcox, S., and Griffith, J.D. (2019). A New View of the T-Loop Junction: Implications for Self-Primed Telomere Extension, Expansion of Disease-Related Nucleotide Repeat Blocks, and Telomere Evolution. *Front. Genet.* 10, 1–9.

Tomita, K. (2018). How long does telomerase extend telomeres? Regulation of telomerase release and telomere length homeostasis. *Curr. Genet.* 64, 1177–1181.

Torres, A.G., Piñeyro, D., Filonava, L., Stracker, T.H., Batlle, E., and Ribas De Pouplana, L. (2014a). A-to-I editing on tRNAs: Biochemical, biological and evolutionary implications. *FEBS Lett.* 588, 4279–4286.

Torres, A.G., Batlle, E., and Ribas de Pouplana, L. (2014b). Role of tRNA modifications in human diseases. *Trends Mol. Med.* 20, 306–314.

Tremellen, K. (2012). Oxidative stress and male infertility: A clinical perspective. *Stud. Men's Heal. Fertil.* 14, 325–353.

Tseng, C.K., Wang, H.F., Schroeder, M.R., and Baumann, P. (2018). The H/ACA complex disrupts triplex in hTR precursor to permit processing by RRP6 and PARN. *Nat. Commun.* 9, 1–12.

Tsakagoshi, H., Busch, W., and Benfey, P.N. (2010). Transcriptional regulation of ROS controls transition from proliferation to differentiation in the root. *Cell* 143, 606–616.

Tsutsumi, S., Sugiura, R., Ma, Y., Tokuoka, H., Ohta, K., Ohte, R., Noma, A., Suzuki, T., and Kuno, T. (2007). Wobble inosine tRNA modification is essential to cell cycle progression in G1/S and G2/M transitions in fission yeast. *J. Biol. Chem.* 282, 33459–33465.

Tucey, T.M., and Lundblad, V. (2013). A yeast telomerase complex containing the Est1 recruitment protein is assembled early in the cell cycle. *Biochemistry* 52, 1131–1133.

Tucey, T.M., and Lundblad, V. (2014). Regulated assembly and disassembly of the yeast telomerase quaternary complex. *Genes Dev.* 28, 2077–2089.

Turgeon, M.O., Perry, N.J.S., and Poulogiannis, G. (2018). DNA damage, repair, and cancer metabolism. *Front. Oncol.* 8.

Tzfati, Y., Fulton, T.B., Roy, J., Blackburn, E.H., Science, S., Series, N., May, N., Monte, E., Tzfati, Y., Fulton, T.B., et al. (2000). Template Boundary in a Yeast Telomerase Specified by RNA Structure Published by: American Association for the Advancement of Science Linked references are available on JSTOR for this article: Template Boundary in a Yeast Telomerase Specified by RNA Stru. 288, 863–867.

Ungar, L., Yosef, N., Sela, Y., Sharan, R., Ruppin, E., and Kupiec, M. (2009). A genome-wide screen for essential yeast genes that affect telomere length maintenance. *Nucleic Acids Res.* 37, 3840–3849.

Uringa, E.J., Lisaingo, K., Pickett, H.A., Brind'Amour, J., Rohde, J.H., Zelensky, A., Essers, J., and Lansdorp, P.M. (2012). RTEL1 contributes to DNA replication and repair and telomere maintenance. *Mol. Biol. Cell* 23, 2782–2792.

Valuchova, S., Fulnecek, J., Prokop, Z., Stolt-Bergner, P., Janouskova, E., Hofr, C., and Riha, K. (2017a). Protection of Arabidopsis Blunt-Ended Telomeres Is Mediated by a Physical Association with the Ku Heterodimer. *Plant Cell* 29, 1533–1545.

Valuchova, S., Fulnecek, J., Prokop, Z., Stolt-Bergner, P., Janouskova, E., Hofr, C., and Riha, K. (2017b). Protection of arabidopsis blunt-ended telomeres is mediated by a physical association with the ku heterodimer. *Plant Cell* 29, 1533–1545.

Vannier, J.B., Pavicic-Kaltenbrunner, V., Petalcorin, M.I.R., Ding, H., and Boulton, S.J. (2012). RTEL1 dismantles T loops and counteracts telomeric G4-DNA to maintain telomere integrity. *Cell* 149, 795–806.

Varela, E., and Blasco, M.A. (2010). 2009 Nobel Prize in Physiology or Medicine: Telomeres and telomerase. *Oncogene* 29, 1561–1565.

Varela, E., Muñoz-Lorente, M.A., Tejera, A.M., Ortega, S., and Blasco, M.A.

(2016). Generation of mice with longer and better preserved telomeres in the absence of genetic manipulations. *Nat. Commun.* *7*.

Vasianovich, Y., Krallis, A., and Wellinger, R. (2020). Telomerase and non-Telomerase Mechanisms of Telomere Maintenance.

Veldman, T., Etheridge, K.T., and Counter, C.M. (2004). Loss of hPot1 function leads to telomere instability and a cut-like phenotype. *Curr. Biol.* *14*, 2264–2270.

Ventura, L., Giovannini, A., Savio, M., Donà, M., Macovei, A., Buttafava, A., Carbonera, D., and Balestrazzi, A. (2013). Single Cell Gel Electrophoresis (Comet) assay with plants: Research on DNA repair and ecogenotoxicity testing. *Chemosphere* *92*, 1–9.

Verdun, R.E., Crabbe, L., Haggblom, C., and Karlseder, J. (2005). Functional human telomeres are recognized as DNA damage in G2 of the cell cycle. *Mol. Cell* *20*, 551–561.

Vodenicharov, M.D., and Wellinger, R.J. (2006). DNA Degradation at Unprotected Telomeres in Yeast Is Regulated by the CDK1 (Cdc28/Clb) Cell-Cycle Kinase. *Mol. Cell* *24*, 127–137.

Vodenicharov, M.D., and Wellinger, R.J. (2007). The cell division cycle puts up with unprotected telomeres: Cell cycle regulated telomere uncapping as a means to achieve telomere homeostasis. *Cell Cycle* *6*, 1161–1167.

Vogan, J.M., and Collins, K. (2015). Dynamics of human telomerase holoenzyme assembly and subunit exchange across the cell cycle. *J. Biol. Chem.* *290*, 21320–21335.

Vulliamy, T., Marrone, A., Goldman, F., Dearlove, A., Bessler, M., Mason, P.J., and Dokal, I. (2001). The RNA component of telomerase is mutated in autosomal dominant dyskeratosis congenita. *Nature* *413*, 432–435.

Walne, A.J., Vulliamy, T., Marrone, A., Beswick, R., Kirwan, M., Masunari, Y., Al-Qurashi, F.H., Aljurf, M., and Dokal, I. (2007). Genetic heterogeneity in autosomal recessive dyskeratosis congenita with one subtype due to mutations in the telomerase-associated protein NOP10. *Hum. Mol. Genet.* *16*, 1619–1629.

Wang, C., and Meier, U.T. (2004). Architecture and assembly of mammalian H/ACA small nucleolar and telomerase ribonucleoproteins. *EMBO J.* *23*, 1857–1867.

Wang, C.Y., Liu, L.N., and Zhao, Z.B. (2013). The role of ROS toxicity in spontaneous aneuploidy in cultured cells. *Tissue Cell* *45*, 47–53.

Wang, F., Podell, E.R., Zaug, A.J., Yang, Y., Baciu, P., Cech, T.R., and Lei, M.



(2007). The POT1-TPP1 telomere complex is a telomerase processivity factor. *Nature* *445*, 506–510.

Wang, L., Wang, C., Liu, X., Cheng, J., Li, S., Zhu, J.K., and Gong, Z. (2019a). Peroxisomal  $\beta$ -oxidation regulates histone acetylation and DNA methylation in *Arabidopsis*. *Proc. Natl. Acad. Sci. U. S. A.* *116*, 10576–10585.

Wang, Y., Ghosh, G., and Hendrickson, E.A. (2009). Ku86 represses lethal telomere deletion events in human somatic cells. *Proc. Natl. Acad. Sci. U. S. A.* *106*, 12430–12435.

Wang, Z., Schwacke, R., and Kunze, R. (2016). DNA Damage-Induced Transcription of Transposable Elements and Long Non-coding RNAs in *Arabidopsis* Is Rare and ATM-Dependent. *Mol. Plant* *9*, 1142–1155.

Wang, Z., Wang, M., Wang, T., Zhang, Y., and Zhang, X. (2019b). Genome-wide probing RNA structure with the modified DMS-MaPseq in *Arabidopsis*. *Methods* *155*, 30–40.

Watson, J.M., and Riha, K. (2010). Comparative biology of telomeres: Where plants stand. *FEBS Lett.* *584*, 3752–3759.

Watson, J.M., and Shippen, D.E. (2007). Telomere Rapid Deletion Regulates Telomere Length in *Arabidopsis thaliana*. *Mol. Cell. Biol.* *27*, 1706–1715.

Wellinger, R.J., and Zakian, V.A. (2012). Everything you ever wanted to know about *Saccharomyces cerevisiae* telomeres: Beginning to end. *Genetics* *191*, 1073–1105.

Wiener-Megnazi, Z., Vardi, L., Lissak, A., Shnizer, S., Zeev Reznick, A., Ishai, D., Lahav-Baratz, S., Shiloh, H., Koifman, M., and Dirnfeld, M. (2004). Oxidative stress indices in follicular fluid as measured by the thermochemiluminescence assay correlate with outcome parameters in in vitro fertilization. *Fertil. Steril.* *82*, 1171–1176.

Wilkinson, K.A., Merino, E.J., and Weeks, K.M. (2006). Selective 2'-hydroxyl acylation analyzed by primer extension (SHAPE): Quantitative RNA structure analysis at single nucleotide resolution. *Nat. Protoc.* *1*, 1610–1616.

Wilusz, J.E., Sunwoo, H., and Spector, D.L. (2009). Long noncoding RNAs: Functional surprises from the RNA world. *Genes Dev.* *23*, 1494–1504.

Wolf, J., Gerber, A.P., and Keller, W. (2002). TadA, an essential tRNA-specific adenosine deaminase from *Escherichia coli*. *EMBO J.* *21*, 3841–3851.

Woodward, A.W., and Bartel, B. (2018). *Biology in bloom: A primer on the*

arabidopsis thaliana model system. *Genetics* 208, 1337–1349.

Wotton, D., and Shore, D. (1997). A novel Rap1p-interacting factor, Rif2p, cooperates with Rif1p to regulate telomere length in *Saccharomyces cerevisiae*. *Genes Dev.* 11, 748–760.

Wu, J., Okada, T., Fukushima, T., Tsudzuki, T., Sugiura, M., and Yukawa, Y. (2012a). A novel hypoxic stress-responsive long non-coding RNA transcribed by RNA polymerase III in *Arabidopsis*. *RNA Biol.* 9, 302–313.

Wu, L., Multani, A.S., He, H., Cosme-Blanco, W., Deng, Y., Deng, J.M., Bachilo, O., Pathak, S., Tahara, H., Bailey, S.M., et al. (2006). Pot1 Deficiency Initiates DNA Damage Checkpoint Activation and Aberrant Homologous Recombination at Telomeres. *Cell* 126, 49–62.

Wu, P., Takai, H., and De Lange, T. (2012b). Telomeric 3' overhangs derive from resection by Exo1 and apollo and fill-in by POT1b-associated CST. *Cell* 150, 39–52.

Wu, R.A., Upton, H.E., Vogan, J.M., and Collins, K. (2017). Telomerase Mechanism of Telomere Synthesis. *Annu. Rev. Biochem.* 86, 439–460.

Wyatt, H.D.M., West, S.C., and Beattie, T.L. (2010). InTERTpreting telomerase structure and function. *Nucleic Acids Res.* 38, 5609–5622.

Wyck, S., Herrera, C., Requena, C.E., Bittner, L., Hajkova, P., Bollwein, H., and Santoro, R. (2018). Oxidative stress in sperm affects the epigenetic reprogramming in early embryonic development. *Epigenetics Chromatin* 11, 60.

Xie, X., and Shippen, D.E. (2018). DDM1 guards against telomere truncation in *Arabidopsis*. *Plant Cell Rep.*

Xie, M., Mosig, A., Qi, X., Li, Y., Stadler, P.F., and Chen, J.J.L. (2008). Structure and function of the smallest vertebrate telomerase RNA from teleost fish. *J. Biol. Chem.* 283, 2049–2059.

Xie, M., Podlevsky, J.D., Qi, X., Bley, C.J., and Chen, J.J.L. (2009). A novel motif in telomerase reverse transcriptase regulates telomere repeat addition rate and processivity. *Nucleic Acids Res.* 38, 1982–1996.

Xin, H., Liu, D., Wan, M., Safari, A., Kim, H., Sun, W., O'Connor, M.S., and Songyang, Z. (2007). TPP1 is a homologue of ciliate TEBP-beta and interacts with POT1 to recruit telomerase. *Nature* 445, 559–562.

Xu, H., Nelson, A.D.L., and Shippen, D.E. (2015a). A Transposable Element

within the Non-canonical Telomerase RNA of *Arabidopsis thaliana* Modulates Telomerase in Response to DNA Damage. *PLOS Genet.* *11*, e1005281.

Xu, W., Wang, T., Xu, S., Xu, S., Wu, L., Wu, Y., and Bian, P. (2015b). Radiation-Induced Epigenetic Bystander Effects Demonstrated in *Arabidopsis thaliana*. *Radiat. Res.* *183*, 511.

Yamaguchi, H., Calado, R.T., Ly, H., Kajigaya, S., Baerlocher, G.M., Chanock, S.J., Lansdorf, P.M., and Young, N.S. (2005). Mutations in TERT, the Gene for Telomerase Reverse Transcriptase, in Aplastic Anemia. *N. Engl. J. Med.* *352*, 1413–1424.

Yang, S.W., Jin, E.S., Chung, I.K., and Kim, W.T. (2002). Cell cycle-dependent regulation of telomerase activity by auxin, abscisic acid and protein phosphorylation in tobacco BY-2 suspension culture cells. *Plant J.* *29*, 617–626.

Yu, Y., Tan, R., Ren, Q., Gao, B., Sheng, Z., Zhang, J., Zheng, X., Jiang, Y., Lan, L., and Mao, Z. (2017). POT1 inhibits the efficiency but promotes the fidelity of nonhomologous end joining at non-telomeric DNA regions. *Aging (Albany, NY).* *9*, 2529–2543.

Zappulla, D.C., and Cech, T.R. (2004). Yeast telomerase RNA: A flexible scaffold for protein subunits. *Proc. Natl. Acad. Sci. U. S. A.* *101*, 10024–10029.

Zeng, J., Dong, Z., Wu, H., Tian, Z., and Zhao, Z. (2017). Redox regulation of plant stem cell fate. *EMBO J.* *36*, 2844–2855.

Zhang, M.J., Zhang, X.S., and Gao, X.Q. (2020). ROS in the Male–Female Interactions During Pollination: Function and Regulation. *Front. Plant Sci.* *11*, 1–8.

Zhang, Q., Kim, N.K., and Feigon, J. (2011). Architecture of human telomerase RNA. *Proc. Natl. Acad. Sci. U. S. A.* *108*, 20325–20332.

Zhang, S., Hu, H., Zhou, J., He, X., Jiang, T., and Zeng, J. (2017). Analysis of Ribosome Stalling and Translation Elongation Dynamics by Deep Learning. *Cell Syst.* *5*, 212–220.e6.

Zhang, W., Xiao, S., and Ahn, D.U. (2013). Protein Oxidation: Basic Principles and Implications for Meat Quality. *Crit. Rev. Food Sci. Nutr.* *53*, 1191–1201.

Zhang, X., Henriques, R., Lin, S.S., Niu, Q.W., and Chua, N.H. (2006). Agrobacterium-mediated transformation of *Arabidopsis thaliana* using the floral dip method. *Nat. Protoc.* *1*, 641–646.

Zhao, Y., Sfeir, A.J., Zou, Y., Buseman, C.M., Chow, T.T., Shay, J.W., and

Wright, W.E. (2009). Telomere Extension Occurs at Most Chromosome Ends and Is Uncoupled from Fill-In in Human Cancer Cells. *Cell* 138, 463–475.

Zheng, Q., Liu, P., Gao, G., Yuan, J., Wang, P., Huang, J., Xie, L., Lu, X., Di, F., Tong, T., et al. (2019a). Mitochondrion-processed TERC regulates senescence without affecting telomerase activities. *Protein Cell* 10, 631–648.

Zheng, Q., Huang, J., and Wang, G. (2019b). Mitochondria, Telomeres and Telomerase Subunits. *Front. Cell Dev. Biol.* 7, 1–10.

Zheng, S., Li, J., Ma, L., Wang, H., Zhou, H., Ni, E., Jiang, D., Liu, Z., and Zhuang, C. (2019c). OsAGO2 controls ROS production and the initiation of tapetal PCD by epigenetically regulating OsHXX1 expression in rice anthers. *Proc. Natl. Acad. Sci. U. S. A.* 116, 7549–7558.

Zhou, J., Hidaka, K., and Futcher, B. (2000). The Est1 Subunit of Yeast Telomerase Binds the Tlc1 Telomerase RNA. *Mol. Cell. Biol.* 20, 1947–1955.

Zhou, J., Chan, J., Lambel , M., Yusufzai, T., Stumpff, J., Opresko, P.L., Thali, M., and Wallace, S.S. (2017). NEIL3 Repairs Telomere Damage during S Phase to Secure Chromosome Segregation at Mitosis. *Cell Rep.* 20, 2044–2056.

Zhou, W., Karcher, D., and Bock, R. (2013). Importance of adenosine-to-inosine editing adjacent to the anticodon in an Arabidopsis alanine tRNA under environmental stress. *Nucleic Acids Res.* 41, 3362–3372.

Zhou, W., Karcher, D., and Bock, R. (2014). Identification of enzymes for adenosine-to-inosine editing and discovery of cytidine-to-uridine editing in nucleus-encoded transfer RNAs of arabidopsis. *Plant Physiol.* 166, 1985–1997.

Zhu, Z., Chung, W.H., Shim, E.Y., Lee, S.E., and Ira, G. (2008). Sgs1 Helicase and Two Nucleases Dna2 and Exo1 Resect DNA Double-Strand Break Ends. *Cell* 134, 981–994.

Zimmermann, M., Kibe, T., Kabir, S., and de Lange, T. (2014). TRF1 negotiates TTAGGG repeat-associated replication problems by recruiting the BLM helicase and the TPP1/POT1 repressor of ATR signaling. *Genes Dev.* 28, 2477–2491.

Zimmermann, P., Heinlein, C., Orendi, G., and Zentgraf, U. (2006). Senescence-specific regulation of catalases in Arabidopsis thaliana (L.) Heynh. *Plant, Cell Environ.* 29, 1049–1060.

Zinshteyn, B., and Nishikura, K. (2009). Adenosine-to-inosine RNA editing.

Zubradt, M., Gupta, P., Persad, S., Lambowitz, A.M., Weissman, J.S., and Rouskin, S. (2016). DMS-MaPseq for genome-wide or targeted RNA structure probing in vivo. *Nat. Methods* *14*, 75–82.

## APPENDIX A

### HIGH YIELD COMET ASSAY TO ASSESS DNA REPAIR COMPETENCE IN

#### *Arabidopsis thaliana*

#### **Abstract**

Living organisms are regularly exposed to biotic and abiotic stressors that can lead to DNA damage and genomic instability. Thus, DNA damage response (DDR) pathways are critical for health and longevity. In order to identify and understand the function of molecular players involved in DDR, it is critical to have reliable methods to gauge DNA damage. The single cell gel electrophoresis (SCGE) or comet assay is the gold standard for assessing DNA damage, and it has been successfully implemented in cells from multiple tissues in humans, mice and *Drosophila*. Modifications to the original assay have been developed to target specific kinds of DNA damage in the sample of interest. Recently, comet assay techniques have also become a regular method to determine damage in plants. Isolation of single cells in plants is difficult because of their strong cell walls; therefore, mechanical stress has been the most common method for generating comet assay samples. Mechanical stress-based methods typically yield few comets and induce secondary damage to the cells, which may impact the final result. In this chapter, we describe an improved comet assay protocol that allows for the automated quantification of large numbers of cells, resulting in a statistically robust assay to evaluate the accumulation of damaged DNA within a specific sample. We also introduce a modification that allows the investigation of DNA repair competence using total protein extracts from plant samples. Altogether we have developed a statistically robust version

of the plant comet assay that can be used to investigate the amount of accumulated DNA damage as well as the damage repair competence in *A. thaliana* genotypes.

## **Introduction**

Keeping the genome healthy and stable is required for a healthy life. Cellular DNA is under constant threat due to intrinsic metabolism that can cause DNA replication errors, overwhelming levels of cellular ROS, and a myriad of extrinsic environmental factors including biotic and abiotic stress (Nisa et al., 2019). In most cases, the genome remains unperturbed due to constant surveillance and repair activities controlled by DNA Damage Response (DDR) (Giglia-Mari et al., 2011). At multiple steps, DDR pathways prevent cell cycle progression to either repair the damaged DNA, or elicit apoptosis if the damage is irreparable (Turgeon et al., 2018). Defective DDR pathways are linked to diseases like immune deficiency disorder, neurological defects, premature aging and cancer (Crasta et al., 2012). Therefore, in order to investigate the function of various molecular players involved in the DDR pathways, it is crucial to have a reliable method for measuring the amount of damaged DNA within an organism.

Since its development in 1984, the comet assay has been the most versatile, sensitive, and easy-to-perform technique for assessing DNA damage (Langie et al., 2015). This assay has been successfully performed on different kinds of samples collected from mammals and insects. The assay harnesses the difference in electrophoretic mobility between intact and damaged DNA, particularly single or double stranded breaks. Unlike intact DNA, damaged DNA separates from the intact DNA and travels faster during electrophoresis, thus creating a trail ahead. This specific movement pattern creates a comet

like structure in which the head is composed of intact DNA and the tail comprises pieces of loose broken DNA (Ventura et al., 2013). Tail length and relative amount of tail DNA serve to qualify and quantify the damage within a sample. Slight modifications to the comet assay conditions provide a variety of information about the type of DNA damage observed in a sample (Nandhakumar et al., 2011). For instance, the alkaline comet assay performed at  $\text{pH} > 13$  helps to detect both single and double-stranded breaks (Singh et al., 1988), whereas the neutral version ( $\text{pH} = 7$ ) only supports the detection of double-stranded breaks (Ostling and Johanson, 1984). Another widely used modification of the assay involves digesting the DNA with endonuclease III or FPG to detect oxidized purines, pyrimidines, and UV induced dimers (Collins et al., 1996).

Besides assessing the total amount of damaged DNA using the standard comet assay, a modified version of the assay can be used to measure DNA repair competence. In this modified version, nuclei prepared from cells with DNA lesions are incubated with protein extracts from different tissues or cells, prior to electrophoresis. The resulting comets are assessed to determine the amount of damaged DNA. The results are compared with comets from untreated nuclei. A difference in the DNA damage level can be correlated with the DNA repair competence of the protein extract donor. This modification has been used to study the potential role of specific enzymes in DNA repair, being instrumental in the understanding of Base/Nucleotide Excision Repair in humans, fruit fly and mice (Azqueta et al., 2014).

Over the past 20 years, a lot of attention has been paid to plant-based comet assay. It is regularly used to assess the negative impacts of environmental stresses on the plant



genome (Santos et al., 2015). Although plant-based comet assay has become a routine experiment, the process of single-cell isolation is technically challenging. Currently, the dominant method is to exert mechanical force (slicing and chopping) without any added step of digesting the plant tissues which yields few isolated cells (Menke et al., 2001). To increase the yield, protoplast isolation has gained traction to provide the individual cells for the comet assay; however, the protoplast isolation techniques described in the previous comet assays typically generates insufficient cells to support robust statistical analyses ( $n < 100$ ) (Bilichak et al., 2014). Also, unlike in humans, mice and flies, there are no available protocols to study the DNA repair competence in plants.

In this chapter, we describe an improved version of the existing plant-based comet assay, with an exciting new feature to study repair competence. In this version we use protoplasts extracted from rosette leaves following the protocol developed by He et. al, in 2007. We were able to use ~1000 protoplasts for each comet assay. Having such a high number of good quality protoplasts allowed us to generate reliable statistical inferences based on robust statistical analysis. We further developed a plant version of DNA repair assay. Nuclei with high levels of DNA damage showed a statistically significant reduction in comet length and DNA when incubated with UV-induced wild type protein extracts. Altogether we offer this improved comet assay protocol to fuel research in DNA repair in plants.

## Comet Assay for plant tissue

### Materials

- ~10 to 12 rosette leaves (1-1.5 cm in length) from 3.5 to 4 week-old wild type and *atr* plants grown in a growth chamber at 22°C under long day light conditions
- Razor blades
- 35 to 75 µm nylon mesh
- 30 mL round bottom polypropylene tubes
- Coplin jars
- Trevigen Comet Assay Kit: low melting agarose, agarose coated slides, lysis buffer

### Reagents

- Propidium Iodide Solution (working solution - 10 µg/ml). Powder obtained from Sigma Aldrich (Catalog - P4170) is dissolved in ultra-pure H<sub>2</sub>O to make a 1000X stock solution. The solution is filtered through 0.45 µm membrane to remove undissolved particles that can interfere during imaging.
- Nail varnish

### Solutions

- Freshly prepared enzyme solution: 15% cellulase R10, 0.4% macerozyme R10, 0.4 M mannitol, 20 mM KCl, 20 mM MES, pH 5.7, 10 mM CaCl<sub>2</sub>
- W5 solution stored at 4°C: 154 mM NaCl, 125 mM CaCl<sub>2</sub>, 5 mM KCl, 2 mM MES pH 5.7
- MMg solution stored at 4°C: 0.4 M mannitol, 15 mM MgCl<sub>2</sub>, 4 mM MES pH 5.7

- 1X TBE electrophoresis buffer stored at 4°C: 1M Tris base, 1M boric acid, 0.02 M EDTA (di-sodium salt)
- Freshly prepared Alkaline Unwinding Buffer: 200 mM NaOH, 1 mM EDTA
- Freshly prepared Protein extraction buffer: 20 mM Tris pH 7.5, 150 mM NaCl, 4 mM MgCl<sub>2</sub>, 75 nM ZnCl, 0.1% Triton X-100, 1mM PMSF, 1X Roche complete – EDTA free (1ml/50 ml).

#### Equipment

- Vacuum chamber
- Centrifuge, swinging bucket
- Light microscope
- Gel running tank
- Fluorescence microscope

### **Standard Comet Assay Protocol**

#### *I. Protoplast Extraction (He et al., 2007)*

- To make the enzyme solution add 1.85 ml of H<sub>2</sub>O, 2.5 ml of 0.8M Mannitol, 50 μL of 1 M KCl and 500 μL of 1M MES (pH - 5.7) to a tube.
- Incubate the tube at 50°C water bath for 10 min.
- Add 0.075g of Cellulase and 0.004g of Macerozyme are added to the heated mix followed by incubation at 50°C for another 10 min with gentle movement to resuspend the enzyme into the solution.

- Transfer the solution to an ice bucket for cooling down. Once the solution reaches room temperature, add 100  $\mu\text{l}$  of 1 M  $\text{CaCl}_2$  solution to the enzyme mix and by transfer the final solution to a six well plate. The total enzyme volume is  $\sim$  5 ml per well.
- Cut well expanded rosette leaves in  $\sim$ 0.5 mm thin strips using a sharp razor blade. This process can be performed on a napkin to have a better grip and trap humidity.
- Immerse the leaf strips in the enzyme solution. Place one sample per well.
- Close and wrap the plate with aluminum foil to protect the enzyme from photo-degradation.
- Place the plate in a vacuum chamber and subject it to vacuum treatment for 30 min.
- Gently release the vacuum. It should take 30 sec -1 min to release all the pressure.
- Allow the digestion to proceed in the vacuum-sealed chamber for 3 h.
- Quench the digestion reaction by adding 5 mL of freshly prepared W5 buffer. Stir the contents of the well with a pipette tip to release the protoplasts.
- Saturate the nylon mesh in W5 solution and use it to line the funnel. Then, assemble the filtering system over a round bottom tube.
- Pour the well contents over the nylon mesh to separate the protoplasts from the leaf strips. The protoplasts collect at the bottom of the tube. Note: Cut the end of a 1000 – 1250  $\mu\text{L}$  pipette tip to widen the mouth prior to aspirating the contents of the well. Do this gently without forming any bubbles.

- Centrifuge the tubes at 30g (acc =1, decc = 1) for 5 min at RT to precipitate the protoplasts.
- Remove the supernatant and resuspend the protoplasts by gently adding 5 ml of W5 buffer. Note: Intact protoplasts pellet at the bottom of the tube while broken protoplasts stick to the wall. Care should be taken not to disturb the protoplast pellet and only remove the protoplasts from the side while changing the buffer. Repeat steps 13 and 14 for three times to enrich the intact protoplasts.
- Resuspend the protoplast pellet in 5 ml of fresh W5 solution and incubate on ice for 30 minutes. This manual incubation step helps to further remove broken protoplasts without losing the intact protoplasts with further centrifugation.
- Remove the supernatant and resuspend the intact protoplasts in 100  $\mu$ l of MMG buffer.
- Use ~20  $\mu$ l of the protoplast solution to assess quality and estimate concentration using a hemocytometer. Count the total number of protoplast present in the four 16-square boundary grids. Calculate the average (A). The protoplast concentration is  $(A) \times 10^4$  protoplasts/ml. You can do this at 20X or using 40X magnification on a light microscope.
- Add the appropriate amount of MMG to dilute the protoplasts to a final concentration of  $2 \times 10^5$  protoplasts/ml. Note: protoplast solution with concentration lower than  $2 \times 10^5$  protoplasts/ml should not be used for the assay.

## *II. Protoplast Lysis*

- Before setting up the lysis experiment, cool down the lysis solution (Trevigen) by adding the buffer to a Coplin jar and placing it at 4°C. Note: do not leave the lysis solution in 4°C for longer than 24 h as the detergent can precipitate and lose its efficacy.
- Melt the low melting agarose (LMA) (Trevigen) in a 42°C water bath. Note: care should be taken to melt the LMA to a uniform consistency. The final temperature should be around RT because heat will rupture the protoplasts.
- Mixed the freshly extracted protoplasts with LMA (Trevigen) in a 1:10 ratio (v/v). Use 50 – 60 µl of this mixture on the precoated comet slides (Trevigen).
- Cool the slides to set the protoplast-embedded agarose. After 10 min of cooling carefully place the slides inside the Coplin jar with lysis solution. Lyse at 4°C for 16 h.
- Transfer the slides to a Coplin jar with cold ultrapure water. Incubate for 5 min at 4 °C. Repeat this step three times to completely remove the lysis solution.
- Transfer the slides into another Coplin jar containing alkaline unwinding solution. Note: The alkaline unwinding buffer used should be freshly made using ultrapure water at 4°C. Allow the alkaline unwinding to proceed for 1 h in 4°C.

## *III. Single cell electrophoresis*

- Place the slide in an electrophoresis tank filled with 1X TBE buffer and run in a dark room at 18V for 10 minutes at 4°C.

- Transfer the slides to a Coplin jar with cold ultrapure water and incubate 5 min in 4°C to remove the TBE buffer from the samples. Repeat this step once.
- Transfer the slides to a Coplin jar with 70% EtOH to remove the chlorophyll and fix the samples.
- Incubate the slides at 37°C for 20-30 min to completely dry the agarose. Note: after drying, the agarose should be completely unnoticeable. The presence of residual agarose will make it difficult to seal the slide with a cover slip and impair image acquisition.
- Add ~20 µL filtered PI stain to the sample. Gently place a coverslip on the slide to avoid trapping bubbles on the sample.
- Seal the coverslip by applying a light layer of nail varnish on the edges. Note: allow varnish to fully dry to avoid damaging the microscope.
- Image the slides at 10X or 20X on a fluorescent microscope. We used the dsRED channel.

#### *IV. Data collection and processing*

- Open the micrographs in Image J and analyze with the Open Comet (Gyori et al., 2014) add-on software (Figure A-1).
- Use the automatic mode to detect comets in the picture.
- Curate the detected comets. Due to the high yield of protoplasts, you may have overlapping comets. These should be removed because they cannot be properly measured. Also, remove all misidentified elements including background speckles and comets whose heads and tails have been incorrectly identified (Figure A-1).

- Measure the comet parameters. Open Comet in Image J generates a comprehensive excel file including percentage DNA in tail (PTD), tail length (TL), tail moment  $TM$ , and olive tail moment (OTM). We chose PTD for our assay validation as it is the most general parameter of DNA damage.
- The DT and TM are directly proportional to DNA damage. The DT is calculated as the ratio of total intensity of the tail and total intensity of the comet (head and tail together), while TM is defined as product of tail length and the DT.

$$DT = \frac{\textit{Total intensity of Tail}}{\textit{Total intensity of Comet}}$$

$$TM = \textit{Tail length} \times DT$$

The TM is a better proxy for DNA damage because it incorporates both a measure of the smallest detectable size of migrating DNA, reflected in the comet tail length, and the number of relaxed and/or broken pieces, represented by the intensity of DNA in the tail. There is a variation on the TM parameter, called Olive TM, which uses the mean tail length as opposed to the absolute tail length. OTM is supposed to be more accurate for representing DNA damage in a sample compared to only PTD or TM (Olive and Banáth, 2006).

$$\textit{Olive TM} = (\textit{Tail mean} - \textit{Head mean}) \times DT$$



- Use a box and whisker plot to assess data quality and identify outliers. There are four parts in the plot which provide information about the data. The lines at the top and bottom of the box represent the upper and lower quartiles, respectively. The horizontal straight line within the box indicates the median and the 'x' represents mean. Overlap between the median and the mean signify normally distributed data.
- If necessary, trim the outliers to normalize the data.
- Use Student's T-test compare samples.

### **Comet Assay Modification to determine DNA repair competence**

To be performed on day 2, after protoplast lysis.

#### *V. Donor Sample preparation*

- Induce DNA damage in the donor plants (the subjects to be tested for DNA repair competence) by exposing them to UV light using a UV-crosslinker (0.12 J for 2 cycles of auto crosslinking). In parallel separate un-induced donor. In our experiment we used WT plants as donors.
- Activate the DDR pathway by allowing the donor plants to recover for 2 h under normal growth conditions with the lights on. Do the same for the un-induced donor.
- Prepare the protein extract from the donor plants. Freeze the plant material in liquid nitrogen and grind it to fine powder. Weigh the ground material and resuspend in three times the volumes of protein extraction buffer (g to ml). In our experiment we used flowers.

- Remove the cellular debris by centrifugation at 21000g for 15 min at 4 °C.
- Carefully transfer the supernatant to a fresh tube, and repeat the centrifugation step.
- Take the clarified protein extract to a third tube and maintain on ice.

#### *VI. DNA repair challenge*

- Thoroughly clean a small slide box (18.0"L x 9.0"W x 21.0"H) by consecutive rinses with nuclease-free ultrapure H<sub>2</sub>O, and dry it completely.
- Add ~500 uL of the protein extract from step V.6 to the box and submerge the comet slide from step II.5, making sure that the whole sample is covered and saturated with the protein extract. We attain this by placing the slide facing down.
- Do this in ice.
- Allow the DNA repair to occur by incubating at 4°C for 4 h.
- Transfer the slide to another Coplin jar with cold ultrapure water to remove the protein extract followed by placing the slides in alkaline unwinding solution for 1 hour at 4°C.
- Repeat step II.5 and continue with the standard comet assay.

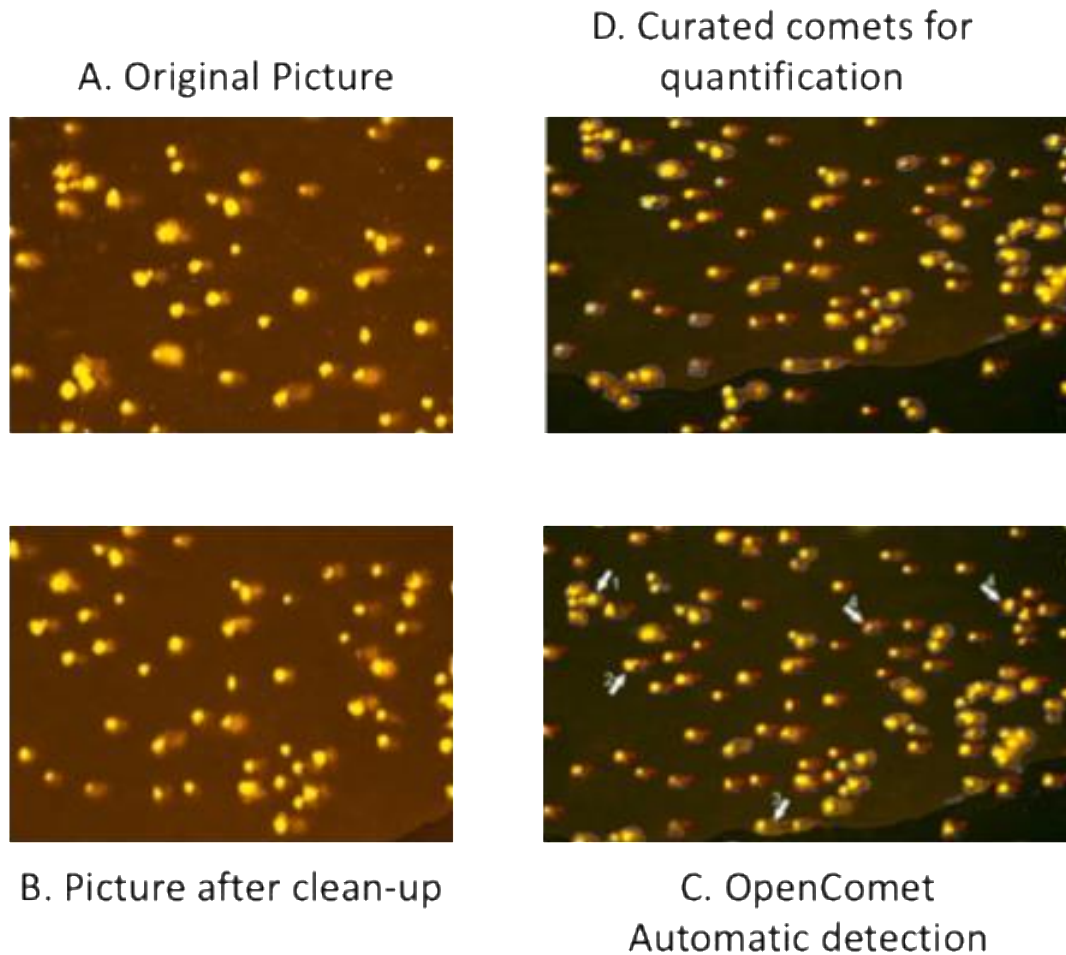


**Figure A-1 Comet assay image processing.**

A. Original picture of the comets embedded in agarose seen at 5X magnification at dsRED channel. B. Picture cleaned up using Adobe photoshop to clean the background without altering the comets themselves. 40pixel diameter “heal brush” with 100% hardness and 25% spacing in “normal” mode using “pen pressure” size was used for clean-up. C. The clean image is then loaded onto the OpenComet plugin in Fiji (ImageJ for MacOS), which graphically identifies the comets as “true” (lined in red), “outliers” (lined in yellow –arrow 3-), and “false” (lined in gray – arrow 1-). We manually click on the false true comets the to exclude them from further analyses. Two common false hits are found, overlapping comets as in arrows 1,2 and 3, or misidentified nuclei as in arrows 4 D. Opencomet parameters from the curated comets used for further analyses. This figure was prepared by Dr. Claudia Castillo-González.

## Results

### **DDR mutants accumulate DNA damage in the absence of environmental insults**

We first analyzed the data obtained from *atr* and wild type samples that were not subjected to additional environmental insults to inquire about the accumulation of DNA damage in plants with defective DDR. We obtained and 917 and 935 comets from WT and *atr* samples. Percentage tail DNA in wild type was ~25%, *atr* mutants showed ~45% of DNA in their comet tails. This result is very statistically significant (Student's T-test, p-value < 0.01). The higher level of PTD in *atr* mutants is consistent with the role of ATR in DDR. Therefore, this result validates our comet assay protocol as a mean to assess endogenous level of DNA damage in plants (Pourrut et al., 2015) (Figure A-2A and 2B).

### **DDR machinery can repair damaged DNA ex vivo**

Next, we analyzed the data from our DNA repair experiment using protein extracts from WT plants DDR-induced, or not, with UV light. We analyzed 303, 109, and 80 comets from *atr* samples untreated or treated with UV-induced and uninduced WT protein extracts, respectively. PTD in the *atr* comets not treated with any extract was calculated at ~55% (Figure A-3). However, the PTD of the *atr* comets treated with WT extract, induced by UV, went down to ~30% (Figure V-3). Comparatively, the PTD of *atr* samples treated with uninduced WT extract only went down to ~45% (Figure A-3). Both treatments significantly reduced the percentage of DNA in the comet tails (Student's t-test, p-value < 0.01)

Based on these results, we conclude that: 1) Total protein extract from WT plants has the capability of repairing damaged DNA in our *ex vivo* set experiment, and 2) UV treatment successfully induced DDR in WT samples, and it efficiently acts damaged DNA even in agarose-embedded lysed nuclei. Altogether, our version of the comet assay is highly robust and versatile as it can be used not only to assess the endogenous levels DNA damage within a sample, it can help to gauge the DNA repair competency of plant samples.

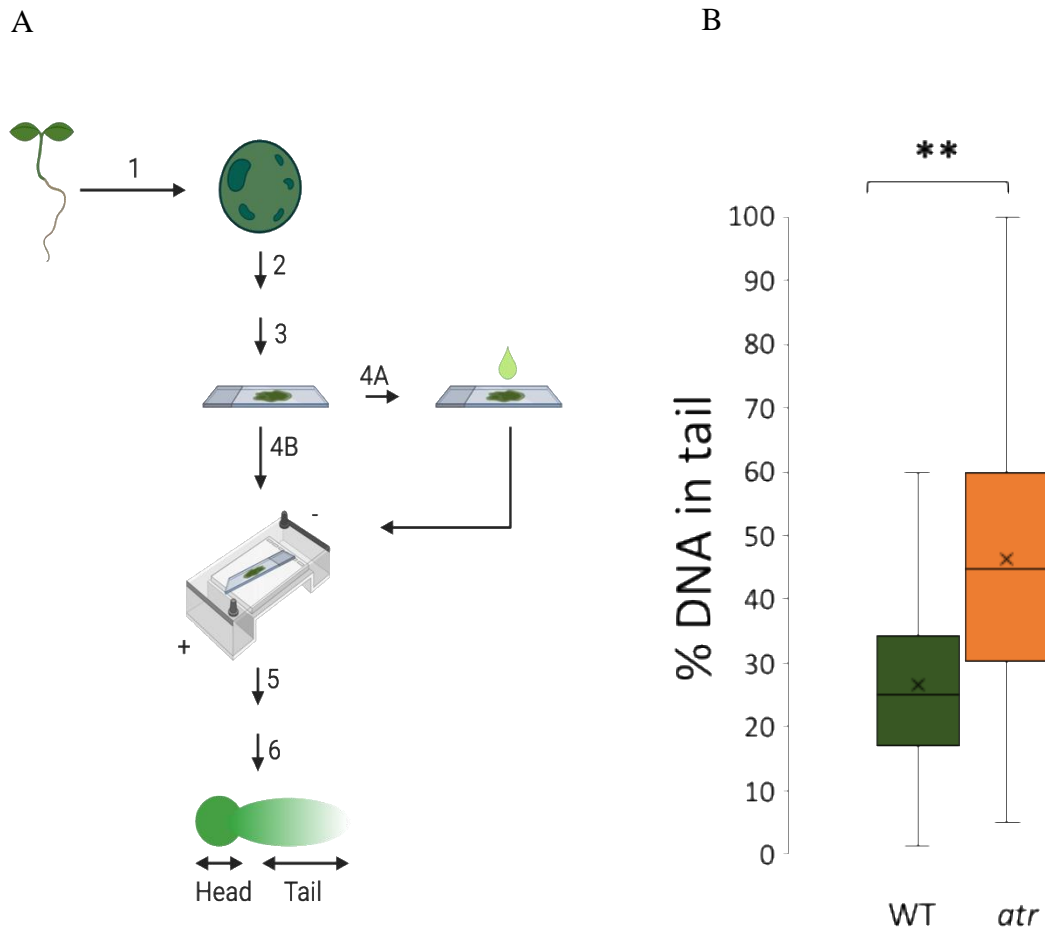


**Figure A-2 Comet assay with plant protoplasts.**

(A) Schematic representation of our version of the comet assay. The assay starts with protoplast extraction from seedlings (step 1) followed by depositing protoplasts mixed with low melting agarose on agarose coated slides (step 2) and overnight lysis reaction (step 3). The samples are either subjected to alkaline unwinding immediately (step 4B) or they are first incubated with the protein extracts (step 4A) followed by alkaline unwinding. Finally, the slides are run in an electrophoretic field, destained (step 5), and stained with PI stain to capture images using a scope (step 6). The comets have a tail comprising the damaged DNA and a head made of intact DNA. (B) Box and whisker plot representation of the comet assay results from *atr* and WT seedlings without any protein incubation. The straight line inside the box represents median while the 'X' is for mean. \*\* = p value < 0.01 using students t – test. n = 917 for WT and n = 935 for *atr*.

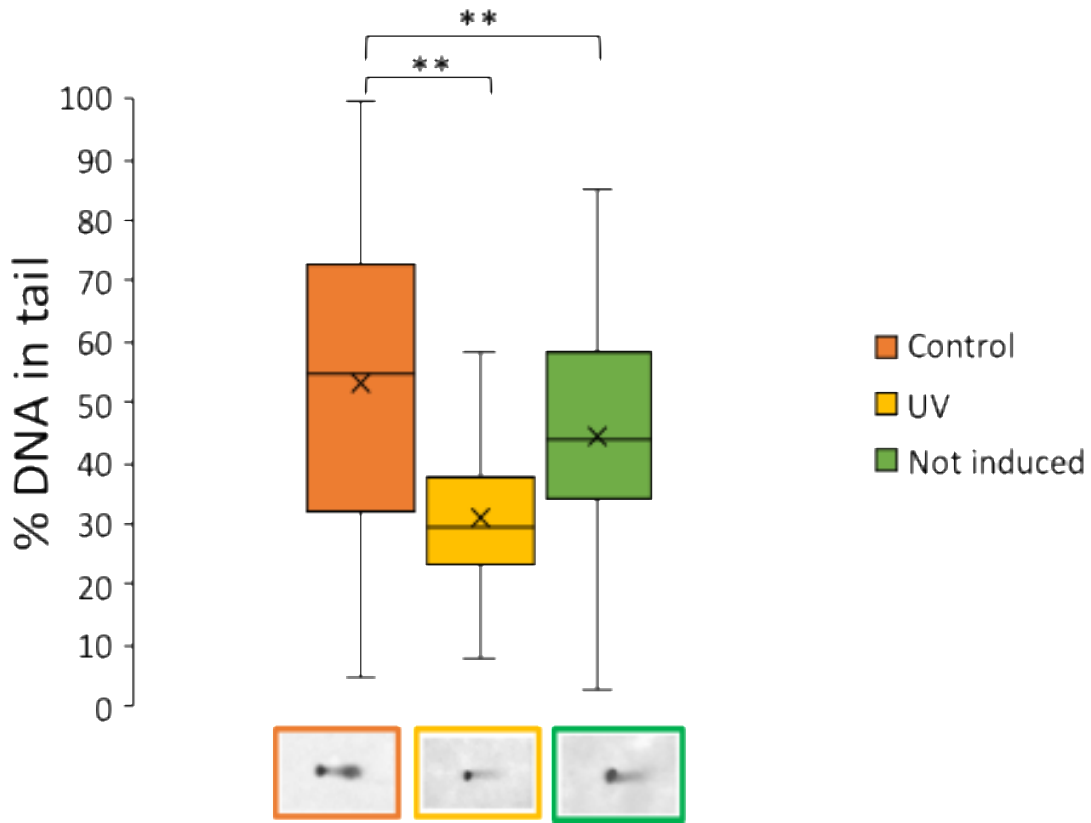


**Figure A-3 Ex vivo DNA Repair potential of WT extract.**

The orange box represents *atr* comets under normal conditions (control). The yellow box is for *atr* comets incubated with protein extract from WT samples treated with UV light (UV) to induce the DDR. The green box represents *atr* comets incubated with WT extracts without any further treatment with UV light (not induced). A representative image of a comet has been displayed under each of the boxes. For control n= 303, for UV induced n= 109 and for not induced n = 80, \*\* = p value < 0.01 using a student's t-test.

## Discussion

The *ex vivo* comet assay developed by our lab describes a robust single cell-based comet assay performed with plant samples without applying any mechanical stress for isolating the individual cells. Protoplasts can be easily extracted from multiple plant

tissues like leaves and seedlings, allowing the study of DNA repair dynamics in both actively dividing tissues and tissues undergoing endoreduplication. Our improved comet assay produces a large comet collection per sample to fuel robust statistical analysis and reliable conclusions. Also, our *ex vivo* DNA repair assay gave us information about the DNA damage repair competence of different genotypes.

There are a couple of caveats to be discussed. First, the chromatin structure plays an important role on the comet shape, so care must be taken when curating the images (Figure A-1). Second, there is great variability of comets from a plant sample, from nuclear content to comet shape and length, therefore, it is paramount to analyze a large population of cells. Note that we observed differences in the *atr* comets between the standard and untreated control of the DNA repair challenge assays. In the former, average PTD calculated from 935 nuclei was ~45%, while average PTD calculated from only 303 nuclei spiked to 55%. This exemplifies how the robustness of the data is dependent on the number of data points observed in the sample. Finally, here we present the analysis based on a single comet parameter, PTD, but other parameters, such tail length and moment, can also be used in parallel to PTD to further characterize the DNA damage and the effects of protein extracts on the genome (Figure -4A and 4B).

While some molecules belonging to the DDR pathway are involved in signaling, others are directly involved in repairing the damaged DNA. The *ex vivo* DNA repair challenge followed by comet assay is an easy and reliable way of identifying molecular players capable of mending the damaged genome. To investigate the role of a specific player in repairing DNA damage, comets prepared from a plant with high levels of



endogenous DNA damage, like *atr*, can be incubated with the protein extracts of a mutant line for our experimental molecule of interest. The inability of the mutant to repair the damaged DNA contrary to WT extract can be correlated to the molecule's involvement in DNA repair pathway *in vivo*.

Here we used the alkaline version of the *ex vivo* assay in our preliminary experiments, similar protein incubation steps can be performed for the neutral comet assay. Being able to rescue the damage in neutral comet assay might provide further information about the probable role of our gene of interest in terms of its ability to repair single-stranded DNA or double-stranded DNA break. We can also investigate the damage repair kinetics of a particular protein extract by analyzing comets subjected to incubation with the protein extract over different time points. Plotting the PTD from those specific time points on the Y– axis against the time points themselves might reveal the damage repair kinetics for a particular genotype. We offer this improved protocol for comet assay in plants because we consider it has great potential to further research in DNA metabolism in plants.

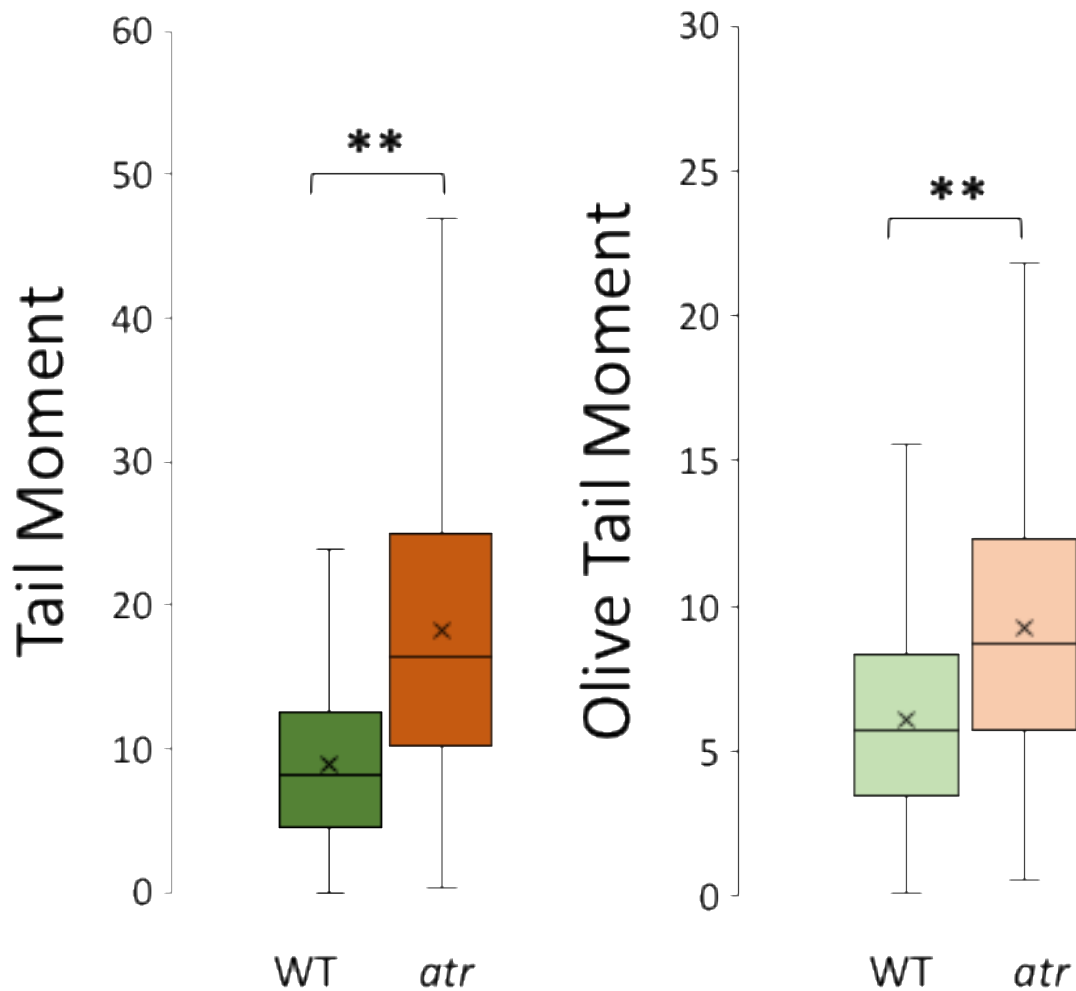


**Figure A-4 Assessing DNA damage accumulation based on parameters beyond PDT.**

Comets from *atr* had higher levels of TM and OTM which corroborate the PDT data showed in Figure Appendix A 1B. Based on the all three parameters (PDT, TM and OTM) *atr* comets have a higher level of damage DNA compared to WT comets.

## APPENDIX B

# THE CONSERVED STRUCTURE OF PLANT TELOMERASE RNA PROVIDES THE MISSING LINK FOR AN EVOLUTIONARY PATHWAY FROM CILIATES TO HUMANS

### **Abstract**

Telomerase is essential for maintaining telomere integrity. Although telomerase function is widely conserved, the integral telomerase RNA (TR) that provides a template for telomeric DNA synthesis has diverged dramatically. Nevertheless, TR molecules retain two highly conserved structural domains critical for catalysis: a template-proximal pseudoknot (PK) structure and a downstream stem-loop structure. Here we introduce the authentic TR from the plant *Arabidopsis thaliana* called AtTR identified through next-generation sequencing of RNAs co-purifying with Arabidopsis TERT. This RNA is distinct from the RNA previously described as the templating telomerase RNA, AtTER1. AtTR is a 268 nt Pol III transcript, necessary for telomere maintenance *in vivo* and sufficient with TERT to reconstitute telomerase activity *in vitro*. Bioinformatics analysis identified 85 AtTR orthologs from three major clades of plants: angiosperms, gymnosperms and lycophytes. Through phylogenetic comparison, a secondary structure model conserved among plant TRs was inferred and verified using *in vitro* and *in vivo* chemical probing.

---

\*Reprinted with permission from “The conserved structure of plant telomerase RNA provides the missing link for an evolutionary pathway from ciliates to humans” by J. Song, D. Logeswaran, C Castillo-González, Y. Li, S. Bose BB Aklilu, Z. Ma, A. Polkhovskiy, JJJ Chen and DE Shippen, 2019. PNAS, 116 (49) 24542-24550  
Copyright 2019 by National Academy of Sciences.

The conserved plant TR structure contains a template-PK core domain enclosed by a P1 stem and a 3' long stem P4/5/6, both of which resemble a corresponding structural element in ciliate and vertebrate TRs. However, the plant TR contains additional stems and linkers within the template-PK core, allowing for expansion of PK structure from the simple PK in the smaller ciliate TR during evolution. Hence, the plant TR provides an evolutionary bridge that unites the disparate structures of previously characterized TRs from ciliates and vertebrates.

### **Introduction**

Many non-coding RNAs (ncRNAs) function as integral components of ribonucleoprotein (RNP) complex enzymes that govern cellular processes such as translation, RNA splicing and telomere maintenance (Wilusz et al., 2009). The telomerase RNA (TR or TER) assembles with the telomerase reverse transcriptase (TERT) protein to form the catalytic core of an enzyme that maintains telomere function and genome integrity by continually adding telomeric DNA repeats onto chromosome ends (Shay and Wright, 2019). TR contains a template for the synthesis of G-rich telomere repeat arrays catalyzed by TERT. In addition, TR harbors highly conserved structural domains that serve as a scaffold for binding accessory proteins that facilitate RNP biogenesis, engagement with the chromosome terminus and regulation of telomerase enzyme activity (Podlevsky and Chen, 2016).

The essential role of telomerase in telomere maintenance is universally conserved across Eukarya, except for a small group of insect species that evolved a retrotransposon-mediated mechanism (Casacuberta, 2017). Nevertheless, key aspects of the telomerase

RNP have diverged dramatically, including the sequence and length of TR, the protein composition of the holoenzyme and the mechanism of RNP maturation (Egan and Collins, 2012). For example, TR genes in ciliated protozoa encode relatively small RNAs (140-210 nt. in length) that are transcribed by RNA polymerase III (Pol III) (Greider and Blackburn, 1989; Lingner et al., 1994). The La-related protein P65 in *Tetrahymena* recognizes the 3' poly-U tail of TR and bends the RNA to facilitate telomerase RNP assembly (Jiang et al., 2015; Singh et al., 2012). In contrast, fungi maintain much larger TR molecules (900 to 2,400 nt.) that are transcribed by RNA polymerase II (Pol II) (Podlevsky and Chen, 2016). The 3' end maturation of fungal TRs requires components of the canonical snRNA biogenesis pathway and results in RNP assembly with Sm and Lsm proteins (Box et al., 2008; Noël et al., 2012). Like fungi, vertebrates also utilize Pol II to transcribe a TR with a size ranging from 312 to 559 nt (Chen et al., 2000). However, vertebrate telomerase RNP processing and biogenesis proceeds via a small nucleolar RNA (snoRNA) maturation pathway (Mitchell et al., 1999b). In vertebrates, a highly conserved structural motif in the 3' H/ACA domain of TR binds the protein components of the H/ACA snoRNP (Dyskerin, NOP10, NHP2, and GAR1) which then protect the 3' end of the mature TR from exonuclease degradation (Egan and Collins, 2010; Tseng et al., 2018; Wang and Meier, 2004).

Within TR, two conserved domains are critical for telomerase catalysis (Qi et al., 2013). The first is the template-pseudoknot domain which bears a single-stranded template region typically corresponding to 1.5-2 copies of the telomeric repeat (Podlevsky and Chen, 2016). The 5' boundary of the TR template is defined by a template boundary

element (TBE) that promotes polymerase fidelity by preventing incorporation of non-telomeric nucleotides into telomeric DNA (Autexier and Greider, 1995; Chen and Greider, 2003a; Jansson et al., 2015; Tzfati et al., 2000). In addition to the template and TBE, the pseudoknot (PK) structure located downstream of the template is essential for TERT-TR interaction and enzyme activity (Blackburn and Collins, 2011; Podlevsky and Chen, 2012b). The PK structures from vertebrates and yeast TRs are generally larger and more stable (Chen et al., 2000; Qi et al., 2013), harboring longer helices than the PK structures of ciliate TR, which are relatively primitive and less stable (Autexier and Greider, 1998; Gilley and Blackburn, 1999). NMR studies of TR reveal a unique triple-helix structure in the PK which plays an essential, but poorly understood, role in promoting telomerase activity (Theimer et al., 2005). Another essential domain of TR, called helix IV in ciliates or CR4/5 in vertebrates, can reconstitute telomerase activity in trans together with the template-PK domain (Chen, 2002; Mason et al., 2003; Mitchell and Collins, 2000; Xie et al., 2008). TRs from other groups of eukaryotes including echinoderms and trypanosomes also possess a second structural domain called eCR4/5 that can bind independently to TERT in trans and is functionally equivalent to the vertebrate CR4/5. The requirement of two conserved structural TR domains for telomerase activity is therefore universally conserved among all major groups of eukaryotes from Trypanosome to vertebrates (Podlevsky et al., 2016).

We previously described the identification of two telomerase-associated RNAs from *A. thaliana* termed AtTER1 and AtTER2 (Cifuentes-Rojas et al., 2011, 2012). AtTER1 was proposed to serve as the template for telomeric DNA synthesis by telomerase

(Cifuentes-Rojas et al., 2011). However, recent data has refuted the role of AtTER1 in telomere maintenance (Dew-Budd et al., 2020; Fajkus et al., 2019). Moreover, Fajkus and colleagues recently reported the identification of a novel telomerase RNA from *A. thaliana* termed AtTR that is required for telomere maintenance and is conserved across land plants (Fajkus et al., 2019). Here we present results of a next-generation sequencing analysis of TERT-associated RNAs, which independently led to the identification of AtTR as the bona fide RNA component for Arabidopsis telomerase. We show that AtTR is crucial for telomere maintenance in vivo and sufficient to reconstitute telomerase activity with *A. thaliana* TERT (AtTERT) protein in vitro. In addition, by employing phylogenetic sequence analysis of homologous TRs from the three distantly related plant lineages including angiosperms, gymnosperms and the early branching lycophytes, we determine a conserved structural model for plant TRs that was verified using chemical probing and mutagenesis. Our findings provide an evolutionary bridge to unite the disparate structures of the previously characterized TRs from ciliates and vertebrates as well as a new platform to explore the evolution of the telomerase RNP enzyme.

## **Results**

### ***AtTR is the predominant RNA associated with active telomerase in Arabidopsis***

Prompted by collaborative work with the Beilstein lab, which indicated that AtTER1 was not the authentic TR component for *A. thaliana* telomerase (Dew-Budd et al., 2020), we developed an unbiased approach to identify ncRNAs associated with the AtTERT protein through RNA immunoprecipitation (RIP) analysis using anti-AtTERT antibody. RIP was performed under native conditions with mild salt and detergent

concentrations to retain weak interactions. Next-generation sequencing of co-purified RNAs identified 177 RNA sequences that were significantly enriched in the wild-type (WT) but not tert null samples (Fig. B-1A). The previously reported telomerase RNA template AtTER1 and the TERT-associated RNA AtTER2 were not found among these AtTERT-associated RNAs. To address the possibility that AtTER1 was masked by other more abundant RNAs, we used more stringent conditions to purify active telomerase by size exclusion chromatography prior to RIP (Fig. B-1B). Telomerase activity was detected by quantitative telomere repeat amplification protocol (qTRAP) with the peak activity in a fraction corresponding to an apparent molecular mass of ~300 kDa (Fig. B-1C). A scatter plot of RNAs purified and sequenced from fractions with peak telomerase activity revealed a single RNA that was enriched more than 100-fold above background (Fig. B-1D). This is the same RNA independently reported by Fajkus et al and dubbed AtTR (34). Since AtTER1 overlaps with the 5' region of RAD52 locus (Samach et al., 2011) (Figure B-2A), we performed additional TERT RIP experiments to directly test if RAD52 mRNA was present in the IP. While RAD52 mRNA could be amplified from the IP, an RNA corresponding to the previously described AtTER1 could not (Figure B-2B and B-2C). These results are inconsistent with AtTER1 being a functional telomerase RNA and instead support the recent findings of Fajkus et al and Dew-Budd et al that AtTER1 is not required for telomere maintenance.



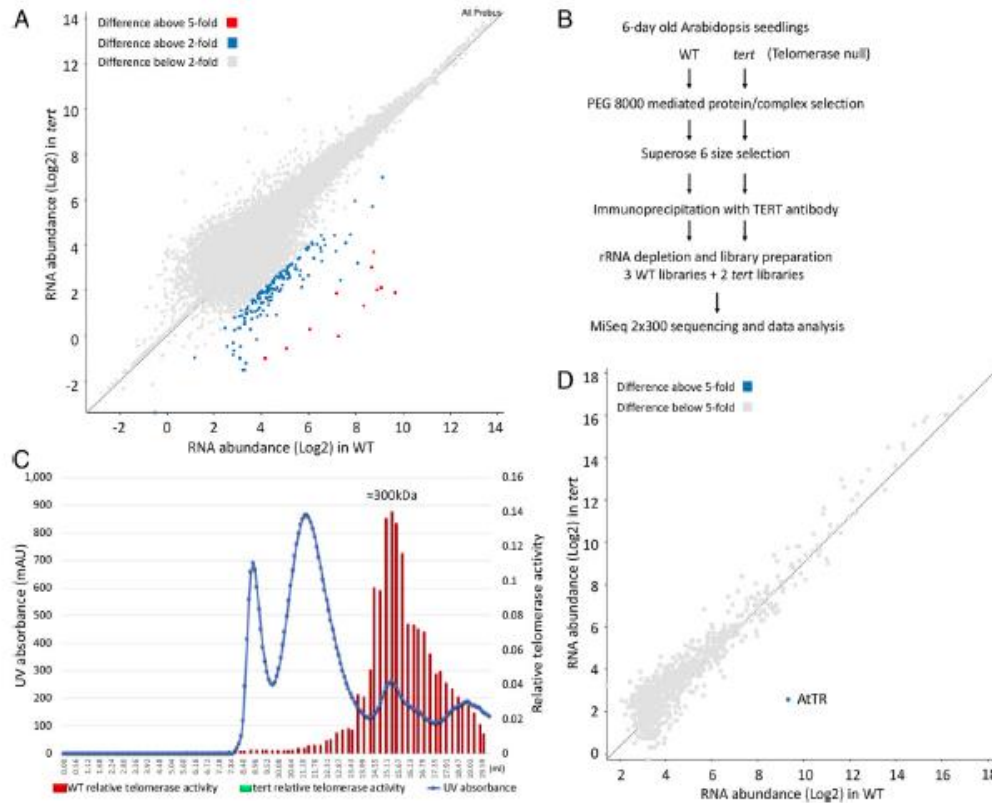


**Figure B-1 A single RNA species is enriched in active telomerase complexes.** (A) Scatter plot representing RNA targets enriched in a direct RIP seq experiment. WT and tert null mutant samples are compared to identify potential AtTERT-associated RNAs labelled as blue or red according to their relative enrichment in WT greater than 2-fold or 5-fold, respectively. (B) Schematic representation of the experimental design for identification of telomerase-associated RNAs. (C) Size exclusion chromatogram of *A. thaliana* protein lysate. Blue curve shows the elution profile and red bars the relative telomerase activity from each fraction. (D) Scatter plot of RNAs copurified with the active *A. thaliana* telomerase complex. AtTR is the only RNA molecule significantly enriched in WT samples compared to tert mutants.

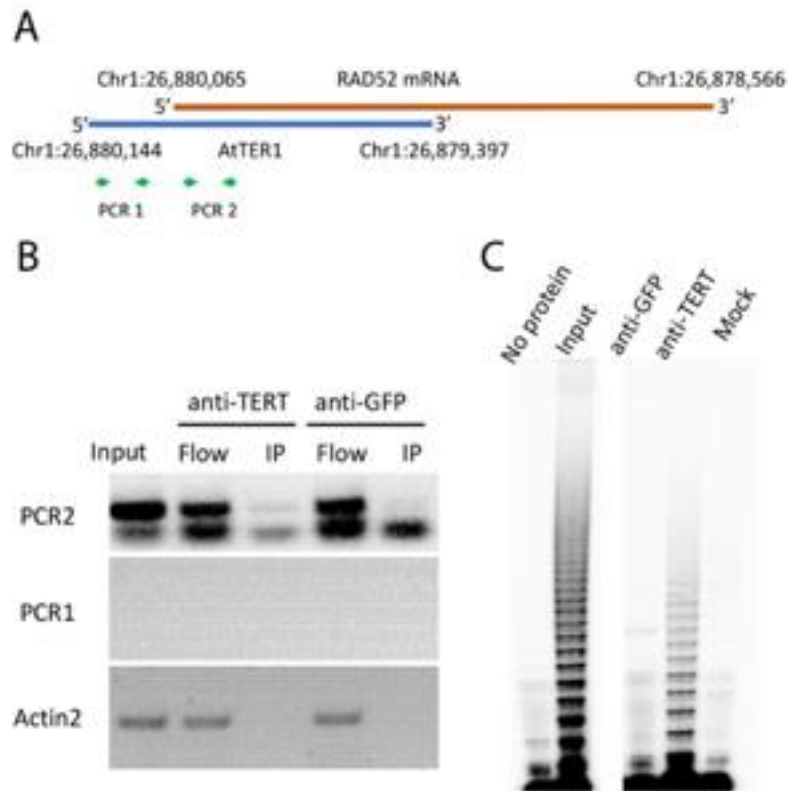


**Figure B-2 AtTER1 is not recovered in an AtTERT IP.**

(A) Schematic representation of the physical map of AtTER1 and RAD52 mRNA. (B) RT-PCR experiments were conducted using RNAs independently collected from AtTERT-IP and GFP-IP. Primers used in the experiments are indicated in panel A. (C) TRAP was performed with identical samples in B to verify that active telomerase was purified from AtTERT-IP but not the GFP-IP.

**AtTR is required for telomere repeat synthesis by *A. thaliana* telomerase**

AtTR was originally described as a noncoding Pol III transcript involved in the stress response (Wu et al., 2012a). AtTR bears a 9-nt sequence of 5'-CUAAACCCU-3' complementary to the *A. thaliana* 7-nt telomeric DNA sequence (TTTAGGG)<sub>n</sub> (Richards and Ausubel, 1988). Mapping of its 5' and 3' ends by rapid amplification of cDNA ends (RACE) revealed that AtTR is 268 nt in length (Figure B-4A). The size of endogenous

AtTR was verified by northern blotting (Figure B-4B). Using direct terminator exonuclease treatment in combination with pyrophosphohydrolase, we found that AtTR bears a 5' triphosphate structure (Figure B-4C). AtTR is widely expressed, but most abundant in actively dividing cell culture. Notably, AtTR is also abundant in mature leaves where AtTERT is conspicuously absent and telomerase activity is negligible (Figure B-4D).

We used two genetic approaches to determine if AtTR is required for telomerase activity and telomere maintenance in vivo. First, we found that a homozygous T-DNA insertion allele of AtTR (Flag\_410H04) completely abolished AtTR RNA production as well as telomerase activity detected by qTRAP, while plants bearing a heterozygous mutation had ~50% of the WT level of AtTR and 50% of the WT telomerase qTRAP activity (Fig. B-3A, B-5A and B-5B). Terminal Restriction Fragment (TRF) analyses showed progressive shortening of the telomere tract in homozygous Flag\_410H04 mutants over five generations (Fig. B-3B), reminiscent of tert null mutants (Riha et al., 2001). Second, two independent CRISPR-mediated deletions that either remove a 49 nt sequence including the template or a 14 nt sequence downstream of the template disrupted telomere maintenance (Figure B-9). We performed genetic complementation experiments on Flag\_410H04 AtTR null mutants using an AtTR construct driven by the U6 promoter (U6::AtTR). Transformants with U6::AtTR expression had restored telomerase activity and increased telomere length (Figure B-3C and Figure B-5C, B-5D). These findings confirm that AtTR is necessary for both telomerase enzyme activity and telomere maintenance in *A. thaliana*.

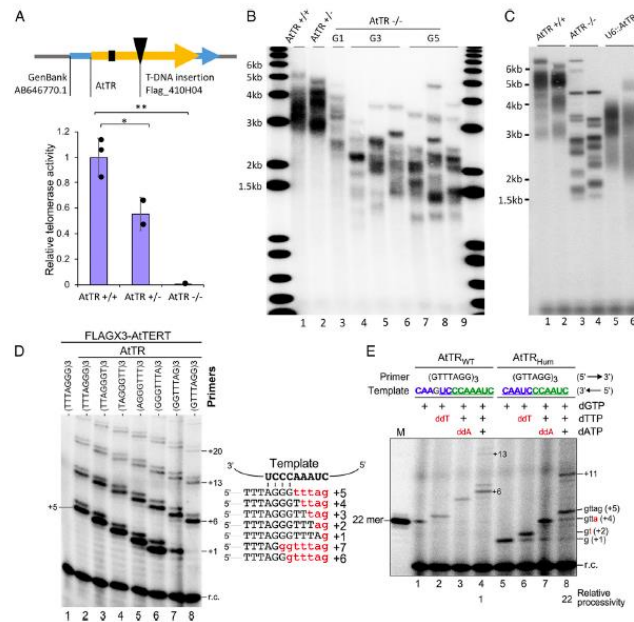


### Figure B-3 AtTR is the RNA template for Arabidopsis telomerase.

(A) Top, schematic representation of the AtTR gene showing the template domain (black box) and the location of a T-DNA insertion. Bottom, relative telomerase activity of WT, heterozygous and homozygous AtTR mutants determined by quantitative TRAP assay. (B) TRF analysis of telomere length in AtTR mutants across multiple generations. (C) TRF results for genetic complementation with AtTR driven by the U6 promoter. Third generation AtTR<sup>-/-</sup> mutants untransformed or transformed with U6::AtTR. (D) In vitro reconstitution of *A. thaliana* telomerase activity. Sequences of the putative template with the annealing position of seven circular permuted telomeric DNA primers are shown (right). The predicted primer-extended products are shown in red. *A. thaliana* telomerase is reconstituted in vitro from synthesized FLAGx3-AtTERT and 1.5  $\mu$ M of T7 transcribed full-length AtTR (268nt). The affinity-purified telomerase was assayed for activity in the presence of 32P-dGTP, dTTP, dATP and seven plant telomeric DNA primers with permuted sequences. A radiolabeled 18-mer recovery control (r.c.) was added before product purification and precipitation. Numbers to the right of the gel denote the number of nucleotides added to the primer. (E) Template-directed nucleotide addition by *A. thaliana* telomerase. Telomerase was reconstituted in vitro with AtTERT and either AtTR<sup>WT</sup> or AtTR<sup>Hum</sup>. The reconstituted telomerase was assayed for activity in the presence of 32P-dGTP and different combinations of dTTP, dATP, ddTTP or ddATP. A 21 nt plant telomeric DNA primer (GTTTAGG)<sub>3</sub> was used for AtTR, and an 18 nt human telomeric DNA primer (GTTAGG)<sub>3</sub> was used for the AtTR<sup>Hum</sup>. A radiolabeled 18-mer recovery control (r.c.) was added before product purification and precipitation. Numbers and sequences of nucleotides added to the primers are indicated.

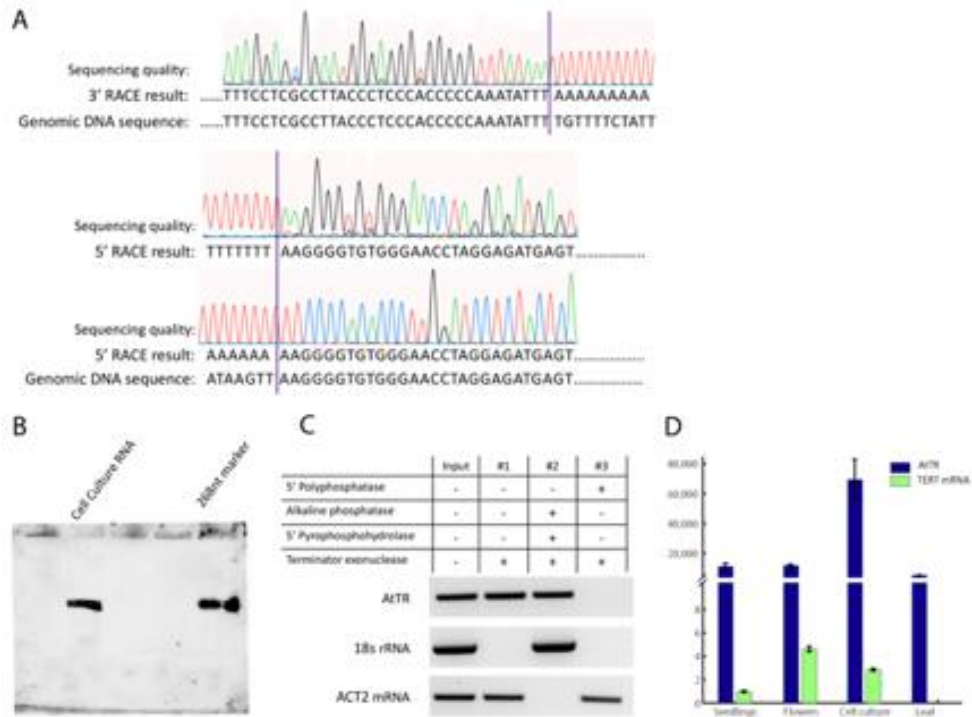


#### Figure B-4 Characterization of AtTR.

(A) 5' and 3' RACE of AtTR define it as a 268nt lncRNA derived from Chr 2 position 12619067 to 12619334. Both polyA and polyT tails were used in 5' RACE to precisely map the transcriptional start site. (B) Northern blotting using total RNA from *A. thaliana* cell line T87 confirmed that AtTR is 268 nt in length. (C) Enzymatic probing of 5' end structure shows that AtTR has a 5' triphosphate. 18s rRNA and ACT2 mRNA served as controls for 5' monophosphate or capped RNAs, respectively. (D) qPCR indicates that AtTR is expressed throughout the plant life cycle and it is enriched in rapidly dividing *A. thaliana* cell culture.

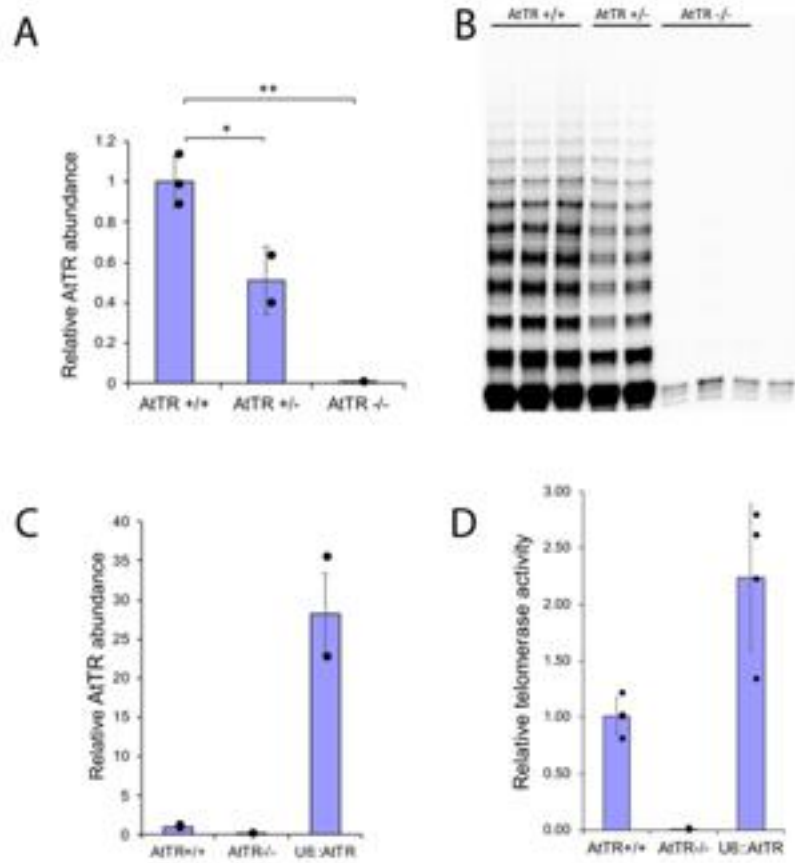


**Figure B-5 AtTR is the bona fide template of *A. thaliana* telomerase.** (A) qPCR analysis of the Flag\_410H04 T-DNA insertion line defines this an AtTR null mutant. (B) Telomerase activities of WT (AtTR +/+), heterozygous (AtTR +/-), and homozygous (AtTR -/-) Flag\_410H04 segregants were determined by TRAP. (C) AtTR abundance was measured by RT-qPCR in untransformed AtTR +/+, AtTR -/- and U6::AtTR complementation lines. AtTR expressed from the U6 promoter in the AtTR -/- background results in a ~28-fold average overexpression of AtTR as compared to WT plants. (D) Telomerase activity was measured by qTRAP in AtTR +/+, AtTR -/- and U6::AtTR complementation lines. Overexpression of AtTR results in increased telomerase activity.

### **AtTR and AtTERT reconstitute active telomerase in vitro**

We next asked whether AtTR can assemble with AtTERT in vitro to reconstitute active telomerase. As shown in Figure B-3D, recombinant FLAGx3-AtTERT protein synthesized in rabbit reticulocyte lysate was assembled with T7 RNA polymerase transcribed AtTR in vitro and the reconstituted telomerase was immuno-purified followed by a direct primer extension assay (Figure B-3D). Importantly, the primer extension activity is AtTR-dependent as no activity was detected in the absence of AtTR (Fig. B-3D, lane 1). Seven *A. thaliana* telomeric DNA primers with permuted sequences of TTTAGGG bearing different 3' terminal sequences were examined using in vitro reconstituted telomerase enzyme. The reaction with (GTTTAGG)<sub>3</sub> generated a 7-nt ladder pattern of products with major bands at positions +6, +13 and +20 (Figure VI-3D, lane 8), consistent with the 7-nt telomeric DNA repeats synthesized by *A. thaliana* telomerase. *A. thaliana* telomerase exhibited similar levels of activity with the different permuted telomeric DNA primers and generated the expected offset banding patterns (Figure B-3D, lanes 2-7), indicating correct primer-template alignment and specific usage of the template.

To further examine the templating function of AtTR, we generated an AtTR template mutant (AtTR<sub>hum</sub>) with a template sequence similar to the human TR (hTR) template that allows the synthesis of 6-nt TTAGGG repeats. The telomeric TTAGGG repeats are ubiquitously conserved in most lineages of eukaryotes. The 9-nt AtTR template sequence 5'-CUAAACCCUGAACC-3' for the synthesis of 7-nt repeats (TTTAGGG)<sub>n</sub> is flanked by a G residue at its 3' boundary and could potentially be expanded to a longer 14

nt template by mutating the G residue to A. To convert the native *A. thaliana* template sequence to a human-like template, we simply deleted one A residue in the polymerization template sequence and the non-conserved G residue in the alignment sequence, which resulted in a 12-nt 5'-CUAACCCUAACC-3' template for synthesizing TTAGGG repeats. As expected, the telomerase reconstituted from the AtTRhum template mutant generates the first major bands at position +5(+gtag) and the second major band at +11, indicating the addition of a 6-nt DNA repeat using the human-like template (Figure B-3E, lane 8). Moreover, the inclusion of dideoxy-ribonucleotides, either ddTTP or ddATP, terminated the primer extension reaction at the expected positions on the template of the AtTRWT and AtTRhum (Figure B-3E, lanes 2-3 and 6-7). In addition, under processive conditions with all three nucleotides, the AtTRhum template with a long 6-nt alignment region led to a significantly high processivity based on the ratio of +11/+5 products (Figure B-3E, lanes 4 and 8), consistent with a previous finding that longer templates correlate with high repeat addition processivity (Chen and Greider, 2003b). Altogether, these data demonstrate that the template sequence 43-CUAAACCCU-51 within AtTR is a bona fide template for telomeric DNA repeat synthesis by *A. thaliana* TERT.

### **Plant TRs share a conserved secondary structure**

To discern the structure of AtTR, we employed phylogenetic comparative analysis to infer a secondary structure model from the sequence alignment of plant TR homologs identified from three major clades of land plant species: angiosperms, gymnosperms and lycophytes (Figure B-6A). Orthologs of AtTR were identified by searching genomic



sequence data from National Center for Biotechnology using sequence homology search tools including BLAST, Fragrep2 (Mosig et al., 2006) and Infernal (Nawrocki and Eddy, 2013). While the BLAST was able to find TR homologs from closely related species, Fragrep2 allowed identification of TR homologs from more distantly related species by utilizing position specific weight matrix (PWM) based searches with PWMs derived from multiple sequence alignments, as opposed to using the primary sequence as the search query. Collectively, we identified 85 AtTR orthologs, 70 from angiosperms, 11 from gymnosperms and 4 from lycophytes (Table B-1). To infer secondary structure, multiple sequence alignment analysis was performed with 16 representative TR sequences (12 angiosperms, 3 gymnosperms and 1 lycophytes) selected from the 85 sequences to allow at least one representative from each individual order spanning three distinct clades (Figure B-10). All TR sequences including those from the basal groups, gymnosperms and lycophytes, can be reliably aligned with the TR sequence from angiosperms, revealing universally conserved structural elements of plant TRs. From the alignment of 16 divergent plant TR sequences, universal or group-specific nucleotide covariations were identified to infer base-paired structural elements (Figure B-6B-6D, B-12). Comparison of TR secondary structures from three representative species, *A. thaliana* from angiosperms, *Picea glauca* (spruce) from gymnosperms and *S. kraussiana* from lycophytes, revealed three common structural features: a conserved template-PK core domain enclosed by stem P1c, a long stem that comprises consecutive short base-paired regions termed P4, P5 and P6, and a long-range base-paired stem P1a formed between the extreme distal 5' and 3' sequences (Figure B-6B-6D).

The plant template-PK (T-PK) core domain resembles those from ciliate, fungal and vertebrate TRs, consisting of a template, a universal PK structure formed by stems P2 and P3, and a core-enclosing stem P1c (Figure VI-6B-6D). However, the plant T-PK core domain contains additional plant-specific stems, namely P1.1 (in *P. glauca* and *S. kraussiana*), P2.1 (in *A. thaliana* and *P. glauca*) and P2.2 (in *P. glauca* and *S. kraussiana*) (Fig. 3B-D). The P1.1 stem can be found in the invertebrate echinoderm and fungal TRs, and could potentially function as a TBE (Qi et al., 2013). The P2.1 and P2.2 stems are not present in all plant TRs, suggesting that they are more adaptable and maybe important for a function specific to some plant groups. One possible role for the variable P2.1 and P2.2 stems is to maintain the length of the linker between the template and the pseudoknot structure within the T-PK core domain.

In addition to the T-PK core domain, the plant TR contains a long helical structure with three consecutive short stems, P4, P5 and P6, located near the 3' end between P1a and P1b (Figure B-6B-6D). The location and structure of the plant P4/P5/P6 stem resembles the vertebrate CR4/5 domain, echinoderm eCR4/5 domain or ciliate helix IV, all of which are essential for telomerase activity (28, 29, 43). The three-way junction formed between P1a, P1b and P4/5/6 appears to be a conserved feature of plant TR (Figure B-6B-6D). This P1a-mediated three-way junction is unique to plant TR and is not found in other known TRs.

This conserved secondary structure model of AtTR is supported by chemical modification probing analysis. Selective 2'-hydroxyl acylation analysis by primer extension (SHAPE) was employed to examine the accessibility of each nucleotide in the

in vitro folded RNA (Wilkinson et al., 2006). N-methylisatoic anhydride (NMIA) modification of individual nucleotides was monitored and SHAPE activity plotted on the structural model to identify unpaired residues (Figure B-6E and Figure B-12). Consistent with our AtTR structural model, most unpaired nucleotides showed significant SHAPE activity.

We also probed the AtTR structure in vivo by dimethyl sulfide (DMS) footprinting and mutational profiling (DMS-MaPseq). DMS methylates the base-pairing faces of single-stranded, unprotected adenosines and cytidines. Such modifications cause the stalling of conventional reverse transcriptases during cDNA synthesis, allowing for footprinting studies. These modifications can also result in mismatches in cDNA when TGIRT reverse transcriptase is used (Zubradt et al., 2016). DMS modifications were analyzed by primer extension (DMS footprinting), while DMS-induced mutational rates per position were calculated by coupling TGIRT cDNA synthesis with high throughput sequencing. DMS footprinting identified 38 accessible nucleotides that mapped to predicted single-stranded residues (Figure B-13). Results of DMS MaPseq extended these findings and revealed a detailed map of nucleotide accessibility (Figure B-6F and Figure B-14). Accessible nucleotides were concentrated in the predicted single-stranded regions within the T-PK and P1b-P1c linker. Altogether, these in vitro and in vivo structural probing results provide strong support for our AtTR secondary structure model.

In addition to inferring the conserved secondary structure, the multiple sequence alignment of the 16 representative plant TRs spanning land plant evolution revealed five highly conserved regions (CR), CR1 to CR5, containing nucleotides that are invariant

among these 16 distantly related species (Figure B-10). Such remarkable conservation of nucleotide identity usually predicts essential functions of these regions as evident in vertebrate TRs (Chen et al., 2000). CR1 corresponds to the template of AtTR. CR2 and CR3 form the universal P2 and P3 stems of the PK, while CR4 and CR5 form a P5 structural element that includes the short 3-bp P5 stem, an asymmetric internal loop and the upper part of stem P4 (Figure B-6B-6D). While lacking the P6.1 stem-loop, the universal P5 structural element of the plant TR resembles the CR4/5 domain conserved in vertebrate, fission yeast and filamentous fungal TRs (Chen, 2002; Qi et al., 2013). This highly conserved P5 stem may serve as a protein binding site or play a crucial role in telomerase function.

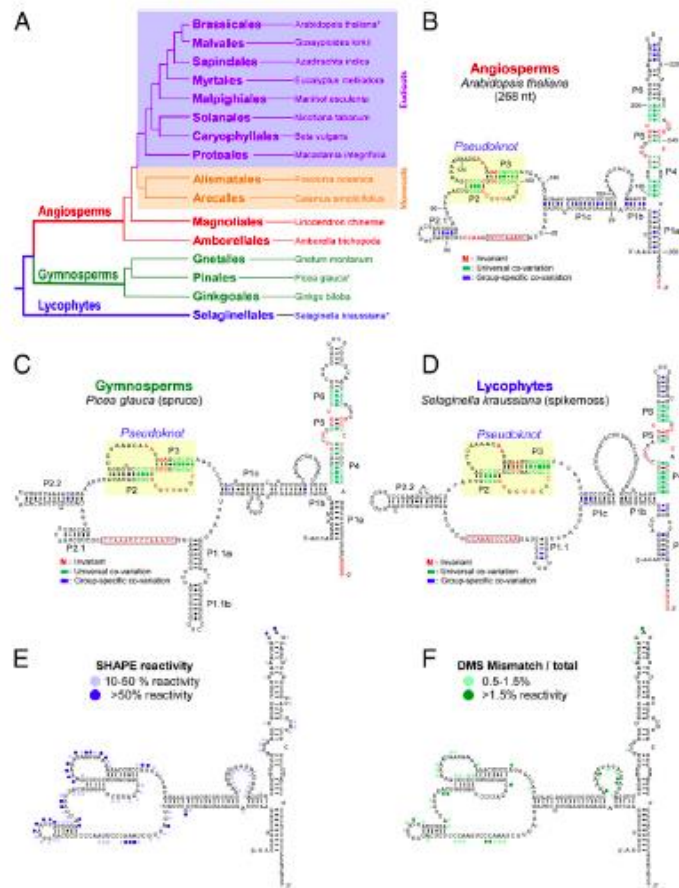


**Figure B-6 Plant TRs share a conserved secondary structure.**

(A) Evolutionary relationship between major land plant clades. A single representative species of each order is included. An asterisk denotes the species with the secondary structure models shown in B, C, D. Representative TR secondary structures determined by phylogenetic sequence analysis are shown for (B) *A. thaliana* from angiosperms, (C) *Picea glauca* (spruce) from gymnosperms and (D) *S. kraussiana* (spike moss) from lycophytes. The characteristic TR pseudoknot (PK) is shaded in yellow. Universal co-variations (green line), group-specific co-variations (blue line) and plant invariant residues (red) are indicated and based on sequence alignment of 16 divergent plant species spanning 8 eudicots, 2 monocots, 2 early branching angiosperms, 3 gymnosperms and 1 lycophyte. The aligned sequences are shown in SI Appendix Fig. S5. (E) In vitro chemical probing of AtTR secondary structure by SHAPE. Chemical reactivities per nucleotide are plotted on the AtTR secondary structure. (F) In vivo chemical probing of AtTR structure by DMS-MaPseq. Average mutation frequencies per nucleotide are plotted on the AtTR secondary structure.

**The AtTR PK domain is essential for telomerase function and homologous to human**

**TR**

With a robust secondary structure model for AtTR, we sought to map the structural elements essential for telomerase activity. Full-length or truncated AtTR constructs were assembled with recombinant FLAGx3-AtTERT in vitro and the immuno-purified enzymes were analyzed for telomerase activity by direct primer extension. Analysis of three truncated AtTR fragments, 11-179, 25-153 and 42-136 (Figure B-7A), showed that AtTR-25-153 is the minimal PK fragment sufficient to reconstitute about 40% of wild-type activity without the P4/5/6 domain (Figure B-7B, lanes 2 and 3). The core-enclosing P1c stem appeared to be important for telomerase function as the AtTR-42-136 fragment with P1c removed was unable to reconstitute any significant activity (Figure B-7B, lane 4). Equivalent to the CR4/5 domain of human TR, the 3' P1a/4/5/6 domain of AtTR can also function in trans as a separate RNA molecule to stimulate the reconstituted activity from the basal 40% to 66% of wild-type level (Figure B-7C). A basal activity of telomerase reconstituted from the T-PK domain alone was previously reported with Trypanosome and Echinoderm TRs (Podlevsky et al., 2016), indicating an evolutionary transition of functional dependence for the two conserved TR domains.

The PK structure of plant TRs highly resembles the PK structures in ciliate and vertebrate TRs with differences in size and complexity. In human TR PK structure, the invariant U residues in the J2/3 upstream region (J2/3u) are essential to telomerase activity (Chen and Greider, 2003a). To determine if the invariant U residues in plant TR PK are functionally homologous to the human TR, we reconstituted telomerases with two AtTR

mutants, U92C and UU94/95CC. The activity assays of the mutant enzyme showed no activity (Figure B-7D, lanes 2 and 3), indicating these U residues in the AtTR PK domain are absolutely required for telomerase activity. Therefore, the T-PK domains of AtTR and hTR are both structurally and functionally homologous.

Another critical function provided by the T-PK domain is defining the functional template boundary through specific structural elements, i.e. the P1 stem in vertebrate TR (Chen and Greider, 2003a). The P1c stem in the T-PK domain of AtTR resembles the P1 stem in human TR, and presumably functions as the template boundary element. To test this idea, we generated an AtTR mutant 38UU with two U residues inserted between the P1c stem and the template to increase the linker length, a critical determinant of the template boundary. In the wild-type AtTR template, a G residue immediately flanks the 5' boundary and does not serve as a template even in the presence of dCTP substrate (Figure B-7E, lanes 1 and 2). However, in the presence of dCTP, the telomerase enzyme reconstituted with the AtTR mutant 38UU utilized the G residue as a template beyond the template boundary (Figure B-7E, lanes 3 and 4). Thus, *A. thaliana* and human telomerases share a homologous mechanism for template boundary definition.

While the overall secondary structure of AtTR is well supported by co-variation evidence and chemical probing data, we performed mutagenesis analysis to provide additional support for the highly conserved P5 stem and the plant-specific P2.1 stem (Figure B-7A). The 3-bp P5 stem is formed by two highly conserved regions, CR4 and CR5, with only limited co-variation support for one of the 3 base-pairs. We thus generated AtTR full-length constructs, P5-m1 and -m2, with two single point mutations, G194C and

C239G, introduced to disrupt the invariant G:C base-pairing in the P5 stem, or a compensatory mutant P5-m3 with both point mutations to restore the base-pairing (Figure B-7A). The activity assay showed that P5-m1 and -m2 single point mutations abolished telomerase activity (Figure B-7F, lanes 2 and 3), while the compensatory mutation P5-m3 restored activity (Figure B-7F, lane 4), consistent with the essential base-paired structure of stem P5. A similar mutagenesis approach was employed to confirm the base-paired structure and the functional importance of stem P2.1 (Figure B-7G). Altogether, these in vitro studies strongly support the robustness of the phylogenetic comparative analysis for inferring RNA secondary structure in plant TR.



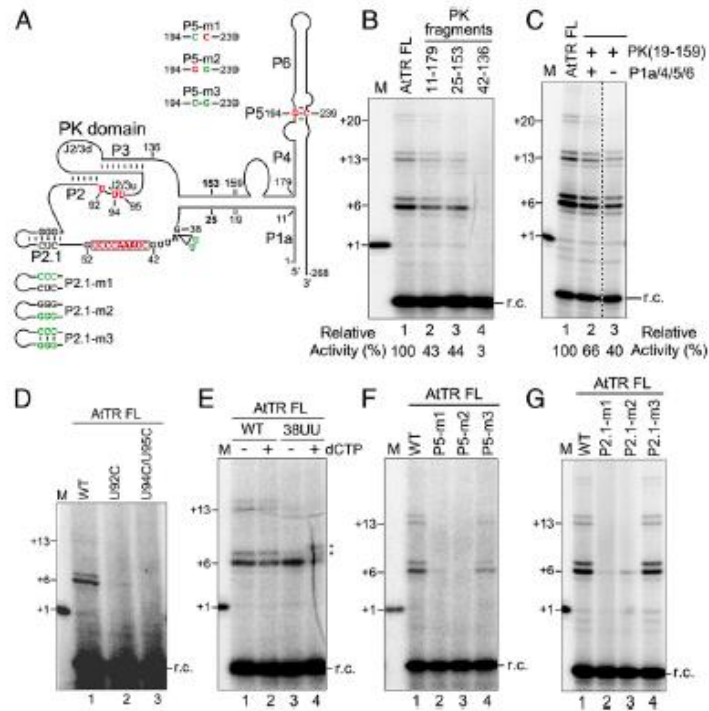


**Figure B-7 Functional characterization of critical structural elements in AtTR.**

(A) A schematic of AtTR secondary structure. The 5' and 3' residues of truncated AtTR fragments are denoted on the AtTR structure. The positions and identities of specific point mutations introduced are indicated. (B) Identification of a minimal PK fragment and (C) functional analysis of stem P1a/4/5/6. Full-length AtTR (AtTR-FL) and various AtTR truncated fragments were assembled with AtTERT in vitro and analyzed for activity by primer extension assay. The number of nucleotides (+6, +13 or +20) added in each major band of product are indicated. The P1a/4/5/6 fragment was generated by deleting residues 25-153 from the AtTR-FL and replacing with a GAAA tetraloop. The relative activities of the reactions are indicated under the gel. A recovery control (r.c.) is shown. (D) The functional requirement of invariant U residues in PK domain. (E) The effect of P1c linker length on template boundary definition. (F) Compensatory mutagenesis analysis of stem P5. (G) Compensatory mutagenesis analysis of stem P2.1. AtTR-FL constructs bearing specific point mutations are assembled with AtTERT in vitro and analyzed for telomerase activity. For analyzing template boundary definition with AtTR-38UU, the reconstituted enzyme was analyzed in the absence (-) or presence (+) of dCTP in addition to dGTP, dATP and dTTP.

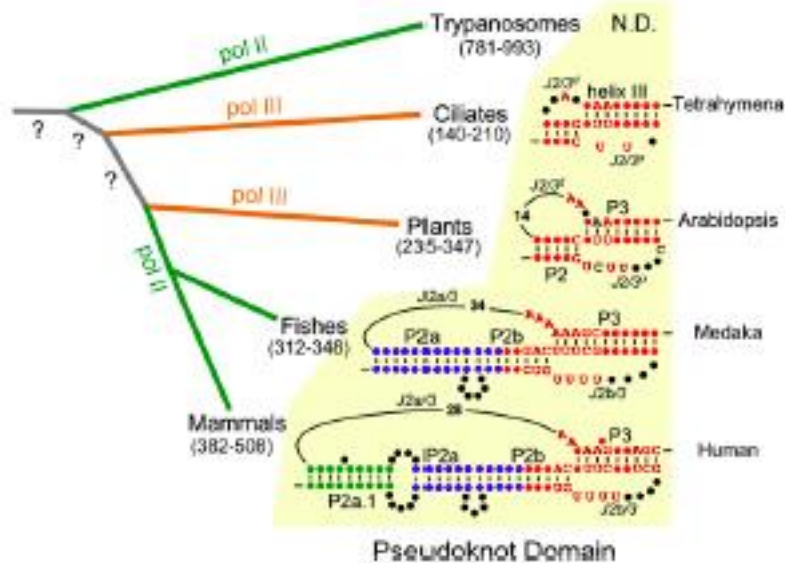


**Figure B-8 Evolution of TR pseudoknot structures.**

A simplified phylogenetic tree of major eukaryotic lineages is shown in the left panel. Branch length in the tree does not reflect evolutionary distance. The lineages with TR transcribed by Pol II (green) and Pol III (orange) are depicted. The size range of TRs from each group is indicated. The PK structures of TRs from the major groups of eukaryotes including ciliates, plants, fishes and mammals are shown in the right panel. Trypanosome TR does not have a PK structure in the template core domain (31). The P2 and P3 stems conserved from ciliates to mammals are shown in red with highly conserved nucleotides explicitly denoted. The vertebrate-specific stem extension P2a is shown in blue while the mammal-specific stem extension P2a.1 is shown in green. The length of joining sequences, J2/3 upstream (J2/3u) or downstream (J2/3d) regions, between stems P2 and P3 are indicated.





**Figure B-10 Multiple sequence alignment of plant TRs.**

Alignment of TR sequences from 8 eudicots, 2 monocots, 2 early branching angiosperms, 3 gymnosperms and 1 lycopphyte species representative of land plants. Multiple sequence alignment was performed using the ClustalW algorithm in the BioEdit program. Highly conserved regions and motifs were aligned first followed by alignment of intervening sequences using conserved regions as anchors. The total number of nucleotides in each TR is indicated at the end of the respective sequence. Individual nucleotides are colored by identity (A; green, G; black, U; red, C; blue) and nucleotides that are conserved in  $\geq 75\%$  of given plant species are shaded (White text on colored background). Five conserved regions (CRs) are indicated with red lines above the alignment. The template and base-paired helices (P1-P6) in the secondary structures are denoted within white boxes below the alignment.

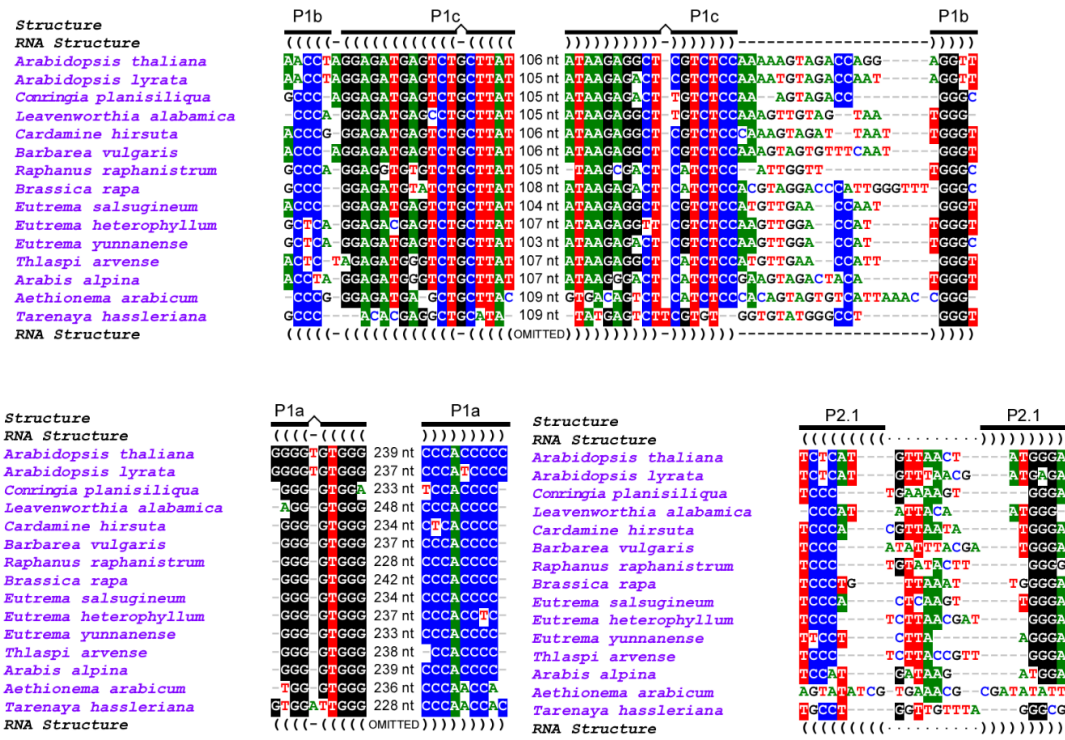
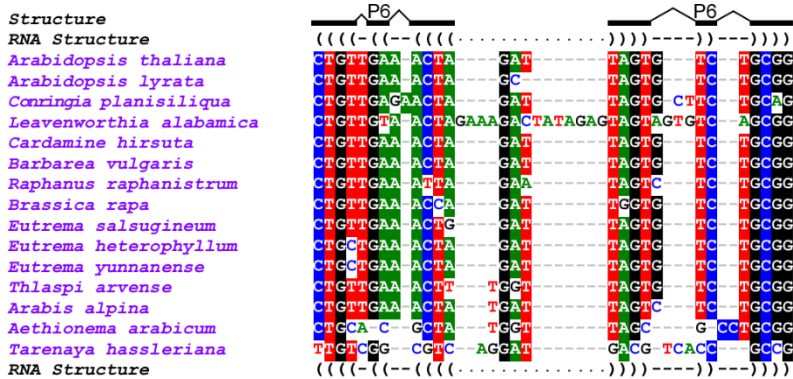


**Figure B-11 Sequence alignments of TR structural elements from respective clades to identify group-specific co-variations.**

Individual nucleotides are colored by identity (A; green, G; black, T; red, C; blue) with shaded residues shown as white text in colored background. Variable shading was applied to show clarity of co-variation. Individual TR elements are indicated above each alignment block with secondary structure representation shown using dot-bracket notations at the bottom. Intervening residues of structural elements that form long range base pairing are omitted and the number of nucleotides omitted are shown between the base paired regions. (A) Sequence alignments of TR structural elements from 15 species belonging to the Brassicales order including AtTR (Figure VI-6A). Shading of P1a (80%), P2.1 (75%), P1b/P1c (60%) and P6 (80%) are shown. (B) Sequence alignments of TR structural elements of 6 species from order Pinales including *P. glauca* TR (Figure VI-6C). Shading of P1b/P1c (50%) and P2.2 (65%) are shown. (C) Sequence alignments of TR structural elements of 4 species from division lycophyta including *S. kraussiana* TR (Figure VI-6D). Shading of 50% shown for all elements P1a, P1c, P1.1 and P6.



Pinales

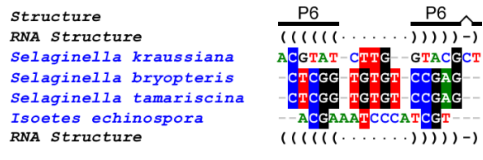
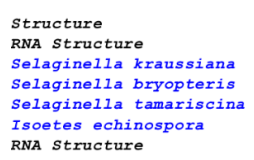
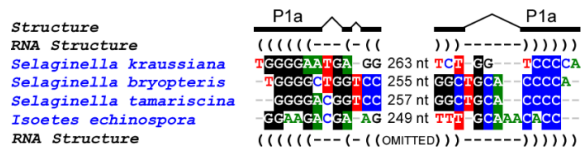
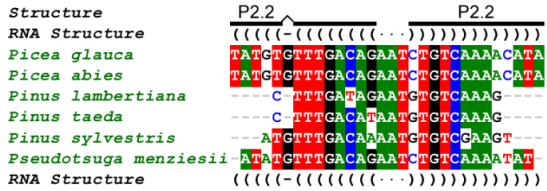
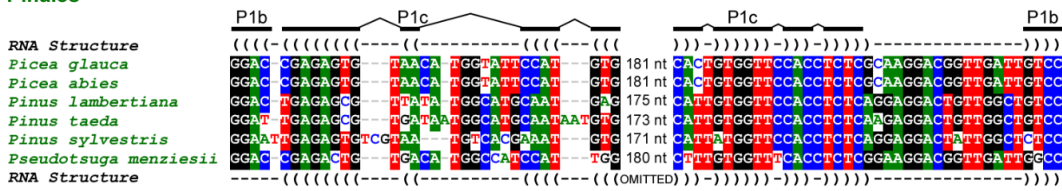
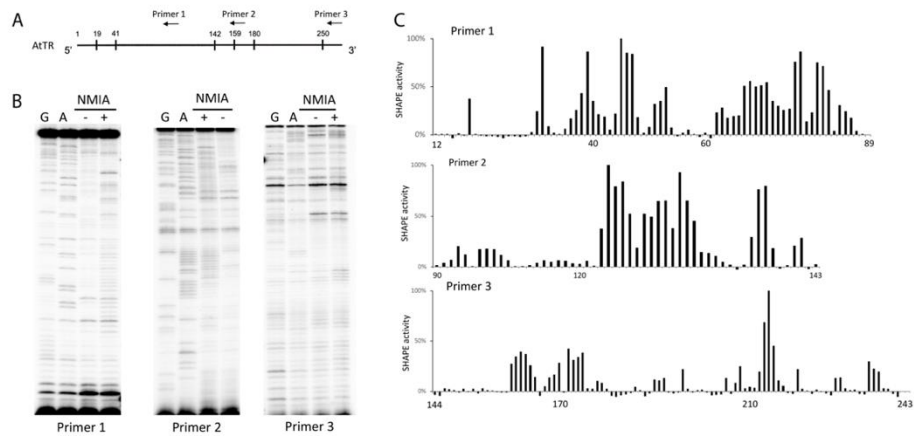
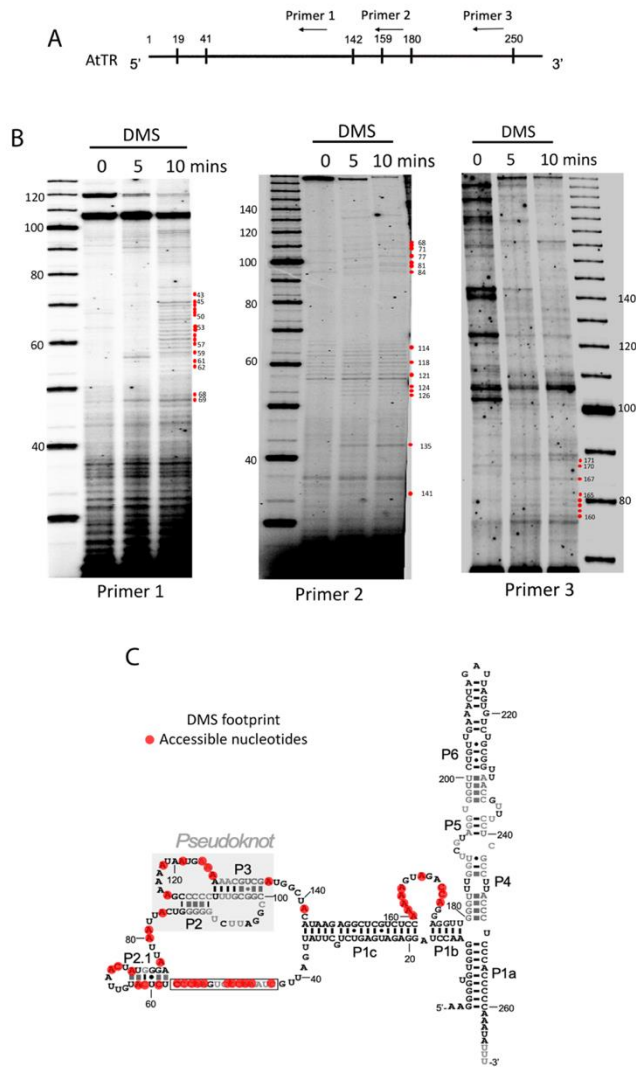


Figure B-11 Continued



**Figure B-12 SHAPE data support the structural model of AtTR.**

(A) Diagram of AtTR and primers used in the SHAPE assay. (B) Primer extension results for in vitro transcribed AtTR in the presence and absence of NMIA. (C) Quantified SHAPE activities are plotted along the AtTR sequence.



**Figure B-13 *In vivo* DMS footprinting uncovers accessible nucleotides in AtTR.**

(A) Schematic representation of AtTR and the primers used in the DMS footprinting assay. (B) Primer extension results using total RNA extracted from *A. thaliana* cell culture. A time course of DMS treatment is indicated. Red dots denote accessible nucleotides. Molecular weight markers (nts) are shown. (C) The DMS-accessible nucleotides (red) are mapped on the AtTR structure.



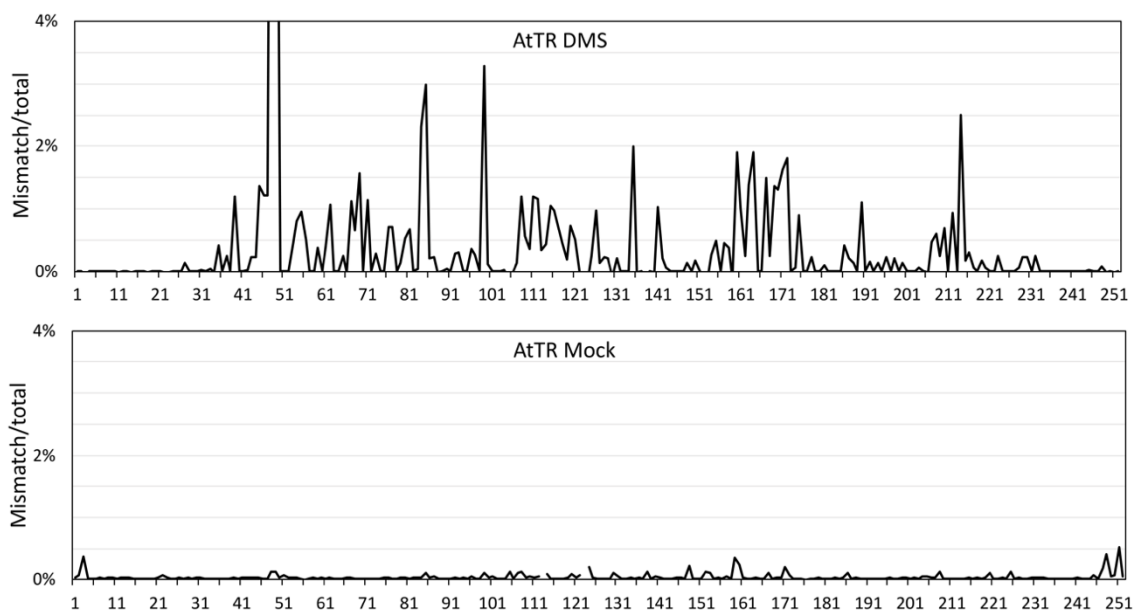


**Figure B-14 DMS MaPseq provides detailed information on accessible nucleotides in AtTR.**

Average mutation frequencies are plotted along AtTR sequences.

**Table B-1 Predictive analysis of telomerase RNA across plants.**

Clade	Order	Species	Accession	Start Coordinates <sup>a</sup>	End Coordinates <sup>b</sup>	Source
Angiosperms	Apiales	<i>Daucus carota</i>	NC_030389.1	27,698,101	27,698,376	NCBI
	Asterales	<i>Chrysanthemum seticuspe</i>	BDUE01009703.1	11,137	11,419	NCBI
	Boraginales	<i>Echium plantagineum</i>	QFAX02000220.1	135,925	136,171	NCBI
	Brassicales	<i>Aethionema arabicum</i>	KE151693.1	19,486	19,752	NCBI
	Brassicales	<i>Arabidopsis halleri</i>	FJVB01000013.1	273,652	273,920	NCBI
	Brassicales	<i>Arabidopsis lyrata</i>	NW_003302193.1	6,235	6,501	NCBI
	Brassicales	<i>Arabis alpina</i>	LT669791.1	32,604,818	32,605,077	NCBI
	Brassicales	<i>Arabis montbretiana</i>	LNCH01009117.1	36,530	36,800	NCBI
	Brassicales	<i>Arabis nordmanniana</i>	LNCG01220153.1	3,675	3,942	NCBI
	Brassicales	<i>Barbarea vulgaris</i>	LXTM01001115.1	52,644	52,908	NCBI
	Brassicales	<i>Boechera stricta</i>	MLHT01000206.1	2,167,990	2,168,256	NCBI
	Brassicales	<i>Brassica cretica</i>	QGKV01138583.1	73	347	NCBI
	Brassicales	<i>Brassica juncea</i>	CM007199.1	42,541,815	42,542,082	NCBI
	Brassicales	<i>Brassica rapa</i>	NC_024798.1	13,226,512	13,226,780	NCBI
	Brassicales	<i>Capsella bursa-pastoris</i>	MPGU01000291.1	544,071	544,341	NCBI
	Brassicales	<i>Cardamine hirsuta</i>	Chr4	14,202,139	14,202,402	MPIPZ
	Brassicales	<i>Conringia planisiliqua</i>	FNXX01000004.1	7,410,188	7,410,452	NCBI
	Brassicales	<i>Crucihimalaya himalaica</i>	SMJT01000124.1	207,463	207,727	NCBI
	Brassicales	<i>Euclidium syriacum</i>	FPAK01000008.1	2,642,798	2,643,063	NCBI
	Brassicales	<i>Eutrema heterophyllum</i>	PKMM01021225.1	255,915	256,145	NCBI
	Brassicales	<i>Eutrema salsugineum</i>	NW_006256908.1	4,817,520	4,817,781	NCBI
	Brassicales	<i>Eutrema yunnanense</i>	PKML01061038.1	473	736	NCBI
	Brassicales	<i>Leavenworthia alabamica</i>	KE157026.1	94,536	94,815	NCBI
	Brassicales	<i>Raphanus raphanistrum</i>	JRQH01003943.1	2,932	3,186	NCBI
	Brassicales	<i>Raphanus sativus</i>	NW_017353142.1	35,244,840	35,245,094	NCBI
	Brassicales	<i>Schrenkiella parvula</i>	CM001190.1	12,955,768	12,956,035	NCBI
	Brassicales	<i>Sisymbrium irio</i>	KE156162.1	139,418	139,686	NCBI
	Brassicales	<i>Tarenaya hassleriana</i>	NW_010971389.1	564,830	565,090	NCBI
	Brassicales	<i>Thlaspi arvense</i>	AZNP01000142.1	120,620	120,884	NCBI
	Caryophyllales	<i>Beta vulgaris</i>	NC_025816.2	46,989,999	46,990,277	NCBI
	Cucurbitales	<i>Cucurbita argyrosperma</i>	SDJN01000158.1	222,899	223,147	NCBI
	Fabales	<i>Pisum sativum</i>	PUCA014342884.1	375	635	NCBI
	Fagales	<i>Casuarina equisetifolia</i>	RDRV01000354.1	115,161	115,414	NCBI
	Gentianales	<i>Coffea eugenoides</i>	NC_040043.1	6,019,019	6,019,286	NCBI
	Lamiales	<i>Olea europaea</i>	NW_019237129.1	278,546	278,801	NCBI
	Malpighiales	<i>Caryocar brasiliense</i>	STGP01026219.1	4,821	5,089	NCBI
	Malpighiales	<i>Manihot esculenta</i>	NC_035172.1	30,848,292	30,848,551	NCBI
	Malpighiales	<i>Populus simonii</i>	CM0117472.2	14,153,485	14,153,758	NCBI
	Malpighiales	<i>Viola pubescens</i>	NBIL01136792.1	11,205	11,463	NCBI
	Malvales	<i>Aquilaria agallochum</i>	KK907007.1	4,840	5,116	NCBI
	Malvales	<i>Aquilaria sinensis</i>	SMDT01003036.1	616,167	616,432	NCBI
	Malvales	<i>Corchorus capsularis</i>	AWWV01006766.1	15,731	16,000	NCBI
	Malvales	<i>Corchorus olitorius</i>	AWUE01012270.1	7,870	8,137	NCBI
	Malvales	<i>Durio zibethinus</i>	NW_019167871.1	10,632,362	10,632,624	NCBI
	Malvales	<i>Gossypioides kirkii</i>	CM008983.1	32,191,550	32,191,784	NCBI
Malvales	<i>Gossypium aroboreum</i>	NC_030666.1	87,580,015	87,580,260	NCBI	

Table B-1 continued

Clade	Order	Species	Accession	Start Coordinates <sup>a</sup>	End Coordinates <sup>b</sup>	Source
Angiosperms	Apiales	<i>Diospyros australe</i>	NC0106629.1	270,698,436	270,698,326	NCBI
	Alismales	<i>Crossidium laticarpum</i>	HM010809703.1	23,878,898	23,879,056	NCBI
	Malvales	<i>Echinops altissimus</i>	QF420000025.1	159,928	159,937	NCBI
	Brassicales	<i>Alchemilla arvensis</i>	NC1518959.1	13,609,850	13,609,742	NCBI
	Brassicales	<i>Arabis alpina</i>	AF0600007457.1	273,656	273,626	NCBI
	Brassicales	<i>Arabis alpina</i>	NS110100045.1	4,217,944	4,217,307	NCBI
	Brassicales	<i>Aristida chilensis</i>	LVXP01036680.1	32,604,842	32,603,077	NCBI
	Brassicales	<i>Cephalanthus foliolaris</i>	RP011001127.1	142,531	142,306	NCBI
	Proteales	<i>Macadamia integrifolia</i>	UZVR01001767.1	83,061	83,327	NCBI
	Brassicales	<i>Arabis horrida</i>	LNC01220153.1	3,675	3,947	NCBI
	Rosales	<i>Rosa chinensis</i>	NC_057093.1	60,849,275	60,849,535	NCBI
	Brassicales	<i>Barbarea vulgaris</i>	LXFT01001115.1	52,644	52,368	NCBI
	Sapindales	<i>Atalantia buxifolia</i>	MKYR01004417.1	843,867	844,129	NCBI
	Brassicales	<i>Boechera stricta</i>	MLHT01000206.1	2,167,990	2,168,256	NCBI
	Sapindales	<i>Azadirachta indica</i>	AMWY02057456.1	1,105	1,362	NCBI
	Brassicales	<i>Brassica cretica</i>	OGKV01138583.1	73	347	NCBI
	Sapindales	<i>Citrus hindsii</i>	QWBT01000927.1	5,076,792	5,077,050	NCBI
	Brassicales	<i>Brassica juncea</i>	CM007199.1	42,541,815	42,542,082	NCBI
	Sapindales	<i>Citrus clementina</i>	NW_006261964.1	4,968,658	4,968,914	NCBI
	Brassicales	<i>Brassica rapa</i>	NC_014798.1	13,226,513	13,229,780	NCBI
	Sapindales	<i>Samolucris sorbifolium</i>	CM010616.1	13,811,758	13,812,020	NCBI
	Brassicales	<i>Capsella bursa-pastoris</i>	MEGJ01000292.1	541,021	543,177	NCBI
	Solanales	<i>Cuscuta australis</i>	NCVE01000692.1	783,927	784,177	NCBI
	Brassicales	<i>Cochlearia hirsuta</i>	GH1520654.1	14,202,130	14,202,402	MPHZ
	Solanales	<i>Cotyledon alba</i>	FNX010000116.1	7,419,188	7,419,462	NCBI
	Brassicales	<i>Cucumis melo</i>	SMWT010093345.1	297,452	297,470	NCBI
	Brassicaceae	<i>Enchiridium aegyptium</i>	EP0601000908.1	2,043,793	2,043,993	NCBI
	Brassicaceae	<i>Erysimum cheiranthoides</i>	RK010100225.1	255,915	256,146	NCBI*
	Brassicaceae	<i>Eutima sinensis</i>	NES006260909.1	4,897,526	4,897,801	NCBI
	Brassicaceae	<i>Eutima sinensis</i>	PKM100000930.1	7,781,426	7,781,726	NCBI
	Brassicaceae	<i>Leiridium chinensis</i>	RP0100200262.1	796,538	796,866	NCBI
	Gymnosperms	Brassicaceae	<i>Raphanus sativum</i>	HE010400943.1	96,872	97,108
Brassicaceae		<i>Rapum sinense</i>	NW010000057.1	35,248,867	35,249,052	NCBI
Ginkgoales		<i>Ginkgo biloba</i>	CM001190.1	261,572,740	261,572,655	GIGA
Brassicaceae		<i>Abies balsamea</i>	refseq1890030163	139,478	139,823	NCBI*
Pinales		<i>Larix sibirica</i>	NW0100000416.1	10,666	11,015	NCBI
Brassicaceae		<i>Taxus hussleriana</i>	CHVK0101923023.1	564,830	563,090	NCBI
Pinales		<i>Picea abies</i>	AZNP01000142.1	6,762	7,140	NCBI
Brassicaceae		<i>Pinus arvensis</i>	ALWZ0101636083.1	120,620	120,884	NCBI
Pinales		<i>Picea glauca</i>	NC_043816	4,036	4,382	NCBI
Caryophyllales		<i>Beta vulgaris</i>	JLMT010003768.1	46,989,999	46,990,297	NCBI
Pinales		<i>Pinus lambertiana</i>	SDJN01000158.1	303,995	304,339	NCBI
Cucurbitales		<i>Cucurbita argyrosperma</i>	sonit_7214027	222,899	223,147	NCBI
Pinales		<i>Pinus sylvestris</i>	PUCAT01454284.1	1,193	1,533	NCBI
Fabales		<i>Pisum sativum</i>	APFE031443769.1	375	635	NCBI
Pinales		<i>Pinus taeda</i>	RDRV01000354.1	20,896	21,241	NCBI
Fagales		<i>Castanea equisetifolia</i>	LPNX010568464.1	115,161	115,414	NCBI
Pinales		<i>Pseudotsuga menziesii</i>	NC_040043.1	175,954	176,301	NCBI
Lycophytes		Gentianales	<i>Coffea eugenioides</i>	NC_040043.1	6,019,019	6,019,286
	Isoetales	<i>Isoetes echinospora</i>	CGKV010093904.1	1,209	1,488	NCBI*
	Lamiales	<i>Olea europaea</i>	NC_019197129.1	278,546	278,801	NCBI
	Malpighiales	<i>Celastrus scandens</i>	ST0100002103.1	4,826	5,089	NCBI
	Malpighiales	<i>Manihot esculenta</i>	NC_035172.1	30,848,292	30,848,551	NCBI
	Selaginiales	<i>Selaginella bryopteris</i>	GEMU01091170.1	1	305	NCBI*
	Malpighiales	<i>Populus simonii</i>	CM017472.2	14,153,485	14,153,758	NCBI
	Malpighiales	<i>Selaginella selaginoides</i>	NC_011007933.1	144,203	141,402	NCBI
	Malvales	<i>Aquilaria agallochum</i>	KK907007.1	4,840	5,116	NCBI
	Malvales	<i>Cochlospermum vitifolium</i>	SMDT01003036.1	616,167	616,432	NCBI

<sup>a</sup>: 5' end predicted based on multiple sequence alignment with ATR

<sup>b</sup>: 3' end of TR inferred on the basis of a *S. pombe* 'SU' tract

NCBI: National Center for Biotechnology Information (Genome Database) <http://www.ncbi.nlm.nih.gov/genomes>  
 NCBI\*: National center for Biotechnology Information - Transcriptome Shotgun Assembly Sequence Database, URL: [www.ncbi.nlm.nih.gov/tx](http://www.ncbi.nlm.nih.gov/tx)  
 MPPIG: Max Planck Institute for Plant Breeding Research - Genomic Resource <http://www.mpi-pz.mpg.de>  
 DRYAD: Dryad digital repository, URL: <http://dx.doi.org>  
 GIGA DB: GigaDB data repository, URL: [gigadb.org](http://gigadb.org)  
 TGDB: TreeGenes database, URL: [treegenes.ucdavis.edu](http://treegenes.ucdavis.edu)

## Discussion

Telomerase emerged in early eukaryotes as a specialized reverse transcriptase with an integral RNA template to counteract the end-replication problem and maintain genomic integrity. While the catalytic TERT component of telomerase is conserved among eukaryotes, the TR component has diverged significantly during evolution. A missing piece in the evolutionary history of telomerase has been plant TR. Recent studies from the Fajkus and Beilstein labs indicated that the previously identified AtTER1 (Cifuentes-Rojas et al., 2011) was not the authentic TR in *A. thaliana*. The results from our independent study support this conclusion. We were unable to detect AtTER1 using two purification schemes, one designed to identify RNAs loosely associated with AtTERT, and a second more stringent approach to identify RNAs associated with partially purified, enzymatically active telomerase. The misidentification of AtTER1 in the previous study may have resulted from a primer extension strategy that employed biased primers corresponding to predicted Arabidopsis TR template, and which inadvertently recovered a low-abundance RNA molecule derived from the RAD52 locus that co-purified with telomerase. Our next-generation sequencing approach also failed to recover AtTER2, a second telomerase-associated RNA proposed to negatively regulate enzyme activity in response to DNA damage (Cifuentes-Rojas et al., 2011, 2012). Re-evaluation of the AtTER2 locus in relation to telomerase and telomeres is now underway.

Nevertheless, the single RNA enriched by 100-fold in enzymatically active telomerase fractions from our more stringent purification scheme was AtTR, the same RNA molecule uncovered independently by the Fajkus lab using an *in silico* strategy to

find plant TRs (Fajkus et al., 2019). To investigate the function of AtTR, we employed a combination of Arabidopsis genetics and in vitro reconstitution experiments using a rigorous non-PCR assay of direct primer extension to test the authenticity of this putative telomerase RNA template. We determined that AtTR was not only required for telomere maintenance in vivo, but also possessed a functional template for telomeric DNA synthesis by AtTERT in vitro. Our observations agree with those of Fajkus et al and confirm that AtTR is the bona fide telomerase RNA subunit for *A. thaliana*.

AtTR was first described in 2012 by Wu and collaborators as a root-specific, conserved Pol III-dependent ncRNA (Wu et al., 2012a). The ATTR gene (Genbank AB646770.1) includes a U6-like Type III promoter and poly(T) terminator. The promoter has a consensus cis upstream sequence element (USE) and a TATA box-like element 25 bp upstream of the transcription start site (TSS). The discovery of plant TRs being Pol III RNA transcripts leads to an interesting question: was the first TR a Pol II or Pol III transcript? TR was originally identified in ciliates as a small Pol III RNA transcript with sizes ranging from 140 to 210 nt (Figure VI-8). RNA polymerase III is generally employed for transcribing small RNA such as 5S rRNA and tRNA due to its sequence-dependent termination at a U-rich termination site. A large RNA would encounter a high frequency of U-rich sequences and suffer premature termination with Pol III transcription, which is consistent with the small size of ciliate TR (Lingner et al., 1994). Surprisingly, TRs identified later in vertebrates and fungi are larger Pol II transcripts with sizes of 312-559 nt and 920-2425 nt, respectively (Chen et al., 2000; Qi et al., 2013). While it seems reasonable to assume that the Pol III TR transcript is more ancestral, TRs from early

branching flagellates, including Trypanosomes, are large Pol II transcripts ranging between 781-993 nt (Figure VI-8). Discerning the origin of TR will require discovery of TRs from the early branching lineages of eukaryotes, a daunting task considering the extremely divergent nature of TR.

The conserved secondary structures of plant TRs presented in this study were determined by employing phylogenetic comparative analysis, a gold standard for inferring RNA secondary structures (Chen et al., 2000; Pace et al., 1989). Moreover, the secondary structure of AtTR was verified by *in vitro* and *in vivo* chemical probing approaches under native conditions as well as mutagenesis analysis using an *in vitro* reconstitution system. In the AtTR structure, the most crucial structural element is the PK, which is conserved in all known TRs except Trypanosome (Figure VI-8). Trypanosome TR contains two structural domains, the template-core and eCR4/5, both of which are required for telomerase activity *in vitro* and can function *in trans* as two separate RNA fragments (Podlevsky et al., 2016). However, the minimal template core domain of Trypanosome TR does not contain a PK, arguing that the critical TR PK was a later adaptation. Nevertheless, helix III of Trypanosome TR is potentially homologous to the PK forming helix III of Tetrahymena TR as both helices are located between the template and the core enclosing helix, i.e. helix I in Tetrahymena TR or P1 stem in other TRs. The PK structure of Tetrahymena TR only requires formation of a 4 bp stem between the loop sequence of helix III and an upstream complementary sequence (Figure VI-8). This 4 bp stem is structurally equivalent to the vertebrate P2 stem which is longer and contains two consecutive stems, P2a and P2b, and with an additional P2a.1 stem in the mammalian TR

PK (Figure VI-8). How this primitive ciliate TR PK evolved to the more complex vertebrate TR PK has been unclear. The structure of plant TR PK now provides an explanation for the structural transition from ciliate to vertebrate PK. Similar to ciliate PK, plant PK contains a short unstable 4 bp P2 stem and a longer 8-9 bp P3 stem. DMS chemical probing of the *A. thaliana* TR PK reveals mild modification of the P2 stem, consistent with a more unstable helix (Figure VI-6F). Notably, the ciliate and plant PK structures differ in the length of the joining sequences, J2/3 upstream (J2/3u) and J2/3 downstream (J2/3d) (Figure VI-8). The length of J2/3u increases from 3 nt in *Tetrahymena* to 8 nt in plants, similar to the 8 nt J2b/3 in vertebrate TR PK (Figure VI-8). The length of J2/3d sequence also increases from 4 nt in *Tetrahymena* to 14 nt in the *A. thaliana* PK. We propose that the longer J2/3d makes it possible to expand the short 4 bp P2 stem to a longer P2a/P2b stem in vertebrate PK during evolution. Notably, plant TR contains additional stems (P2.1 and P2.2) located between the template and the P2 stem (Figure VI-8). These additional stems may reflect selective pressure to maintain the spatial constraints for the enzyme active site as the P2 stem expands during evolution. Therefore, the plant TR PK provides an evolutionary bridge for the structural transition from ciliate TR to vertebrate TR.

## **Material and Methods**

### ***RIP seq***

Anti-AtTERT antibody was affinity purified with an EpiMAX affinity purification kit (abcam) following the manufacturer's protocol. It was preincubated with protein A

magnetic beads (Dynabeads) before IP experiments. For the direct RIP seq, 1.2 g of WT (Col-0) and tert Arabidopsis flowers were ground in liquid nitrogen and homogenized in buffer RIP (100 mM Tris-OAC pH7.5, 100 mM KGlu, 1 mM MgCl<sub>2</sub>, 0.5% Triton X-100, 0.1% Tween 20, 20 ul/ml Plant protease inhibitor cocktail (Sigma), 1 ul/ml RNase OUT (Thermo Fisher) and 2.5 mM DTT). After clearing by centrifugation, protein complexes were immunoprecipitated using preincubated anti-AtTERT magnetic beads for 2.5 h at 4°C. After incubation, beads were washed with buffer RIP for seven times and resuspended with 1 ml TRIzol reagent (Invitrogen) to extract RNA. For RIP seq after gel filtration, fractions with peak telomerase activity were incubated in buffer TERT (50 mM Tris-OAC pH7.5, 150 mM KGlu, 5 mM MgCl<sub>2</sub>, 5% Glycerol, 20 ul/ml Plant protease inhibitor cocktail (Sigma), 1 ul/ml RNase OUT (Thermo Fisher), 0.1 mM PMSF, and 1.5 mM DTT) with preincubated anti-AtTERT magnetic beads for 3 h at 4°C. Beads were washed with buffer RIP seven times, and the remaining RNA was extracted following Direct-zol RNA kits (ZYMO research) including in-column DNase treatment. After rRNA depletion, construction of Illumina sequencing libraries was performed with the NEBNext Ultra Directional RNA Library Prep Kit, and libraries were sequenced on an 300x2 Illumina MiSeq platform by Texas A&M AgriLife Genomics and Bioinformatics Service.

#### Target-specific DMS-MaPseq

Target-specific DMS-MaPseq was performed as described (Ding et al., 2014; Zubradt et al., 2016) with modifications. Total RNA was extracted from DMS or Mock treated samples using RNA Clean & Concentrator-5 (ZYMO research) with in-column DNase digestion. RNA quality was analyzed on agarose gels. 5 µg high quality RNA was



combined with gene-specific primers (5 pmol each) in a total volume of 11  $\mu$ l. The mixture was heated at 75°C for 3 min and annealed at 55°C for 15 min. TGIRT reaction buffer including 4  $\mu$ l 5x First-Strand buffer (Thermo Fisher), 1  $\mu$ l 0.1M DTT, 1  $\mu$ l RNaseOUT (Thermo Fisher) and 1  $\mu$ l TGIRT-III (Ingex, Cat#: TGIRT50) was added and the solution was incubated at room temperature for 30 min. Then, 2  $\mu$ l 10 mM dNTP was added and the well-mixed reaction was processed at 60°C for 2.5 h. After RT, 1  $\mu$ l cDNA solution was directly added into a 50  $\mu$ l PCR reaction using Phusion High-Fidelity DNA Polymerase (NEB) to amplify AtTR or ACT2 mRNA with an approximate product size of 260 bp. PCR products were gel purified and quantified by the Qubit dsDNA BR assay kit (Thermo Fisher). Without fragmentation, the cleaned PCR products were directly assembled into Illumina sequencing libraries using the NEBNext Ultra II DNA Library Prep Kit with 25 ng input. One Mock library and two DMS libraries were built for each genotype. Finally, the libraries were quantified using Agilent TapeStation before sequencing on an 150x2 Illumina NextSeq 500 platform at Texas A&M University.

#### Telomerase direct primer extension

12  $\mu$ l of in vitro reconstituted telomerase enzyme was immuno-purified with 3  $\mu$ l of anti-FLAG M2 magnetic beads (Sigma M8823) at room temperature for 1 hr. The telomerase enzyme on beads was assayed in a 10  $\mu$ l reaction containing 1X telomerase reaction buffer (50 mM Tris-HCl, pH 8.0, 50 mM NaCl, 0.5 mM MgCl<sub>2</sub>, 5 mM BME and 1mM spermidine), 1 $\mu$ M DNA primer, and specified dNTPs or ddNTPs and 0.18 $\mu$ M of <sup>32</sup>P-dGTP (3,000 Ci/mmol, 10 mCi/ml; Perkin-Elmer). Reactions were incubated at 30°C for 60 min and terminated by phenol/chloroform extraction, followed by ethanol

precipitation. The 22-mer size marker was prepared in a 10  $\mu$ l reaction containing (GGGTTTA)<sub>3</sub> oligo, 1x TdT reaction buffer, 5 units of terminal deoxynucleotidyl transferase (TdT, Affymetrix) and 0.1  $\mu$ M of 32P-dGTP. The reaction was incubated at room temperature for 3 sec and terminated by addition of 10  $\mu$ l 2x formamide loading buffer (10mM Tris-HCl, pH8.0, 80% (vol/vol) formamide, 2 mM EDTA, 0.08% bromophenol blue, and 0.08% Xylene cyanol). The DNA products were resolved on a 10% (wt/vol) polyacrylamide/8 M urea denaturing gel, dried, exposed to a phosphorstorage screen and imaged on a Typhoon gel scanner (GE Healthcare).

*Plant material, growth conditions, and transformation*

*Arabidopsis thaliana* accession Col-0, WS, attr (Flag\_410H04), and tert (SALK\_041265C) were used in this study. Cell line T87 was obtained from ABRC and was originally derived from *A. thaliana* accession Col-0. The cell culture was maintained as indicated by the ABRC, passed every seven days in NT-1 media and grown under continuous light at room temperature with constant shaking at 120 rpm. Seeds were sterilized in 50% bleach with 0.1% Triton X-100 and then plated on half Murashige and Skoog (half MS) medium with 0.8% agar. Plants were grown at 22°C under long day light conditions. AtTR was placed under the control of the U6 promoter in the pHSN6A01 vector. Guide RNAs targeting the sequences surrounding the template of AtTR were cloned into the pDs-Sa-Cas9 vector for transformation into Col-0 plants using *Agrobacterium*-mediated transformation as described (Zhang et al., 2006). For genetic complementation, third generation AtTR<sup>-/-</sup> were transformed with *A. tumefaciens* GV3101 containing pHSN6A01 U6::AtTR. Transformants were selected on hygromycin

in T1 and analyzed for telomere phenotypes. In parallel, untransformed fourth generation AtTR<sup>+/+</sup> and AtTR<sup>-/-</sup> plants were analyzed.

#### Gel filtration of active telomerase

Five-day-old WT (Col) and tert seedlings were ground in liquid nitrogen and homogenized in extraction buffer (50 mM Tris-OAC pH7.5, 100 mM KGlu, 5 mM MgCl<sub>2</sub>, 20 mM EGTA, 15 g/L Polyvinylpyrrolidone (PVP), 10% Glycerol, 20 ul/ml Plant protease inhibitor cocktail (Sigma), 1 ul/ml RNase OUT recombinant ribonuclease inhibitor (Thermo Fisher), 0.2 mM PMSF, and 1.5 mM DTT). The homogenates were centrifuged at 14,000 r.p.m for 15 min at 4°C and the supernatant was combined with 10% final concentration of PEG8000 to precipitate protein complexes for 45 min at 4°C. The precipitation was collected and resuspended with buffer TERT (50 mM Tris-OAC pH7.5, 150 mM KGlu, 5 mM MgCl<sub>2</sub>, 5% Glycerol, 20 ul/ml Plant protease inhibitor cocktail (Sigma), 1 ul/ml RNase OUT (Thermo Fisher), 0.1 mM PMSF, and 1.5 mM DTT). After three rounds of centrifugation, supernatant was injected into an AKTA FPLC system, and the proteins were fractionated through a Superose6 Increase 10/300 GL column (GE Healthcare) driven by buffer TERT. Fractions were collected to measure telomerase activity by qTRAP.

#### In vivo DMS modification

DMS treatment was performed as described with a few modifications (Wang et al., 2019b; Zubradt et al., 2016). For DMS footprinting, Arabidopsis cell culture in growth medium was mixed with DMS (Sigma, Cat#: D186309) to a final concentration of 0.75%. Incubation was applied with gentle shake in vacuum condition for 5 or 10 min. After

adding  $\beta$ -mercaptoethanol to quench the reaction, materials were washed five times with miracloth wrap. The dry materials were immediately frozen in liquid nitrogen and stored at  $-80^{\circ}\text{C}$ .

For DMS MaPseq, four-day-old WT (WS) seedlings were treated with 1% DMS or water (Mock samples) in DMS reaction buffer (40 mM HEPES pH7.5, 100 mM KCl and 0.5 mM  $\text{MgCl}_2$ ). 7.5 min of vacuum incubation was applied twice with a thorough mix in between. Materials after DMS incubation were washed and collected as described previously (Zubradt et al., 2016).

#### DMS footprinting

10  $\mu\text{g}$  total RNA extracted from each DMS-treated sample was mixed with  $^{32}\text{P}$ -radiolabelled gene-specific primers in annealing buffer (10 mM Tris-HCl pH7.5 and 20 mM KCl) of total 10  $\mu\text{l}$  volume. The mixture was heated at  $75^{\circ}\text{C}$  for 3 min, annealed at  $55^{\circ}\text{C}$  for 15 min, and stabilized at  $4^{\circ}\text{C}$  for 2 min. After annealing, 10  $\mu\text{l}$  reverse transcription (RT) reaction including 1x SuperScript IV buffer, 1 mM DTT, 1 mM dNTPs, 1  $\mu\text{l}$  RNaseOUT (Thermo Fisher) and 1  $\mu\text{l}$  SuperScript IV reverse transcriptase (Thermo Fisher) was added. The reaction proceeded for 1 h at  $60^{\circ}\text{C}$ . Reaction products were alkali-treated to hydrolyze the RNA, neutralized and precipitated before loading into a 7M Urea 8% (19:1) polyacrylamide gel. The gel image was collected with a Typhoon FLA 9500 (GE Healthcare) and bands were quantified using Quantity One (Bio-Rad).

#### SHAPE

SHAPE was performed as described with modifications (Wilkinson et al., 2006). 2 pmol gel purified AtTR was folded in SHAPE buffer (100 mM HEPES pH8.0, 100 mM

NaCl, and 7 mM MgCl<sub>2</sub>) at 37°C for 30 min. NMIA of 6.5 mM final concentration was used for RNA modification. After resolving primer extension products on a 7M Urea 8% (19:1) polyacrylamide gel, the image was collected with a Typhoon FLA 9500 (GE Healthcare) and bands were quantified using Quantity One (Bio-Rad).

#### Terminal Restriction Fragment (TRF), TRAP, and quantitative TRAP (qTRAP)

TRF, TRAP, and qTRAP assays were performed as previously described (Kobayashi et al., 2019; Surovtseva et al., 2007; Xu et al., 2015a) with one modification. For TRAP and qTRAP, partially purified telomerase was incubated with corresponding reactions at room temperature for 30 min instead of 37.

#### Northern Blotting

Total RNA was extracted from Arabidopsis cell culture by Direct-zol RNA kits (ZYMO research) including in-column DNase treatment. 15 µg total RNA was fractionated on a 7M Urea 4% (19:1) polyacrylamide gel together with in vitro transcribed AtTR as a molecular weight marker. RNA was semi-dry transferred to a Hybond+ membrane (GE Healthcare) and hybridized for 16 h at 65°C with a combination of three <sup>32</sup>P-radiolabelled oligonucleotides complementary to AtTR. After the membrane was washed, the gel image was collected with a Typhoon FLA 9500 (GE Healthcare).

#### Bioinformatics analysis

AtTR orthologs were identified by standalone BLAST (version 2.2.31+) searches initially using AtTR as query from closely related species. The BLASTN search was performed with the -task dc-megablast parameter to allow for identification of more variable sequences. For more distantly related species, position weight matrix (PWM)

search using fragrep 2 (Mosig et al., 2006) was performed for candidate identification. The PWM was created using sequence alignment from AtTR orthologs identified via BLAST and the match scores were relaxed during PWM searches to allow for identification of more divergent sequences. Once a reliable secondary structure was established using the TRs identified via BLAST and fragrep2, secondary structure-based searches were performed using Infernal (Nawrocki and Eddy, 2013) for identification of orthologs from more distantly related species.

#### Sequence alignment analysis

Multiple sequence alignment of land plant TRs was performed initially using the ClustalW algorithm of the Bioedit program. Manual refinements were made to preliminary alignments with highly conserved regions and invariant primary sequence motifs as anchor points. Sequences from closely related species of the Brassicaceae family were aligned first and the alignment was expanded by including sequences in order of phylogenetic relationships to the existing alignment.

#### In vitro reconstitution of Arabidopsis telomerase

3xFLAG tagged Arabidopsis TERT (AtTERT) was expressed in rabbit reticulocyte lysate (RRL) from the p3xFLAG-AtTERT plasmid using the TNT Quick Coupled transcription/translation kit (Promega) following manufacturer's instructions. The AtTR fragments were in vitro transcribed by T7 RNA polymerase, gel purified and assembled with TERT protein for 30 min at 30°C at a final concentration of 1.5  $\mu$ M (Podlevsky et al., 2016).

## APPENDIX C

### MISCELLANEOUS INFORMATION

**Table C-1 Primer Sequences.**

Primer Name	Primer Sequence
<b>Genotyping Primers</b>	
Lb1.3	ATTTTGCCGATTTTCGGAAC
LB1 SAIL1	GCCTTTTCAGAAATGGATAAATAGCCTTGCTTCC
tad3-1_LP_SAIL	GACGACAACCTAAACCCTACGCTTACA
tad3-1_RP_SAIL	CGATGTTGTTTTCTGCTTAGGACACA
tad3-2_LP	ATGGTCAGGTGACAATGAAGG
tad3-2_RP	ACCTTAGCCACTAACAACCCC
ku70_LP	TTACTTTGTTGTTTCGGGTGC
ku70_RP	CTCTTGGCAAGTACACGCTTC
pot1a_LP	ATGGCGAAGAAGAGAGAGAGTCCCA
pot1a_RP	CTATCTTGATCTCTCTCAAGAAGGA
pot1a_T-DNA	CATTTTATAATAACGCTGCGGACATC
ctc1_LP	GGTGCTTGAGAAGATGTTTGC
ctc1_RP	ACTTTTAAATTCGCAGGGTGG
<b>qPCR Primers</b>	
TAD3_F	TAGATGGCATCGGTGGGTTCAG
TAD3_R	TCACTGCAGCATTCAAGTGG
TER2_F	CGCTTACATAAAAACGCGACC
TER2_R	CACGTCTCTCTTACGTCGTC
TER2_3'_F	CAAAC TTGTGCCTAAGCAG
TER2_3'_R	GCAAAC TGATTCCTGAAGTTGG
TERT_F	ACCGTTGCTTCGTTGACTTCACG
TERT_R	CGACCCGCTTGAGAAGAAACTCC
POT1A_F	TTCCGTCACCTCCTGGATTAACAG
POT1A_R	TCTGTACTTGCAATGTAACCTTGGG
<b>Fusion PCR Primers</b>	
1R	CTATTGC CAGAACCTTGATATTCAT
1L	ACAAGGATAGAAATAGAGCATCGTC
2R	CAACATGGCCCATTTAAGATTGAACGGG
3L	CATAATTCTCACAG CAGCACCGTAGA
4R	TGGGTGATTGTCATGCTACATGGTA
<b>Others</b>	
qTRAP_F Primer	CACTATCGACTACGCGATCAG
qTRAP_R Primer	CCCTAAACCCTAAACCCTAAA
UDG-PENT Primer	CCCTAAACCC TAAA
HairPin Assay Oligo	P-GGATCCGACTTTTGTCTGGATCC
4X G-probe	(TTTAGGG)X4
4X C-probe	(CCCTAAA)X4